The Functional Relevance of BIN1: Implications for Endocytosis in Alzheimer's Disease

Submitted to Cardiff University for the Degree of Doctor of Philosophy by

Anna Lucie Burt

Division of Psychological Medicine and Clinical Neurosciences

School of Medicine, Cardiff University

September 2017

Declaration

This work has not been submitted in substance for any other degree or award at this or any other university or place of learning, nor is being submitted concurrently in candidature for any degree or other award.

Signed …… (candidate) Date ……..……..……

STATEMENT 1

This thesis is being submitted in partial fulfillment of the requirements for the degree of ……(insert MCh, MD, MPhil, PhD etc, as appropriate)

Signed …… (candidate) Date ……..……..……

STATEMENT 2

This thesis is the result of my own independent work/investigation, except where otherwise stated, and the thesis has not been edited by a third party beyond what is permitted by Cardiff University's Policy on the Use of Third Party Editors by Research Degree Students. Other sources are acknowledged by explicit references. The views expressed are my own.

Signed …… (candidate) Date ……..……..……

STATEMENT 3

I hereby give consent for my thesis, if accepted, to be available online in the University's Open Access repository and for inter-library loan, and for the title and summary to be made available to outside organisations.

Signed …… (candidate) Date ……..……..……

STATEMENT 4: PREVIOUSLY APPROVED BAR ON ACCESS

I hereby give consent for my thesis, if accepted, to be available online in the University's Open Access repository and for inter-library loans **after expiry of a bar on access previously approved by the Academic Standards & Quality Committee.**

Signed …… (candidate) Date ……..……..……

This thesis is dedicated to my grandmother, Sheila Readings, for seeing the good in everything.

Your example will forever inspire me.

Acknowledgements

Firstly, I would like to extend my utmost appreciation and thanks to Rhian Thomas, for her invaluable expertise, support, encouragement and unending enthusiasm, without which, quite frankly, this thesis would not have been possible. Rhian has been a fantastic academic mentor, stepping in as a supervisor when things didn't quite go to plan and playing a pivotal role in the transformation of my project. The passion and precision with which she works in addition to her incredibly thorough feedback have truly shaped me as a scientist. Rhian's patience and unwavering optimism in my moments of doubt have influenced me throughout this project and will continue to do so through life. Rhian, I will forever be grateful for you taking me in and only hope that I have done you proud.

Next, I'd like to thank my supervisors Mel Dunstan and Beccy Sims for their guidance and support in this project. Mel, thank you for embarking on the iPSC journey with me, sharing the parental responsibility of weekend feeds, always looking on the bright side and providing a constant source of amusing anecdotes! Thanks also to Beccy who has provided invaluable advice and feedback, both in in this project and for my future ambitions. Thank you also to my supervisor Julie Williams for giving me the opportunity to work on this project, it has been a fascinating and challenging experience.

Thanks must be extended to those who have helped me through the challenge of iPSC culture, particularly Claudia Tamburini and Zoe Noakes. Thank you to Lyle Armstrong at Newcastle University and Sally Cowley and the team at the James Martin Stem Cell Facility, Oxford University, for their time, expertise and willingness to help. I would like to thank Mark Gumbleton, Jack Sim and Arwyn Jones for their time and guidance in mastering the endocytic trafficking assays. Also thanks to Ann Ager for kindly providing me with the hCMEC/D3 cell line required to complete this project. Thank you to Catherine Matheson and Rob Greening, two brilliant project students who assisted with the Western blots contributing to Chapters 5 and 6. Thank you also to Emyr Lloyd-Evans for your interest, help and guidance with Chapter 6 and your team, particularly Helen Waller-Evans and Luke Haslett. Special thanks must be extended to Emily Kirkham for her generosity, technical assistance and always making me feel welcome in the lab.

I am grateful to all those in the Alzheimer's team who have helped me out with training, advice, support, cell feeding, Western washing, forgetting my woes, celebrating successes or have just been there to listen. Particular mention must go to Helen, Jodie, Gareth, Rachel, Matt, Nicola and Sarah for the time they have given me throughout this project and Taniesha, Rhodri and Adele for getting me through many a long day.

To "the other" Anna, my fellow PhD-er, well, what can I say? It's been emotional! I can't thank you enough for completing this journey alongside me and sharing the load. Thank you for your support, both emotional and technical, for listening, celebrating, commiserating, persevering, ranting, raving, drinking, dancing, and most of all laughing with me for the past four years. We may have been mistaken for the same person on multiple occasions, but I can't imagine my PhD experience any other way. I'm so pleased we will be able to celebrate completing this challenge together. We did it!

To all my ever-supportive friends, who may be more relieved that I have finally finished than I am! Thank you for your patience, encouragement and friendship while I have been otherwise engaged, for ensuring my social life is minimally affected and for always showing a genuine interest in what I do. A particular mention must go to Jess for being a constant source of support, companionship and laughter throughout the PhD and my time in Cardiff, for always being there to listen and showing me that it will all be worth it. Thank you for being the best friend I could ask for, I couldn't have done it without you.

Finally, to my family, thank you to my parents for everything you have done for me to get me through my academic studies. Thank you for your encouragement, love and support and never once doubting me, even when I have doubted myself. Mum, you have been an invaluable source of strength and reassurance. Thank you for always taking an interest, I don't mind if you don't understand the title, I know you are proud of me. Thank you to Max and to Mandy, Jim and Nan for all your support and interest throughout. Dad, thank you for your encouragement and help throughout my studies and the practical side of life alongside and to my brother Chris, cheers for being there for me and for finally learning what I do.

Last but by no means least, to my fiancé Chris. Thank you for never failing to put a smile on my face at the end of a long day, for always believing in me and reminding me that I can do anything but not everything. Thank you for sharing in my triumphs and my tears. You have been a pillar of strength, getting me through the stressful times, reaffirming my self-confidence and providing unconditional support and encouragement. This is as much your achievement as it is mine.

"I may not have gone where I intended to go, but I think I have ended up where I needed to be."

~ Douglas Adams

Thesis summary

Alzheimer's disease is a complex neurodegenerative disorder, characterised by progressive neurological and cognitive impairment. Genome-wide association studies have shown the significant association of several endocytosis-related genes with Alzheimer's disease, including *BIN1*. With multiple tissue-specific isoforms, BIN1 functions are wide-ranging and its involvement in mediating Alzheimer's disease risk is not fully understood.

The initial aim of this thesis was to develop a neuronal cell model from induced pluripotent stem cells (iPSCs) derived from peripheral blood mononuclear cells (PBMCs) for the study of endocytosis in Alzheimer's disease. The development of PBMC-derived iPSC models is a novel field and this thesis demonstrates that PBMC-derived iPSCs can be differentiated into cortical neurons through dual SMAD inhibition. This protocol was carried out for the first time in the current lab and has therefore established these iPSC protocols for future use.

Secondly, this thesis aimed to further develop knowledge on the role of BIN1 in clathrin-mediated endocytosis (CME) in a non-neuronal context. The hCMEC/D3 human brain microvascular endothelial cell line was used as an *in vitro* model of the blood-brain barrier (BBB) to investigate the effect of siRNA-mediated BIN1 depletion. Evidence is presented suggesting BIN1 is involved in the amyloidogenic processing of APP by an increase in β-CTF upon BIN1 depletion, in the absence of changes in levels of APP, Aβ and soluble APP or putative α- β- and γ- secretases. This was not suggested to be due to altered CME as transferrin uptake and recycling remained unaffected. While caveolin-2 levels increased with BIN1 depletion, lactosylceramide internalisation, a measure of caveolar endocytosis, was not affected, suggesting BIN1 was not crucial for this mechanism in hCMEC/D3 cells. Impaired degradative clearance of β-CTF was also hypothesised, however an absence of gross changes in lysosome morphology suggested that BIN1 was not central to normal lysosome function. This thesis provides novel insight into the role of BIN1 in the amyloidogenic processing of APP and endocytosis at the BBB, furthering understanding on the functional relevance of AD risk mediated by BIN1.

Table of Contents

Abbreviations

Aβ	Beta-amyloid
ABC	ATP-binding cassette
ACH	Amyloid cascade hypothesis
AD	Alzheimer's disease
ADAM	A disintegrin and metalloproteinase
ADAS-cog	Alzheimer's Disease Assessment Scale-cognitive Subscale
AICD	APP intracellular domain
AME	Adsorptive-mediated endocytosis
AMPH1	Amphiphysin 1
APH-1	Anterior pharynx-defective 1
APOE	Apolipoprotein E
APP	Amyloid precursor protein
APPL1	Adaptor protein containing pleckstrin homology domain, phosphotyrosine binding domain and leucine zipper motif
APS	Ammonium persulphate
AP2	Adaptor protein 2
BACE1	β-site APP cleaving enzyme 1
BAR	BIN1/Amphiphysin/RVS167-related
βCTF	APP Beta carboxy-terminal fragment
BIN1	Bridging integrator 1
BM	Basement membrane
BMP	Bone morphogenetic protein
BODIPY	Boron-dipyrromethene
BSA	Bovine serum albumin
CAA	Cerebral amyloid angiopathy
CAV1	Caveolin-1
CAV2	Caveolin-2
CAV3	Caveolin-3
CCP	Clathrin-coated pit
CCV	Clathrin-coated vesicle
cDNA	Complementary deoxyribonucleic acid
CHARGE	Cohorts for Heart and Aging Research in Genomic Epidemiology
CHC	Clathrin heavy chain
CHO	Chinese hamster ovary
CIE	Clathrin independent endocytosis
CLAP	Clathin-AP2 binding
CME	Clathrin-mediated endocytosis
c-Myc	Cellular homolog of avian myelocytomatosis virus oncogene
CNS	Central nervous system
CRISPR	Clustered regularly interspaced short palindromic repeats

CSF	Cerebrospinal fluid
CT	Computerised tomography
CTF	Carboxy-terminal fragment
CTIP2	Chicken ovalbumin upstream promoter transcription factor-interacting protein 2
ctxB	Cholera toxin B subunit
DHA	Docosahexaenoic acid
dH_2O	Distilled water
DIV	Days *in vitro*
DMSO	Dimethyl sulfoxide
DNase	Deoxyribonuclease
dNTP	Deoxynucleotide
dsRNA	Double-stranded RNA
EAL	Endosomal-autophagic-lysosomal
EB	Embryoid body
EEA1	Early endosome antigen 1
EGM2	Endothelial growth medium
Ehbp1l1	EH domain-binding protein 1-like protein 1
EOAD	Early-onset Alzheimer's disease
ER	Endoplasmic reticulum
ERC	Endosome recycling complex
ESC	Embryonic stem cell
EQTL	Expression quantitative trait loci
F-actin	Filamentous actin
FACS	Fluorescence-activated cell sorting
fAD	Familial Alzheimer's disease
FBS	Fetal bovine serum
FCHO1/2	Fer/Cip4 homology domain only proteins 1 and 2
FITC	Fluorescein isothiocyanate
FOXG1	Forkhead box G1
GAK	cyclin G-associated kinase
GAPDH	Glyceraldehyde-3-Phosphate Dehydrogenase
GFAP	Glial fibrillary acidic protein
GFP	Green fluorescent protein
GSL	Glycosphingolipid
GTPase	Guanosine triphosphate hydrolase
GWAS	Genome-wide association study
HCl	Hydrochloric acid
HEK	Human embryonic kidney
hESC	Human embryonic stem cell
hPSC	Human pluripotent stem cell
HRP	Horseradish peroxidase
HSC70	Heatshock cognate 70
HSC70	Heatshock cognate 70
hTERT	Human telomerase reverse transcriptase

HUVEC	Human umbilical vein endothelial cells
IDO1	Indoleamine 2,3-dioxygenase
IGAP	International Genomics of Alzheimer's Project
iPSC	Induced pluripotent stem cell
ISF	Interstitial fluid
JAM	Junctional adhesion molecule
KLF4	Kruppel-like factor 4
KO-DMEM	Knockout Dulbecco's Modified Eagle Medium
KPI	Kunitz protease inhibitor
LacCer	Lactosylceramide
LAMP1	Lysosomal associated membrane protein-1
LAMP2	Lysosomal associated membrane protein-2
LD	Linkage disequilibrium
LOAD	Late-onset Alzheimer's disease
LRP1	Lipoprotein receptor-related protein 1
MAF	Minor allele frequency
MAP	Microtubule-associated protein
MAPT	Microtubule-associated protein tau
MBD	Myc-binding domain
MCI	Mild cognitive impairment
MDCK	Madin-Darby Canine Kidney
MEF	Mouse embryonic fibroblast
MMSE	Mini-Mental State Exam
MoCA	Montreal Cognitive Assessment
M_r	Relative molecular mass
MRI	Magnetic resonance imaging
MVB	Multivesicular bodies
NaCl	Sodium chloride
NGS	Next generation sequencing
NINCDS-ADRDA	National Institute of Neurological and Communicative Disorders and Stroke and the Alzheimer's Disease and Related Disorders Association
NPC	Niemann-Pick type C
NPC	Neural precursor cell
NTID	N-terminal insert domain
NVU	Neurovascular unit
N2a	Neuro-2a
OCT4	Octamer-binding transcription factor 4
OR	Odds ratio
PAX6	Paired box 6
PBMC	Peripheral blood mononuclear cell
PBS	Phosphate buffered saline
PBST	Phosphate buffered saline with tween
PCR	Polymerase chain reaction
PDGFRB	Platelet Derived Growth Factor Receptor Beta

PEN-2	Presenilin enhancer 2
PET	Positron emission tomography
PFA	Paraformaldehyde
Pgp	P-glycoprotein
PICALM	Phosphatidylinositol binding clathrin assembly protein
PIP_2	Phosphatidylinositol-(4,5)-bisphosphate
PSEN1	Presenilin 1
PSEN2	Presenilin 2
pTau	Phosphorylated tau
RAGE	Receptor for advanced glycation end products
RNA	Ribonucleic acid
RT	Room temperature
sAD	Sporadic Alzheimer's disease
sAPPα	Soluble APP-alpha
sAPPβ	Soluble APP-beta
SDAT	Senile dementia of Alzheimer's type
SDS	Sodium dodecyl sulphate
SDS-PAGE	Sodium dodecyl sulphate polyacrylamide gel electrophoresis
SEM	Standard error of the mean
SeV	Sendai virus
SH3	SRC homology 3
siRNA	Short interfering RNA
SNP	Single nucleotide polymorphism
SNV	Single nucleotide variant
SNX9	Sorting nexin 9
SOX2	Sex determining region Y box 2
T_A	Annealing temperature
TBR1	T-Box Brain Protein 1
TBR2	T-Box Brain Protein 1
TEER	Transendothelial electrical resistance
TEMED	N,N,N'N' – Tetramethylethylenediamine
Tf	Transferrin
TfR	Transferrin receptor
TGFβ	Transforming growth factor beta
TJ	Tight junction
T_m	Melting temperature
T-tubule	Transverse tubule
VWF	Von Willebrand Factor
WGA	Wheat germ agglutinin
ZO	Zonula occludens

List of Tables

List of Figures

Chapter 1

Introduction

1.1 Alzheimer's Disease

1.1.1 History

Alzheimer's disease is a neurodegenerative disorder characterised by progressive neurological impairment and decline in cognitive function. In 1906, Alois Alzheimer first described an unusual psychiatric disease with severe cerebral histopathology in the brain of a 51-year-old female patient named Auguste Deter (Alzheimer, 1907). Her symptoms included rapidly increasing memory impairment, disorientation, aphasia, poor comprehension, paranoia and auditory hallucinations. Following her death, after 4 ½ years of illness, Alzheimer studied the neuropathology of her brain, where he observed "military foci", now known as β-amyloid plaques, and neurofibrillary degeneration. In 1909, Gaetano Perusini reinvestigated Auguste Deter's symptoms and histopathology in addition to three further cases and presented illustrations of the amyloid plaques and neurofibrillary tangles (Perusini, 1909).

Emil Kraepelin, director of the Royal Psychiatric Clinic in Frankfurt where Alzheimer worked, first introduced the aponym Alzheimer's disease (AD) in 1910 following other reports of cases with similar symptoms and histopathology with extremely serious cell alterations and cell death (Kraepelin, 1910). While this diagnosis was originally referred to as presenile dementia, a rare disease occurring in middle age, it later became apparent that the disease commonly affected the elderly and the terminology was later extended to describe the largest cause of primary dementia; Senile Dementia of Alzheimer Type (SDAT, (Maurer et al., 1997). Over 100 years later and Alzheimer's original observations still form the basis of the well-known pathological hallmarks of the disease.

1.1.2 Clinical diagnosis

In 1984, the National Institute of Neurological and Communicative Disorders and Stroke and the Alzheimer's Disease and Related Disorders Association (NINCDS-ADRDA) assembled a uniform set of criteria for the clinical diagnosis of AD (McKhann et al., 1984). The diagnoses were divided into possible, probable and definite AD. Possible AD was diagnosed on the basis of the dementia syndrome; the decline of memory and other cognitive functions in comparison to a patient's previous level of functioning. While a clinical diagnosis of definite AD could only be made by histopathological evidence from biopsy or autopsy, probable AD was characterised by dementia as established by neuropsychological tests, deficits in two or more areas of cognition, described below, accompanied by progressive decline in memory and cognition, onset between the ages of 40-90 and the absence of other systemic disorders or brain disease (McKhann et al., 1984).

The major cognitive domains impaired in AD are memory, orientation, language, attention, motor coordination, visual perception, problem-solving and social functioning. Cognitive tests such as the Mini-Mental State Exam (MMSE), Montreal Cognitive Assessment (MoCA) and Alzheimer's Disease Assessment Scale-cognitive Subscale (ADAS-cog) are used to assess an individual's ability in these areas (Folstein et al., 1975, Nasreddine et al., 2005, Rosen et al., 1984). These are often combined with physical and neurological assessments, in addition to structural imaging by computerised tomography (CT) and magnetic resonance imaging (MRI). Although impairments in memory and cognitive function are thought to be the primary features of AD, many non-cognitive neuropsychiatric symptoms also present with the disease, such as apathy, hallucinations and delusions, aggression, depression, disinhibition, and motor impairments (Lyketsos et al., 2011).

With advances in our understanding of the disease, the NINCDS-ADRDA criteria were reviewed as it is now recognised that the AD spectrum is broader than previously thought (McKhann et al., 2011). This is based on literature emerging since the mid 1990s showing a transitional state between the cognitive changes of normal aging and AD, known as mild cognitive impairment (MCI) (Petersen et al., 2013). These gradual impairments in cognitive function precede the point where significant interference in daily activity occurs but they do not meet the accepted criteria for clinical probable AD and not all MCI leads to AD. The reviewed guidelines were published in 2011 and also introduced recommendations for

a newly defined stage of disease intended purely for research purposes; the diagnosis of preclinical (presymptomatic) AD, reflecting emerging evidence that measurable biomarker changes in the brain may occur years before symptoms become apparent (Dickerson et al., 2011). While research is ongoing to source an easily testable biomarker for AD, the strongest candidates include brain imaging studies such as molecular tracing by MRI or positron emission tomography (PET).

1.1.3 Prevalence

Over 46.8 million people worldwide are living with dementia, of which AD is recognised as the leading cause, accounting for up to 70% of all dementia cases (Prince, 2015). Globally, the number of people living with dementia is predicted to increase to 131.5 million by 2050, an increase of 281% (Prince, 2015). Within the UK, 850,000 people are thought to suffer from dementia, accounting for 7.1% of people over the age of 65 while 40,000 people in the UK under the age of 65 suffer from early onset forms of dementia (Prince, 2014). With age being the biggest risk factor for dementia, increasing life expectancy is the key driving force behind the projected rise in cases to over 1 million by 2025 (Prince, 2014). Indeed, the risk of developing dementia rises from 1 in 14 over the age of 65, to 1 in 6 over the age of 80 (Prince, 2014). Women are more likely to develop dementia in their lifetime, with 65% dementia sufferers being female (Prince, 2014). While this may partly be accounted for by the longer life expectancy of women, research is ongoing to elucidate the reason for this gender difference, which is still unclear. Dementia not only causes huge emotional burden for people who have a close friend or relative with the condition, but the financial burden to UK society is estimated at £24 billion in health and social care costs, with a projected rise to £59 billion by 2050 (Lewis, 2014).

1.1.4 Neurobiology and Pathological hallmarks

Post mortem analysis of brain tissue from AD patients has revealed the presence of distinct neuropathological changes at both the anatomical and cellular level. The primary hallmarks of AD are extracellular neuritic protein aggregations, or plaques, predominantly composed of the Aβ peptide, intracellular neurofibrillary tangles (NFTs), comprising filamentous aggregates of hyper phosphorylated tau protein (ptau) and neuronal and synapse loss.

1.1.4.1 Brain atrophy

One of the most distinctive hallmarks of AD is the considerable neuronal loss observed throughout the cortical and subcortical structures upon examination of post-mortem brain tissue. **Error! Reference source not found.** shows the spread of AD pathology throughout the brain with progression of disease and highlights the areas particularly affected by comparison to a healthy brain. A typical symmetric pattern of brain atrophy affecting the medial temporal lobes while relatively sparing the primary motor, sensory and visual cortices is characteristic of AD pathology (Dickerson et al., 2009). Reliable atrophy was identifiable in asymptomatic individuals nearly a decade before dementia onset, representing a potentially important biomarker of neurodegeneration (Dickerson et al., 2011). The symptoms of AD arise from the selective neuronal loss within the paralimbic and heteromodal association areas with early neuronal loss occurring in the entorhinal, parahippocampal and temporo-parietal cortex (Juottonen et al., 1998, Jack et al., 1992). This mirrors the time course of cognitive impairment, extending into anterior regions as the disease progresses (Serrano-Pozo et al., 2011). The use of MRI has allowed researchers to non-invasively monitor cerebral volume throughout disease progression. Cortical thinning in AD patients has been shown to increase with decreasing cognitive performance (Sabuncu et al., 2011). This association followed a sigmoidal pattern, exhibiting early acceleration followed by deceleration while hippocampal volume loss exhibited positive acceleration throughout disease progression. MRI volumetric measurements have shown a 40% loss in entorhinal cortex volume compared to controls, which correlated significantly with severity of the disease (Juottonen et al., 1998). Hippocampal volumes have shown a 24% reduction between AD patients and controls, with a 3.3% loss in hippocampal volume over just 6 months, compared with a 0.9% loss in volume in the age-matched control group (Schuff et al., 2009). Therefore, hippocampal volume may also be an early indicator of AD.

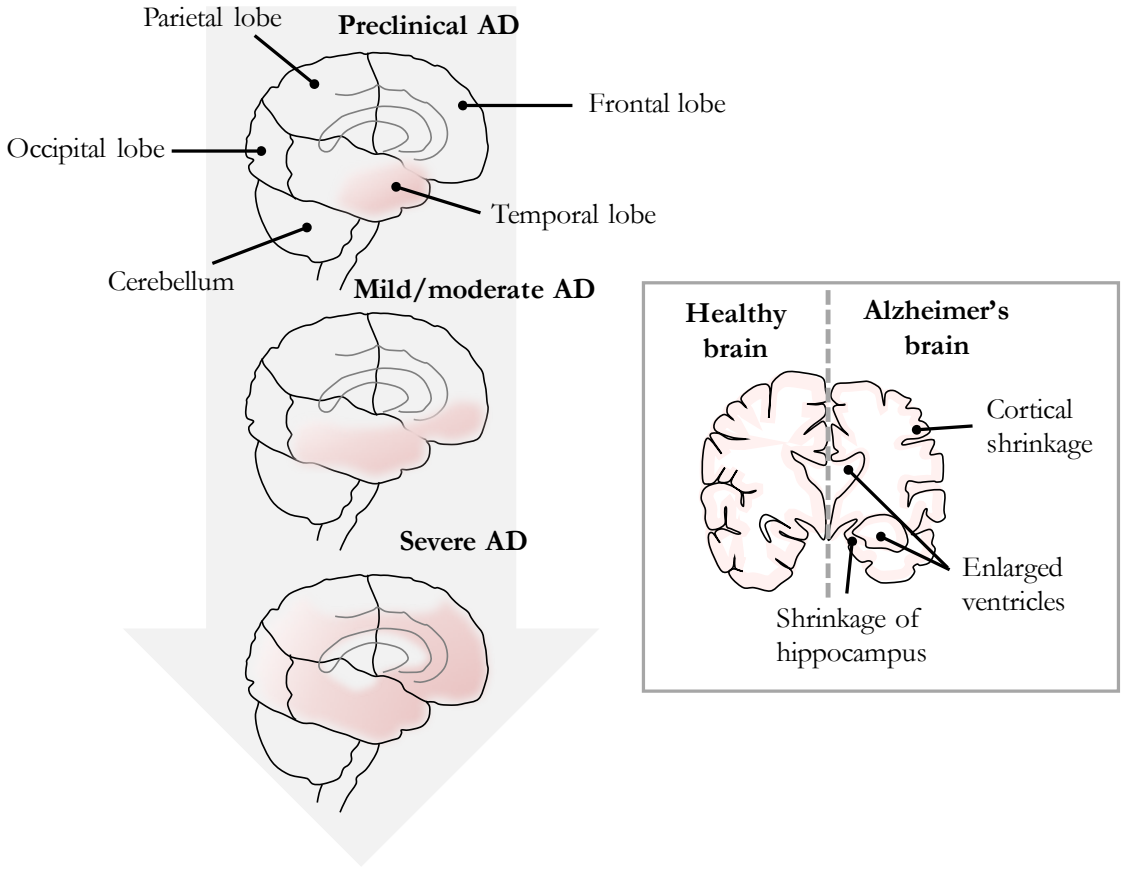

Figure 1.1: The progression of Alzheimer's pathology in the human brain

A schematic depicting the progression of Alzheimer's disease pathology starting in the medial temporal lobes, where the hippocampus and associated structures are first affected. The pathology spreads in a symmetrical pattern, extending to the anterior regions as the disease progresses. A schematic representing a coronal cross-section of the brain is also shown, illustrating the shrinkage of the cortex and hippocampus, and enlargement of the ventricles.

1.1.4.2 Neuritic plaques

Neuritic plaques are microscopic foci of extracellular beta-amyloid (Aβ) deposition which principally occurs in the filamentous form with a high content of β-pleated secondary structure. The plaques contain dystrophic neurites which are defective in synaptic function and neurotransmission (Ferrer et al., 1998). Aβ is a 39-43 amino acid peptide of 4 kDa and is produced from the sequential cleavage of amyloid precursor protein (APP), a type I transmembrane glycoprotein (Kang et al., 1987), by β- and γ -secretases on the N- and C-terminal ends of the Aβ region, respectively. The most common forms of Aβ produced are 40 and 42 residues in length, with much of the Aβ found in neuritic plaques comprising the

more hydrophobic 42 amino acid species which is particularly prone to aggregation (Jarrett et al., 1993). The mechanisms underlying the pathological accumulation of Aβ are yet to be fully determined, however the formation of plaques is known to involve the polymerisation of monomeric Aβ into oligomers, protofibrils and amyloid fibrils (Ward et al., 2000). The accumulation of Aβ in the brain is thought to arise from increased Aβ production, decreased clearance from the brain or a culmination of the two (Selkoe and Hardy, 2016). Heiko and Eva Braak categorised the progression of amyloid deposition throughout the brain in AD into three stages (Braak and Braak, 1991). In stage A, low densities of amyloid deposits were present, particularly in the basal frontal, temporal and occipital lobes while no amyloid was present in the hippocampus. Stage B tissue demonstrated more extensive amyloid deposition in almost all isocortical areas with only the primary motor and sensory areas free of, or showing minimal, amyloid deposits and the hippocampus showed only mild pathology. Stage C tissue exhibited a greater extent of amyloid pathology throughout isocortical layers but the hippocampus remained mildly affected. The striatum and nuclei of the thalamus and hypothalamus showed evidence of deposition, while the substantia nigra and pars compacta remained amyloid-free. These defined stages, known as Braak stages, are used to classify the degree of pathology both in research and in clinical diagnoses of disease from post-mortem. A further six stages (I- VI) were also defined to characterise neurofibrillary changes throughout disease progression which are further described in Section 1.1.4.3.

Together with extracellular Aβ deposits in the parenchyma, fibrillary amyloid deposition is also commonly observed in the cerebral blood vessels, a feature known as cerebral amyloid angiopathy (CAA). CAA increases with age, occurring in approximately half of elderly individuals (Yamada et al., 1987), while the prevalence in AD patients is estimated at 80-90% (Yamada, 2002). CAA is mainly observed in the leptomeningeal and cortical vessels where amyloid fibrils are initially deposited in the outer basement membrane of vessels and later accumulate in place of degenerated smooth muscle cells of the media (Yamada, 2015).

1.1.4.3 Neurofibrillary tangles

Hyperphosphorylated tau is the major component of intracellular neurofibrillary tangles, one of the key pathological hallmarks of AD. Tau is a microtubule-associated protein (MAP) that stimulates tubule assembly into microtubules, which act as a scaffold for the

cell cytoskeleton and are involved in vesicular trafficking (Weingarten et al., 1975). Tau has been the focus of much research since it was discovered to form the paired helical filaments of NFTs in the AD brain (Grundke-Iqbal et al., 1986). Phosphorylation of tau at critical sites inhibits it binding to microtubules by varying degrees (Sengupta et al., 2017) with further phosphorylation promoting self-aggregation into filaments. Hyperphosphorylated tau appears to gain the toxic ability to sequester normal tau and other MAPs, causing microtubule disassembly (Alonso et al., 1997). Despite extensive research, the causes leading to the abnormal phosphorylation of tau are still not fully elucidated and the exact molecular basis of its toxicity remains an area of intense research. The development of NFTs throughout the brain was categorised into six stages with the stages I-II classified as transentorhinal, stages III-IV as the limbic stages and stages V-VI as the isocortical stages (Braak and Braak, 1991). As AD progresses, tau pathology spreads from the entorhinal cortex in a uniform and reproducible fashion, suggesting that tau pathology may be transmitted between neighbouring neurons (Pooler et al., 2013). Although the complex interplay between Aβ and tau is yet to be defined, the prevailing hypothesis of AD pathogenesis is that deleterious effects on synaptic function leading to cognitive impairment caused by tau are initiated by Aβ. This theory was coined The Amyloid Cascade Hypothesis (ACH) and is further explained in Section 1.2.3.

1.1.4.4 Protein aggregates: cause or consequence?

While gross aggregations of Aβ and hyperphosphorylated tau are hallmarks of AD pathology, the extent to which these end products of polymerisation contribute towards neuronal toxicity has recently come under scrutiny. Amyloid plaque burden correlates much less well with degree of cognitive impairment than neurofibrillary tangle pathology (Nelson et al., 2012, Guillozet et al., 2003) while plaques have been detected in cognitively normal individuals (Erten-Lyons et al., 2009), some with plaque burdens equivalent to those seen in demented patients (Rentz et al., 2010). The presence of significant plaque burden without brain atrophy or cognitive impairment (Erten-Lyons et al., 2009) suggests that Aβ plaques are not directly responsible for neurodegeneration.

Soluble Aβ oligomers, however, have been shown to produce cognitive deficits in APP-overexpressing mice in the absence of plaques (Gandy et al., 2010) and evidence of neurodegeneration in MCI patients has been reported without observed amyloid

deposition, suggesting that large Aβ aggregates are not essential for cognitive impairment (Petersen et al., 2013). Aβ oligomers bind to post-synaptic excitatory sites in neurons (Lacor et al., 2004) and interfere with synaptic plasticity by blocking long term potentiation (LTP) (Wang et al., 2002). They have also been shown to interfere with calcium homeostasis in neurons, inducing oxidative stress and tau hyperphosphorylation (De Felice et al., 2008). Other brain cell types have also shown evidence of toxic responses to Aβ oligomers such as disruption of blood-cerebrospinal fluid (CSF) barrier integrity (Brkic et al., 2015). DaRocha-Souto et al. (2011) demonstrated that oligomeric Aβ deposits, but not total plaque burden, correlated with neuronal loss in the entorhinal cortex of double-transgenic mice overexpressing human mutant APP and tau. Therefore, there is much evidence to suggest that Aβ is neurotoxic in its oligomeric form.

Likewise, studies have challenged the idea that NFTs are causative of neuronal death. For example, a mouse model expressing a mutant form of human tau (rTg4510) showed dissociation of neuronal loss and NFT pathology, with neurodegeneration observed before neurofibrillary lesions appeared in the dentate gyrus while NFTs appeared without major cell loss in the striatum (Spires et al., 2006). Growing evidence suggests that pre-filamentous forms of tau, specifically oligomers, are neurotoxic. Indeed, tau oligomers derived from human AD brain can induce synaptic and mitochondrial dysfunction and memory impairment when intracranially-administered to wild-type mice (Lasagna-Reeves et al., 2011). Although the debate between the correlation of oligomers or mature fibrils with disease severity is ongoing, recent progress in this area is promising. The identification of toxic oligomeric species formed during protein aggregation has presented Aβ and tau oligomers as potential biomarkers for the accurate and early detection of AD (Holtta et al., 2013, Sengupta et al., 2017).

1.2 The Genetic Landscape of Alzheimer's Disease

Historically, Alzheimer's disease has been categorised into two broad categories; early-onset Alzheimer's disease (EOAD), which is characterised by disease onset before the age of 65 and accounts for 5% of all AD cases (Zhu et al., 2015) and the more common late-onset Alzheimer's disease (LOAD), with onset after the age of 65. The genetics of AD also falls into two categories, Mendelian or familial forms of AD (fAD) and sporadic forms of AD (sAD). Mendelian forms of AD are rare, accounting for less than 1% of all AD cases (Wingo et al., 2012), typically characterised by early-onset and have heritability estimates of 92-100% (Wingo et al., 2012). Rare mutations in the amyloid precursor protein (*APP*) and presenilin 1 and 2 (*PSEN1* and *PSEN2*) genes have been shown to cause early-onset cause fAD and will be further described in Section 1.2.1. However, only 5% of EOAD patients carry a known pathogenic mutation, with the majority of EOAD cases remaining unexplained (Cacace et al., 2016). The vast majority of AD cases, however, fall under the sAD category which has a much more complex pattern of inheritance. The majority of sAD comprises the late-onset form of the disease, while early-onset forms of sAD are rare, accounting for less than 5% of all early-onset AD cases. For clarity, this project will predominantly refer to the genetically-defined categories of AD, familial and sporadic.

1.2.1 Familial Alzheimer's Disease

Initial attempts to understand the genetic basis of AD focused on autosomal dominant early-onset forms of the disease, resulting in the discovery of pathogenic mutations in *APP* (Goate et al., 1991), *Presenilin 1* (Broeckhoven et al., 1992) and *Presenilin 2* (Sherrington et al., 1996) through autosomal dominant AD pedigrees. These findings provided the basis for much of our understanding of AD pathogenesis today and underpin the ACH, further described in Section 1.2.3.

1.2.1.1 Amyloid Precursor Protein

The *APP* gene is located on chromosome 21 and encodes a transmembrane glycoprotein. Alternative splicing of the APP transcript generates 3 major isoforms; the 695 amino acid

isoform is predominantly expressed in neurons while the 751 and 770 isoforms are expressed both in the brain and ubiquitously (Rohan de Silva et al., 1997). APP is a transmembrane protein which is proteolytically processed by α-, β- and γ -secretases, following one of two pathways (Figure 1.2).

The non-amyloidogenic pathway involves an initial α -cleavage of APP by members of the ADAM (a disintegrin and metalloproteinase) family of transmembrane proteins, such as ADAM17 (Buxbaum et al., 1998), ADAM10 (Lopez-Perez et al., 2001) and ADAM9 (Koike et al., 1999). This cleaves APP within the Aβ domain, therefore precludes Aβ generation. The α-cleavage of APP occurs at a site in the extracellular domain, releasing a large soluble ectodomain, termed sAPPα, thought to be involved in neuronal plasticity and protective against excitotoxicity (Furukawa et al., 1996). The carboxy-terminal fragment (α -CTF) remains membrane-bound and is subsequently cleaved by γ -secretase to release P3, which is rapidly degraded, and the APP intracellular domain (AICD). AICD has been implicated in the transcriptional regulation of multiple genes, including APP itself (von Rotz et al., 2004, Muller et al., 2008).

The amyloidogenic pathway of APP proteolysis involves cleavage of APP by β-secretase which releases the soluble ectodomain, sAPPβ, that has been reported to function in axonal pruning and neuronal cell death (Nikolaev et al., 2009). Following β-cleavage, the membrane-associated carboxy-terminal fragment, β-CTF, is further cleaved by γ -secretase to release intact Aβ and the AICD. The length of the Aβ fragment produced depends where exactly the γ -cleavage occurs, the majority of Aβ produced is of the 40 amino acid species, Aβ40 and to a lesser extent Aβ42, the more aggregation-prone species predominantly present in neuritic plaques. The β-secretase was identified as the transmembrane aspartic protease, β-site APP-cleaving enzyme 1 (BACE1) (Sinha et al., 1999, Vassar et al., 1999) while Presenilin 1 (PSEN1) and Presenilin 2 (PSEN2) proteins are catalytic subunits of the γ-secretase complex (Wolfe et al., 1999). The γ-secretase enzyme is a multiprotein complex comprised of Presenilin, Nicastrin, Anterior pharynx-defective 1 (APH-1), and Presenilin enhancer 2 (PEN-2) in a 1:1:1:1 ratio and all four proteins are necessary for full proteolytic activity (De Strooper, 2003). The fate of APP largely depends on where in the cell it is proteolytically cleaved and this will be further described within a cellular trafficking context in Section 1.4.3.

According to the Alzheimer Disease & Frontotemporal Dementia Mutation Database (http://www.molgen.ua.ac.be/ADMutations), a total of 51 mutations in 121 families have been identified in the *APP* gene (Cruts, 2017). *APP* mutations located close to the β- or γ - cleavage sites can increase overall Aβ production, but most affect the ratio of Aβ species produced in favour of Aβ42 (Citron et al., 1992, De Jonghe et al., 2001, Zhou et al., 2011). Additionally, *APP* duplications in autosomal dominant early-onset families (Rovelet-Lecrux et al., 2005) lead to abundant parenchymal and vascular deposits of amyloid-beta peptides. A recessive mutation has been identified in *APP* that only resulted in AD in its homozygous state, with co-incubation of mutated and wild-type peptides conferring instability on Aβ aggregates, inhibiting amyloidosis and neurotoxicity (Fede et al., 2009). A coding mutation in *APP* was also recently identified that confers a protective value against sAD, this will be further described in Section 1.2.2.3.

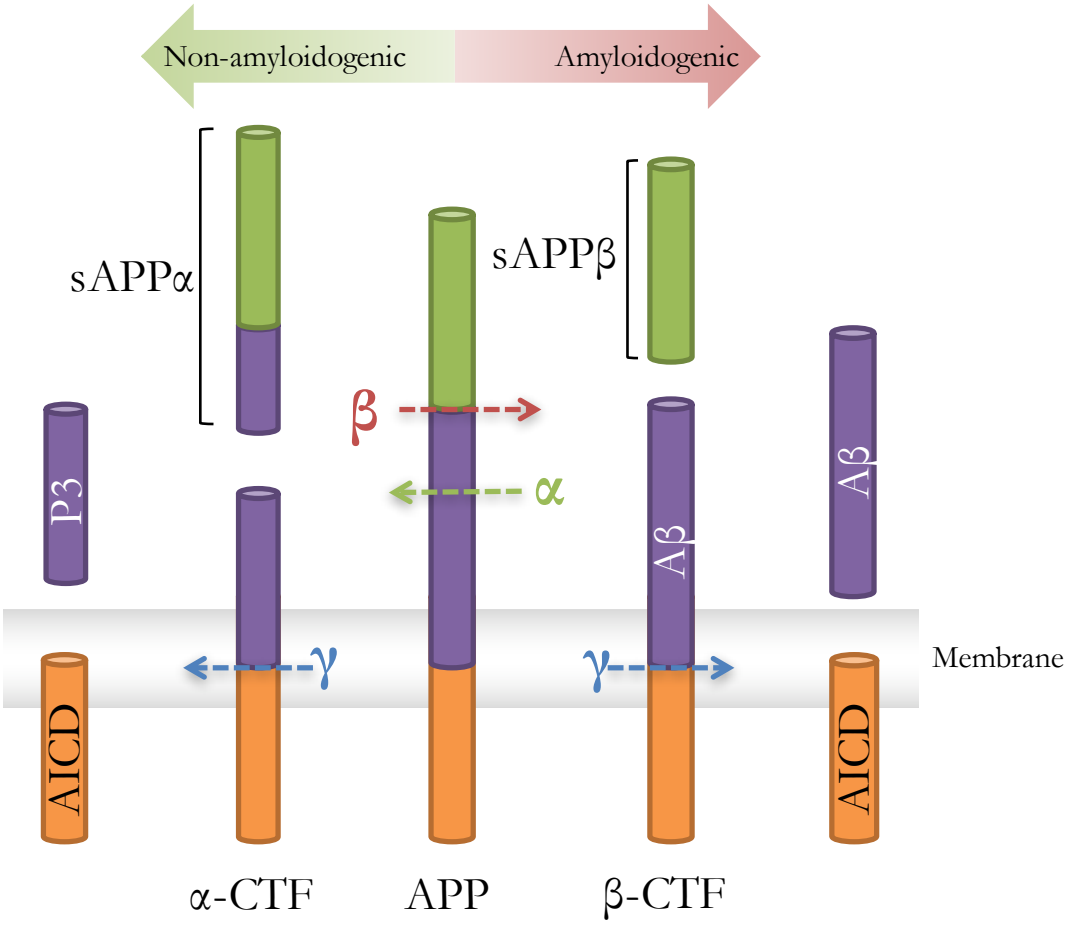

Figure 1.2: The pathways of APP processing

A schematic depicting the non-amyloidogenic and amyloidogenic routes of APP processing. In the non-amyloidogenic pathway, the α-secretase cleaves APP within the Aβ region, forming sAPPα and α-CTF which is subsequently cleaved into P3 and the membrane-bound AICD. In the amyloidogenic pathway, β-secretase cleavage results in the production of sAPPβ and β-CTF which is subsequently cleaved by γ -secretase to form Aβ. This amyloidogenic processing of APP is thought to occur predominantly in the endocytic pathway.

1.2.1.2 The Presenilins

PSEN1 and *PSEN2* are highly homologous genes that encode essential components of the catalytic site of the γ -secretase complex which cleaves membrane proteins, including APP. With 219 AD-causing mutations identified in *PSEN1* and a further 16 in *PSEN2* (Cruts, 2017), they contribute a considerable proportion of the known causes of fAD. Mutations in *PSEN1* are highly variable in terms of their effect on age of onset, disease severity and rate of progression. However, all *PSEN1* mutations show complete penetrance and can cause severe forms of AD with age of onset as early as 25 years (Tanzi, 2012). Gene knockout studies in mice suggest that PSEN1 is the major γ-secretase and that it contributes disproportionately to Aβ generation, whereas PSEN2 plays a more minor role (Herreman et al., 1999). This is consistent with an earlier age of onset and death observed in fAD patients with *PSEN1* mutations compared to those harboring *PSEN2* mutations (Lippa et al., 2000).

The precise mechanism by which *PSEN* mutations cause fAD has undergone much debate, with early reports suggesting a gain-of-function mechanism mediated by selective overproduction of Aβ42 (Borchelt et al., 1996, Scheuner et al., 1996). However, several lines of evidence have brought into question this view, suggesting that loss of PSEN function could better explain neurodegeneration in AD. Firstly, conditional *PSEN* inactivation in mice results in progressive memory impairment and neurodegeneration, which models based on Aβ overproduction have failed to demonstrate (Saura et al., 2004). Secondly, expression of *PSEN* mutants on a *Psen*-negative background resulted in accumulation of APP-CTFs and decreased generation of cytoplasmic AICD, suggestive of decreased PSEN activity (Bentahir et al., 2006), (Kumar-Singh et al., 2006). Furthermore, *PSEN1* knockin mice carrying fAD mutations have shown a complete loss of PSEN1 function *in vivo*, abolishing γ -secretase activity, suggesting *PSEN1* mutations cause fAD by a loss-of-function mechanism (Xia et al., 2015).

Loss of PSEN function is thought to result in the incomplete digestion of APP, with fewer but longer Aβ peptides generated (Yagishita et al., 2006). This is because the proteolytic function of γ –secretase is thought to occur sequentially. The first cut represents the endopeptidase cleavage which releases the C-terminal domain of substrates. The enzyme remains bound to the N-terminal fragment which is then processed by carboxypeptidase-like activity which successively removes short peptides (Chavez-Gutierrez, 2013). Although

the precise molecular mechanisms of different *PSEN* mutations vary considerably, in all cases the mutations appear to decrease the carboxypeptidase-like activity of γ –secretase, resulting in an increase in the relative production of longer Aβ peptides. Szaruga et al. (2015) reported that brain samples from fAD patients harbouring *PSEN1* mutations had similar overall γ -secretase activity levels to controls, suggesting that loss of the endopeptidase function of γ-secretase is not an essential part of fAD pathogenesis. However impaired carboxypeptidase function was observed in all fAD brains (Szaruga et al., 2015). Interestingly, the authors also reported that some sAD patient brain samples displayed γ -secretase dysfunction, suggesting that γ -secretase may also play a role in some sAD cases, however the majority of sAD samples displayed normal endo- and carboxypeptidase-like γ -secretase activity. Nevertheless, more than 99% of all AD patients, including sporadic and all other forms of fAD, express wild-type presenilins, therefore it is highly unlikely that the loss of PSEN function is a general mechanism of AD pathogenesis.

1.2.2 Sporadic Alzheimer's Disease

Sporadic forms of AD account for over 95% of all cases and predominantly manifest as LOAD (Zhu et al., 2015). The inheritance pattern of sporadic forms of AD is complex. With heritability estimates of 58-79% (Gatz et al., 2006), both genetic and environmental factors are thought to play a role in pathogenesis. The search for genetic factors contributing to sAD has evolved significantly since the identification of fully penetrant mutations in *APP*, *PSEN1* and *PSEN2* as a cause of autosomal dominant fAD.

1.2.2.1 Apolipoprotein E

The first locus identified to reliably associate with AD risk was within the apolipoprotein E (*APOE*) gene where the expression of the *APOE* type epsilon 4 (ε4) allele had a highly significant association with sAD (Saunders et al., 1993). The differential expression of three *APOE* alleles (ε2, ε3, and ε4) is dependent on two single nucleotide polymorphisms (SNPs), rs429358 and rs7412, within exon 4 of the gene (Weisgraber et al., 1981). In humans, these variants result in three homozygous (ε2/ε2, ε3/ε3, and ε4/ε4), and three heterozygous (ε2/ε3, ε2/ε4, and ε3/ε4) phenotypes. Based on these variants, the *APOE* gene encodes 3 possible protein isoforms; E2, E3 and E4 (Agosta et al., 2009). The ε3 allele is the most common, followed by ε4 and ε2, although these frequencies vary between

populations (Singh et al., 2006). Homozygosity for the ε4 allele confers a nearly 15-fold increased risk of developing AD, while heterozygous individuals carrying only one copy have a 3-fold increased risk (Farrer et al., 1997) compared to those homozygous for *APOE* ε3, the most common genotype (Corbo and Scacchi, 1999). The *APOE* ε2 allele, on the other hand, confers a protective effect with individuals carrying at least one copy having a 40% decreased risk of developing AD compared to ε3 homozygous individuals (Farrer et al., 1997). Genin et al. (2011) assessed AD lifetime risk of 7351 cases and 10 132 controls from Caucasian ancestry based on *APOE* genotype and concluded that findings were consistent with semi-dominant model of inheritance whereby the homozygous ε4 or ε2 genotypes confer a greater risk or protective value, respectively, than ε3ε4 or ε3ε2 heterozygotes.

Mechanistic studies have explored the functional relationship between APOE and AD and found that APOE has an important role in Aβ metabolism. Studies in humans and transgenic mice showed that brain Aβ levels and amyloid plaque loads are APOE isoform-dependent as fibrillary amyloid deposits increased progressively with each additional ε4 allele in the brains of cognitively normal individuals (Reiman et al., 2009). Increased vascular and plaque Aβ deposits have also shown greater abundance in ε4 carriers compared to non-carriers (Schmechel et al., 1993). Despite the clear association of *APOE* with AD risk and amyloid pathology, the pathway(s) by which APOE4 may increase Aβ levels are unclear and the subject of continued inquiry. APOE is a glycoprotein mainly expressed in the brain by non-neuronal cells, such as astrocytes and microglia (Pitas et al., 1987). It functions as a ligand in receptor-mediated endocytosis of lipoproteins and plays a major role in calcium homeostasis (Mahley, 2016). There is no current consensus on the mechanism by which APOE isoforms affect AD risk, however, the prevailing view involves the modulation of Aβ metabolism. Studies have suggested that APOE4 accelerates Aβ deposition to form amyloid plaques (Wisniewski et al., 1994). In an AD mouse model expressing mutated human APP and human APOE isoforms under control of the mouse regulatory elements, APOE4 was shown to increase Aβ deposition relative to APOE3 and APOE2 due to defective clearance of Aβ from the brain (Castellano et al., 2011). Whether the *APOE* ε4 allele influences AD pathogenesis by a gain of toxic function, a loss of protective function or a combination of both remains to be elucidated.

1.2.2.2 Common Genetic Variants associated with Alzheimer's Disease

With the advent of genome wide association studies (GWAS), our knowledge of the genetic landscape of sAD has vastly improved. Since 2009, several well-powered GWAS have been published in addition to a landmark meta-analysis carried out by the joint International Genomics of Alzheimer's Project (IGAP) consortium. This included 17,008 sAD cases and 37,154 controls, with replication in an independent sample of 8,572 sAD cases and 11,312 controls, which identified 11 new susceptibility loci (Lambert et al., 2013). While *APOE* remains the most significant genetic risk factor for sAD, genetic analyses over the past decade have led to the discovery of over 20 susceptibility loci for sAD that consistently reach the genome-wide significance threshold of $p < 5 \times 10^{-8}$.

Early GWAS identified variants in or near the *CLU*, *PICALM* and *CR1* genes to be associated with sAD risk (Harold et al., 2009, Lambert et al., 2009). *BIN1* was first identified as a significant AD susceptibility gene in 2010 (Seshadri et al., 2010) followed by *EPHA1*, *MS4A*, *CD2AP* and *ABCA7* in 2011(Hollingworth et al., 2011, Naj et al., 2011). A further 11 novel susceptibility loci were identified in 2013: *HLA-DRB5/ HLA-DRB1*, *PTK2B*, *SORL1*, *SLC24A4 - RIN3*, *INPP5D*, *MEF2C*, *NME8*, *ZCWPW1*, *CELF1*, *FERMT2* and *CASS4*(Lambert et al., 2013). In 2014, 2 further novel loci, *TP53INP1* and *IGHV1–67*, showed genome-wide association for sAD (Escott-Price et al., 2014). *TRIP4* was also confirmed as a sAD susceptibility gene when SNP data from the IGAP dataset was combined with additional genotyping in an independent follow-up study (Ruiz et al., 2014).

Although the precise biological function of these polymorphisms in AD is yet to be defined, the susceptibility loci identified tend to converge onto select areas of biology. Pathway analysis has been carried out to explore whether certain biological pathways are significantly enriched in the genetic association data, including loci that associate with disease but failed to reach the genome-wide significance threshold. A significant enrichment for certain biological pathways was identified within the IGAP dataset, including the immune response, endocytic regulation, cholesterol transport and proteasome-ubiquitin activity (Jones et al., 2015). This enrichment was shown to be independent of known genetic risk factors as the association remained once all genes within linkage disequilibrium (LD) of *APOE* or any of the genes reaching genome-wide significance in the IGAP meta-analysis had been removed. These biological processes

therefore represent prime targets for AD therapeutics. However, it has been estimated that over 60% of the genetic variance of sAD is not accounted for by the identified common variation from GWAS studies or that available by imputation (Ridge et al., 2013). It is likely that the remaining heritability is accounted for by susceptibility genes of small effect that current GWAS are underpowered to detect, in addition to rare variants that are poorly represented on GWAS platforms.

1.2.2.3 Rare Genetic Variants associated with Alzheimer's Disease

Rare variants in the population can have substantial effect sizes which may account for some of the missing heritability following GWAS studies. Next generation sequencing (NGS) has been used to detect rare SNPs that may be associated with sAD. Through studying whole-genome sequence data from 1,795 Icelanders, a rare coding mutation in the *APP* gene was identified that protects against Alzheimer's disease and cognitive decline in the elderly by encoding a sub-optimal BACE1-cleavage site resulting in decreased Aβ production (Jonsson et al., 2012). This finding provided proof of principle that reduced BACE1 cleavage of APP may protect against AD. Furthermore, the *APP* mutation also protected against cognitive decline in the elderly without AD, suggesting the possible shared pathogenesis of AD and normal cognitive decline of the elderly.

NGS has also resulted in the discovery of *TREM2* as an AD risk gene which showed a highly significant association with sAD (Guerreiro et al., 2013). The same study corroborated this association by analyzing *Trem2* expression in APP transgenic mice and found *Trem2* expression was increased compared to wild-types and found to be expressed in large activated microglia (Guerreiro et al., 2013), suggesting increased Trem2 expression may represent a response to rising levels of Aβ. In the same year, Jonsson et al. (2013) identified the same missense mutation in *TREM2* to be associated with sAD and further found that carriers of the risk allele (rs75932628) aged 80-100 who did not have sAD, showed poorer cognitive function than non-carriers. While a SNP is defined as a single nucleotide polymorphism which is found in more than 1% of the population, a single nucleotide variant (SNV) is variation in a single nucleotide without any limitations of frequency. A significant SNV in *TREM2* was recently published from genome-wide exome genotyping of the IGAP dataset (Sims et al., 2017). In addition to a new association in *TREM2*, two novel susceptibility loci, *PLCG2* and *ABI3* were identified (Sims et al., 2017),

all three of which are predominantly expressed in microglia (Zhang et al., 2010). Together with the aforementioned implication of the immune system in AD from pathway analysis, these findings further corroborate a role for microglial-mediated innate immunity in sAD pathogenesis.

1.2.2.4 The Heritability of Alzheimer's Disease

Despite recent success in the genetics field through GWAS and NGS studies, the estimate of heritability explained by genetic findings to date remains relatively low due to the small effect sizes of known variants, illustrating the multifactorial nature of AD. Polygenic risk scores take into account SNPs that fail to meet the GWAS threshold and are based on a calculation of the collective contribution of common SNPs and their associated effect sizes. Using the IGAP data, significant evidence that individuals with higher polygenic risk scores were at greater risk of AD was reported after *APOE* and other genome-wide associated regions were excluded (Escott-Price et al., 2015). This suggested that the association was not dependent on previously identified susceptibility loci or associations as a result of linkage disequilibrium (LD). As sAD is thought to develop 10-30 years before the onset of symptoms, the predictive utility of polygenic risk scores was also analysed, with the probability of correctly predicting a case status reaching 75% when *APOE* genotype and SNPs with sAD association p values <0.5 were included (Escott-Price et al., 2015). Individuals at the extremes of polygenic risk score (highest and lowest 2%) can give prediction accuracy of over 90% (Escott-Price et al., 2015). This could allow the identification of asymptomatic populations at greatest and lowest risk of AD which would have important benefits for clinical diagnosis and selection of participants for clinical trials. Furthermore, polygenic signals for specific biological pathways can also be calculated, allowing for the development of cell models to explore functional outputs through reprogrammed induced pluripotent stem cells from individuals with selected risk profiles.

1.2.3 The Amyloid Cascade Hypothesis

The most widely recognised theory of AD pathogenesis to date is the ACH, proposed by Hardy and Allsop in 1991, which was formed on the basis that AD is driven by the accumulation of Aβ in the brain and that NFTs, cell loss, vascular damage and neurodegeneration follow as a direct result of Aβ deposition (Hardy, 1992, Selkoe, 1991). It

was argued that impaired cleavage of APP results in increased Aβ, particularly the longer 42-residue peptide. This hypothesis was formed on the basis of several lines of evidence, including the discovery that the principal component of neuritic plaques is Aβ (Masters et al., 1985), evidence that people with Trisomy 21, resulting in triplication of the *APP* gene, inevitably develop AD-like pathology (Olson and Shaw, 1969) and that genetic mutations near the cleavage sites of *APP* favour amyloidogenic processing by β- and γ -secretases (Citron et al., 1992). The mechanism by which Aβ results in tangle formation and neuronal loss was not elucidated (Hardy and Allsop, 1991).

The later discovery that *PSEN* mutations alter Aβ production in fAD further supported the ACH (Borchelt et al., 1996). Furthermore, mutations in the gene encoding the tau protein do not lead to Aβ deposition, even in the most severe cases of NFT pathology, suggesting NFTs in AD are likely deposited after changes in Aβ metabolism (Hardy et al., 1998). Transgenic mice overexpressing human *APP* and mutant human *MAPT,* the gene that encodes tau, further substantiated this hypothesis. These mice showed increased formation of NFTs, without altering amyloid plaque load, suggesting altered APP processing occurs before tau alterations (Lewis et al., 2001). Indeed, mouse hippocampal neurons expressing either mouse or human tau proteins degenerated in the presence of Aβ while tau-depleted neurons showed no signs of degeneration in the presence of Aβ, suggesting its toxicity is tau-dependent (Rapoport et al., 2002).

Initially, the ACH was based on Aβ plaque load but was later updated to reflect the fact that soluble oligomeric species of Aβ are thought to be the toxic species and this reappraisal was published 100 years after Alzheimer's first description of the disease (Hardy, 2006). The ACH indeed offers a tractable and testable theory of pathogenic events underlying AD. However, it fails to provide a detailed explanation for the origin of the disease and several lines of evidence fail to fit with the hypothesis. Critics have argued that the theory cannot account for many aspects of AD pathogenesis (Hardy and Selkoe, 2002). Significant plaque burden has been demonstrated in individuals, by positron emission tomography (PET) scan, without evidence of cognitive impairment (Klunk et al., 2009). However, Aβ oligomer levels per plaque in these cases were shown to be much lower than in AD brains (Esparza et al., 2013). Furthermore, the theory that deposition of Aβ triggers the formation of NFT ultimately leading to cell death can be disputed by the lack of correlation in the temporal and regional distribution of NFTs and Aβ plaques in AD

(Serrano-Pozo et al., 2011). In fact, Braak and Braak (1991) showed evidence that tau pathology first develops in the transentorhinal cortex, often in the absence of plaque pathology, suggesting that NFTs may precede Aβ plaque formation (Schonheit et al., 2004). However, it was argued that such studies may not have taken into account diffuse plaques or soluble Aβ oligomers in the brain which require a more systematic search effort (Selkoe and Hardy, 2016). Arguments against Aβ being the preceding factor in AD pathogenesis also include the fact that amyloid plaque burden correlates much less well with degree of cognitive impairment than do neurofibrillary tangle counts (Nelson et al., 2012). However, Selkoe and Hardy (2016) argue that Aβ deposits are an early pathological event that may occur some length of time before clinical dementia and can lead to downstream cellular changes, such as neuritic dystrophy and tangles, that are more causative of neuronal dysfunction. The proposed relationship between Aβ and tau is further questioned by the lack of NFT pathology in APP and APP/PSEN1 transgenic mice, despite producing elevated levels of Aβ (Sasaguri et al., 2017). However, the absence of tauopathy in these models may be due to the time course of the disease, with mice living less than 3 years while at least two decades are required for Aβ amyloidosis to induce cortical tauopathy and neurodegeneration in humans (Bateman et al., 2012). Furthermore, it has been suggested that mouse and human brains express different profiles of tau species (McMillan et al., 2008) and therefore the adequacy of transgenic AD mice, from which much of our knowledge of Aβ physiology derives, is brought into question. As these mice carry mutations found in fAD patients, it is also difficult to establish the extent to which their pathophysiology is applicable to sAD, despite the two forms of AD showing similar neuropathological features (Serrano-Pozo et al., 2011).

Many studies investigating the genetic basis of sAD have shown support for the ACH, including the discovery that the APOE ε4 allele markedly increased AD risk by decreased brain clearance of Aβ, leading to excess Aβ aggregation and typical AD neuropathology (Castellano et al., 2011). The identification of other risk loci for sAD, through GWAS and, more recently, exome and genome sequencing have helped in identifying important biological processes in the context of AD pathogenesis, in particular cholesterol/sterol metabolism, the immune system and endocytosis (Jones et al., 2015). Follow-up studies investigating the function of susceptibility genes within these pathways have provided new support for the ACH as a driving factor in AD pathogenesis. For example, the *SORL1*, *PICALM* and *BIN1* genes are associated with risk of sAD (Lambert et al., 2013) and all

have involvement in endocytic processes. SORL1 has been shown to act as a sorting receptor for APP, protecting it from amyloidogenic processing (Andersen et al., 2005), PICALM has been implicated in regulating Aβ clearance from the brain and BIN1 was reported to be involved in the endocytic trafficking of β-secretase, ultimately regulating Aβ production (Miyagawa et al., 2016). These mechanistic studies, among others, have linked several recently identified sAD risk genes to aspects of Aβ homeostasis, providing further support for the ACH.

1.3 The AD Risk Gene *Bridging Integrator 1 (BIN1)*

Bridging Integrator 1 (*BIN1*) is currently identified as the second most significant sAD risk gene, after *APOE* (www.alzgene.org). *BIN1* first came to light in the field of sAD genetics in 2009 in a two-stage GWAS involving over 16,000 individuals from the Genetic and Environmental Risk in Alzheimer's Disease (GERAD) consortium (Harold et al., 2009). Two loci approximately 30 kb 5' of the *BIN1* gene, rs7561528 and rs744373, showed suggestive association with sAD but did not reach the genome-wide significance threshold with p-values of 3.0×10^{-6} and 3.2×10^{-6}, respectively (Harold et al., 2009). The rs744373 polymorphism, however, reached genome-wide significance ($p = 1.6 \times 10^{-11}$) in a subsequent three-stage GWAS in the Cohorts for Heart and Aging Research in Genomic Epidemiology (CHARGE) consortium (Seshadri et al., 2010), which was then combined with data from the GERAD consortium at Stage 3. The odds ratio (OR) of rs744373 was 1.13 and the minor allele frequency (MAF) 0.29. The OR is the unit used to report effect sizes in GWAS and is the ratio of two odds: the odds of having disease for individuals with a specific allele and the odds of having disease for individuals who do not have that same allele. MAF, on the other hand, is the frequency at which the second most common allele is found in a population. The association of *BIN1* was further confirmed at the rs7561528 SNP in a GWAS in The Alzheimer's Disease Genetics Consortium (ADGC) showing significance at $p = 4.2 \times 10^{-14}$ (Naj et al., 2011). A combined analysis of four GWAS datasets was then carried out and termed GERAD+ which further supported the association at rs744373 ($p = 2.6 \times 10^{-14}$) (Hollingworth et al., 2011). The GERAD, CHARGE, ADGC and EADI1 consortia were combined in the largest AD GWAS to date, with a total of 25,580 cases and 48,466 controls of European ancestry, comprising the IGAP (Lambert et al., 2013). In addition to the *APOE* locus, 21 loci reached genome-wide significance, of which *BIN1* was the most highly associated with the top SNP, rs6733839, reaching $p = 6.9 \times 10^{-44}$. This was a newly-identified SNP, located 27.1 kb upstream from the *BIN1* coding locus, with the minor allele (T) conferring a genetic risk for AD (OR = 1.22, MAF = 0.409) (Lambert et al., 2013). Table 1.1 shows a summary of the key GWAS results implicating *BIN1* as a sAD susceptibility gene. All the aforementioned sAD-associated SNPs were found to lie within a 6.7 kb LD block approximately 30 kb upstream of the *BIN1* promoter (Chapuis et al., 2013), suggesting they are representative of the same association signal.

Table 1.1: Key GWAS Identifying BIN1 as a sAD Susceptibility Gene

Consortium	SNP	Odds Ratio	Minor Allele Frequency	P-value	Reference
CHARGE	rs744373	1.13	(G) 0.29	1.6×10^{-11}	(Seshadri et al., 2010)
ADGC	rs7561528	1.18	(A) 0.35	4.2×10^{-14}	(Naj et al., 2011)
GERAD+	rs744373	1.17	(G) 0.29	$2.6\text{x}10^{-14}$	(Hollingworth et al., 2011)
IGAP	rs6733839	1.22	(T) 0.409	$6.9\text{x}10^{-44}$	(Lambert et al., 2013)

1.3.1 The Functional Relevance of the Genetic Association of *BIN1* with sAD

While GWAS identified a large number of novel risk-influencing loci, understanding the functional link between these genetic determinants and sAD presents a challenge given the functional risk variant(s) are yet to be determined. The sAD-associated index variant rs7561528, 5' of the *BIN1* gene, has been reported to show a *cis*-regulatory effect on the transcription of *BIN1* in peripheral blood mononuclear cells (PBMCs) (Raj et al., 2012), suggesting, that changes in gene expression may be a possible mechanism by which BIN1 mediates sAD risk. The 6.7 kb LD region containing the *BIN1* association SNPs was sequenced from 47 sAD cases and 47 controls, resulting in the identification of 8 new polymorphisms (Chapuis et al., 2013). A sample of 338 controls was used for genotyping of these 8 polymorphisms which then acted as a reference for imputation in the GWAS EADI1 cohort where a three base pair insertion, rs59335482, was associated with higher risk of sAD (OR = 1.21, $p = 1.3 \times 10^{-6}$) (Chapuis et al., 2013). This insertion allele was shown to affect the transcriptional activity through a luciferase assay, showing a 101% and 33% increase in luciferase activity in the human neuroblastoma SH-SY5Y and human embryonic kidney (HEK) cell lines, respectively. Furthermore, rs59335482 was associated with an increase in *BIN1* mRNA expression levels in the brain and lymphoblastoid cell

lines, suggesting that BIN1 polymorphisms may mediate AD risk by increasing BIN1 expression. The originally identified *BIN1* SNP rs744373 (Hollingworth et al., 2011, Seshadri et al., 2010) has also shown association with *BIN1* expression levels in temporal lobe epilepsy patients with severely impaired memory performance. Higher *BIN1* mRNA expression levels were significantly associated with individuals homozygous for the risk allele at rs744373 compared to the non-risk allele (Bungenberg et al., 2016).

Conditional analysis on the top *BIN1* SNP (rs6733839) has identified a secondary association signal at rs7584040 within the first intron of BIN1, ~30kb from rs6733839 (In house unpublished data). Both these SNPs showed evidence of a functional role as expression quantitative trait loci (eQTLs). These are regions of the genome containing variants that influence the expression of one or more genes. Furthermore, rs7584040 has been reported to lie within a differentially methylated region (DMR) in lymphoblastoid cell lines (Kuleshov et al., 2014). DMRs are genomic regions which differ in DNA methylation status across phenotypes and are regarded as possible functional regions involved in gene transcriptional regulation. Methylation at intragenic sites is thought to associate with a decrease in gene expression (Lorincz et al., 2004). Further evidence of BIN1 methylation in sAD comes from the identification of a CpG locus, cg22883290, which is located 5 kb from the 5' end of the *BIN1* gene that was significantly associated with burden of AD pathology in 708 brain autopsy samples (De Jager et al., 2014). Methylation of CpG dinucleotides is a prime epigenetic mechanism and a frequent biochemical modification of DNA in the human genome. The *BIN1* index SNP rs744373, located 92 kb from cg22883290, was moderately associated with level of methylation at this CpG locus ($P = 0.0003$). However, the association of this methylation site with sAD was not found to be driven by rs744373 as adjusting for this variant did not change the effect size of CpG association to sAD burden (De Jager et al., 2014). Collectively, however, these studies suggest that genetic and epigenetic associations of *BIN1* with sAD may have functional consequences for *BIN1* expression.

1.3.2 BIN1 Expression in Alzheimer's disease

With the region of association in *BIN1* implicated in AD pathogenesis by multiple genetic analyses (Harold et al., 2009, Lambert et al., 2009, Seshadri et al., 2010, Naj et al., 2011, Hollingworth et al., 2011), BIN1 protein expression levels in AD became the next source

of interest. Evidence of BIN1 expression in AD to date has been conflicting. Glennon et al. (2013) reported that BIN1 protein was reduced by 87% in 24 frontal cortex samples from sAD patients compared to age-matched controls. In the same study, no significant difference was found in BIN1 expression when comparing 6 hippocampal samples from fAD patients compared to age-matched controls, suggesting that BIN1 expression level changes may be specific to the sporadic form of the disease. While the brain areas analysed differed, both the frontal cortex and the hippocampus are pathologically affected in AD (Braak and Braak, 1991, Jack et al., 1992). The sAD-specific nature of BIN1 expression changes suggest that BIN1 is a primary contributor to the disease rather than a secondary consequence of sAD. Glennon et al. (2013) also reported that BIN1 levels showed a trend towards a decrease with age in a cohort of 16 control samples between 25-88 years, although this observation did not reach statistical significance and requires replication.

In contrast, *BIN1* mRNA transcript levels have been reported to show an increase in sAD prefrontal cortex samples compared to controls in two independent studies (Chapuis et al., 2013, De Jager et al., 2014). Karch et al. (2012) reported that BIN1 mRNA expression levels were marginally upregulated with sAD ($p = 0.0540$) in 112 parietal lobe samples, however this did not reach statistical significance. Interestingly, however, the same study reported that higher BIN1 expression levels were associated with later age at onset and shorter disease duration in neurons of sAD brain tissue from the parietal lobe (Karch et al., 2012), therefore it still remains unclear how BIN1 expression changes are associated with AD pathogenesis.

Subcellular changes in BIN1 expression with AD have been reported (Adams et al., 2016), suggesting that analysis of expression levels in brain samples containing a mixed population of cells may be too broad and this could, in part, account for the discrepancy in findings. Adams et al. (2016) reported that AD patients showed decreased BIN1-immunoreactive neuropil areas, rich in unmyelinated axons, dendrites and glial cells compared to controls, but an increase in the number of BIN1-positive neurons in the prefrontal cortex and CA1 region of the hippocampus, the site of the earliest AD-associated neurodegeneration (West et al., 2000), compared to controls. Furthermore, the percentage of BIN1-positive pyramidal neurons in the CA1 region positively correlated with hippocampal neuritic plaque score in patients with AD (Adams et al., 2016). These findings further implicate altered BIN1 expression in AD pathogenesis and highlight the diversification of BIN1

expression among cell types of the brain. BIN1 has also shown isoform-dependent expression in AD (Holler et al., 2014). *BIN1* is subject to extensive alternative splicing, generating at least 10 tissue-specific isoforms, as discussed in detail in Section 1.3.3. The largest isoform, isoform 1, showed significantly reduced expression in sAD brain tissue compared to age-matched controls whereas smaller BIN1 isoforms showed increased expression (Holler et al., 2014). The conflicting direction of evidence in addition to the differential expression patterns presented by different BIN1 isoforms suggests that BIN1 expression does relate to AD pathogenesis, albeit it in a tissue-, cell-type- or isoform-dependent manner.

1.3.3 Genetic Architecture and Protein Structure of BIN1

The *BIN1* gene is 58,975bp in length and is found at position 2q14.3. It contains at least 20 exons, of which 7 are differentially spliced (Wechsler-Reya et al., 1997). Initially identified as box-dependent myc-interacting protein 1 (Sakamuro et al., 1996), a tumour suppressor, BIN1 was originally denoted Amphiphysin 2 as it is a close homologue of the endocytic protein Amphiphysin 1 (AMPH1), sharing 55% protein homology (Butler et al., 1997). Together with the yeast protein RVS167, Bin1 and Amph1 comprise the founding members of the BIN1/Amphiphysin/RVS167-related (BAR) domain family of proteins, defined by the presence of a homologous α -helical domain of 250-280 amino acids (Sivadon et al., 1995, Sakamuro et al., 1996). While BAR domain proteins have been implicated in a wide range of cellular functions, this conserved feature suggests a common molecular mechanism may be underlying these diverse processes (Ren et al., 2006).

The protein structure of BIN1 and its major splice variants are illustrated in Figure 1.3. All isoforms of BIN1 contain an N-terminal BAR domain: a kinked, tri-helical banana-shaped homodimer exhibiting a positive charge on its concave surface to induce membrane curvature (Casal et al., 2006). The C-terminal SRC homology 3 (SH3) domain of BIN1 mediates the interaction with endocytic proteins such as dynamin by binding to its proline-rich domain (Grabs et al., 1997), an interaction which is important for clathrin-mediated endocytosis (CME) (Wigge et al., 1997b) which will be further described in Section 1.4.2.

BIN1 isoforms exhibit tissue-specific expression and differ by the alternative splicing of 7 exons: 6a, 10, 12a-d and 13 (Wechsler-Reya et al., 1997). The original nomenclature described by Wechsler-Reya et al. (1997) has been used here for consistency, but it should

be noted that exon 6a was previously overlooked and is more recently referred to as exon 7, with all subsequent exons $n + 1$ from their original designation (Ren et al., 2006). Exon 6a encodes a brain-specific 31-residue N-terminal insert domain (NTID) which has been shown to strongly promote an interaction with dynamin 2 (Ellis et al., 2012) and is important for membrane targeting and dimerization of Bin1 during endocytosis (Ramjaun et al., 1999). Exon 10 is predominantly found in the muscle-specific BIN1 isoform, which is involved in transverse tubule (T-tubule) biogenesis in striated muscle (Lee et al., 2002). Exon 10 encodes a 15-residue sequence which associates with certain phosphoinositides to enable membrane association, crucial for the T-tubule localization, and induces tubulation (Lee et al., 2002). Exon 12 includes a series of brain-specific exons divided into subtypes a-d that encode the clathrin and AP2 binding (CLAP) domain. This facilitates binding with clathrin and associated adapter proteins, such as adaptor protein 2 (AP2), during CME (Ramjaun and McPherson, 1998). While exons 12a-d are spliced only into BIN1 isoforms found in the brain, the inappropriate inclusion of exon 12a in melanoma cells has been reported, which abolished the ability of Bin1 to inhibit c-Myc (malignant transformation by cellular homolog of avian myelocytomatosis virus oncogene) and to induce programmed cell death (Ge et al., 1999). Exon 12d is also found in BIN1 isoforms without exons 12a-c however the functional relevance of these exons to BIN1 function, when expressed in isolation, is yet to be elucidated. Finally, exon 13 encodes part of the Myc-binding domain (MBD) which binds c-Myc, an important regulator of cell proliferation and terminal differentiation which is mutated in human cancers (Pineda-Lucena et al., 2005). BIN1 was first identified as a protein that interacts with the N-terminus of c-Myc (Sakamuro et al., 1996) and acts as a tumour suppressor by actively inhibiting c-Myc activation (Elliott et al., 1999).

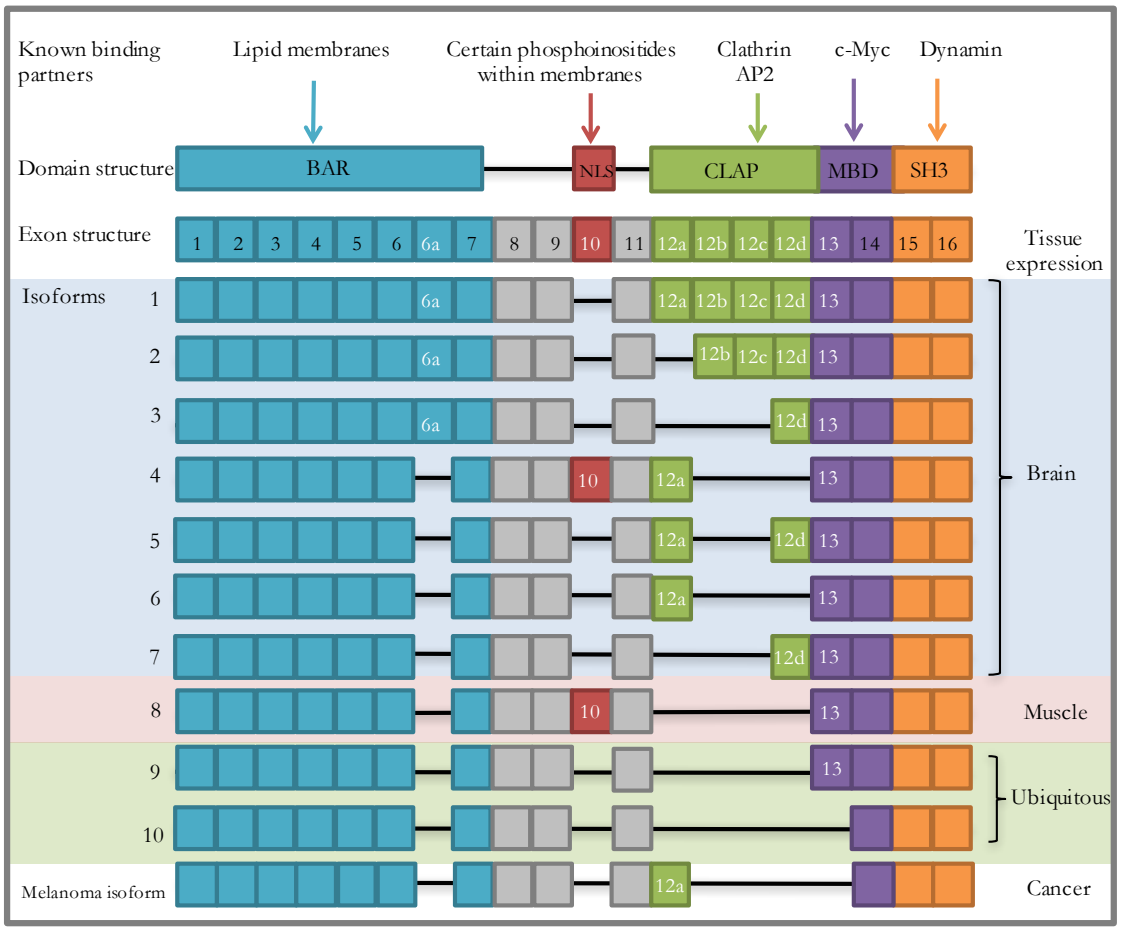

Figure 1.3: The Isoforms of BIN1

A schematic depicting the protein domain structure and corresponding exons that comprise the 11 alternatively-spliced isoforms of BIN1. Known binding partners of the protein domains are indicated. Exons 1-7 encode the BAR domain, exon 10 encodes a nuclear-localisation-signal-like motif (NLS). Exons 12a-2 encode the clathrin-associated protein binding region (CLAP) domain while the Myc-binding domain (MBD) is encoded by exons 13 and 14. Finally, exons 15 and 16 encode the C-terminal SH3 domain. Isoforms 1-7 show brain-specific expression while isoform 8 is muscle-specific and isoforms 9 and 10 are ubiquitous. Inclusion of exon 12a has been identified in cancers (Ge et al., 1999). Alternatively-spliced exons are indicated in white text. Schematic adapted from Prokic et al. (2014).

1.4 The Functional Role of BIN1

The mammalian genome contains two distinct amphiphysin genes denoted *Amphiphysin 1* (*AMPH1*) and *Amphiphysin 2/BIN1*. While *AMPH*1 is predominantly expressed in the brain (Wigge et al., 1997b), showing strict neuronal expression and presynaptic localisation (De Rossi et al., 2017), BIN1 shows widespread expression with brain-specific, muscle-specific and ubiquitous isoforms (Tsutsui et al., 1997, Wechsler-Reya et al., 1997). All isoforms contain the N-terminal BAR domain that binds lipid membranes, inducing membrane curvature in numerous contexts including T-tubules in muscular cells, endocytic pits and intracellular membranes (Wechsler-Reya et al., 1997, Peter et al., 2004). The concave shape of the membrane-binding face of the BAR domain provides a simple mechanical explanation for its preferential binding to curved membranes. Membrane invagination/tubulation is mediated through dimerisation of the BAR domains of BIN1 (Peter et al., 2004). The formation of both Bin1 homodimers and Bin1/Amph1 heterodimers has been demonstrated in rat brain extracts (Ramjaun et al., 1999). *Drosophila* only possess a single Amphiphysin gene and studies suggest this is always present in membrane domains that undergo great changes in curvature and surface area, for example at the apical membrane of epithelial cells (Zelhof et al., 2001).

The mechanisms that underlie the pathogenic nature of BIN1 in sAD are not yet fully understood. However, BIN1 has shown involvement in two of the key biological pathways to be implicated in sAD from genetic studies; immune function and endocytosis. Aged mosaic *BIN1* knockout mice show a higher incidence of inflammation compared to age-matched controls (Chang et al., 2007) while *BIN1* mouse knockout studies indicate that BIN1 regulates the expression of indoleamine 2,3-dioxygenase (IDO1) (Muller et al., 2005). This is upregulated as an immune defence mechanism and is also found to be associated with Aβ plaques and NFTs (Bonda et al., 2010).

As a member of the Amphiphysin family, BIN1 binds to the GTPase dynamin and is thought to play an important role in CME (Wigge and McMahon, 1998). There are 7 brain-specific isoforms of BIN1, all of which contain at least one of the exon 12 variants (a-d), exon 13 and three of which contain exon 6a (Figure 1.3). Isoform 4 also contains exon 10 although the functional relevance of this in the brain is unclear. In neurons, Bin1 binds dynamin 1 through its SH3 domain (Ramjaun et al., 1997) and forms heterodimers with

Amph1 which are thought to aid endocytic uptake at the synaptic clathrin coated pit (Wigge et al., 1997a). Evidence both supporting and questioning the role of BIN1 in CME is further described in Section 1.4.2.

1.4.1 Clathrin-mediated Endocytosis

Endocytosis is the process by which cells internalise molecules from their environment by invagination of the plasma membrane and the formation of a membrane-bound vesicle called an endosome. It is a universally important cell function, enabling nutrient uptake, receptor recycling and degradation and the delivery of cargo to intracellular organelles. Internalised cargo may be shuttled through this internal membrane system for metabolic utilization or trafficked to late endosomes for further sorting resulting in retrograde transport to the Golgi apparatus, transcytosis to the opposing plasma membrane or degradation in lysosomes. There are multiple methods by which mammalian cells endocytose material from their extracellular environment. Macroscale endocytic processes include phagocytosis, the ingestion of larger objects, such as viruses, bacteria, or other particles, and macropinocytosis, the bulk non-selective uptake of solute molecules, nutrients and antigens (Kumari et al., 2010). Microscale endocytic events can also be non-selective, such as fluid-phase and adsorptive endocytosis which describe the non-specific uptake of solutes from the immediate extracellular environment. Adsorptive endocytosis involves electrostatic interactions and requires the solute to have an excess positive charge, allowing it to bind the negatively-charged plasma membrane (Tamai et al., 1997). Microscale endocytic events are often categorised according to their requirement for dynamin scission. For example, CME and caveolar endocytosis depend on dynamin activity for vesicle formation (Wigge et al., 1997b, Oh et al., 1998), while the flotillin-mediated endocytic route can be independent of dynamin function (Glebov et al., 2006, Kumari et al., 2010). With BIN1 possessing both clathrin and dynamin-binding domains, this project will principally investigate CME and other dynamin-dependent endocytic processes such as caveolar endocytosis.

To date, the best characterised endocytic mechanism is CME. As illustrated in Figure 1.4, it involves the formation of clathrin-coated pits (CCPs) around transmembrane receptors and their ligands at the plasma membrane, which subsequently develop into intracellular clathrin-coated vesicles (CCVs) (Mousavi et al., 2004). Clathrin is a soluble cytosolic

protein which functions as a heterohexamer, consisting of three heavy chains and three light chains in a triskelion shape (Young, 2007). It has no direct contact with the plasma membrane but is recruited by adaptor proteins, polymerising into a lattice around the inward-budding pit. There are five major steps of CME including nucleation, cargo selection, coat assembly, vesicle scission and uncoating.

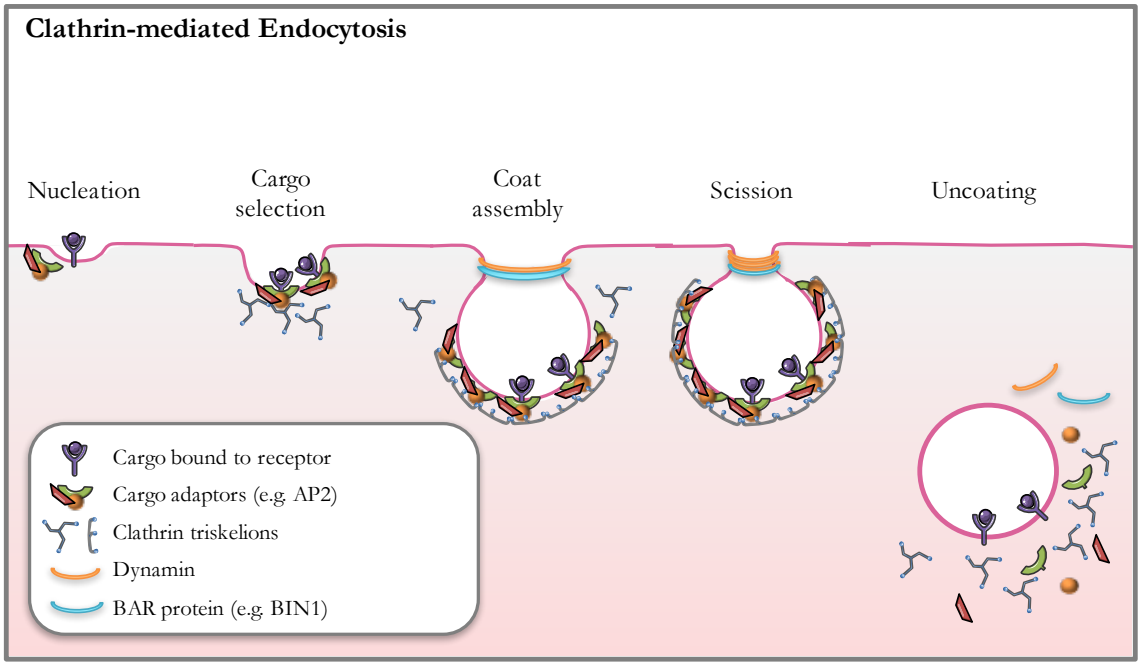

Figure 1.4: Clathrin-mediated Endocytosis

A schematic illustrating the five key stages in CME. Firstly, a nucleation module forms around the cargo-bound receptor and adaptor proteins are recruited to the endocytic pit. The adaptor proteins bind to the cargo-receptor complex and the assembly of the clathrin coat occurs. Meanwhile, BAR-domain proteins, such as BIN1, enable curvature of the membrane to produce the clathrin-coated pit and dynamin is recruited which results in scission of the vesicle from the plasma membrane. Once the vesicle is internalised, the clathrin coat and associated adaptor proteins disassemble and uncoat the vesicle. Adapted from (McMahon and Boucrot, 2011).

1.4.1.1 Nucleation

CME is initiated by the assembly of various endocytic accessory proteins at the plasma membrane into CCPs. However, many of the CCPs formed quickly diminish into abortive events, with the remainder undergoing stabilization and maturing into CCVs (Ehrlich et al., 2004). Although not yet fully understood, the initiation of the CCP is thought to involve the formation of a nucleation module. F-BAR domain-containing FCHo1/2 proteins (Fer/Cip4 homology domain only proteins 1 and 2) bind Phosphatidylinositol-(4,5)-bisphosphate (PIP_2)-rich regions of the plasma membrane (Jost et al., 1998) and recruit AP2 via interactions with scaffold proteins eps15 and intersectin (Henne et al., 2010). At least five adaptor protein complexes have been identified in eukaryotes (Hirst et al., 2011), each have a distinct localisation and function but all are involved in the sorting of cargo into vesicles for transport between membrane-bound compartments. AP2, the most thoroughly characterised of the five complexes, facilitates CME by linking clathrin and accessory proteins to the plasma membrane during CME, acting as a hub of interactions. AP2 is recruited to the nucleation module in addition to other cargo-specific adaptor proteins to mediate cargo selection (McMahon and Boucrot, 2011).

1.4.1.2 Cargo selection

The heterotetrameric complex of AP2 comprises two large subunits α and β2, the medium subunit μ2 and the smallest subunit σ2 (Owen et al., 2004, Figure 1.5). The large subunits can be divided into a trunk and an appendage domain, joined by a flexible hinge region. Initially, the α subunit of AP2 interacts with PIP_2 in the plasma membrane {Rohde, 2002 #276} while the μ2 subunit targets cargo for internalisation by binding to linear internalization motifs on the cytoplasmic tails of transmembrane cargo molecules (Owen et al., 1998). The appendage domains are attached to the trunk domain by long flexible hinge regions, allowing for recruitment of accessory proteins from the cytosol such as BIN1, AMPH1, AP180 (or its functional homologue PICALM) and auxilin (Owen et al., 1999). AP2 binds clathrin via interactions with the β2 hinge region and the appendage domains (Shih et al., 1995, ter Haar et al., 2000, Owen et al., 2000), completing the interaction between the endocytic cargo, accessory proteins and the clathrin coat. AP2 is the major hub of interactions in the maturing CCP and is essential for CCP and CCV formation at the plasma membrane (Boucrot et al., 2010).

1.4.1.3 Coat assembly

Clathrin molecules comprise a triskelia shape and are recruited from the cytosol by the AP2 hub, polymerising through their simultaneous binding to the β2 appendage and the β2 hinge region (Owen et al., 2000) into hexagons and pentagons to form a coat around the nascent pit. Clathrin polymerises at the forming pit and stabilises membrane curvature. The two-site binding of clathrin to both the β2 hinge region and appendage domain of AP2 displaces accessory proteins from the appendage domains to which they are bound (Owen et al., 2000).

1.4.1.4 Vesicle scission

Budding of the CCV from the plasma membrane requires the GTPase dynamin (Damke et al., 1994) which is recruited by BAR domain-containing proteins, such as BIN1, through binding of their SH3 homology domains to the C-terminal proline-rich domain of dynamin (Shpetner et al., 1996). BAR domain-containing proteins form dimers and mediate membrane curvature through electrostatic interactions with lipid head groups (Peter et al., 2004). Vesicle scission is facilitated by dynamin forming a helical collar around the neck of the invaginating CCV. *In vitro* evidence suggests that upon GTP hydrolysis, this helix extends lengthways (Stowell et al., 1999), eventually pinching the vesicle from the membrane. Both GTPase activity of dynamin and this associated conformational change are required for endocytosis (Marks et al., 2001).

The self-assembly of dynamin into a multimeric ring structure during endocytosis greatly enhances its GTPase activity (Warnock et al., 1996). It is therefore essential that the formation of this structure is temporally and spatially regulated. BIN1 and Amph1 have been proposed to selectively bind dynamin in its dissociated form, targeting it to the CCP prior to ring formation (Owen et al., 1998). This is based on evidence that dynamin ring formation and amphiphysin binding are mutually exclusive events and the SH3 domains of BIN1 and Amph1 prevent the formation of dynamin rings in solution (Owen et al., 1998). Indeed, the amphiphysin SH3 domains are unique in their ability to inhibit CME when overexpressed in fibroblasts (Wigge et al., 1997b) which may be due to the sequestration of dynamin away from the CCP.

1.4.1.5 Uncoating

Once detached from the plasma membrane, the clathrin coat is disassembled from the vesicle prior to fusion with the target endosome by the ATPase heatshock cognate 70 (HSC70) (Schlossman et al., 1984) and in conjunction with auxilin in neuronal cells (Ungewickell et al., 1995) or cyclin G-associated kinase (GAK) in non-neuronal cells (Greener et al., 2000). Both these cofactors function catalytically to support uncoating of the clathrin basket by binding to clathrin triskelia and recruiting HSC70 (Schlossman et al., 1984). Uncoating releases clathrin and other endocytic machinery into the cytoplasm to be used in the next round of CME.

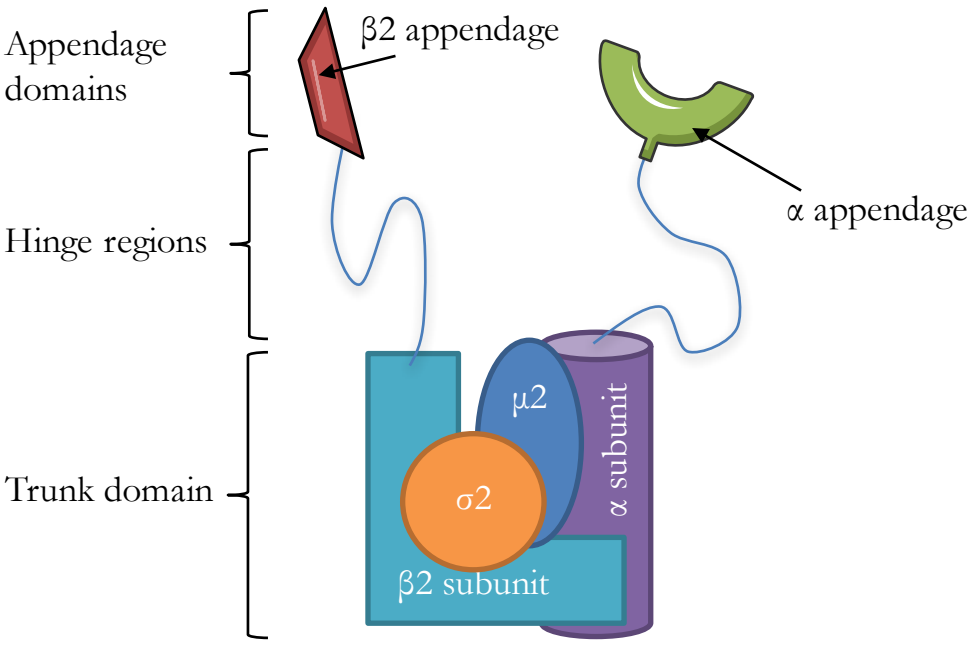

Figure 1.5: The protein structure of AP2

A schematic of the AP2 adaptor complex, a multimeric protein consisting of four adaptin subunits in the trunk domain, β2, σ2, μ2 and α, and two appendage domains attached by polypeptide hinges. The trunk domain binds to membranes and cargo via the β2 and μ2 subunits while the hinge regions bind clathrin and the appendage domains bind endocytic accessory proteins, such as BIN1. Adapted from Owen et al. (2004).

1.4.2 The Role of BIN1 in Clathrin-mediated Endocytosis

As a member of the amphiphysin family, BIN1 binds the GTPase dynamin through interactions with its SH3 domain (Wigge et al., 1997b) and brain-specific isoforms demonstrate binding to both clathrin and AP2 through the CLAP domain (Ramjaun and McPherson, 1998), implicating BIN1 in CME in a number of cell types. The evidence for the role of BIN1 in CME originates from research into the role of AMPH1, which shares 55% homology with BIN1 (Butler et al., 1997). The enrichment of AMPH1 at presynaptic terminals in the brain (Ramjaun et al., 1997) and interactions with dynamin and AP2 first implicated this family of proteins in the endocytic pathway (David et al., 1996). Furthermore, *in vivo,* disruption of the Amph1-dynamin interaction has been demonstrated to block synaptic vesicle endocytosis in the lamprey reticulospinal synapse, suggesting that this interaction is essential for this process (Shupliakov et al., 1997). Following the discovery of BIN1, much research focused on investigating whether, like AMPH1, BIN1 had a role in CME. Early *in vitro* studies supported a role for BIN1 in CME and suggested that AMPH1 and BIN1 interact to form heterodimers in the brain (Wigge et al., 1997a). Indeed, *Amph1* knockout mice were found to exhibit dramatically reduced expression of the brain-specific *Bin1* isoforms (Di Paolo et al., 2002). Expression of either full-length *Amph1* or *Bin1* alone inhibited endocytosis in COS monkey fibroblast cells, possibly due to a dominant negative effect, while coexpression of these two genes rescued endocytic inhibition (Wigge et al., 1997a). This suggested that both Amph1 and Bin1 were required in these cells for endocytic function. Indeed, depletion of both Amph1 and Bin1 by siRNA in the skin fibroblast cell line SK-MEL-2 led to defective uptake of transferrin, a marker of CME (Meinecke et al., 2013).

However, immunohistochemical analysis of human brain sections for BIN1 and AMPH1 provides compelling evidence that these homologs show a different pattern of expression in the brain. Unlike AMPH1, the large majority of BIN1 immunoreactivity was not associated with neurons and showed predominant expression in mature oligodendrocytes (De Rossi et al., 2016). This suggests that BIN1 and AMPH1 may also function independently. The role of BIN1 in CME has been questioned by several findings. For example, the disruption of the sole BAR domain-containing gene identified in Drosophila (likely the Bin1 homolog) did not detectably affect synaptic vesicle endocytosis (Zelhof et al., 2001). Furthermore, primary neurons from *Bin1* knockout mice showed no deficiency

in synaptic vesicle uptake (Muller et al., 2003), suggesting that the function of Bin1 in the brain may differ from Amph1. Indeed, Bin1 is broadly expressed in many tissues, unlike Amph1, and shows tissue-specific expression of at least 10 different isoforms (Wechsler-Reya et al., 1997). The relative importance of the alternatively-spliced CLAP domain for CME is unclear and while Bin1 may be important for CME in certain cell types, it may lack a necessary functional role in generalised endocytosis.

1.4.3 The Endocytic Pathway and the Fate of APP

Following internalization by CME, cargo contained within CCVs are trafficked through the cell via a number of highly dynamic membrane-enclosed tubulo-vesicular structures. Firstly, the newly budded vesicles can fuse with each other or early endosomes under the direction of the small GTPase Rab5 (Gorvel et al., 1991). The early endosome acts as a major sorting station, from which some receptors and membrane-bound lipids may be recycled back to the plasma membrane of origin via the endosome recycling complex (ERC) (Grant and Donaldson, 2009). Dissociated ligands are transported to late endosomes and lysosomes, where they are proteolysed. Endosomes transition from early to late by the transition from association with Rab5 to Rab7 (Poteryaev et al., 2010). During the transition, endosomes move along microtubules to the perinuclear region which is accompanied by increasing intravacuolar acidification (Hu et al., 2015). Late endosomes are involved in the formation of intraluminal vesicles, which bud inward from the endosome membrane. Late endosomes containing many intraluminal vesicles are referred to as multivesicular bodies (MVBs). Late endosomes and MVBs fuse with lysosomes where cargo proteins and intraluminal vesicles are degraded. Alternatively, MVBs may directly fuse with the plasma membrane, releasing their contents as exosomes. The luminal pH decreases along the endo-lysosomal pathway from pH 6-6.5 to pH 4.5-5.5 in late endosomes and lysosomes, reflecting the optimal pH of the enzymes that function within these vesicles (Hu et al., 2015).

CME is an important mechanism in the context of LOAD as APP is internalised via this method (Carey et al., 2005) and alterations in intracellular trafficking are thought to influence whether it enters the non-amyloidogenic or amyloidogenic pathway. BACE1 has an acidic pH optimum and therefore resides predominantly in endosomes (Vassar et al., 1999) whereas α-secretase has been shown to cleave APP almost exclusively at the cell

surface (Parvathy et al., 1999). This suggests that the cleavage of APP by β-secretase, and the amyloidogenic processing of APP, is more likely to occur if APP undergoes endocytosis. The importance of the endocytic pathway to APP processing and Aβ generation is illustrated by observations of reduced Aβ production when APP internalization is inhibited in APP transgenic mice (Carey et al., 2005). Furthermore, acceleration of APP metabolism and Aβ secretion upon endocytosis stimulation was demonstrated by overexpressing Rab5, a positive regulator of endocytosis, in mouse fibroblasts (Grbovic et al., 2003). Altered endocytosis has also been implicated in early AD pathogenesis as an increase in the number and size of Rab5-positive endosomes was one of the earliest detectable pathologies in post-mortem AD brains, preceding Aβ deposition (Cataldo et al., 2000). Inhibition of CME by the expression of a Rab5-specific GTPase-activating protein in Neuro-2a (N2a) mouse neuroblastoma cells significantly reduced levels of β-CTF and secreted Aβ without affecting APP biosynthesis, suggesting endocytosis is important for the β-cleavage of APP (Ehehalt et al., 2003). With aforementioned evidence implicating BIN1 in CME, research investigating BIN1 function in APP processing has yielded interesting results to suggest it is involved in Aβ production in both neuronal and non-neuronal cell lines (Miyagawa et al., 2016). The tissue-specific expression of BIN1 isoforms brings into question whether BIN1 has a generalised function in endocytosis or if this is cell-type specific. Further findings implicating BIN1 function in APP processing will be described in Chapter 4.

1.5 Endocytosis at the Blood-Brain Barrier

The blood-brain barrier (BBB) is a crucial interface between the nervous tissue of the brain and the circulating blood within the brain microvasculature. It is composed of an extensive network of endothelial cells which, alongside neurons, pericytes and astrocytes, form the neurovascular unit (Figure 1.6). The BBB is highly specialised to maintain the precise microenvironment required by the central nervous system by regulating the flux of nutrients, ions and other molecules, while providing protection from toxins and pathogens (Keaney and Campbell, 2015). Brain microvascular endothelial cells (BMECs) line the capillaries and form intercellular tight junctions, severely restricting the paracellular diffusion of macromolecules, ions and other polar solutes (Smith and Gumbleton, 2006).

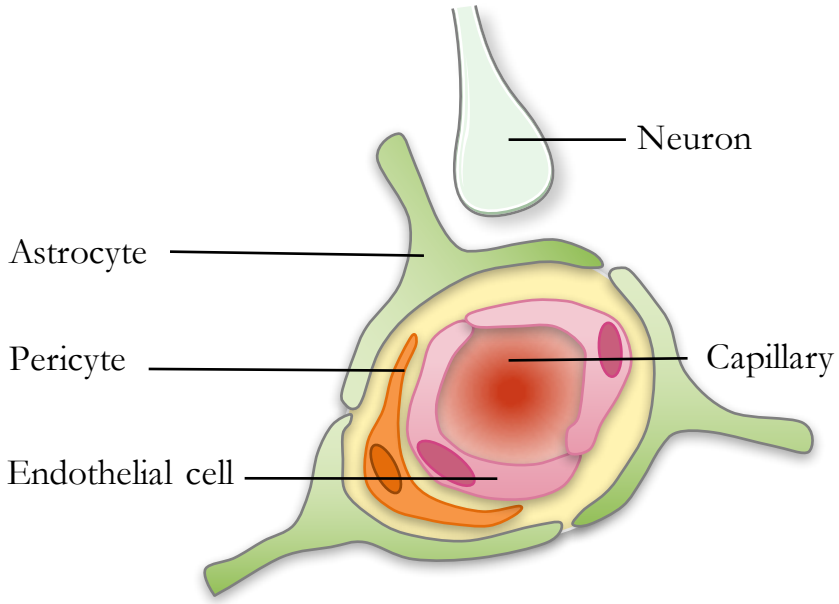

Figure 1.6: The Neurovascular Unit

A schematic showing the structure of the neurovascular unit of the blood-brain barrier as a cross-section through a brain capillary. Brain microvascular endothelial cells line the capillary and are supported in their barrier function through interactions with pericytes, astrocytes and neurons. Adapted from Wolff et al., (2015).

1.5.1 The Neurovascular Unit

1.5.1.1 Brain microvascular endothelial cells

The primary anatomical units of the BBB are BMECs which line the brain capillaries, bearing much resemblance to other somatic endothelial cell types. However, these cells are highly specialized with unique properties that facilitate essential functions of the BBB, including acting as a barrier to passive diffusion, enabling active transport of molecules and facilitating communication between the CNS and the periphery (Keaney and Campbell, 2015), further described in Section 1.5.2. BMECs form a tightly packed lining and maintain this structural integrity through intercellular adherens junctions. These are regions of cell-to-cell contact composed of cadherin proteins spanning the intercellular cleft and are anchored to the cell cytoplasm by the scaffolding proteins α β and γ catenin (Keaney and Campbell, 2015). Adherens junctions provide structural support and are a vital component for BBB function as they are essential for the formation of tight junctions (TJs) which also span the intercellular cleft (Niessen, 2007).

TJs are dynamic structures consisting of a number of transmembrane and membrane-associated cytoplasmic proteins with the principal function of severely restricting paracellular diffusion (Keaney and Campbell, 2015). The transendothelial electrical resistance (TEER) is a powerful, non-invasive measure of the tightness of a cellular barrier *in vitro* and TJs allow the BBB to obtain a high *in vivo* TEER of 1000 Ωcm^2 (Butt et al., 1990). TJs consist of a complex of occludins, claudins and junctional adhesion molecules (JAMs) involved in intercellular contact and interactions with intracellular scaffold proteins such as zonula occludens (ZO) – proteins which anchor TJ proteins to the cytoskeleton (Fanning et al., 1998). While occludins are not required for the formation of tight junctions, they regulate barrier properties including maintaining the tightness of TJs and are involved in the formation of the apical (blood-facing) and basolateral (brain-facing) domains, as discussed below (Balda et al., 1996). Claudin-3 and claudin-5 are expressed in BMECs and support TJ integrity (Wolburg et al., 2003, Ohtsuki et al., 2007) while JAMs are thought to be involved in the facilitation of TJ assembly and the establishment of cell polarity (Ebnet et al., 2004).

The apical-basolateral polarity of BMECs is an essential property of the BBB which enables these cells to segregate receptors into plasma membrane domains, specific to their required direction of transcytosis. The receptor for the iron-binding ligand transferrin, for example, which undergoes CME, is predominantly found on the apical side of BMECs, largely limiting its endocytosis to the blood side and transport in a blood-to-brain direction (Roberts et al., 1993). The lipid composition also differs in the apical and basolateral membranes of BMECs and the basolateral membrane has been reported to display more caveolae, flask-shaped invaginations involved in clathrin-independent endocytosis (Bendayan et al., 2006). This suggests that endocytic mechanisms are also polarised at the BBB and that this is an important feature to maintain the function of the BBB. The establishment and maintenance of polarity in BMECs is thought to involve polarity regulator proteins and endocytic regulators which coordinate and promote each others activities (Shivas et al., 2010). While the molecular mechanisms governing endothelial apical-basolateral polarity are not fully elucidated, the regulation of polarity in epithelial cells is more fully understood. Indeed, differential regulation of endocytic mechanisms at the apical and basolateral domains has been demonstrated in polarised epithelial MDCK cells where clathrin-independent endocytosis of the protein toxin ricin was able to be stimulated on the apical membrane without increasing the uptake at the basolateral side (Eker et al., 1994).

1.5.1.2 Basement membranes

There are two basement membranes (BMs) that separate the endothelium from associated cell types within the brain; the endothelial BM and the astroglial BM. Integrins expressed by the endothelial cells can bind to most proteins of the BM while astrocyte end feet attach to the BM through dystroglycan, therefore the BMs act as important scaffolding structures allowing endothelial cells close proximity to astrocytes for optimal communication (Alvarez, 2013).

1.5.1.3 Astrocytes

While the endothelial cells make up the primary component of the BBB, their function is highly regulated by associated cell types which comprise the neurovascular unit. Microglia, astrocytes and nerve terminals all release vasoactive agents and cytokines which can modify

tight junction assembly and barrier permeability (Abbott et al., 2006). The contribution of astrocytes to BBB formation and maintenance was first demonstrated in 1987 both *in vivo* and *in vitro* by the groups of Raff and Brightman, respectively. Subcultured bovine BMECs showed fragmentation and decreased frequency of tight junctions, however when co-cultured with rat astrocytes, enhancement of tight junction width and complexity was shown (Tao-Cheng et al., 1987). Janzer and Raff (1987), meanwhile, demonstrated that astrocytes have the ability to enhance tightness of microvascular endothelial cells *in vivo*. In this study, both purified rat cerebral cortex astrocytes and neonatal meningeal cells formed vascularised aggregates when injected into the rat anterior eye chamber. While endogenous albumin was detected in meningeal cell aggregates, it was not present in astrocyte aggregates, thus the endothelial cells lining the vasculature were functionally tight in the presence of astrocytes but functionally leaky in meningeal cell aggregates (Janzer and Raff 1987). Indeed, more recently it has been demonstrated that significantly higher TEER can be induced in BMECs *in vitro* by co-culturing with astrocytes (Wang et al., 2015).

1.5.1.4 Pericytes

Pericytes are peripheral cells of mesodermal origin which show extensive coverage of CNS vasculature and have an important role in regulating cerebral blood flow, BBB permeability and clearing toxic cellular byproducts (Keaney and Campbell, 2015). Pericytes, like endothelial cells, are attached to extracellular matrix proteins of the basement membrane by integrins and project elongated processes that ensheath the capillary wall (Stratman et al., 2009). Platelet-derived growth factor receptor β (*Pdgfrβ)* knockout mice have defects in pericyte generation and demonstrate structural abnormalities in TJs, increased BBB permeability and increased rate of transcytosis (Daneman et al., 2010b). This suggests that pericytes are required for BBB formation during development and that pericyte coverage controls BBB permeability. Furthermore, purified wild-type murine BMECs cultured alone showed large gaps between cell connections, whereas when cultured with a feeding layer of purified brain pericytes, the endothelial junctions sealed and a 4-fold increase in TEER was recorded (Daneman et al., 2010b).

1.5.2 Function of the Blood-Brain Barrier

The primary function of the BBB is to regulate the flux of molecules between the blood and the brain in order to maintain different homeostasis of these separate compartments. It is essential that the ionic composition of the brain is kept optimal for synaptic signalling function and therefore specific ion channels and transporters are present in brain endothelial cells to regulate this (Smith and Gumbleton, 2006). The concentration of ions in blood plasma may dramatically differ from that of the interstitial fluid (ISF) surrounding neurons and this may also fluctuate with environmental stimuli which could have neurotoxic effects if disseminated to the brain (Begley, 2007). The BBB therefore needs to prevent passive diffusion from either side while ensuring the essential uptake and removal of molecules to/from the brain.

The BBB also serves as a protective barricade to neurotoxic substances that may be circulating in the blood, such as endogenous metabolites, proteins and xenobiotics. Brain endothelial cells have ATP-binding cassette (ABC) transporters which actively pump many of these damaging agents out of the brain. There is a much lower protein content in CSF than blood plasma (Begley, 2007) and therefore the transport of macromolecules between blood and brain is also restricted by the BBB, which prevents exposure of nervous tissue to factors that may convert endogenous proteins to damaging products in the brain.

1.5.3 Methods of transport at the Blood-Brain Barrier

Transport of substances across the BBB is predominantly an active process due to the severe restriction of the passive paracellular transport pathway. Passive diffusion across BMECs is limited to lipid-soluble molecules of approximately <180 Da in size due to the obstruction of the paracellular space by TJs (Kozler and Pokorny, 2003). Active transport, on the other hand, occurs at the BBB in the form of specialised transcellular transport systems that tightly restrict entry and exit of hydrophilic molecules to and from the CNS.

Figure 1.6 shows the various modes of transport across BMECs. Some substrates, such as glucose, have specific protein transporters found in the plasma membrane of BMECs that mediate the facilitated diffusion of these polar substrates across the BBB. For example, the glucose transporter GLUT-1 is highly expressed in BMECs on both apical and basolateral membranes (Laterra et al., 1999) and mediates the transport of glucose into the brain by

carrier-mediated transport (Winkler et al., 2015). Receptor-mediated transport mechanisms are also found in BMECs, such as CME. Cargo is transported across the cell through endocytic vesicles which bypass the lysosome for exocytosis at the opposing domain by means of transcytosis. Electrostatic charge may also mediate the uptake of cationic substances and transport across the BBB by interactions with anionic sites on the cell surface, termed adsorptive-mediated endocytosis (Tamai et al., 1997). While the aforementioned transport mechanisms may be involved in both influx and efflux from the brain, a number of transport and carrier systems are expressed and polarised on the apical or basolateral surface of BMECs. Protein transporters such as ABC active efflux transporters are integral membrane proteins that use the energy of ATP hydrolysis to translocate neurotoxic substances from the brain and also prevent them entering in the first instance. P-glycoprotein (Pgp) is an ABC transporter involved in Aβ efflux and is further discussed in Section 1.5.4.

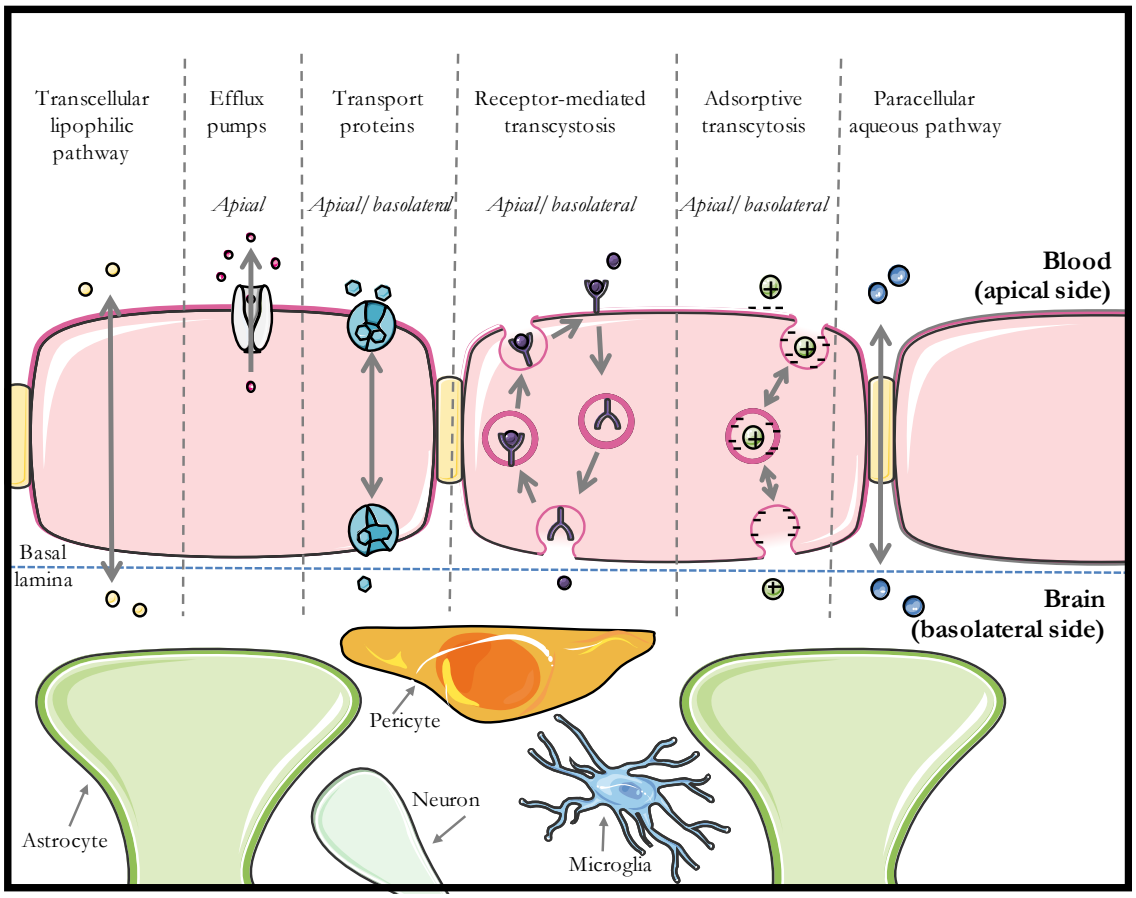

Figure 1.7: Methods of transport across the BBB

A schematic illustrating the structure and various modes of transport at the BBB. The membrane location of the receptors or where the cargo binds (apical/basolateral) is indicated and the arrows signify whether the process occurs from blood to brain, brain to blood or both. Methods of transport at the BBB include transcellular diffusion of lipophilic molecules, active efflux pumps, carrier-mediated transcytosis by transport proteins, receptor-mediated transcytosis, adsorptive transcytosis and the largely restricted paracellular diffusion pathway. Adapted from Abbott et al. (2006).

1.5.4 Aβ transport at the Blood-Brain Barrier

1.5.4.1 Influx and efflux of Aβ across the BBB

APP is expressed in a variety of tissues and can also be detected at low levels in blood (Seubert et al., 1992). Aβ is therefore continuously produced by cells of the CNS and peripheral tissues, raising the question of whether circulating Aβ in the periphery could contribute to Aβ in the brain parenchyma. Maness et al. (1994) demonstrated that radioactive Aβ40 is capable of crossing the murine BBB and accumulating in the brain (Maness et al., 1994). Cerebral capillary sequestration and specific transport of synthetic Aβ40 and Aβ42, identical to endogenous Aβ, into guinea pig brain parenchyma was subsequently demonstrated by an intracarotid brain infusion method (Martel et al., 1996). The BBB expresses several transporter systems that are involved in receptor-mediated flux of Aβ, including receptor for advanced glycation end products (RAGE), low-density lipoprotein receptor-related protein (LRP1), and P-glycoprotein (Pgp). RAGE has been identified as the likely transporter responsible for mediating apical-to-basolateral transcytosis of Aβ across the BBB (Deane et al., 2003). Interruption of the RAGE-ligand interaction prevented circulating Aβ passing across the brain endothelium *in vivo*, reducing Aβ-mediated vasoconstriction and neurovascular stress, while BBB transport of Aβ in RAGE-null mice was undetectable (Deane et al., 2003). This study further demonstrated that RAGE contributes to the transport of pathophysiologically-relevant concentrations of Aβ in a mouse model overexpressing APP. These levels were comparable to baseline plasma Aβ levels. While RAGE is capable of rapidly transporting free Aβ into the CNS, Aβ in the brain parenchyma is primarily cleared to the bloodstream across the BBB by LRP1 (Shibata et al., 2000). LRP1 is expressed mainly at the basolateral side of the BBB (Zhao et al., 2015) where it is involved in the endocytosis of more than 40 different ligands including APOE, APP and Aβ (Zlokovic et al., 2010). Pgp is an ABC transporter that is highly expressed in BMECs, showing strong enrichment in the apical membrane (Beaulieu et al., 1997), consistent with its role as an efflux pump. Pgp actively transports a wide variety of agents from BMECs into the vascular lumen and is important for mediating Aβ efflux from the brain (Cirrito et al., 2005). Indeed, in Pgp-null mice, decreased Aβ clearance and enhanced Aβ deposition were reported (Cirrito et al., 2005). Based on its apical location in BMECs, it has been suggested that Pgp functions to expel Aβ into the bloodstream which

has been internalised from the brain by LRP1 (Hartz et al., 2010). However, antioxidant treatment that preserves LRP1 but not Pgp under inflammatory conditions also preserves Aβ efflux, suggesting that LRP1 can also function independently of Pgp (Erickson et al., 2012).

1.5.4.2 Defective Aβ transport in AD

Changes in transport mechanisms across the BBB have a critical impact on the concentration of soluble Aβ in the CNS which is central to the formation of neurotoxic Aβ oligomers. The observation that LRP1 expression was decreased in the AD brain microvasculature (Shibata et al., 2000) lead to the neurovascular hypothesis of AD, originally stating that defects in Aβ efflux across the BBB because of LRP1 deficiency contributed to Aβ accumulation in the brain (Zlokovic, 2005, Jaeger et al., 2009). Indeed, depletion of LRP1 in the BBB by antisense oligonucleotides impairs Aβ efflux, resulting in Aβ accumulation in the brain and cognitive impairment in young wild-type mice (Jaeger et al., 2009). Reports of decreased Aβ efflux in rodent models of AD and human AD patients have substantiated the association between the disease and impaired Aβ efflux (Banks et al., 2003, Kandimalla et al., 2005, Mawuenyega et al., 2010). Alterations in Pgp-mediated transport have also been reported in association with AD with PET imaging studies indicating Pgp dysfunction in human AD patients (van Assema et al., 2012). An increase in RAGE expression levels has been reported in AD endothelium (Yan et al., 1996), suggesting enhanced Aβ influx may be associated with AD pathogenesis. Indeed, RAGE inhibition was shown to reduce Aβ40 and Aβ42 levels in the brain and rescued cognitive performance in aged transgenic mice overexpressing human APP, representing a transgenic mouse model of AD with established Aβ pathology (Deane et al., 2012). Collectively, these data suggest that the cumulative effects of reduced expression of LRP1 and Pgp, with increased expression of RAGE may contribute to brain Aβ accumulation in AD.

Recent evidence has implicated *PICALM*, one of the AD susceptibility genes, in regulation of Aβ efflux across the BBB, citing it as having a central role in Aβ clearance and thus demonstrating a mechanistic role in AD pathogenesis (Zhao et al., 2015). While a role for PICALM in CME of APP has previously been established in neuronal-like cell lines (Xiao et al., 2012, Thomas et al., 2016), Zhao *et al.* were the first to bring together a mechanistic role for PICALM at the BBB(Zhao et al., 2015). This study demonstrated that PICALM

regulated CME of Aβ bound to LRP1 and its transcytosis across the BBB. Furthermore, the AD risk SNP rs3851179 decreased PICALM expression by *cis*-regulation in induced pluripotent stem cell (iPSC)-derived endothelial cells and this resulted in higher Aβ clearance compared to isogenic controls containing the non-risk SNP (Zhao et al., 2015). This study therefore demonstrated the mechanism by which an AD susceptibility variant, identified by GWAS (Harold et al., 2009, Seshadri et al., 2010), is associated with reduced risk of sAD. With advances in sequencing efficiency, the number of genes identified to be associated with AD risk is ever-increasing, yet the function of these genes remains largely unknown. This demonstration of a mechanism that may explain the association of *PICALM* with sAD provides promise for future work elucidating the functional role of other AD risk genes.

1.6 Thesis Aims

With the aforementioned research in Section 1.4.2 implicating BIN1 in CME and the demonstration that internalisation of APP via CME is important for Aβ production (Carey et al., 2005), the extent to which BIN1 may mediate AD risk by its involvement in APP processing remains to be elucidated. Much of the *in vitro* research to date into the role of BIN1 in APP processing and CME has been conducted in cell lines derived from neuronal tumours, including mouse and human neuroblastoma cell lines (Glennon et al., 2013, Miyagawa et al., 2016). The use of an oncogenically-transformed cell line does not accurately reflect neuronal physiology and the degree to which these cell lines can recapitulate the *in vivo* physiology of polarised neurons with functional excitatory synapses is a key aspect regarding the validity of these models. Research into a potential role for BIN1 in other brain-associated cell types is also limited. The ubiquitous expression of BIN1, in addition to its 10 alternatively spliced isoforms indicate that it may function in multiple mechanisms, which may be tissue- or cell type-specific. While much work investigating the role of BIN1 in AD has focused on its function in neuronal-like cells, endocytic mechanisms involved in transcytosis at the BBB are also highly relevant in the context of AD. With its high level of splicing, it is important to consider the role BIN1 has in other brain cell types. Indeed, BMECs of the BBB also express BIN1 but a possible role in brain endothelial transport mechanisms is yet to be investigated.

The aims of this project are two-fold. Firstly, this project aims to utilise novel advances in the development of iPSCs in order to create a more accurate neuronal cell model to study the role of BIN1 and endocytic mechanisms in neurons. In particular, the creation of a cortical neuronal model from PBMC-derived iPSCs offers an attractive prospect to the AD research field whereby an extensive resource of blood samples is available, accompanying the genetic data obtained from GWAS. This currently untapped resource offers the potential to reprogram iPSCs from patients with a known genetic background in order to develop models to investigate the function of AD susceptibility genes. This project will address the initial stages of this research, involving the demonstration of a protocol to produce cortical neurons from blood-derived iPSCs. The hypothesis of this study is that cortical neurons can be differentiated from blood-derived iPSCs.

Secondly, this study aims to further develop knowledge in the field of BIN1 function in the brain, in a non-neuronal context, by investigating the role of BIN1 in CME at the BBB. The current knowledge of BIN1 function is largely limited to its role in CME in a neuronal context, however its involvement in the pathogenesis of AD and its general function in non-neuronal cells is largely unknown. Through siRNA-mediated BIN1 depletion, the function of BIN1 in a human brain endothelial cell line, as an *in vitro* model of the BBB, will be investigated. With previous studies demonstrating the involvement of BIN1 in APP processing through endocytic trafficking, products of APP proteolysis will be analysed in order to elucidate whether the amyloidogenic processing of APP is affected by BIN1 depletion. Furthermore, trafficking of fluorescence-conjugated ligands will be used to analyse whether BIN1 attenuation affects clathrin-dependent and independent forms of endocytosis to further examine the normal functioning of BIN1 in these cells. Ultimately, this study will expand on current knowledge regarding the function of BIN1 in a novel cellular context which may give further insights into the possible mechanisms by which BIN1 mediates risk of sAD. The hypothesis of this study is that the depletion of BIN1 affects APP processing in hCMEC/D3 brain endothelial cells.

Chapter 2

Materials and Methods

All experiments used analytical grade chemicals from either ThermoFisher Scientific (Waltham, Massachusetts, USA) or Sigma (St. Louis, Missouri, USA) unless otherwise indicated.

2.1 The hCMEC/D3 cell line

2.1.1 Origin

The hCMEC/D3 cell line was derived from human temporal lobe microvessels isolated from an adult female with epilepsy in the lab of Prof. Pierre-Olivier Couraud, Cochin Institute, Paris, France and were obtained for the present work from Dr. Ann Ager, Cardiff University. Cells were immortalized by lentiviral vector transduction with the human telomerase catalytic subunit (hTERT) and SV40 large T antigen, as previously described (Weksler et al., 2005).

2.1.2 Maintenance

All culture vessels were pre-coated with 100 µl per cm^2 of 50 µg/ml human plasma fibronectin (Millipore, Billerica, Massachusetts, USA) for at least 30 min which was then removed prior to cell culture. Cells were grown in 75 cm^2 cell culture treated flasks in EGM-2 media, supplied as the EGM-2 BulletKit (Catalogue numbers: CC-3156 and CC-4176, Lonza, Basel, Switzerland) which comprised 475 ml Endothelial Cell Basal Medium-2, 50 µl Hydrocortisone, 500 µl hFGF-B, 125 µl VEGF, 125 µl R3-IGF-1, 125 µl Ascorbic Acid, 125 µl Heparin, 125 µl hEGF and 125 µl GA-1000 supplemented with 25ml FBS (ThermoFisher Scientific)) in a 37°C, 5% CO_2 humidified incubator. Growth medium was

changed every other day and cells passaged once 90-95% confluency was reached. In order to passage cells or for plating, media was aspirated from the culture vessel and cells were washed twice with 10 ml room temperature (RT) phosphate buffered saline (PBS). Cells were incubated at RT in PBS for 10-15 min before replacing this with 8 ml 0.025% Trypsin/EDTA (Lonza) until cells were in suspension, aided by gentle tapping of the side of the flask every 30 seconds. 4ml of 0.025% trypsin neutralizing solution (Lonza) was added to the culture vessel and cell suspension was transferred to a sterile tube. The flask was rinsed with 8 ml 25 mM HEPES Buffered Saline Solution (Lonza) to collect residual cells, and the rinse added to the cell suspension. The harvested cells were centrifuged at 130 x g for 5 min, supernatant removed and cells resuspended in 1 ml EGM-2 media. Cells were split at a ratio of 1:15 and added to a fibronectin-coated culture vessel containing EGM-2 media. The culture vessel was gently rocked to evenly distribute the cells and returned to the 37°C incubator.

2.1.3 Thawing

Culture vessels were pre-coated with human plasma fibronectin, as described in section 2.1.2. One million cells were quickly thawed from a single cryovial in a 37°C bead bath and centrifuged at 130 x g for 4 min. The supernatant was poured off and 1ml of EGM-2 media was added to resuspend the cells. Cell suspension was dispensed into a fibronectin-coated 75 cm^2 culture vessel with 15 ml EGM-2 media. The culture vessel was gently rocked to evenly distribute the cells and returned to the 37°C incubator.

2.1.4 Cryopreservation

Cells were counted using the Trypan Blue (Sigma) exclusion method, as detailed below, in a haemocytometer and pelleted by centrifugation at 130 x g for 5 min. Cells were then resuspended at a concentration of 1 million cells per ml of RT freezing medium (30% FCS (ThermoFisher Scientific), 10% DMSO (Sigma) in EGM2 medium) and 1 ml was dispensed into each cryovial (Greiner, Kremsmünster, Austria) which were placed in a RT Mr Frosty™ freezing container (ThermoFisher Scientific) at -80°C overnight. The next day, cryovials were transferred to liquid nitrogen storage.

2.1.5 Trypan Blue Exclusion

The hemocytometer was cleaned with 70% ethanol before use and a moistened coverslip affixed to the surface. The cell suspension was mixed thoroughly and 20 µl of cells was added to 20 µl 0.4% Trypan Blue (ThermoFisher Scientific) and gently mixed. Using a pipette, the Trypan Blue-treated cell suspension was applied to the hemocytometer until both chambers underneath the coverslip were full, allowing the cell suspension to be drawn out by capillary action. Using a microscope, the live, unstained cells were counted in each set of 16 squares and the average cell count from each set of 16 corner squares was calculated. To calculated the total number of cells per ml, the average was multiplied by 2, to account for the dilution factor, then multiplied by 10^4 to give the number of cells per ml.

2.2 siRNA Transfection

For transfection, cells were plated at 21,000 cells per cm^2 (2 million cells per well of a 6-well plate) of a Nunc cell culture treated multidish (ThermoFisher Scientific) 18-20 hours prior to treatment. For lysates, 6-well plates were used with the volumes described here. Volumes were adjusted accordingly for 12-well and 24-well plates. Custom-designed oligonucleotides were designed *in silico* using Eurofins Genomics (Ebersberg, Germany) as 21mer oligonucleotides with dTdT overhangs for nuclease resistance. Sequences used in this thesis are shown in Table 2.1. Oligonucleotide and Oligofectamine™ transfection reagent (Invitrogen) complexes were pre-formed for 20 min at RT using the optimised concentration of oligonucleotide as indicated in Table 2.1 per 4 µl Oligofectamine in a total volume of 200 µl OptiMEM reduced serum medium (ThermoFisher Scientific). Cells were washed once with OptiMEM and the complex added to give the final oligonucleotide concentration specified in Table 2.1 in a total of 1ml OptiMEM. For each treatment, cells were incubated with media alone, siRNA targeting green fluorescent protein (GFP) to control for off-target effects and target siRNA sequences for 4 hours before 500 µl OptiMEM supplemented with 15% FBS was added directly to cells, to give a final concentration of 5% FBS in the media. After a further 48 hours, cells were processed as required.

Table 2.1 siRNA sequences used to knock down protein expression.

siRNA target	Sequence	Amount added per reaction	Final concentration	Reference
Total BIN1 'a'	5'-CCAGAACCUCAAUGAUGUGdTdT-3'	50 pmol	50 nM	Custom designed
Total BIN1 'b'	5'-GGAGAUGAGCAAGCUCAACdTdT-3'	50 pmol	50 nM	Custom designed
AP2µ2	5'-AAGUGGAUGCCUUUCGGGUCAdTdT-3'	25 pmol	25 nM	(Moody et al., 2015)
CAV1	5'-AGACGAGCUGAGCGAGAAGdTdT-3'	50 pmol	50 nM	(Al Soraj et al., 2012)
GFP	5'-GGCUACGUCCAGGAGCGCAdTdT-3'	To match target siRNA	To match target siRNA	(Moody et al., 2015)

2.3 Protein Quantification

2.3.1 Cell Lysis

Lysates were prepared from the treated cells in 6-well plates using 100 µl per well of lysis buffer (20 mM Tris-HCl (pH 7.5), 150 mM NaCl, 1 mM Na_2EDTA, 1 mM EGTA, 1% Triton, 2.5 mM sodium pyrophosphate, 1 mM beta-glycerophosphate, 1 mM Na_3VO_4, 1 µg/ml leupeptin, Cell Signaling, Danvers, Massachusetts, USA) with 1 mM PMSF added immediately before use, according to manufacturer's instructions. Briefly, conditioned media was removed and stored at -20°C, cells were washed once with PBS then incubated on ice for 5 min, collected using a cell scraper (VWR, Radnor, Pennsylvania), briefly sonicated and centrifuged at 14,000 x g for 10 minutes at 4°C. Supernatant was removed for use and stored at -20°C.

2.3.2 Protein concentration

Total protein concentration of lysate was quantified by Pierce BCA assay (ThermoFisher Scientific) as per manufacturers guidelines. Briefly, 5 µl of each sample was tested in

duplicate alongside a 9-point standard curve ranging from 0-2 mg/ml protein concentration in a flat-bottomed plate. Pierce BCA reagents A and B were added to samples at a ratio of 50:1, respectively, with 200 µl per well and incubated for 30 min at 37°C. Absorbance was read at 562 nm on a uQuant plate reader (Biotek, Winooski, Vermont, USA).

2.3.3 Sample Preparation

Protein samples to be resolved by SDS-PAGE were diluted in ¼ volume of 5X sample buffer (0.125M Tris pH 6.8, 4% (w/v) sodium dodecyl sulfate (SDS), 20% (v/v) Glycerol, 5% 2-mercaptoethanol, 0.001% (w/v) bromophenol blue). Proteins were denatured by boiling samples at 95°C for 5 min prior to loading.

2.3.4 Sodium Dodecyl Sulphate Polyacrylamide Gel Electrophoresis (SDS-PAGE)

The Mini-PROTEAN® Tetra Handcast System (Bio-Rad, Hercules, California, USA) was used for SDS-PAGE. Depending on the molecular mass of the protein of interest, proteins were routinely visualized using 7% or 10% resolving gels (380mM Tris-HCL pH 8.8, 7-8% (v/v) acrylamide (30% (w/v) acrylamide: 0.8% Bis-acrylamide (37.5:1), 0.1% (w/v) SDS, 0.1% (w/v) ammonium persulphate (APS), 0.08% N,N,N'N' – Tetramethylethylenediamine (TEMED)). Isopropanol was layered on the resolving gel to ensure a level interface with the stacking gel. Once the gel had polymerised, the isopropanol was washed off three times with dH_2O and the stacking gel was applied (125mM Tris-HCl pH 6.8, 5% (v/v) acrylamide (30% (w/v) acrylamide: 0.8% Bis-acrylamide (37.5:1)), 0.1% (w/v) SDS, 0.1% (w/v) APS, 0.1% TEMED) with a 10-well comb inserted. Gels were submerged in SDS-PAGE running buffer (25mM Tris-base, 192mM glycine, 1% (w/v) SDS) and 20µg sample loaded per well with 2 µl molecular weight marker (Prism Ultra Protein Ladder, Abcam). Gels were run at 150V for approximately 90 min, dependent on the molecular weight of the protein of interest, until appropriate resolution of the protein standard was achieved.

2.3.5 Western Blotting

Protein was transferred onto 0.2 μm nitrocellulose membranes (GE Healthcare, Amersham, England) for 60 minutes at 85V in transfer buffer (20% methanol in SDS-PAGE running buffer). Blots were blocked in 5% milk for 1 hour, washed three times in PBST (Phosphate Buffered Saline with 0.1% Tween 20) and incubated with the relevant primary antibody in 2% BSA or 1-5% milk in PBST for 2-20 hours, depending on optimised conditions. Blots were washed three times in PBST and incubated with the relevant horseradish peroxidase-conjugated secondary antibody (Vector Laboratories, Burlingame, California) at 1:15,000 in 1-5% milk in PBST. Blots were initially detected using SuperSignal West Dura Extended Duration Substrate (ThermoFisher Scientific) and SuperSignal West Femto Maximum Sensitivity Substrate if a stronger signal was required. Blots were then developed on Amersham hyperfilm (GE Healthcare) using an Ecomax automatic developer (Wolflabs, York, England).

2.3.6 Densitometric Analysis

Signal intensity of protein bands from Western blots was determined by densitometric analysis using ImageJ software, as described in Figure 2.1. The grey mean value for each protein band was measured using a defined identical-sized area and the same for the background of each well. An inverted value was calculated by subtracting the Background values were subtracted from the white pixel value of 255. The inverted background value was subtracted from the corresponding protein of interest inverted value to give the net protein of interest value. The same was carried out for each corresponding housekeeping protein band and a ratio of protein of interest : housekeeping protein was generated. These ratios were then expressed as a percentage of expression in the non-transfected cells.

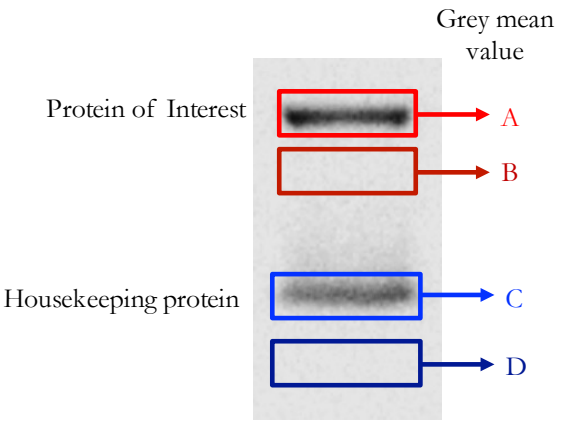

$$\frac{(255 - A) - (255 - B)}{(255 - C) - (255 - D)} = \frac{\text{Net protein of interest}}{\text{Net housekeeping protein}} = \text{Protein of interest : Housekeeping protein ratio}$$

Figure 2.1: The Method used for Densitometry analysis of Western blots

The grey mean value was determined for each protein of interest band (A) and its corresponding background (B) using identical sized rectangles. Values were also obtained for the housekeeping protein (C) and corresponding background (D) by the same method. These values were inverted by subtracting from the white pixel value of 255 and the background inverted value was then subtracted from the corresponding protein inverted value. A ratio of protein of interest to housekeeping protein was then determined for each sample.

2.4 Protein Visualisation

Cells were fixed either by paraformaldehyde (PFA) or methanol prior to immunocytochemistry. The method used is identified in the relevant section.

2.4.1 Paraformaldehyde Fixation

To fix cells, 4% (w/v) paraformaldehyde (PFA) (Sigma) was prepared by dissolving 4 g PFA in 60 ml dH_2O at 60°C and adding a drop of 2M NaOH to adjust the pH. A third of the total volume (33.3 ml) of 3x PBS was then added and the pH adjusted to 7.2 with HCl. The volume was made up to 100 ml with dH_2O and the solution cooled to 4°C. Media was removed and cells were gently washed twice with PBS at RT. Cells were fixed in 4% PFA at RT for 10-15 min before washing three times with PBS. Cells were stored in PBS at 4°C with plates wrapped in parafilm until staining.

2.4.2 Methanol Fixation

Media was removed and cells were gently washed twice with PBS at RT before fixing for 5 min in ice-cold 100% methanol. Cells were washed three times with PBS and stored in PBS at 4°C with plates wrapped in parafilm until staining.

2.4.3 Immunocytochemistry

Round 13 mm glass coverslips (VWR) were pre-sterilised by washing with 70% ethanol, air-drying and exposing to UV light for at least 1 hour. Coverslips were then pre-coated with fibronectin, as previously described in Section 2.1.2. Cells were PFA or methanol-fixed, as described in sections 2.4.1 and 2.4.2. Cells were permeabilised with 0.1% Triton-X (Sigma) in PBS for 15 minutes, blocked with 5% bovine serum albumin (BSA), 5% goat serum, 0.3% Triton-X (all Sigma) in PBS and incubated with the appropriate primary antibodies diluted in antibody diluent (0.1% BSA, 0.3% Triton-X in PBS) overnight at 4°C. Cells were washed 3 x 3 minutes with antibody diluent before incubating with the appropriate secondary antibody diluted in antibody diluent for 2 hours at RT, minimizing light exposure from now on. The Alexa Fluor secondary antibodies used in this thesis were: goat-anti-mouse 594 (1-2 μg/ml), goat-anti-mouse 488 (2 μg/ml), goat-anti-rabbit 594 (2 μg/ml), goat-anti-rabbit 488 (2 μg/ml) and goat-anti-rat 488 (2 μg/ml, all ThermoFisher

Scientific). Cells were washed 3 x 3 minutes with antibody diluent before incubating with 1 μg/ml DAPI for 5 minutes at RT. Cells were washed 3 x 3 minutes with PBS before mounting onto glass slides with ProLong Gold Antifade Mountant (ThermoFisher Scientific). IPS cells were not cultured on coverslips and were instead overlaid with coverslips directly into the well using Vectashield mounting medium (Vectorlabs, Peterborough, England). Plates were imaged on either the Evos FL imaging system (ThermoFisher Scientific), the DMI6000B Inverted Time-lapse Microscope (Leica, Wetzlar, Germany) or the Axio Observer A1 (Zeiss, Oberkochen, Germany) and images processed using LAS AF software (Leica) and ImageJ. For each experiment, negative controls were performed (see Appendix I) using the secondary antibody only, to confirm a lack of background staining.

2.5 Cell Viability Assay

Cell viability following siRNA treatment was assessed using the CellTiter 96 AQueous One Solution Cell Proliferation Assay (Promega, Madison, Wisconsin, USA). Cells were plated and transfected as previously described in Section 2.2 in 96-well cell culture plates. 48 hours post-transfection, cells were incubated with CellTiter 96® Aqueous One Solution Reagent 1-4 hours. Readings were taken at 1, 1.5, 2, 3 and 4 hours on a uQuant plate reader at 490nm. Absorbance readings were plotted against time. The absorbance at 1.5 hours best represented the exponential phase of the curve and was therefore selected for comparisons between siRNA treatments. In addition to BIN-depleted, GFP siRNA-treated cells and non-transfected cells, a control without cells was included to measure background absorbance levels which was subtracted from all other readings.

2.6 Statistical Analysis

Western blots were quantified using ImageJ, as described in Section 2.3.6, And expressed as percentage of the non-transfected control. Absorbance readings from ELISA assays were quantified by comparing to standard curves generated on each plate using GraphPad Prism 7. Data were then normalized to total protein concentration of each sample, calculated as described in Section 2.3.2, and expressed as the percentage of non-transfected control values. Data from flow cytometry experiments were expressed as the geometric mean of fluorescent intensity.

All statistical analysis was calculated using GraphPad Prism 7. For data with sufficient replicates (at least 8), the D'Agostino-Pearson test for normality was used in addition to an F test for equality of variance. For normally-distributed data, where there were only two factors, data were compared to GFP siRNA-treated values using unpaired Student's t tests. For comparisons of more than two factors, ANOVA was used as specified in the appropriate experiments. Data that was not normally-distributed was analysed using the non- parametric Mann-Whitney test, as specified in the appropriate experiments. Unless otherwise stated, a sample size (n) of at least 3 was used for all quantified experiments. N is defined as a sample taken from a separate culture vessel and using separate reagents to all other replicate samples within the experiment.

Chapter 3

Neuronal Differentiation of Human Induced Pluripotent Stem Cells

3.1 Introduction

Cell culture has been the mainstay of biomedical research for decades, providing countless novel insights into normal cellular biology and pathologically processes. *In vitro* culture of human primary cells has limited potential for long term objectives due to the short lifespan of primary cells in culture. Human cell lines, either derived from cancerous tissue or that have undergone artificial immortalization, evade normal cellular senescence and can undergo division indefinitely. Many cell lines are now available for a huge variety of cell types, permitting long term culture and reproducibility. However, the culture of neuronal cells for the study of neurodegenerative disease, in particular, is challenging as mature neurons do not undergo cell division at all. This has largely been overcome through the use of cell lines derived from neuronal tumours, including the mouse and human neuroblastoma cell lines N2a and SH-SY5Y, respectively. These can be differentiated into a neuronal-like phenotype (Pahlman et al., 1984, Tremblay et al., 2010), however still retain the genetic and epigenetic signatures of neuroblastoma tissue which may impact on disease-specific networks in AD (Krishna et al., 2014).

Induced pluripotent stem cells (iPSCs), on the other hand, provide the opportunity to reprogram patient-specific somatic cells and differentiate these into cells of any type whilst retaining the genetic signature of the individual from which they were originally derived. Chapter 3 describes the process of differentiating iPSCs derived from PBMCs into cortical neurons as an *in vitro* model for the study of BIN1 function in the context of AD. While

still a relatively new field, studies researching iPSC models in sAD to date have mainly focused on fibroblast-derived iPSCs (Israel et al., 2012, Kondo et al., 2013). However, with an extensive bank of blood samples alongside genome-wide genotyping data available, the opportunity for furthering genetic leads in PBMC-derived iPSC models offers great scope for disease modelling in AD. Furthermore, much of the *in vitro* research surrounding endocytic mechanisms in AD to date has involved the use of neuroblastoma, neuroglioma or non-neuronal cell lines, such as human embryonic kidney (HEK) or human cervical cancer HeLa cells (Chapuis et al., 2013, Miyagawa et al., 2016). These cannot recapitulate the morphology and physiology of neurons *in vivo*. A gap in the literature is therefore apparent within the AD field to create human cortical neurons from a peripheral blood source.

3.1.1 Discovery of Stem Cells

The presence of stem cells in human cord blood was discovered in 1978 (Prindull et al., 1978), shortly followed by the very first isolation and establishment of embryonic stem cells (ESCs) *in vitro* from mouse blastocysts in 1981 (Evans, 1981). These ES cell lines were among the first demonstrated to grow in culture in an undifferentiated state for long periods, and were capable of differentiating both *in vitro* and *in vivo* by teratoma formation in a mouse host (Evans, 1981). Teratoma formation *in vivo* demonstrates 3-germ-layer differentiation capability and is considered the most rigorous test for pluripotency (Hentze et al., 2009). This was a revolutionary discovery in the field of disease modeling, leading to the creation of gene targeting technology in mouse ES cells in order to create genetically modified mouse models for a host of human diseases.

Human embryonic stem cells (hESCs) were first derived from early embryos in 1998 (Thomson et al., 1998) and were demonstrated to proliferate in an undifferentiated state for 4-5 months, owing to their high telomerase activity, maintaining the potential to differentiate into derivatives of all three embryonic germ layers; endoderm, mesoderm and ectoderm. These cells not only offered insights into developmental events in the human embryo, but also provided a platform by which directed differentiation could offer a potentially limitless source of specific cell types for regenerative medicine and drug discovery. Human pluripotent stem cells (hPSCs), by definition, have the ability to give rise to any cell of the human body and can self-propagate indefinitely in an undifferentiated

state (Thomson et al., 1998). Indeed, in 2000, somatic differentiation of hESCs *in vitro* was demonstrated for the first time (Reubinoff et al., 2000.) By culturing at high density without replacement of the feeder layer, Reubinoff et al. (2000) observed cells at the early neuroectoderm stage develop. These were then isolated and went on to demonstrate morphology and expression of markers characteristic of mature neuronal differentiation (Reubinoff et al., 2000). The possibility of creating hESC-derived cells of any type *in vitro* greatly excited the research community, offering the prospective of novel disease-relevant models, particularly for which standard cell culture lines do not exist and which are difficult to obtain in their primary form from patients, such as neurons.

3.1.2 Induced Pluripotent Stem Cells and Reprogramming

The stem cell field moved rapidly and while hESCs provided a revolutionary research tool, the ethical concerns surrounding their source and the way they are acquired could not be escaped. In 2006, the creation of pluripotent stem cells by the ectopic expression of just four genes led to the invention of iPSCs (Takahashi and Yamanaka, 2006). The four factors were selected from 24 candidate genes based on their hypothesised role in maintaining ESC identity. By systematically withdrawing factors one at a time from the pool of factors transduced into mouse embryonic fibroblasts (MEFs), Takahashi and Yamanaka (2006) determined Octamer-binding transcription factor 4 (*OCT4)*, sex determining region Y box 2 (*SOX2), c-Myc* and kruppel-like factor 4 (*KLF4)* were necessary and sufficient for reprogramming. By retroviral transduction, the four factors were incorporated into the genome of terminally differentiated MEFs, reprogramming them back to a pluripotent state. This was later replicated in adult human fibroblasts, where pluripotency was characterised by the ability to form teratomas *in vivo* and embryoid bodies *in vitro* that expressed markers of all three germ layers (Takahashi, 2007). The ability to generate patient-specific human iPSCs and differentiate them into pathophysiologically-relevant cell types offers the potential for previously inaccessible insights into disease mechanisms. Development of human disease can be observed at the single cell level using models that are isogenic with the patient from whom they were derived. For the AD field, this was revolutionary; allowing direct observation of genetic variation on phenotype while eliminating the need to obtain primary brain tissue. However, this procedure presents challenges, while being technically difficult in itself, obtaining fibroblasts from elderly

subjects and reprogramming cells at this late stage may add an additional level of complexity.

There are multiple methods to generate iPSCs. Initially, retroviruses were used to insert their DNA into the genome of the somatic cell (Takahashi and Yamanaka, 2006). However, integration of viral DNA into the host genome carried the risk of multiple insertions and tumorigenicity, posing safety concerns for potential gene therapy applications (Okita et al., 2007). Non-integrating reprogramming methods were therefore sought, such as the use of Sendai Virus (SeV) vectors, which replicate in the form of negative-sense single-stranded RNA in the cytoplasm of infected cells (Fusaki et al., 2009). Each vector contains one of the four Yamanaka factors and replicates independent of the cell cycle, producing very high copy numbers of the target gene without the requirement for cell division to occur. The SeV is lost from the iPSCs after propagation for 10-13 passages (Chen et al., 2013) so no genomic integration or viral remnants remain. In addition, SeV can infect a broad host range and is non-pathogenic to humans. The efficiency of iPSC reprogramming by SeV has been shown to significantly surpass that of retroviral transduction (Takahashi, 2007,Fusaki et al., 2009). The reprogramming efficiency was calculated as the number of alkaline phosphatase-positive, ESC-like colonies formed per number of infected cells seeded, which reached 1% using SeV (Fusaki et al., 2009) compared to just 0.02% using retrovirus (Takahashi, 2007).

3.1.3 Stem Cell Characterisation

Stem cells are characterised by their capacity for indefinite self-renewal and differentiation into all three germ layers. Therefore, the confirmation of true pluripotency is a prerequisite for any experiment involving the use of ESCs or iPSCs. Pluripotency can be determined by the expression of well characterised and widely accepted pluripotency markers, including alkaline phosphatase, OCT4, TRA-1-60, SSEA4 and NANOG and demonstrating the ability of cells to differentiate into ectoderm, endoderm and mesoderm by the formation of embryoid bodies (Baghbaderani et al., 2016). Karyotype analysis ensures the starting material undergoing the reprogramming process is normal and that no chromosomal abnormalities are incurred in the reprogramming and expansion process.

3.1.4 Induction of Neural Fate

For neurodegenerative disorders, whereby disease-relevant cell types are difficult to obtain in their primary form, iPSCs have been used to create neuronal *in vitro* models. While this field is still in its infancy, several groups have demonstrated neuronal differentiation to produce cellular models to study AD (Israel et al., 2012, Shi et al., 2012b, Kondo et al., 2013, Vazin et al., 2014). Neural induction represents the earliest step in the determination of cell fates from the ectoderm (Chambers et al., 2009). Inhibition of bone morphogenetic protein (BMP) signaling activates neural rather than epidermal fates in ectodermal cells while inhibition of the activin/nodal branch of the transforming growth factor beta (TGFβ) signaling pathway prevents induction of mesodermal gene expression in ectodermal cells (Hemmati-Brivanlou and Melton, 1994). Efficient neurogenesis in chemically defined medium is based on minimising these extrinsic and intrinsic signals that divert differentiation to alternate fates and allowing cells to follow the default model of neurogenesis. Inhibition of both the activin/nodal and BMP arms of the TGFβ signaling pathways, through dual inhibition of SMAD (an acronym from the fusion of *Caenorhabditis elegans Sma* genes and the *Drosophila Mad*, Mothers against decapentaplegic) signaling, was shown to be necessary for rapid and complete neural conversion of hESCs (Chambers et al., 2009), forming the basis by which different neuronal cell types can be created. SB431542, a small molecule activin/nodal receptor kinase inhibitor, and Noggin, an endogenous mammalian BMP inhibitor (Groppe et al., 2002), were administered to hESCs and iPSCs for an 11-day treatment period resulting in uniform neural conversion (Chambers et al., 2009). Derivation of relevant neuron subtypes, including motor neurons and dopamine neurons, was subsequently demonstrated presenting an efficient, defined and robust platform for the rapid generation of iPSC-derived neurons.

3.1.5 Cortical Differentiation

3.1.5.1 Human neurulation

During human embryonic development, the process of neurulation takes place to form the neural tube, the embryonic structure that ultimately forms the brain and spinal cord. The neural tube develops from elongated neural plate cells of the ectoderm migrating towards the midline of the embryo where they form the neural groove (Caviness et al., 1995). This

then fuses at the dorsal midline, creating a hollow neural tube (O'Rahilly and Muller, 1994). Induction of neural fate *in vitro* results in the cells undergoing similar morphological changes in the formation of neural rosettes (Shi et al., 2012c). These rosettes bear striking resemblance to the neural tube *in vivo* with a radially arrangement of progenitor cells possessing apical-basolateral polarity (Shi et al., 2012a). Neural rosettes are the developmental signature of neural precursors *in vitro*, from which neuronal subtypes then develop.

3.1.5.2 Corticogenesis in vitro

In order to create a neuronal model for the study of AD, the desired neuronal subtype must be designated to direct iPSCs down this lineage. Early histopathological studies reported widespread damage and loss of cortical and hippocampal neurons in AD brains (Mann et al., 1985). Pyramidal neurons, which constitute at least 70% of the total neuron population in the healthy mammalian cortex (Hendry et al., 1987), were shown to be particularly affected by NFT pathology in AD (Mann et al., 1985). Cortical pyramidal neurons are thought to utilise the excitatory amino acid transmitter glutamate and disruption of glutamatergic circuits is associated with cognitive impairment in AD (Francis et al., 1993). The creation of cortical glutamatergic projection neurons *in vitro* has been demonstrated by several groups through directed differentiation of iPSCs (Shi et al., 2012a, Espuny-Camacho et al., 2013 Vazin et al., 2014). The adult cortex undergoes development by the stereotyped generation of six layers in a temporal manner from deep layer neurons through to the upper layers (Leone et al., 2008). This process takes over 70 days in humans and just 6 in mice (Caviness et al., 1995). The identity and proportions of different types of cortical projection neurons can be defined by their combinatorial expression of a core set of transcription factors (Shi et al., 2012c) and depicted in Figure 3.1.

Two major classes of neurons are found in the neocortex; interneurons and projection neurons (Leone et al., 2008). While interneurons make local connections within the neocortex and are largely inhibitory, excitatory projection neurons reach their axons to distant brain targets. Cortical projection neurons are derived from mitotically active progenitor cells found within two populations: radial glial cells in the ventricular zone and radial glia-derived basal progenitors in the subventricular zone (Leone et al., 2008). Newborn neurons migrate towards the margin of the cerebral wall and take their positions

in the cortical plate in an inside-out sequence, with newly arriving cells migrating through existing cell layers to reach the top of the plate (Bystron et al., 2008). The cortex is organised radially into six layers (Figure 3.1) with the first neurons to exit the cell cycle from the ventricular zone forming the deepest cortical layers, 6 and 5 while the subventricular zone provides the source of neurons in layers 2-4. Each layer contains neurons with distinct morphologies, neurotransmitter phenotype and projection patterns. Layer 1, referred to as the molecular layer, is the latest born upper layer which contains many dendritic and axonal synapses extending from the lower levels of the neocortex with very few cell bodies (Leone et al., 2008). Layers 2 and 4 correspond to the external and internal granule layers, respectively, and are composed of many granular neurons with very small cell bodies. These encase layer 3, the external pyramidal layer containing small and medium-sized pyramidal neurons while layer 5 comprises the internal pyramidal layer with cells larger than those in layer 3 (Leone et al., 2008). Finally, layer 6 has a very heterogeneous composition and is therefore known as the multiform layer with all morphological forms present.

While the layers of the cortex were primarily defined based on morphological assessment, a large extent of cellular heterogeneity exists across the cerebral cortex rendering classification based on developmental age and cellular morphology alone difficult (Leone et al., 2008). However, a number of molecular markers have been identified for neurons of distinct cortical layers, many of which are not expressed uniformly within a given layer, but can be used to confirm cortical developmental stages *in vitro*. Well-recognised markers of cortical development stages including primary progenitor, secondary progenitor and layer-specific markers are indicated in Table 3.1 and have been used in several studies demonstrating cortical development from iPSCs (Chambers et al., 2009, Shi et al., 2012a, Shi et al., 2012c, Espuny-Camacho et al., 2013).

3.1.5.3 Directed cortical differentiation in vitro

Directed differentiation of iPSCs *in vitro* can generate all classes of cortical neurons over a period of several weeks, providing a suitable model by which patient-specific neurons can be examined to investigate the aetiology of AD (Shi et al., 2012c). These human iPSC-derived neurons exhibited action potential generation and formed functional excitatory glutamatergic synapses after 50 days in culture. The process encapsulated a number of

crucial steps, starting with the formation of a complex population of cortical stem and progenitor cells, followed by an extended period of cortical neurogenesis, astrocyte genesis, neuronal terminal differentiation and the acquisition of electrophysiological properties, culminating in synaptogenesis and network formation (Shi et al., 2012c). An effective cellular model for AD should not only accurately represent the physiology of the appropriate cell type, but also develop the relevant molecular pathology including Aβ aggregation and tau hyperphosphorylation in a reproducible manner within a practical time frame. One of the major hurdles facing iPSC cell models within AD research is whether a disease of ageing that takes decades to manifest in humans can be effectively recapitulated *in vitro* within a realistic timescale.

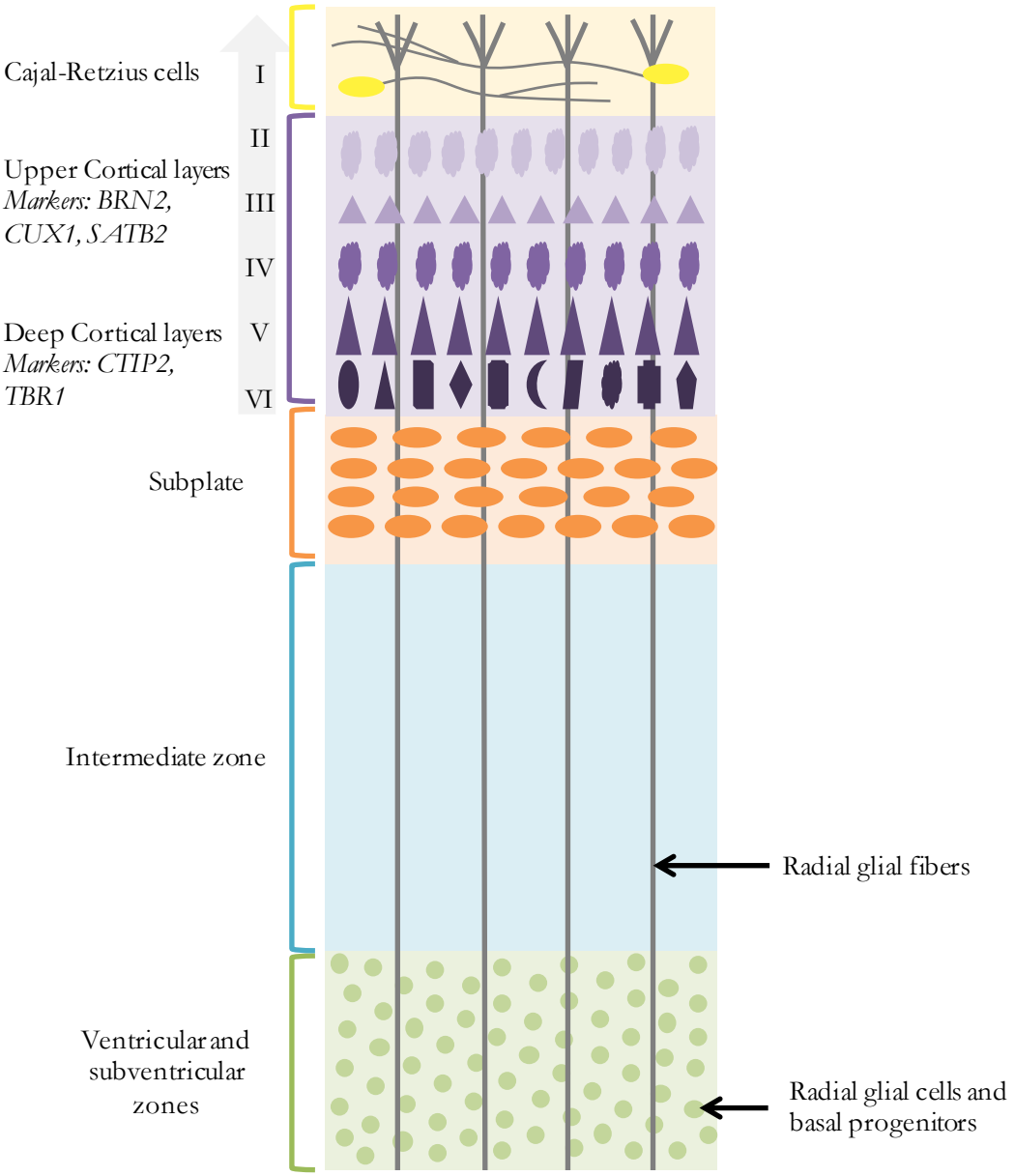

Figure 3.1: Cortical development in vivo

A schematic adapted from depicting the layers of the human cortex, and the pattern of layer-specific cortical neuron markers used in the present study. Newly-born neurons migrate through the intermediate zone to form the cortical layers in an inside-out arrangement, from layer VI to layer I.

3.1.6 Stem Cell Models of Familial AD

Much of what we know about the molecular mechanisms of sAD is based on studies of fAD. Yagi et al. (2011) were the first to successfully demonstrate AD-related phenotypes in iPSC-derived neuronal models of fAD by reprogramming fibroblasts derived from a patient with mutations in the *PSEN1* (A246E) and *PSEN2* (N141I) genes. Both mutations have previously been reported to increase Aβ42 levels in human plasma, patient-derived fibroblasts and transgenic mice (Scheuner et al., 1996, Borchelt et al., 1996, Oyama et al., 1998). Neurons from these fAD-iPSCs had increased Aβ42 secretion and an increased Aβ42:Aβ40 ratio compared to controls, recapitulating the pathological mechanisms established for these fAD mutations (Yagi et al., 2011). However, abnormal tau protein accumulation or tangle formation was not detected suggesting the culture period of 2 weeks may not have been sufficient for tau pathology to develop. These results were subsequently supported by Mahairaki et al. (2014) who found the extracellular Aβ42:Aβ40 ratio was significantly higher in iPSC-derived neurons from patients with the A246E *PSEN1* mutation compared to controls. (Sproul et al., 2014) took a different approach to modelling fAD using iPSCs by not continuing differentiation right through to the neuron stage. Instead, comparisons between control cells and those with the A246E *PSEN1* mutation were made at the neural precursor cell stage as this was considered a more homogenous population than the wide variety of neurons produced by general neuronal differentiation protocols at the time (Sproul et al., 2014). Interestingly, greater ratios of Aβ42 to Aβ40 were reported in *PSEN1* neural precursors relative to their control counterparts and this elevated ratio was even more prominent in neural precursor cells compared to the original fibroblasts from which they were derived, demonstrating more pronounced Aβ-related changes following neuronal differentiation (Sproul et al., 2014).

3.1.7 Modelling Sporadic AD through Patient-derived iPSCs

The success in demonstrating AD-related phenotypes in iPSC-derived neurons harboring fAD mutations led studies to explore the possibility of modelling sAD in this manner. Israel et al. (2012) generated two iPSC lines from sAD patients and two from patients with an *APP* duplication before differentiating them into neurons by BMP and activin/nodal inhibition and subsequent fluorescence-activated cell sorting (FACS) purification. The cell surface marker signature CD184(+)/CD271(-)/CD44(-)/CD24(+) was used for

purification, which had previously been identified as a cell-surface signature for isolating neural stem cell populations (Yuan et al., 2011). Higher levels of secreted Aβ40 were reported compared to non-demented control neurons in both fAD lines and one sAD line but Aβ42 did not reach sufficient detection levels due to the small number of purified neurons (Israel et al., 2012). Tau phosphorylation at Thr231 correlates with neurofibrillary tangle number and cognitive decline (Buerger et al., 2006) therefore the amount of phosphorylated tau at Thr231 (p-tau) was measured relative to total tau in fAD, sAD and control neurons. Neurons from both fAD patients showed a significant increase in p-tau/total tau compared to controls, as did the same sAD line that showed increased Aβ40 previously (Israel et al., 2012). GSK-3β levels were also investigated as this kinase can phosphorylate tau at Thr231 *in vitro* and colocalises with NFT in AD post-mortem brain tissue (Goedert et al., 1994, Buerger et al., 2002, Buerger et al., 2006). The cell lines showing an increase in p-tau also showed significant increases in the amount of GSK-3β lacking phosphorylation at Ser 9, indicating its active form. Collectively, this study demonstrated strong correlations between Aβ40, p-tau/total tau and active GSK-3β in fAD and sAD-derived neuronal cultures suggesting AD-related phenotypes were achieved (Israel et al., 2012). However, the second sAD line showed no difference in these measures compared to controls, illustrating the difficulties in reproducibility when modelling a complex disease with lines from different individuals. This also highlights that AD in different individuals is likely attributed to defects in different cell types which a neuronal model alone cannot recapitulate.

Subsequently, Kondo et al. (2013) generated seven iPSC lines, five from two fAD patients each carrying a different *APP* mutation and two sAD lines from unrelated patients. The authors differentiated iPSCs into cortical neurons by BMP and activin/nodal inhibition and showed that Aβ oligomers accumulated inside iPSC-derived neurons derived from a patient with the *APP* (E693D) mutation and one of the patients with sAD. Aβ oligomers were not present in *APP* (V717L) iPSC-derived neurons but there was an increase in the extracellular Aβ42/Aβ40 ratio, suggesting a distinction in pathology between intracellular and extracellular Aβ production. Again, one of the sAD lines failed to show the AD-related phenotypes measured in this study, emphasizing the importance of individual differences in AD and the selection of patients for related studies.

These studies provide an important proof-of-principle for the field of iPSC modelling in the context of AD; that iPSC technology can be used to observe phenotypes of AD patients, despite the disease taking decades to manifest *in vivo* (Israel et al., 2012, Kondo et al., 2013). However, they also illustrate the challenges presented by patient-derived iPSC models of a complex disease, without a known cause, with much inter-individual variability making reproducibility difficult. Minimising intra-individual variability, however, is paramount and was demonstrated in the study by Israel et al. (2012) with each individual represented by three clonal iPSC lines. In order to map out the metabolic pathways involved in AD pathogenesis, patient-derived iPSC models should be informed by genetic data to determine the appropriate cell type to create and functional assays to pursue.

3.1.8 Aims of this Chapter

While the aforementioned studies used dermal fibroblasts as a starting source, the vast repositories of blood available, in addition to the invasive nature of skin biopsies, makes PBMCs an attractive source for iPSC creation. As part of the large scale GWAS conducted by the IGAP consortium, an untapped potential resource of patient blood samples with GWAS data for over 1500 participants is available for analysis. While still a novel field, transgene-free iPSCs can be reliably produced directly from peripheral blood mononuclear cells (Trokovic et al., 2014). Differentiation of PBMC-derived iPSCs into cortical neurons, however, is yet to be documented. Therefore, the initial aim of this work is to characterise and successfully differentiate PBMC-derived iPSCs into cortical glutamatergic neurons. This nature of work has not yet been carried out in my home lab and it will therefore be the aim to set up and establish these iPSC and differentiation protocols within the lab for intended future use on participant-derived iPSCs.

The creation of these iPSCs will provide an *in vitro* model in which early pathology features of AD can be modelled such as endocytic pathway abnormalities which have been shown to precede the extracellular deposition of Aβ (Cataldo et al., 2000). In the aforementioned study by Israel et a. (2012), accumulation of large Rab5-positive early endosomes was observed in neurons from sAD patients, which are evident in pyramidal neurons of the post-mortem brain from early stage AD patients (Cataldo et al., 2000, Israel et al., 2012). As an early disease phenotype, the regulation of endocytosis presents an ideal pathway to study through iPSC creation.

The creation of iPSC-derived neurons from patients with known genotypes would allow novel insights into cellular mechanisms in AD. Previous work investigating the role of AD susceptibility genes *in vitro* have largely involved the use of neuronal-type cell lines, such as the SHSY5Y neuroblastoma cell line (Glennon et al., 2013) and the H4 neuroglioma cell line (Thomas et al., 2016). While hugely informative, these are not ideal models as they only provide a neuronal-like phenotype and there is a need for a more representative *in vitro* neuronal model to accurately assess the function of these genes. The primary aim of this chapter is to optimise a protocol for differentiation of cortical neurons from PBMC-derived iPSCs with a view to utilizing the IGAP GWAS cohort (Harold et al., 2009) for iPSC modelling in the future. This will create a more representative *in vitro* neuronal model to study the role of AD susceptibility genes in endocytic function.

3.2 Experimental Design

3.2.1 Induced Pluripotent Stem Cells (iPSCs)

3.2.1.1 Isolation and storage of PBMCs

Processing of blood samples and the isolation of PBMCs was carried out by Newcells Biotech (Newcastle, England) by the following methods. A blood sample donated from a 30-year-old female with a chromosome 20 duplication was separated by Ficoll-Paque® density gradient, with the PBMC layer removed and washed in RPMI 1640 medium (ThermoFisher Scientific) and centrifuged. This was repeated and cells were resuspended in 10% DMSO (Sigma) in FBS (ThermoFisher Scientific). Cells were frozen in a rate-controlled freezer at -80°C and transferred to liquid nitrogen for long-term storage.

3.2.1.2 Reprogramming

PBMCs were reprogrammed using Cytotune 2.0 Sendai Reprogramming Kit (ThermoFisher Scientific) according to the manufacturer's instructions by Lyle Armstrong and colleagues at Newcells Biotech. The kit utilises SeV particles to deliver the Yamanaka factors *Klf4, Oct3/4, Sox2* and *c-Myc* within a single transfection. Twenty-one days post-transfection, clonal iPSC colonies were picked and cultured for expansion, according to section 3.2.1.3

3.2.1.3 Maintenance

Culture vessels were coated with Matrigel matrix (Corning, New York, USA), using 1 ml per well of a 6-well plate at 37 °C for at least 1 hour and washed with RT PBS prior to plating of cells. iPSCs were cultured on matrigel-coated vessels in mTeSR1 medium (Stem Cell Technologies, Vancouver, Canada) at 37°C in a 5% CO_2 humidified chamber. Media was warmed to 37°C and replaced every day. All cell culture was carried out in sterile conditions in a biosafety cabinet. When iPSCs reached 70% confluency, colonies were cleaned manually for differentiated areas using a 10 µl pipette tip. This involved removing any cells forming dense clumps in the centre of colonies or those losing characteristic iPSC

morphology, such as round defined borders and high nuclear:cytoplasm ratio. Cells were washed once with RT PBS and once with 0.02% EDTA (Lonza) before incubating for 2-5 min in 0.02% EDTA at 37°C. EDTA was then carefully removed and cells were flushed with RT mTeSR1 media to allow resuspension of small clumps of cells. Cells from one well of a 6-well plate were then divided between 3-6 matrigel-coated wells for expansion, with 1.5 ml mTeSR1 per well, manually shaken to allow even distribution and left to attach at 37°C for at least 24 hours before the first media change.

3.2.1.4 Cryopreservation

The iPSC cultures were cleaned for areas of differentiation as previously described in Section 3.2.1.3. Cells were washed with RT PBS and RT 0.02% EDTA before incubating in 0.02% EDTA for 2-5 min at 37°C. EDTA was carefully removed and cells flushed with cold mTeSR1 media. Cells were pooled from all dishes and centrifuged at 200 x g for 4 min before resuspending in cold mTeSR1 medium. Cells were counted according to the trypan blue exclusion method (Chapter 2, Section 2.1.4) and resuspended in equal volumes of mTeSR1 and 2x freezing medium (20% DMSO, 60% FBS, 20% knockout (KO)-DMEM) to achieve 1 million cells/ml. Cryovials containing 1 ml cells each were transferred to a chilled Mr Frosty and stored at -80°C overnight. Cryovials were transferred to liquid nitrogen storage the following day.

3.2.1.5 Thawing

IPSCs were removed from liquid nitrogen and quickly thawed by swirling in a 37°C bead bath until only a small ice crystal remained. Cells were transferred to a 15 ml centrifuge tube and 11 ml mTeSR1 with 10 μM Y-27632 dihydrochloride (inhibitor of Rho-associated, coiled-coil containing protein kinase (ROCK), Abcam) at RT was added dropwise. Cells were washed by centrifugation at 200 x g for 5 min and resuspended in mTeSR1 with 10 μM Y-27632 dihydrochloride at RT. The vial of cells was divided between two wells of a matrigel-coated 6-well plate with 80% in the first well and 20% in the second and manually shaken in vertical and horizontal motions to allow even plating. Cells were left to attach for at least 24 hours in the incubator before the first media change.

3.2.2 Immunofluorescence Staining

Immunocytochemistry was used to confirm expression of key pluripotency and differentiation markers. Cells were fixed in plates with 10% neutral buffered formalin solution (Sigma) for 15-20 min at RT before washing 3x 5 min with 500 µl PBS. If storing long-term, 1 drop of 10% sodium azide (0.5g sodium azide (Sigma) in 5 ml dH_20) was added to each well before storing at 4°C. Immunocytochemistry was carried out as previously described in Chapter 2, Section 2.4.3 with the antibodies used in Table 3.1: Primary antibodies used in . For surface markers, SSEA4 and Tra-1-60, the permeabilisation step was omitted. As cells were grown in plates and not plated onto coverslips, cells were mounted by adding a drop of Vectashield directly onto the cells and covering with a glass coverslip. Cells were then imaged using either the Evos FL imaging system or the Leica DMI6000B Inverted Time-lapse Microscope and images processed using LAS AF software and ImageJ. For each experiment, negative controls were performed (see Appendix I) using the secondary antibody only, to confirm a lack of background staining.

Table 3.1: Primary antibodies used in Chapter 3

Antibody (clone)	**Antigen location**	**Species**	**Supplier**	**Concentration**	**Expression**
OCT4	Nucleus	Mouse	Santa Cruz	4 µg/ml	Pluripotent stem cells
SOX2	Nucleus	Rabbit	Millipore	10 µg/ml	Pluripotent stem cells
Tra-1-60 (2A6)	Cell membrane	Mouse	Abcam	20 µg/ml	Pluripotent stem cells
SSEA-4 (MC813)	Cell membrane	Mouse	Abcam	0.3 µg/ml	Pluripotent stem cells
Nanog	Nucleus	Rabbit	Abcam	2 µg/ml	Pluripotent stem cells
AFP	Cytoplasm	Rabbit	Dako	2.8 µg/ml	Endoderm
SMA (ASM-1)	Cytoplasma, cytoskeleton	Mouse	Millipore	1 µg/ml	Mesoderm
TUJ1 (Poly18020)	Cytoplasma, cytoskeleton	Mouse	Biolegend	1 µg/ml	Ectoderm Neural lineage
PAX6 (Poly19013)	Nucleus	Rabbit	Biolegend	6.67 µg/ml	Primary progenitor cells
FOXG1	Nucleus	Rabbit	Abcam	3.33 µg/ml	Primary progenitor cells
Nestin (10C2)	Cytoplasm	Mouse	Abcam	3.33 µg/ml	Primary progenitor cells
Ki-67 (B56)	Nucleus	Mouse	BD Biosciences	0.42 µg/ml	Cycling cells
CTIP2 (25B6)	Nucleus	Rat	Abcam	3.33 µg/ml	Deep-layer neurons
TBR1	Nucleus	Rabbit	Abcam	3.3 µg/ml	Layer 1 and deep layer neurons
TBR2	Nucleus	Rabbit	Abcam	5 µg/ml	Secondary progenitor cells
CUX1(M-222)	Golgi	Rabbit	Santa Cruz	0.67 µg/ml	Upper layer neurons
BRN2 (H-60)	Nucleus	Rabbit	Santa Cruz	0.5 µg/ml	Upper layer neurons
SATB2 (SATBA4B10)	Nucleus	Mouse	Abcam	0.1 µg/ml	Upper layer neurons

3.2.4 Spontaneous Differentiation into Embryoid Bodies

IPSCs were cultured until 70–80% confluency was reached and cleaned of differentiated areas, as described in section 3.2.1.3. Media was aspirated and cells were washed twice with RT PBS. Fresh embryoid body (EB) medium (20% Knockout Serum Replacement, 1% GlutaMAX, 1% non-essential amino acids, 0.1mM 2-mercaptoethanol in KO-DMEM/F-12, all ThermoFisher Scientific) was added to each well. Wells were scored with a 26-gauge needle (ThermoFisher Scientific) into a grid of 10x10 sections and cells were gently scraped off the surface in large clumps using a cell scraper. IPSC colonies were transferred to a non-treated bacterial grade dish (Corning) and incubated at 37°C. Media was replaced every other day by transferring the entire cell suspension to a 15 ml centrifuge tube and allowing colonies to settle at the bottom for 5 min. The supernatant was then removed and fresh EB medium added to cells and the suspension returned to the dish. After 4 days the EBs were transferred to 0.1% gelatin-coated 24-well plates to allow attachment and further differentiation. EBs were cultivated for a further 16 days before fixing in 10% formalin solution and staining for AFP, SMA and TUJ1, markers of endoderm, mesoderm and ectoderm respectively, as previously described in Section 3.2.2.

3.2.5 Cortical Neuron Differentiation

Neural induction was based on the SMAD inhibition method (Chambers et al., 2009), previously described in Section 3.1.4, with the use of the small molecule inhibitors LDN193189 (Stemcell Technologies, Cambridge, UK) and SB431542 (Tocris Bioscience, Bristol, England) which inhibit BMP type I receptors and TGF-β type I receptor activin receptor-like kinases, respectively. The cortical differentiation protocol was adapted to feeder-free culture conditions from that published by (Shi et al., 2012a). This protocol provided detailed descriptions of a simple and robust culture system to generate both deep- and upper-layer excitatory neurons from hPSCs. Unless otherwise stated, all media was added to cells pre-warmed to 37°C and cells were incubated at 37°C in a 5% CO_2 humidified chamber.

3.2.5.1 Preparation of iPSCs for neural differentiation

Plates were coated with growth factor-reduced Matrigel (Corning) using 1 ml per well of a 6-well plate for 1 hour at 37°C. Wells were washed with PBS before iPSCs were plated in mTeSR1 medium at a density of approximately 45,000-50,000 cells/cm^2, as described in Section 3.2.1.3, and maintained until 70-80% confluent up to a maximum of 4 days with daily media changes.

3.2.5.2 Neural induction

To commence neural induction, cells were washed with PBS and cultured in N2B27 medium (2/3 DMEM/F-12, 1/3 Neurobasal, 1% L-Glutamine, 0.5% N2 supplement, 1% B-27 supplement without vitamin A and 0.1 mM 2-mercaptoethanol, all Life Technologies) with 100 nM LDN193189 and 10 nM SB431542. This was denoted Day 0, or 0 days *in vitro* (DIV). Cells were cultured for 8 days with half media changes every other day. Once a tightly compacted neuroepithelial sheet had formed at 8 DIV, media was changed to N2B27 with 10μM Y-27632 dihydrochloride and cells incubated at 37°C for 1 h. This media was then removed and kept aside while cells were washed once with RT PBS and incubated with 0.02% EDTA for 1-2 min at 37°C. EDTA was then carefully removed and the N2B27 media with 10μM Y-27632 dihydrochloride, saved from the previous step, was added to cells. The surface of the well was gently scratched with the tip of a 5 ml serological pipette in a zig-zag pattern, holding it perpendicular to keep large clusters of cells which were then gently triturated off the surface. Cells were collected and added to the appropriate amount of N2B27 with 10μM Y-27632 dihydrochloride to split the cells at a 2:3 ratio (based on the area of the wells). Cells were divided into plates which had been coated in 25 μg/ml fibronectin (Millipore) for 1 hour at 37°C and washed with RT PBS. Plates were shaken vertically and horizontally to allow even distribution of cells. At 13 DIV, a sample of cells were fixed and stained as previously described in Section 3.2.2 for PAX6, TUJ1, FOXG1 and Nestin to confirm neural progenitor identity, as per Table 3.1.

3.2.5.3 Neural maturation

After passaging onto fibronectin-coated plates, cells were cultured for a further 8 days with half media changes every other day. Upon widespread appearance of neural rosettes at 16

DIV, cells were passaged at a ratio of 1 well : 3 wells onto poly-D-lysine (10µg/ml, Sigma) and Laminin (10µg/ml, ThermoFisher Scientific) coated plates. For this second passage, the media was removed and cells washed with PBS. Cells were incubated in 0.02% EDTA for 1-2 min at 37ºC before removing this and adding N2B27 medium. The plate surface was scratched with the tip of a 5ml serological pipette, this time keeping small clusters of cells. The cells were then collected into a 15 ml centrifuge tube and resuspended before plating. At 21 DIV, a sample of cells was fixed and stained for CTIP2, TBR1, PAX6, TUJ1, TBR2 and Ki-67, as described in section 3.2.2, to identify deep-layer neuron formation and the expression pattern of neural rosettes. Remaining cells were then cultured in N2B27 medium with media changes every other day until 26 DIV when B-27 supplement with vitamin A replaced B-27 supplement without vitamin A in the N2B27 media. Half media changes took place every day and cells were cultured for up to 90 days. A sample of cells were fixed and stained for CTIP2, TBR1, CUX1, TUJ1 and BRN2 at 35 DIV and CUX1, TUJ1, BRN2 and SATB2 at 50 DIV, as described in section 3.2.2, in order to monitor the development of deep-layer and upper-layer cortical neurons.

3.3 Results

3.3.1 iPSC Characterisation

The characterisation of iPSCs for pluripotency is essential to ensure a uniform starting population of pure iPSCs for differentiation. For the current project, characterisation assays were performed as guided by the StemBANCC iPSC workflow (www.stembancc.org) and included immunocytochemical staining for hPSC markers and spontaneous *in vitro* EB differentiation. A thorough characterisation including karyotype analysis and gene expression profiling constitute a considerable expense and were therefore not deemed necessary in this optimisation stage but would be carried out an any future newly generated iPSC line.

3.3.1.1 Pluripotency markers

In terms of morphology, iPSCs formed characteristic ESC-like colonies with smooth borders and a high nuclear to cytoplasmic ratio (Figure 3.2). Intracellular transcription factors OCT4, SOX2 and Nanog and the extracellular membrane glycosphingolipid stage-specific embryonic antigen 4 (SSEA-4) and the Tra-1-60 antigen are well-recognised markers used to confirm pluripotency. These are expressed in hPSCs and are lost upon differentiation (Schöler et al., 1989, Loh et al., 2006, Choi et al., 2011, Barrett et al., 2014). OCT4 and SOX2 were both readily expressed in the vast majority of iPSCs, showing uniform expression within colonies (Figure 3.3). Very few, if any, cells were detectable that lacked OCT4 and SOX2 expression and both proteins colocalised with DAPI, showing their expression within the nuclei. NANOG is a homeodomain-containing transcription factor that is essential for the maintenance of pluripotency (Silva et al., 2009). Uniform expression of Nanog was apparent throughout iPSC colonies, showing diffuse expression throughout the cytoplasm of iPSCs (Figure 3.3). SSEA-4 and Tra-1-60 are stage-specific embryonic antigens that are tightly regulated during embryogenesis and widely used as PSC markers. The Tra-1-60 antibody reacts with an epitope of a proteoglycan on the cell surface of hPSCs (Schopperle and DeWolf, 2007) and is widely used as a marker of identifying and isolating ESCs and iPSCs. Both cell surface antigens showed widespread cell surface expression in iPSC colonies (Figure 3.3). Tra-1-60 cell surface expression showed variation

across the colony with strong expression in some cells and weaker expression in others but this did not follow a specific pattern. SSEA4 showed more uniform expression across the cell surface of iPSCs, with slightly stronger expression observed at the colony edges. Collectively, the positive expression of these proteins confirmed the pluripotent state of iPSCs.

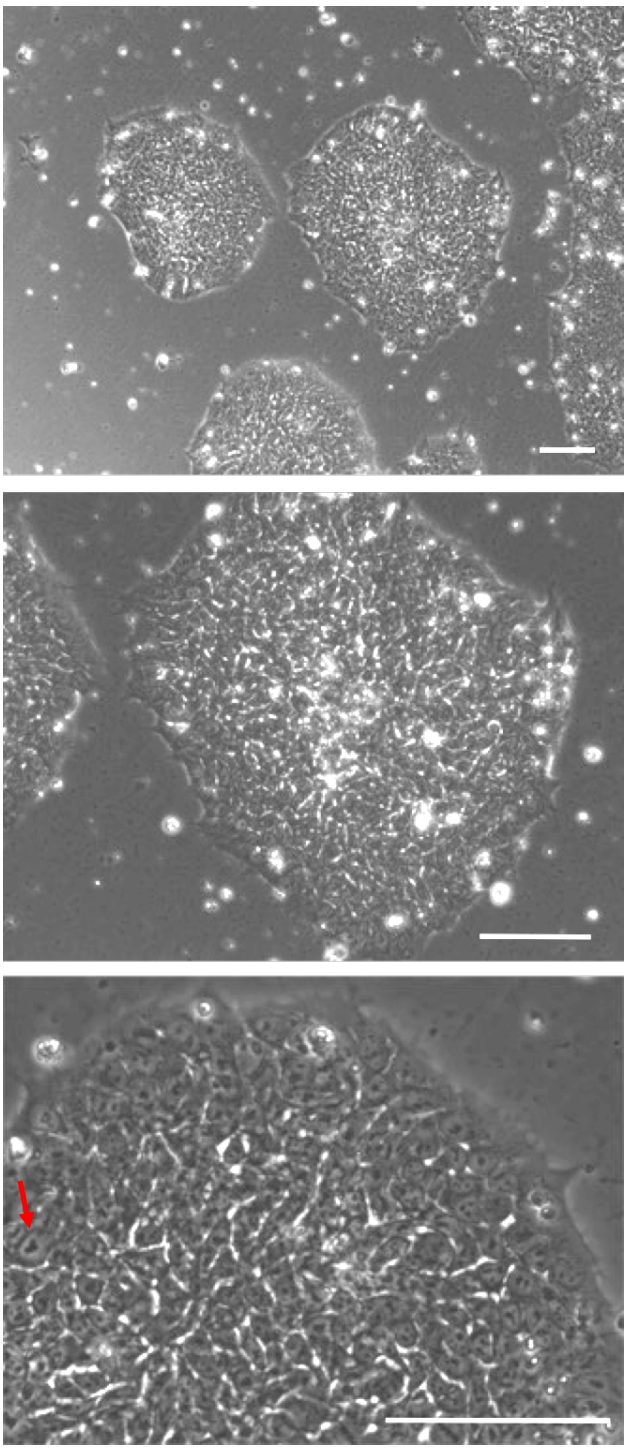

Figure 3.2: PBMC-derived iPSC colonies displaying characteristic iPSC morphology

Phase-contrast images of iPSC colonies in culture at x10, x20 and x40 magnification (top to bottom). Colonies are rounded in shape with smooth defined borders containing tightly packed iPSCs with a high nuclear to cytoplasmic ratio (example indicated with red arrow). Scale bar = 100μm

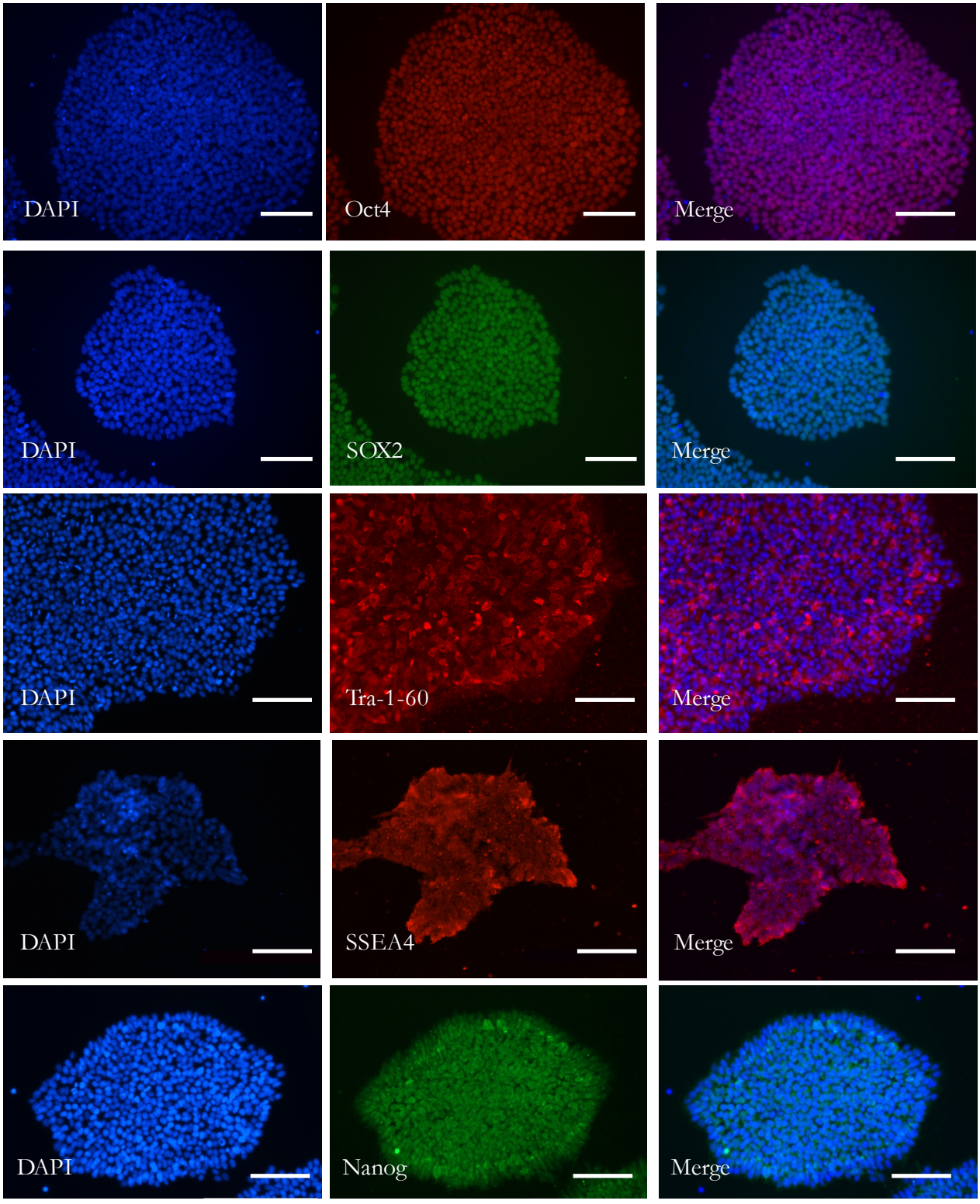

Figure 3.3: Pluripotency markers to characterise PBMC-derived iPSCs

Representative images of immunocytochemical staining of iPSCs with pluripotency markers OCT4, SOX2, Nanog, Tra-1-60 and SSEA4. DAPI was used to counterstain the nuclei and images were taken at x20 magnification, scale bar = 100 μm.

3.3.1.2 Spontaneous differentiation into embryoid bodies demonstrating three germ layers

To confirm the ability of iPSCs to differentiate into all three germ layers; endoderm, mesoderm and ectoderm, the formation of EBs and subsequent undirected differentiation was permitted. IPSCs were cultured in suspension for 4 days in non-tissue-culture treated dishes to encourage 3D colony formation rather than the formation of an adherent monolayer (Figure 3.4). After 4 DIV, the EBs were plated onto tissue culture-treated dishes to continue growth and encourage further differentiation. EBs continued to grow, showing a 3-fold increase in size and had started to loosely adhere to the plate surface 8 days after re-plating (Figure 3.4). Over time, this attachment allowed further differentiation of neural-like cells at the edge of the EBs, evident by the neural processes projecting from the EB core (Figure 3.4). After 20 DIV, the adherent EBs were fixed and showed expression of markers representative of all three germ layers α-fetoprotein (AFP, endoderm), α-smooth muscle actin (SMA, mesoderm) and β-III tubulin (TUJ1, ectoderm). SMA and TUJ1 showed more widespread expression than AFP. The cells of endoderm lineage, expressing AFP, were more often found within the dense cell mass of the EB, possibly reducing their exposure to the antibody. However, all three germ layer markers showed evidence of expression in multiple embryoid bodies, therefore confirming the pluripotent capability of these iPSCs.

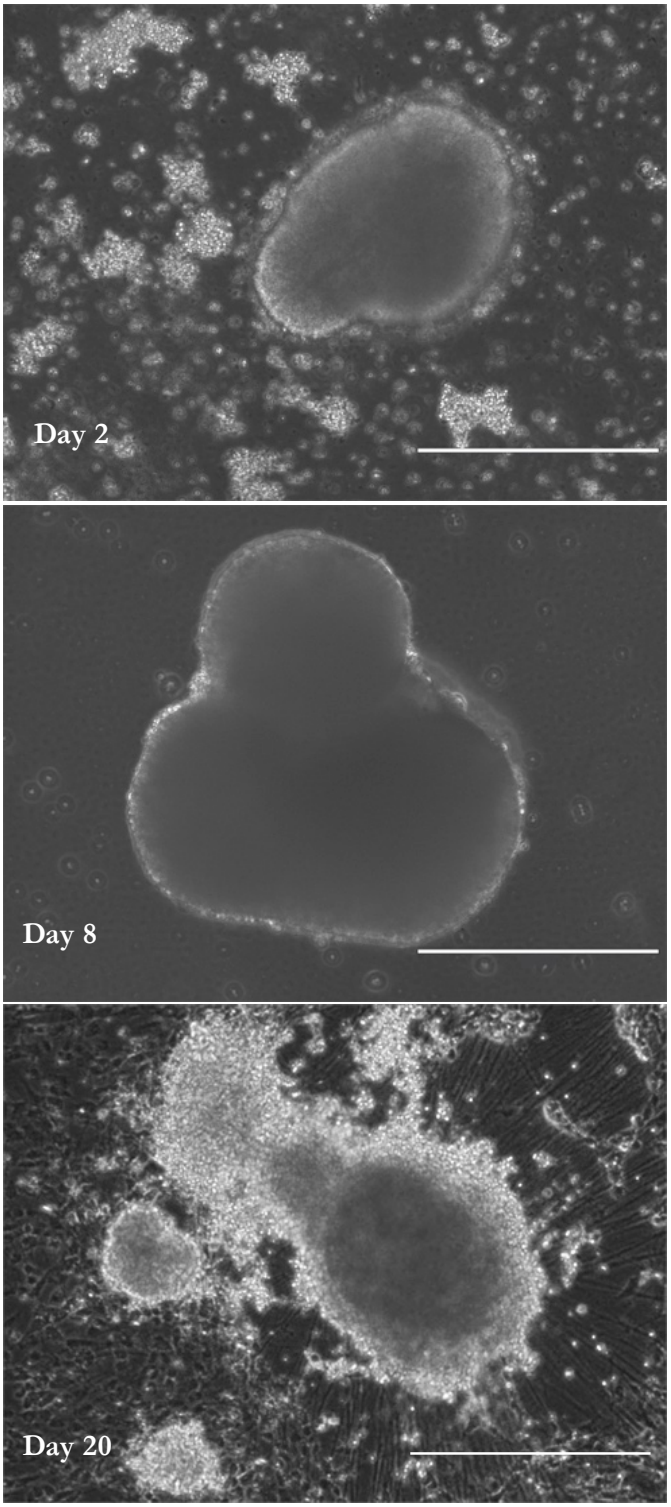

Figure 3.4: Spontaneous EB differentiation of PBMC-derived iPSCs

Representative photographs of embryoid bodies on day 2, 8 and 20 of differentiation taken at x10 magnification. After day 2, large cell masses began to form and these were plated onto gelatin-coated plates on day 4. By day 8, EBs had increased in size 3-fold and adhered to the plate surface. By day 20, EBs showed evidence of a variety of cell types, including neural-like processes emanating from the EB core. Scale bar = 400 μm

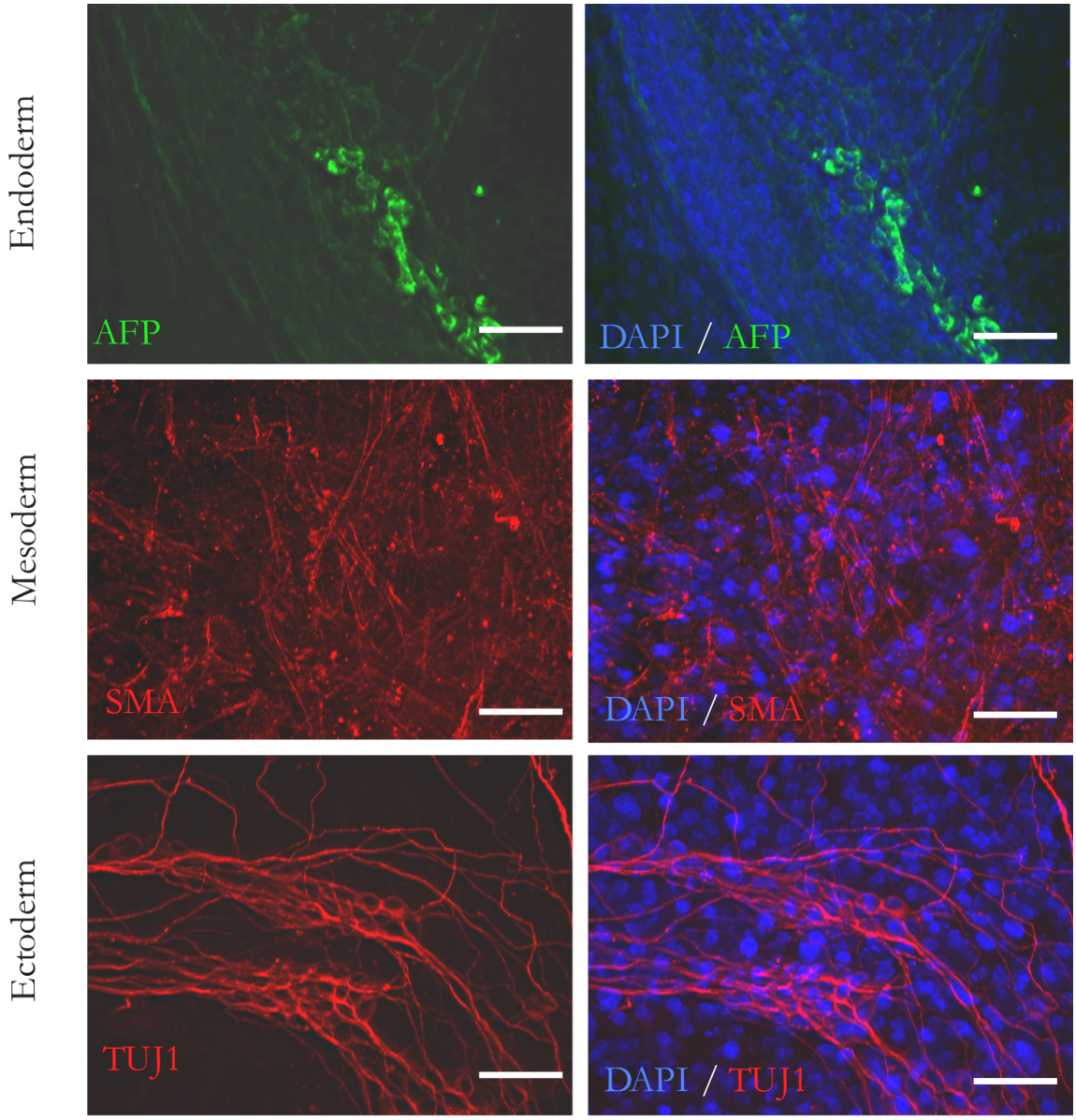

Figure 3.5 Expression of germ layer-specific markers in embryoid bodies

Representative immunofluorescence images of PBMC-iPSC-derived embryoid bodies fixed at 20 DIV, showing positive cells for AFP (marker for endoderm), SMA (marker for mesoderm) and TUJ1 (marker for ectoderm). DAPI was used to counterstain the nuclei and images were taken at x40 magnification, scale bar = 50 μm.

3.3.2 Differentiation of PBMC-iPSCs to Neural Stem Cells

Over 8 days in vitro (DIV), in which SMAD signalling inhibitors LDN193189 and SB431542 were administered, iPSCs became gradually more compacted as they formed a neuroepithelial sheet (Figure 3.6). The cells were closely monitored for morphological changes during differentiation and iPSCs with large nuclei were gradually replaced by tightly packed neuroepithelial cells with notably smaller nuclei (Figure 3.6). At this stage (8 DIV) they were passaged onto fibronectin. As neural progenitors are very fragile, the cells were passaged in as large clumps as possible by scraping each well in a large zig-zag pattern and gently triturating the cell clumps off the surface. Confirmation of neural progenitor identity was performed at 13 DIV by immunocytochemical analysis. By observation, almost all of the cells in the culture (>90%) stained positive for paired box 6 (PAX6), which colocalised with DAPI, suggesting nuclear localisation (Figure 3.7). Expression of the neuron-specific tubulin TUJ1 showed the presence of neural processes emanating from the neural progenitor cells, confirming neural identity (Figure 3.7), however this was not detected in all PAX6-positive cells. The neural stem cell marker Nestin showed cytoplasmic expression in nearly all cells, which also stained positively for Forkhead box G1 (FOXG1), found to colocalise in the nucleus with DAPI (Figure 3.8). SOX2 is expressed at high levels in the neuroepithelium of the CNS and was indeed abundantly expressed in these cells, with an observational estimate of >95% positive staining (Figure 3.9). Ki-67 is a mitotic marker and its expression was apparent in approximately 60% of SOX2-positive cells, illustrating actively cycling neural progenitors (Figure 3.9). Together, these data show that a neural identity can be induced over 8 DIV in PBMC-derived iPSCs.

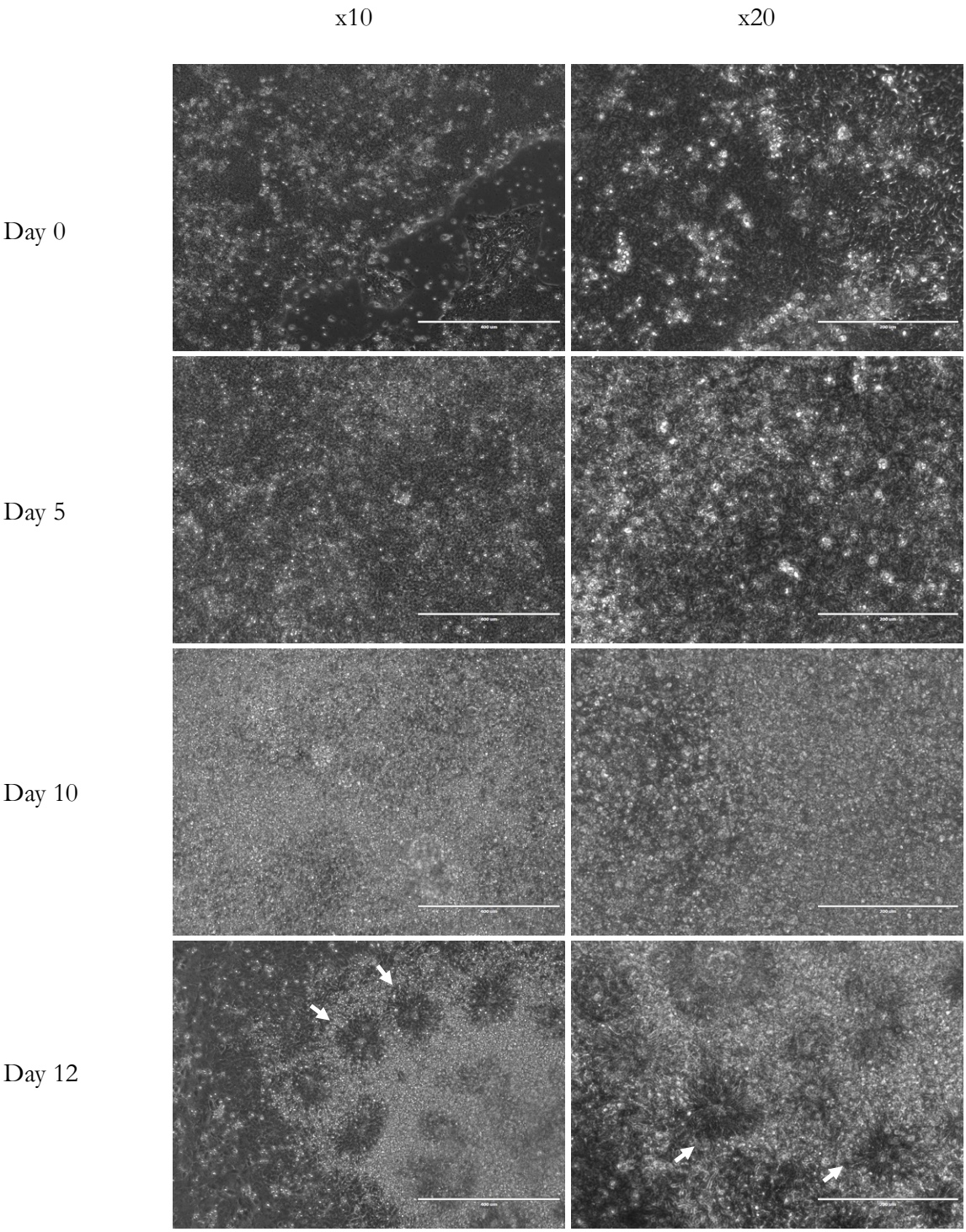

Figure 3.6: Neural induction and rosette formation of PBMC-derived iPSCs

Representative images of PBMC-derived iPSCs up to 12 DIV. Cells were subjected to dual SMAD inhibition for 8 days and passaged onto fibronectin matrix without inhibitors thereafter. Cells became gradually more compacted over this time with cells containing large nuclei gradually replaced by tightly packed neuroepithelial cells with notably smaller nuclei. By day 12, neural rosettes containing radially arranged columnar cells, began to appear (indicated by arrows). Photographs were taken at x10 and x20 magnification, scale bars represent 400μm and 200 μm, respectively.

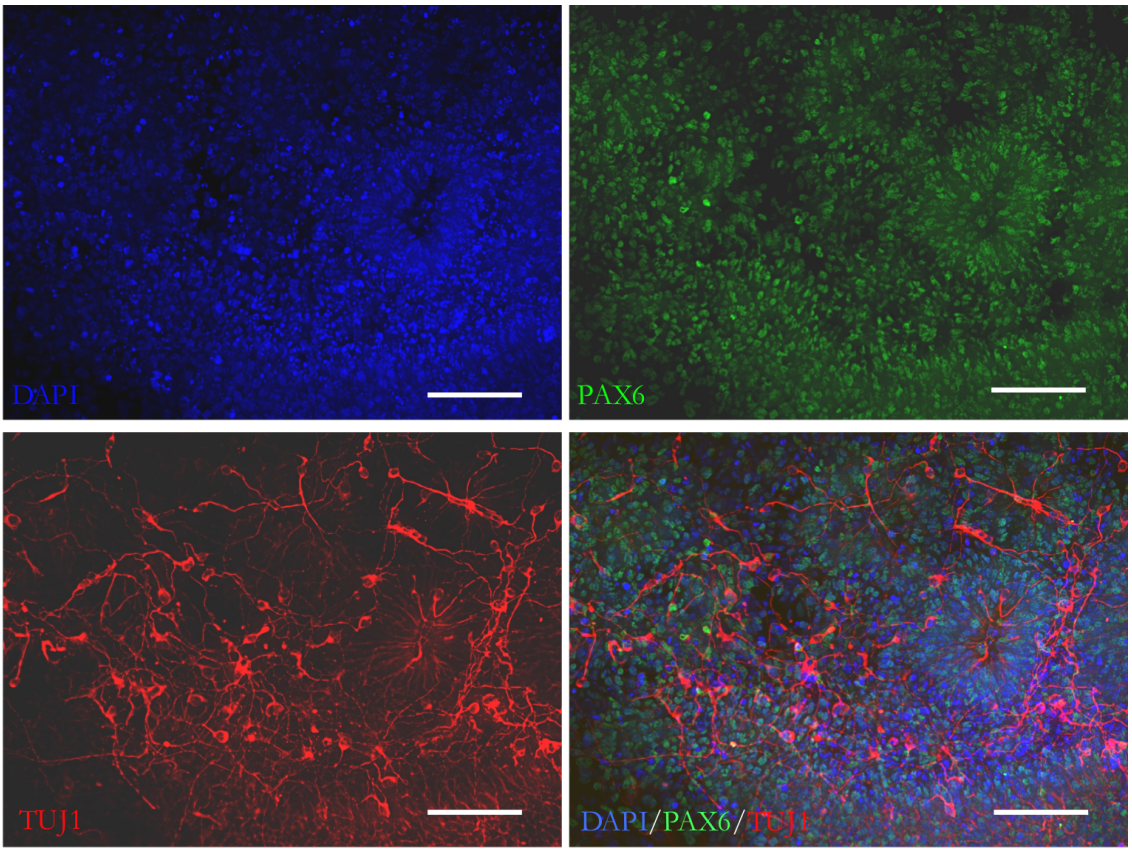

Figure 3.7: Immunofluorescence staining with PAX6 and TUJ1 to confirm the neural identity of induced neural tissue at 13 DIV

Representative immunofluorescence images of PBMC-iPSC-derived neural progenitors fixed at 13 DIV, showing positive nuclear staining for PAX6 and expression of neuron-specific tubulin TUJ1 in the emanating processes of neural progenitors. DAPI was used to counterstain the nuclei. Images taken at x20 magnification, scale bar = 100 μm.

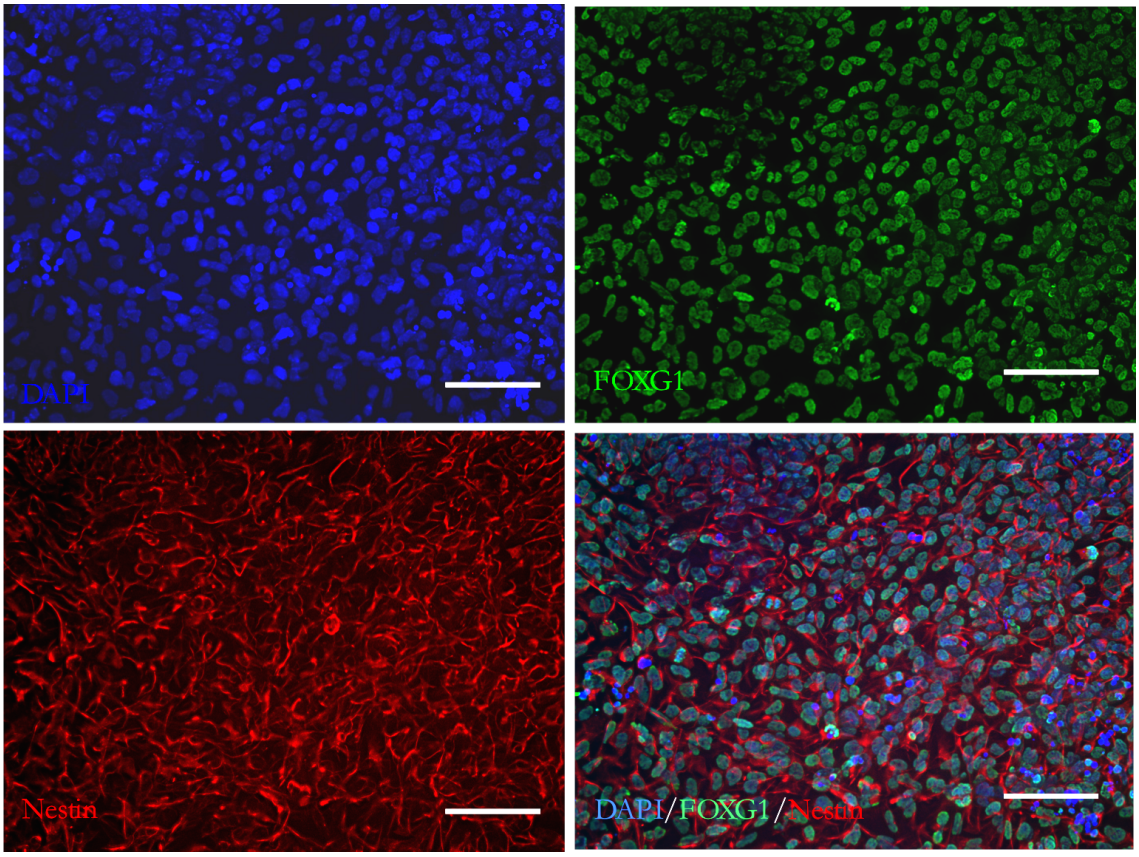

Figure 3.8: Immunofluorescence staining with FOXG1 and Nestin to confirm the neural identity of induced neural tissue at 13 DIV

Representative immunofluorescence images of PBMC-iPSC-derived neural progenitors fixed at 13 DIV, showing strong nuclear staining of FOXG1 and cytoplasmic expression of Nestin in almost all cells in culture. DAPI was used to counterstain the nuclei. Images taken at x20 magnification, scale bar = 100 μm.

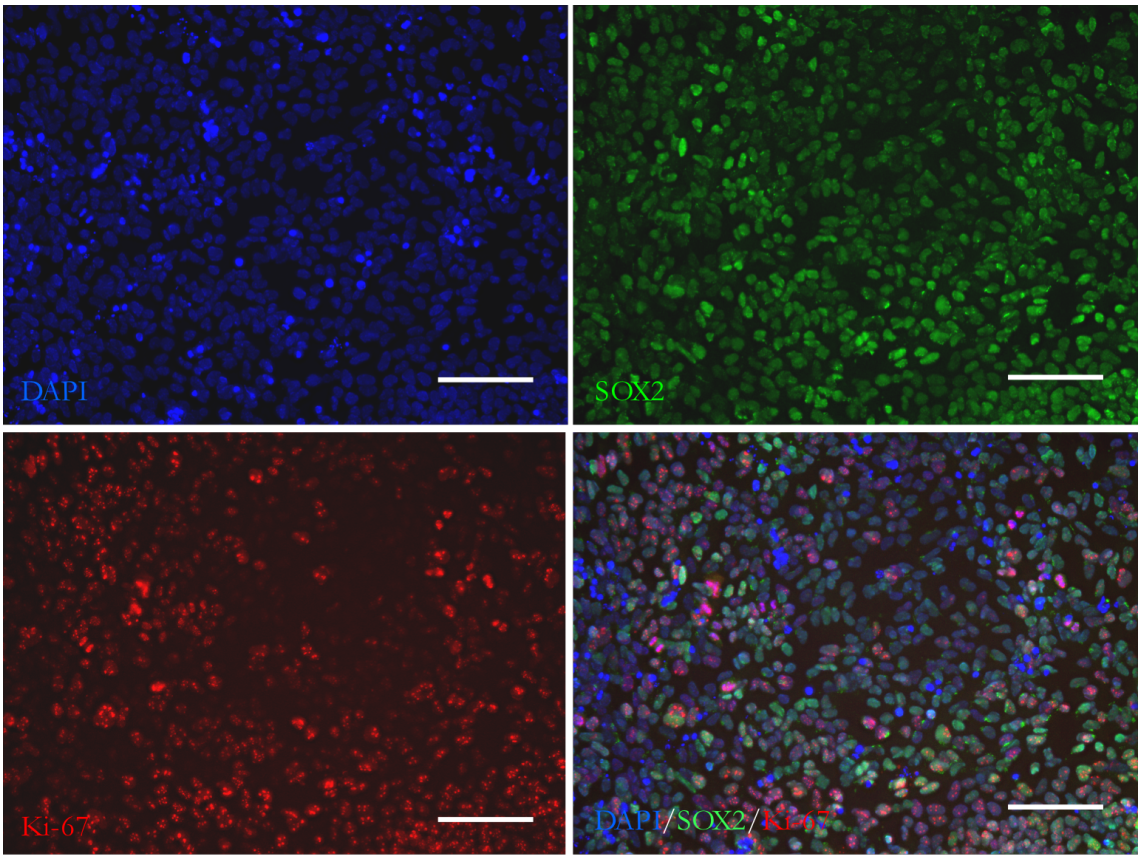

Figure 3.9: Immunofluorescence staining with SOX2 and Ki-67 to confirm the cortical identity of induced neural tissue at 13 DIV expression

Representative immunofluorescence images of PBMC-iPSC-derived neural progenitors fixed at 13 DIV, showing positive nuclear staining for SOX2 in nearly all cells and the pool of actively cycling neural progenitors staining positively for Ki67. DAPI was used to counterstain the nuclei. Images taken at x20 magnification, scale bar = 100 μm.

3.3.3 The Formation of Neural Rosettes

From 12 DIV, neural rosettes started to become apparent (Figure 3.6), consistent with expectations from the literature (Shi et al., 2012a). The neural rosette is the developmental signature of differentiating neural progenitors *in vitro*. It comprises a radial arrangement of elongated columnar neural progenitor cells, which express many proteins that are present in the neuroepithelium of the neural tube *in vivo* (Wilson and Stice, 2006). On the widespread appearance of neural rosettes at 16 DIV, cells were passaged onto poly-D-lysine/laminin-coated plates for expansion. In order not to disturb the cells too vigorously, the same principle as the first passage was applied but creating a finer zig-zag pattern to generate smaller clumps. Cells were fixed at 21 DIV and strong PAX6 expression was still observed, indicating the presence of cortical stem and progenitor cells (Figure 3.10). Ki-67 expression indicated actively cycling cells, which could be seen predominantly at the apical and basal areas of the rosette (Figure 3.10). T-box brain protein 2 (TBR2) and Ki-67 co-expression identifies secondary progenitor cells that form a basal layer around the rosette structure (Shi et al., 2012a). However, TBR2 was not identified by immunofluorescence. TUJ1 expression shows neuronal processes are present, mainly localised to the periphery of neural rosettes (Figure 3.10). To assess the development of early-born deep-layer cortical neurons, expression of T-Box Brain Protein 1 (TBR1) and chicken ovalbumin upstream promoter transcription factor-interacting protein 2 (CTIP2) was analysed. While TBR1 expression was apparent around the edges of the rosettes, a minimal proportion of cells showed strong positive staining. CTIP2 expression was not detected at all at this stage in of differentiation, suggesting early born deep-layer neurons had not yet developed.

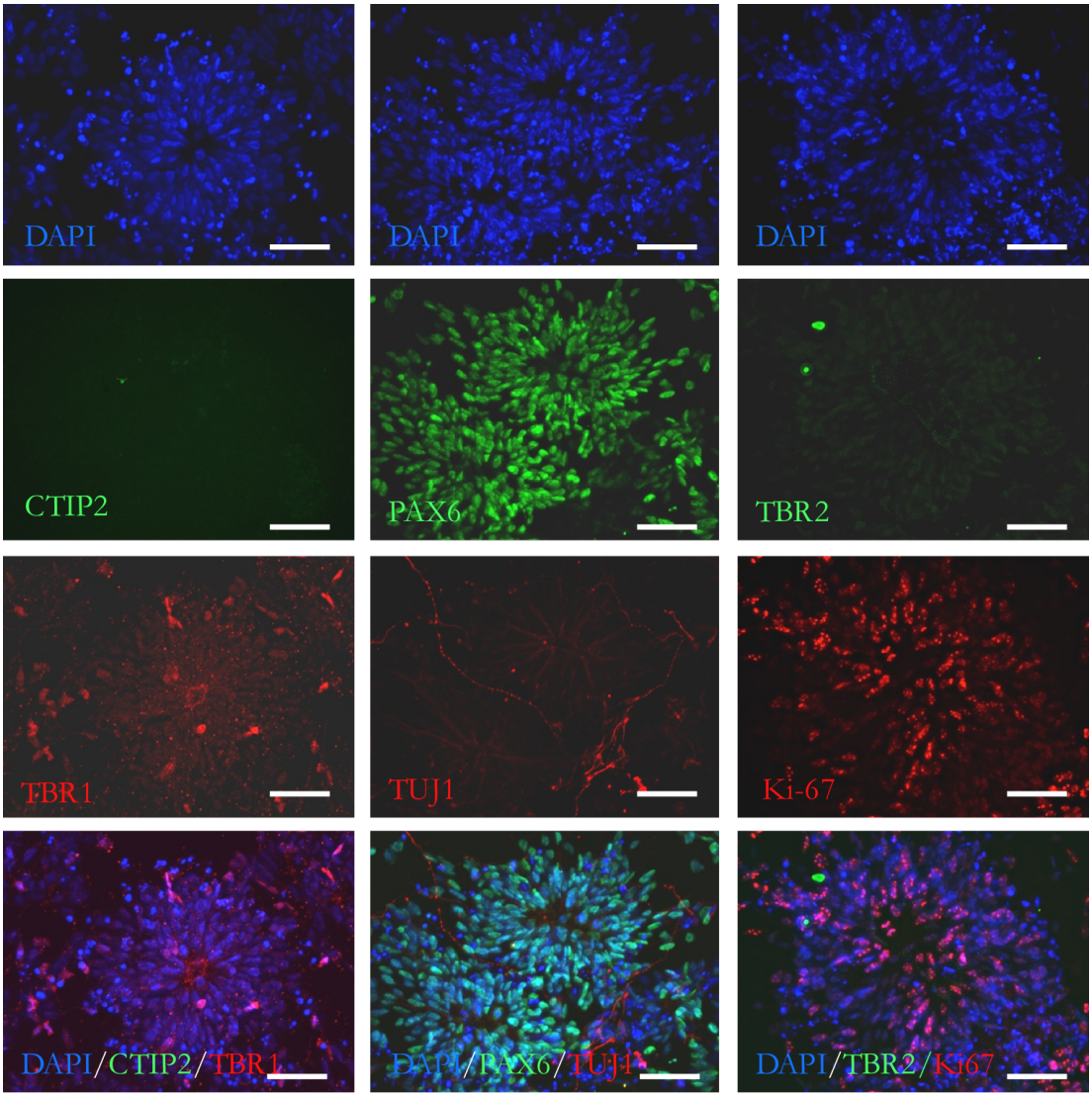

Figure 3.10: Immunofluorescence staining of neural rosettes at 21 DIV derived from PBMC-iPSCs

At 21 days after neural induction, neural rosettes plated on poly-D-lysine/laminin were analysed for CTIP2, TBR1, PAX6, TUJ1, and Ki-67 expression to confirm neural progenitor identity. CTIP2 and TBR2 failed to show positive staining. Minimal expression of TBR1 was shown while Ki-67^{+} cycling progenitors were evident in the apical and basal regions of rosettes and PAX6 was abundantly expressed. DAPI was used to counterstain the nuclei. Images were taken at x40 magnification, scale bar = 50µm.

3.3.4 Differentiation of Cortical Neurons

Following the second passage at 16 DIV, it became apparent with further culture that the clusters of neural rosettes were not broken up sufficiently to allow neural expansion, thus impairing the differential potential of cells to progress from the compacted neural rosette stage. Neuronal-like processes became apparent at the edge of rosettes suggesting the formation of neurons, however the large dense clusters of neural rosettes became loosely attached over time and some were lost during media changes. Cells were fixed at 35 DIV and expression of CTIP2 and TBR1 were again tested. Both were shown to be expressed in cultures, colocalising with DAPI in the nucleus and suggesting the successful development of deep-layer cortical neurons (Figure 3.11). The absence of BRN2 and CUX1 expression also supports this identification, as these define later-born upper-layer neurons (Shi et al., 2012a). At this stage, the cells tend to become very fragile and passaging cells after day 35 was not recommended in the protocol, due to a low survival rate following passage (Shi et al., 2012a). Despite the observed clumping and loss of some neural rosettes, the positive expression of deep layer cortical neuron markers CTIP2 and TBR1 gave rationale to continuing culture without further passaging.

Neurons were maintained in culture, with media changes every second day for a further 55 days. As cells approached day 50, cultures were becoming increasingly sparse as many of the pools of progenitor cells contained within the neural rosettes had formed dense clumps and detached. Cells were fixed at 50 DIV and tested for expression of later-born, upper-layer neuron markers CUX1, BRN1 and SATB2 (Figure 3.12) Despite the sparse distribution of neurons, expression of CUX1 in the cytoplasm was detected while colocalisation of BRN2 with DAPI in the nucleus was apparent, suggesting the successful development of upper-layer neurons. However, SATB2 expression was not detected. Cells were successfully maintained in culture up to 90 DIV, however became further fragmented and fragile over this time which did not allow for further analysis of neuronal marker expression. Large clumps of cells developed with processes extending from them and a large variation in morphology was evident in cell cultures, suggesting a heterogeneous population of cell types was present (Figure 3.13).

For exploratory purposes, one well of cells was passaged, as before, at 40 DIV but resuspending more vigorously, to determine if cells would survive passaging at this late stage and if this would help their morphological development. This well was denoted

Culture B. Indeed, these cells showed much less clumping than the non-passaged cells (Culture A) and displayed more neuronal-like processes and morphology (Figure 3.13). At 68 DIV, Culture B exhibited clear neuronal-like morphology with many neural processes, far fewer were observed in Culture A where many of the cells were contained within dense three-dimensional clumps. However, upon long term culture up to 90 DIV, Culture B still developed dense, clumped morphology, similar to that observed in Culture A (Figure 3.13).

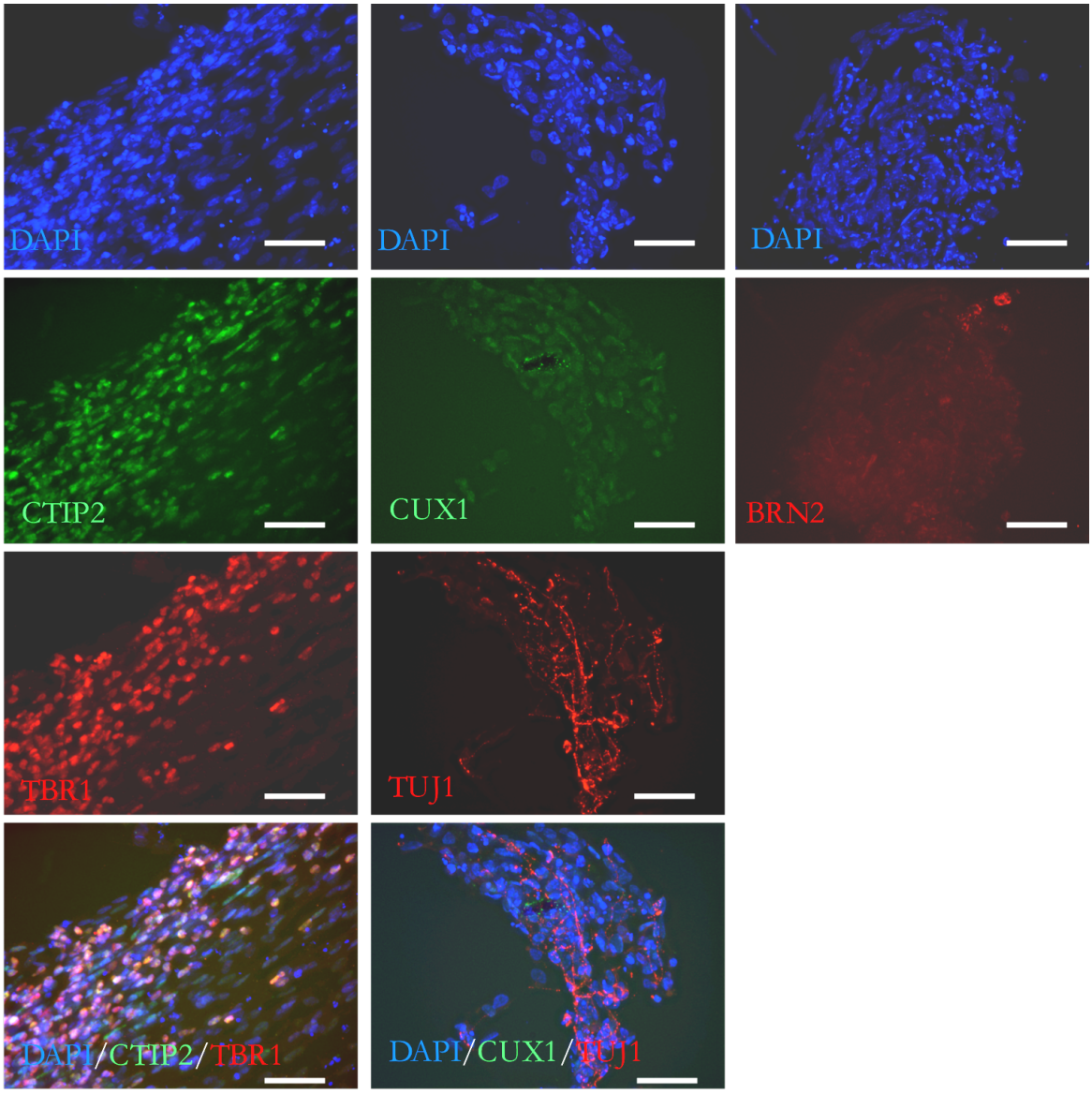

Figure 3.11: Immunofluorescence staining of markers indicating the presence of early-born deep-layer cortical neurons at 35 DIV

Representative immunofluorescence images of PBMC-iPSC-derived cortical neurons fixed at 35 DIV, showing positive staining for CTIP2, TBR1 and TUJ1. Cells were negative for CUX1 and BRN2 expression, consistent with a deep-layer cortical phenotype. DAPI was used to counterstain the nuclei. Images taken at x40 magnification, scale bar = 50 μm.

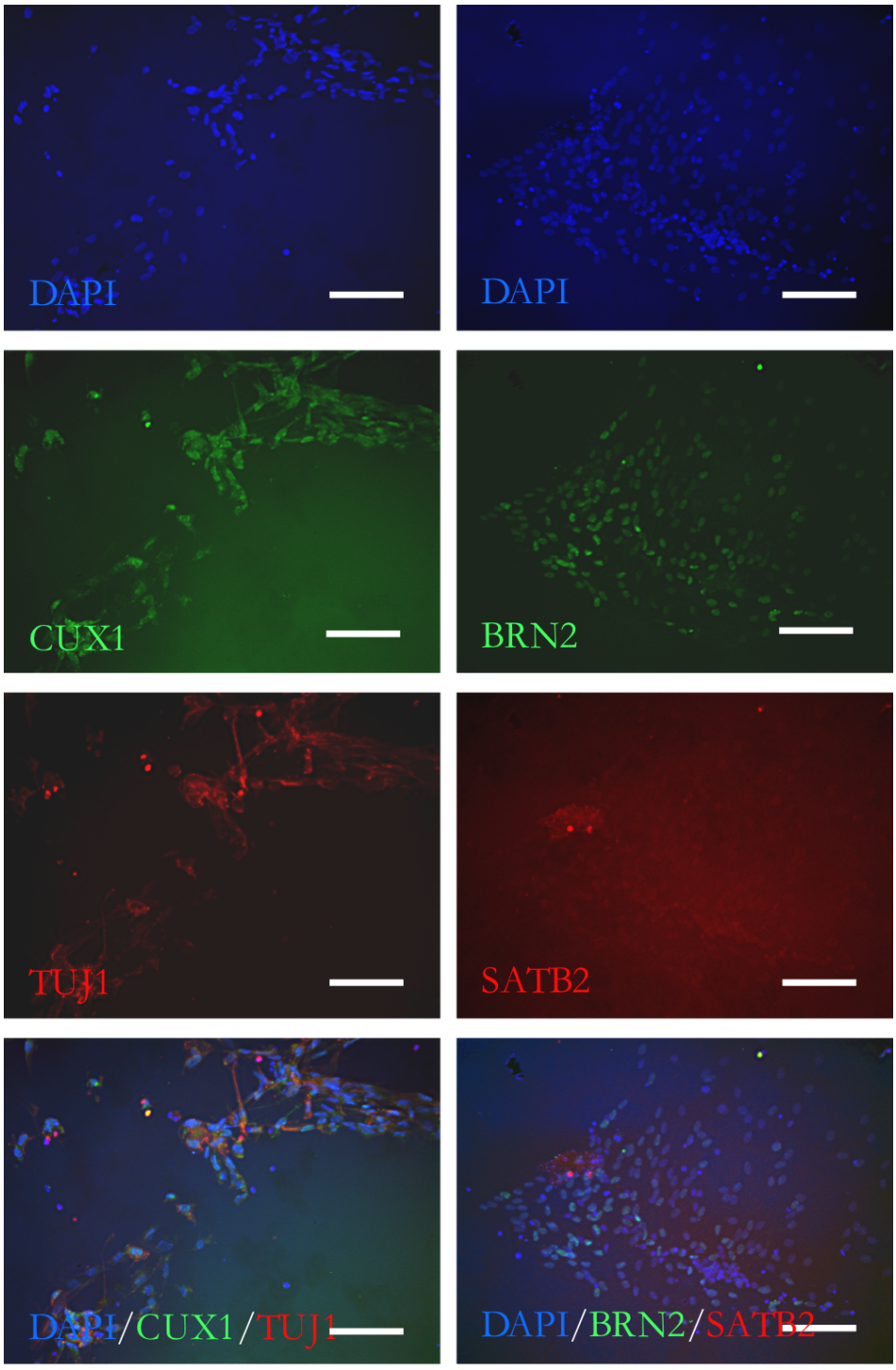

Figure 3.12: Immunofluorescence staining indicating the presence of late-born upper-layer cortical neurons at 50 DIV

Representative immunofluorescence images of PBMC-iPSC-derived cortical neurons fixed at 50 DIV, showing positive staining for CUX1, BRN2 and TUJ1. Cells were negative for SATB2 expression. DAPI was used to counterstain the nuclei. Images taken at x40 magnification, scale bar = 50 μm.

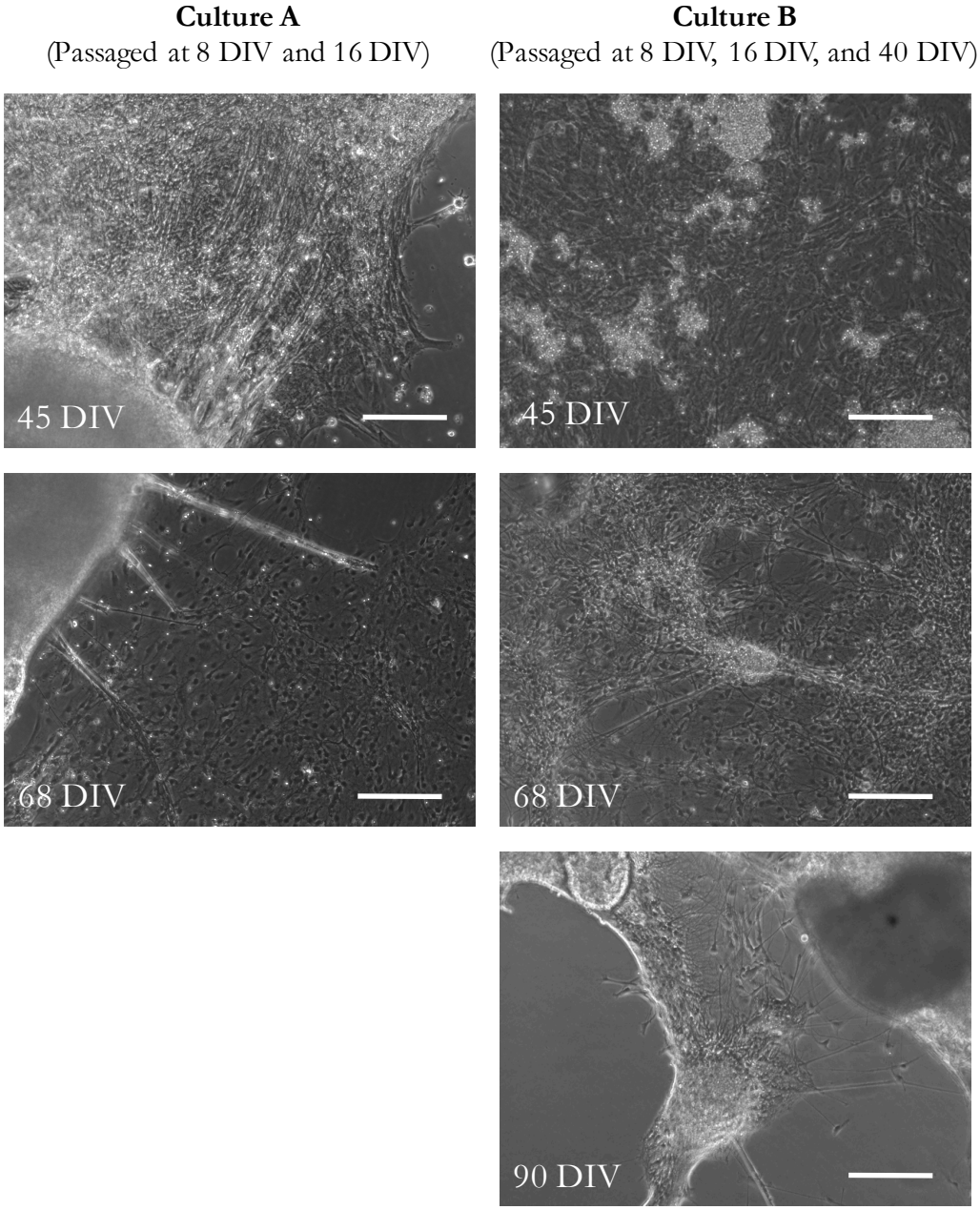

Figure 3.13: The effect of a third passage at 40 DIV on cellular morphology

Representative images showing a comparison between cortical neurons that were only passaged twice at 8 DIV and 16 DIV (Culture A) compared to those that underwent an additional passage with vigorous resuspension at 40 DIV (Culture B). At 45 DIV, Culture A showed areas of dense clumped cells and heterogeneous morphology whereas Culture B showed a more uniform morphology and dense three-dimensional clumps were not apparent. At 68 DIV, Culture B exhibited clear neuronal-like morphology with many neural processes however far fewer were observed in Culture A where many of the cells were contained within the dense clumps. By 90 DIV, however, Culture B exhibited similar cell clumping to that observed in Culture A. Images were taken at x20 magnification, scale bar = 100 μm.

3.4 Discussion

This study has confirmed the expression of pluripotency markers OCT4, SOX2, Nanog, TRA-1-6- and SSEA4 in PBMC-iPSCs and demonstrated the ability of PBMC-iPSCs to differentiate into all three germ layers by layer-specific gene expression in embryoid bodies. This provided an ideal starting population of stem cells for neural differentiation. By dual SMAD inhibition, neural identity was induced in PBMC-iPSCs to form a neuroepithelial sheet followed by the efficient formation of neural rosettes. Successful neural induction was confirmed by positive staining for key progenitor markers. Evidence of deep-layer cortical neurons was confirmed at 35 DIV by CTIP2 and TBR1 expression, while CUX1 and BRN2 expression were indicative of later-born, upper-layer neurons present at 50 DIV.

3.4.1 Confirmation of Pluripotency

IPSCs are characterised by the observation of ESC-like morphology (high nuclear to cytoplasmic ratio and forming colonies with clear-cut borders), expression of pluripotency markers and the ability to differentiate into all three germ layers (Baghbaderani et al., 2016). This study successfully demonstrates these characterisation steps to ensure the cells are truly pluripotent. The positive expression of pluripotency markers is routinely carried out in iPSC studies (Yagi et al., 2011, Shi et al., 2012b, Espuny-Camacho et al., 2013). Both OCT4 and SOX2 are two of the four reprogramming factors shown by Takahashi and Yamanaka to be required for induction of pluripotency in somatic cells (Takahashi and Yamanaka, 2006) and showed strong nuclear staining across iPSC colonies in this study. Oct4 is a member of the POU family of transcription factors and is a key developmental regulator with important roles in early embryogenesis, showing expression in unfertilised oocytes, early embryos and primordial germ cells but not in adult tissues (Schöler et al., 1989). SOX2 is also critical in controlling pluripotency and differentiation of hPSCs. SOX2 is indispensable for embryonic development (Avilion et al., 2003) and critical for maintaining pluripotency of ESCs and iPSCs, forming a core transcriptional regulatory network with OCT4 and NANOG to maintain self-renewal (Loh et al., 2006). NANOG, a homeodomain-containing transcription factor, was surprisingly not among the quartet of reprogramming factors sufficient to create iPSCs (Takahashi and Yamanaka, 2006).

However, it is critical for the maintenance of pluripotency in stem cells and, although required at a later point than OCT4 during development, both control a cascade of pathways to govern self-renewal and pluripotency (Yuin-Han Loh, 2006). NANOG is in fact a target of TGFβ/Activin-mediated SMAD signaling and the binding of SMADs to the NANOG promoter plays an essential role in sustaining stem cell self-renewal (Xu et al., 2008). The cell surface pluripotency markers SSEA4 and Tra-1-60 showed strong expression across iPSC colonies in this study, however showed less uniform expression compared to the aforementioned intracellular markers. As the cells grow within tightly packed colonies and were not permeabilised for the staining of these two antibodies, access of the antibody to the cell surface may have been impaired. The pattern of staining is however consistent with that observed in the literature confirming the pluripotency of blood-derived iPSCs (Choi et al., 2011, Barrett et al., 2014).

The creation of cells expressing endodermal, mesodermal and ectodermal markers through spontaneous differentiation into EBs demonstrated the pluripotent capacity of PBMC-iPSCs in this study. While the expression of AFP, a marker of endodermal origin, was not as widespread as SMA and TUJ1, it was expected that only certain areas would show positive staining due to the heterogeneous nature of the EBs. This assay provides a cheaper and less labour-intensive alternative to teratoma assay, which is considered the gold standard for demonstrating stem cell pluripotency (Hentze et al., 2009). This involves the injection of PSCs into immunodeficient mice to form a non-malignant tumour comprising cells of all three germ layers. However, these assays are expensive and the cost, in terms of animal usage, was not justified for this study. Both of these pluripotency assays, however, are limited in their ability to distinguish between high quality iPSC lines, with a high proportion of pure PSCs, and those that are more heterogeneous in nature, with a smaller proportion of truly pluripotent cells. This is particularly important due to the large number of cells lines required in any iPSC study to exclude the interference of variability, including multiple clones from each individual. Fluorescent cytometry can be used to stain for cell surface markers, such as TRA-1-60 and SSEA4, quantifying the fluorescence per sample, thus distinguishing between high quality uniform cultures and those that are heterogeneous in pluripotency. Gene expression-based assays can also provide an extensive characterisation of pluripotency, such as the robust open-access bioinformatic assay PluriTest (Muller et al., 2011). This can give an accurate view of pluripotency by comparing the expression of a large number of genes to a database of ~450 genome-wide

transcriptional profiles from diverse stem cell preparations, including 223 hESC and 41 iPSC lines, in addition to differentiated cell types, and developing and adult human tissues (Muller et al., 2011). While these approaches were not justified in this optimisation study, they would be incorporated into the thorough characterisation necessary for determining pluripotency in newly-generated patient-derived iPSCs.

3.4.2 Successful Neural Induction of PBMC-iPSCs

This study has demonstrated the ability to induce neuronal differentiation in a PBMC-derived iPSC line. Neural induction appeared to be highly efficient by the abundant formation of neural rosettes by day 12 and their positive staining for neural progenitor markers PAX6, FOXG1, Nestin and TUJ1. PAX6 expression was observed in >90% cells at both the neuroepithelial (13 DIV) and neural rosette (21 DIV) stage. This is in line with that previously demonstrated in the literature using dual SMAD inhibition protocols, with Shi et al. (2012) reporting that >95% of cells were PAX6-positive 15 days after initiation of neural induction (Shi et al., 2012a) and further studies demonstrating similar expression levels after 15-19 DIV (Shi et al., 2012b, Espuny-Camacho et al., 2013). Although colocalisation of PAX6 and FOXG1 was not possible in the present study due to the antibodies available being derived from the same species, similar expression and localisation of these two proteins was observed in neural progenitors at 13 DIV, confirming their cortical identity (Shi et al., 2012a).

Nestin and SOX2 also showed widespread expression at 13 DIV, consistent with the levels of coexpression with FOXG1 during neural induction in the literature (Shi et al., 2012a). The neuron-specific tubulin, TUJ1, was expressed at 13 DIV and throughout differentiation, confirming neural identity. Prominent TUJ1 staining was localised predominantly outside or at the periphery of rosettes, resembling the accumulation of neurons at the basal domain of the neural tube, outside of the apical proliferative zone. Shi et al. (2012c) also stated that the critical step in generating cortical neurons is the highly efficient differentiation to neural progenitor cell rosettes and the genesis of apical and basal progenitors in the system (Shi et al., 2012c). This was demonstrated in the present study, with apical and basal Ki-67 expression within the rosettes replicating that reported by Shi et al. (2012c) and confirming the presence of mitotically cycling neural progenitors. Due to the small starting pool of cells for this differentiation, only observational estimates of the

percentage of positive staining per marker was possible, however an expansion of this study in patient-derived iPSCs would allow an accurate quantification of immunofluorescence positive staining. This would enable comparisons to be made between lines and a more thorough analysis of differentiation efficiency. Collectively, however, the abundance of these markers, as judged by eye, was considered sufficient to confirm their expression.

The lack of CTIP2 expression at 21 DIV may be due to the neural progenitors not yet being mature enough to express this protein therefore it would perhaps be more appropriate to stain for this protein at a later time point. Espuny-Camacho et al. (2013) differentiated cortical neurons by dual SMAD inhibition and found CTIP2/TBR1 co-expression at 24-28 DIV and CTIP2 positive layer V neurons at 37 DIV while others also report early-born deep-layer neurons only becoming a major population around day 35 (Shi et al., 2012a). Neural rosettes were fixed at 21 DIV which is likely too early for these markers, particularly as PAX6-positive progenitors were still abundant. Indeed, CTIP2 and TBR1 expression were observed at 35 DIV, with many of the neurons showing positive double staining for both these markers, indicating the successful development of layer VI cortical neurons (Espuny-Camacho et al., 2013). The same may be true for TBR2 expression as this identifies newly-born post-mitotic neurons which may not yet have developed. TBR2 was not present at 21 DIV but expression has been shown at day 24 in the literature (Shi et al., 2012a) and as the primary progenitor marker PAX6 expression was still abundant at 21 DIV in the present study, it may be that the cultures were fixed too early for secondary progenitor cells to have developed.

Upper layer CUX1/BRN2-positive neurons were detected at 50 DIV and TUJ1 further confirmed neural identity of cells in culture, however this expression was not as widespread as published results have shown (Shi et al., 2012a, Chambers et al., 2009), suggesting heterogeneous cell types in the cultures. SATB2 expression, which corresponds to callosal neurons, could not be detected. Espuny-Camacho et al. (2013) found that SATB2 and CUX1/BRN2-positive cells started to appear at the latest time points in culture around 61-72 DIV. It could be that the upper layer callosal neurons had not yet developed at 50 DIV and further immunocytochemistry at 70 DIV would have been informative. One of the great limitations with neuronal differentiation studies is the post-mitotic nature of mature neurons which does not allow sources to be replenished. This means that a very large

starting batch of neural precursors is essential for sufficient quantities of neurons to be generated, both for characterisation and the final population for functional assays. Due to the insufficient separation of neural rosettes at the second passage, large clumps of neural precursors formed and were prevented from differentiating. Many of these detached over time, therefore further reducing the number of cells available for characterisation. For this reason, cells were not fixed as frequently after 50 DIV as was planned with the aim of fixing at 90 DIV to maximise the chance of observing late-born mature neuronal markers. Unfortunately, this was not possible due to a cell culture infection, demonstrating the challenges of long-term culture in the absence of antibiotics. In future, expansion of cell cultures at the progenitor stage to produce frozen stocks would be employed to ensure a plentiful supply of neural precursors. This would save the time required to prepare iPSCs from scratch for neural induction and also allow back-up stocks to be cultured simultaneously in case of such unforeseen circumstances.

3.4.3 The use of PBMCs for iPSC Modelling

While the precise timing of differentiation is highly line-dependent and likely to differ when it comes to sAD patient-derived iPSCs, testing the procedure in this trial PBMC-derived iPSC line provides promise that the method will be effective in future PBMC-derived iPSC models and validates their use in this project. Until recently, the most common source from which to derive human iPSCs has been skin fibroblasts. However, PBMCs provide an ideal starting source for iPSC models of neurodegeneration as they eliminate the requirement for patient skin biopsies to generate dermal fibroblast lines. This is particularly invasive for elderly participants as it can cause bleeding, infection, and scarring and may also be unethical to carry out on an individual who lacks the mental capacity to understand the procedure. Blood, on the other hand, is a cell source that can easily be obtained from patients and several groups have successfully generated iPSCs from PBMCs (Loh et al., 2010, Mack et al., 2011, Seki et al., 2010).

PBMCs collected from blood are advantageous as they can be reprogrammed immediately following extraction due to the large numbers of cells available in a blood sample whereas time is required for the expansion of dermal fibroblasts obtained from a skin biopsy before reaching adequate numbers for reprogramming (Takahashi and Yamanaka, 2006). Blood collection is routinely performed therefore reduces the need for highly-specialised staff

trained in skin biopsy collection. The less invasive nature of the procedure also helps participants to overcome the psychological barrier of participating in research which may lead to greater recruitment for such studies. Undeniably, blood is becoming a routinely used source for iPSC generation and studies differentiating these into neuronal cell types are on the increase. DeRosa et al. (2012), for example, generated patient-specific iPSCs from individuals with autistic spectrum disorder and differentiated these into GABAergic neurons (DeRosa et al., 2012). Recent studies have also demonstrated the successful derivation of iPSCs from PBMCs collected from elderly AD patients (Tancos et al., 2016, Chandrasekaran et al., 2016, Ochalek et al., 2016, Nemes et al., 2016, Zhang et al., 2017) providing evidence that this approach is suitable and effective for AD research. Indeed, reprogramming success is not adversely affected when performed on PBMCs from elderly patients, unlike dermal fibroblasts extracted from elderly participants (El Hokayem et al., 2016).

While an exciting emerging field, PBMC-iPSCs are subject to limitations, including the handling of samples immediately following collection. Temperature fluctuations and an extended time period before PBMCs are isolated from whole blood can adversely affect sample quality (El Hokayem et al., 2016). Agu et al. (2015) demonstrated that iPSCs can be derived from whole blood held for 48 hours at room temperature before isolating PBMCs, however reprogramming efficiency at 48 hours was 10-fold lower than those held for 5 hours. Furthermore, evidence from mouse iPSCs derived from fibroblasts, hematopoietic and myogenic cells has suggested that early-passage iPSCs retain a transient epigenetic memory of their somatic cells of origin (Polo et al., 2010). Epigenetic marks carried over from PBMCs to iPSCs could make differentiation into certain cell types difficult, however, the demonstration of neural induction in the current study suggests this is not problematic. Polo et al. (2010) reported that the retention of PBMC epigenetic marks could be circumvented by extending the number of passages iPSCs undergo, indicating that reprogramming is a gradual process extending beyond the activation of pluripotency genes. While several recent studies have demonstrated the successful derivation of iPSCs from PBMCs collected from elderly AD patients (Tancos et al., 2016, Chandrasekaran et al., 2016, Ochalek et al., 2016, Nemes et al., 2016), studies demonstrating successful terminal differentiation of PBMC-iPSCs into disease-relevant cell types are scarce suggesting the field is in its infancy and may still be subject to methodological issues.

While the storage of PBMC samples in liquid nitrogen for 4 months prior to reprogramming results in no obvious change in reprogramming efficiency (Agu et al., 2015), the implications of longer term frozen storage of PBMCs on reprogramming efficiency has yet to be determined. The PBMC samples available for AD research purposes within the GERAD cohort have been collected over many years and have therefore undergone a long-term period in liquid nitrogen storage. Attempts by Lyle Armstrong to reprogram 2 case and 2 control PBMCs samples collected between 2002-2004 took much longer than the 21-day protocol described in the Cytotune 2.0 protocol for reprogramming PBMCs. The cells were slow to eliminate the SeV reprogramming vector and produced very small numbers of pickable colonies, representing low reprogramming efficiency. The colonies were also difficult to expand because they were very prone to differentiation down a neuroepithelial pathway. It was thought that this behaviour was likely due to the PBMCs being in storage over 10 years, based on anecdotal reports of this behaviour in fibroblasts which had been in storage for a number of years. It is possible that storage for this length of time had affected their quality.

3.4.4 Models of Neurodegeneration: Future Challenges

3.4.4.1 Recapitulating ageing in vitro

It has proven difficult to generate *in vivo* models that recapitulate typical late-stage features of AD including the presence of plaques, tangles and neuronal death, with rodent models relying on the overexpression of multiple mutant genes to demonstrate this pathology (Oddo et al., 2003). A key finding that would support the recapitulation of true AD pathology in iPSC models is the demonstration of these advanced stage features which would ultimately allow iPSC models to be used to probe the links between Aβ and tau. Despite iPSC-derived neuronal models from sAD patients showing elevated levels of toxic amyloid-β species and phosphorylated tau (Kondo et al., 2013, Israel et al., 2012), amyloid-β plaques or neurofibrillary tangles have not been demonstrated. Recent implementation of 3D culture models has uncovered a breakthrough in reproducing these hallmark features, previously unseen in cellular or animal AD models. Choi et al. (2014) successfully recapitulated amyloid-β and tau pathology in an immortalised human neural precursor cell line derived from fetal brain but this also required the overexpression of mutant genes.

APP and *PSEN1* containing fAD mutations were overexpressed in human neural stem cells and differentiated into 3D cultures of neuronal and glial cells, representative of different brain regions (Choi et al., 2014). The authors hypothesised that a 3D culture system would accelerate Aβ deposition by limiting its diffusion, which classically occurs into a large volume of media in 2D cultures. Indeed, robust extracellular deposition of Aβ and the formation of plaques was demonstrated in fAD 3D cultures in addition to high levels of p-tau aggregates in the soma and neurites (Choi et al., 2014). The use of β- or γ-secretase inhibitors not only decreased Aβ pathology but attenuated tauopathy, supporting the amyloid hypothesis that accumulation of Aβ drives tauopathy (Hardy, 1992). Together, these data support the utility of 3D organoids for AD research, yet it remains to be determined whether both amyloid and tau tangle pathologies can be recapitulated *in vitro* in the absence of mutant fAD genes.

This lack of late-stage pathology recapitulation in sAD models could be due to the resetting of donor age during somatic cell reprogramming, removing all biological signatures of ageing. Gene expression profiling of iPSC-derived neurons has shown that these cells differentiate at a rate comparable to their fetal counterparts (Mariani et al., 2012). How can 90 days in culture effectively recapitulate 80 years in the human brain? Efforts to genetically trigger age-like features in iPSC derivatives have involved manipulation of a genetic mutation responsible for premature ageing (Miller et al., 2013) and telomere shortening (Vera et al., 2016). However, with the complex pathogenesis that AD already presents, introduction of further impairments through 'artificial ageing' has the potential to interfere with true readouts.

3.4.4.2 Inter-line variability

The demonstration of AD-related phenotypes in iPSC-derived neurons from patients with sAD (Israel et al., 2012, Kondo et al., 2013) provides great promise for modelling such complex disorders *in vitro*. However, both these studies reported contradictory results between different sAD cell lines, with only one of the two demonstrating phenotypes consistent with the fAD lines (Israel et al., 2012, Kondo et al., 2013). This variability speaks to the complexity of each human genetic background and the challenge of modelling complex diseases in this manner still hinders progress in the field. It also illustrates that there are likely multiple causes of sAD which cannot all be modelled by one system.

Furthermore, iPSC models cannot escape from the interference of individual differences in genetic background when multiple patient lines are used. Recent advances in genome editing technology with the use of clustered regularly interspaced short palindromic repeats (CRISPR) and their associated protein-9 nuclease (Cas9) have allowed the creation of isogenic iPSC lines to eliminate this source of variation. The CRIPSR/Cas9 system efficiently introduces targeted double stranded breaks which can be repaired by homology-directed repair using a DNA repair template. The repair template supplied can be designed to selectively introduce a mono- or bi-allelic sequence to allow a targeted mutational knock-in of single alleles to model heterozygous or homozygous mutations. The generation of knock-in iPSC-derived cortical neurons with the *APP* or *PSEN1* mutation has recently been demonstrated (Paquet et al., 2016). These neurons displayed genotype-dependent disease-associated phenotypes such as increased total Aβ generation and secreted Aβ42:Aβ40 ratio, which correlated with mutation load. This approach has also been applied to investigating the genetic basis of sAD by genetically modifying iPSCs to incorporated AD risk SNPs into the genome. For example, Zhao et al. (2015) investigated whether certain AD-associated *PICALM* variants could influence *PICALM* expression and Aβ clearance in iPSC-derived endothelial cells. CRISPR/Cas9 genome editing was used to generate isogenic homozygous iPSC lines for two homozygous allelic variants, one of which was associated with a decreased risk of AD (Harold et al., 2009, Lambert et al., 2009, Lambert et al., 2013). Indeed, they reported that iPSC-derived endothelial cells homozygous for the protective rs3851179^{A} allele had higher *PICALM* mRNA and protein levels and increased Aβ clearance than those expressing the non-protective rs3851179^{G} allele (Zhao et al., 2015). This presents an avenue for the future use of iPSC models, such as the cortical neurons demonstrated in this chapter, to investigate the function of SNPs associated with sAD risk through the creation of isogenic lines by genome editing.

3.4.4.3 Selection of appropriate cell type

This study investigating PICALM function in brain endothelial cells also highlights the importance of creating iPSC models of the appropriate cell type for the gene of interest. While much of the focus for modelling AD *in vitro* has surrounded the generation of neuronal models, other brain cell types including astrocytes, microglia, oligodendrocytes and endothelial cells have remained relatively underexplored, despite each showing evidence suggesting participation in the pathogenesis and progression of AD (Olabarria et

al., 2010, Desai et al., 2010, Zhao et al., 2015). Atrophic astrocytes, for example, have been detected in the early stages of disease in AD mouse models (Olabarria et al., 2010). Recently, Jones et al. (2017) reported that both fAD and sAD iPSC-derived astrocytes display cellular atrophy and a smaller degree of branching compared to controls, as calculated using the astrocyte marker glial fibrillary acidic protein (GFAP) to measure surface area, volume and the relative ratio. The enormous potential of iPSCs for AD modelling has been demonstrated through neuronal models and extended with the recent introduction of 3D culture systems to better reflect the *in vivo* system. Specific selection of appropriate cell type is crucial when applying these methods to analyse gene function in AD and the field is now being extended to include these equally important non-neuronal cell types.

3.4.5 Conclusion

This chapter has provided proof of principle that iPSCs derived from PBMCs can be directed to differentiate into cortical neurons through dual SMAD inhibition. This protocol was carried out for the first time in the current lab and has therefore established these iPSC protocols for future use and optimisation. This approach to *in vitro* modelling of AD is limited in terms of the feasibility of reprogramming samples from patients with AD. Whether the difficulties encountered during the reprogramming of these samples were due to the age of the donor or the long duration in storage is yet to be determined. Unfortunately, with the unanticipated delay in reprogramming the patient-derived PBMCs, the feasibility of optimising neural differentiation in an AD patient line was not possible within the time constraints of this PhD project. However, the protocols are now available for the future use of the team, allowing the potential creation of iPSC-derived neuronal cultures for the study of AD susceptibility genes.

Chapter 4

The Involvement of BIN1 in APP Processing at the Blood-Brain Barrier

4.1 Introduction

Chapter 4 introduces the exploration of the role of *BIN1*, a gene implicated in LOAD aetiology by numerous genetic studies (Chapter 1, Section 1.3) in the proteolytic processing of APP at the BBB. The amyloidogenic processing of APP by neurons coupled with poor Aβ clearance across the BBB have been classically attributed to plaque formation. However, APP from BMECs and the peripheral circulation represents a significant potential source of Aβ in the brain and surrounding vasculature (Devraj et al., 2016). With APP processing evident in BMECs (Devraj et al., 2016) and CME central to this mechanism, this chapter seeks to explore whether BIN1 has a role in APP proteolysis at the BBB. BIN1 function has not previously been investigated in BMECs, therefore a well-characterised immortalised human brain endothelial cell line will be used to investigate the effect that siRNA-mediated depletion of BIN1 has on APP processing.

4.1.1 APP Processing at the BBB

While the role of the BBB in the clearance of brain-derived Aβ has been studied in great detail, the involvement of BMECs in the amyloidogenic processing of APP is yet to be fully investigated. Several studies have reported that over 70% of AD cases also demonstrate CAA with deposition of Aβ in the walls of cerebral blood vessels (Mandybur, 1975, Attems and Jellinger, 2004) yet the origin of these deposits remains unclear. The

formation of Aβ plaques and CAA have classically been attributed to the production and release of Aβ by neurons, coupled with poor clearance of Aβ at the BBB. However, BMECs have been shown to express APP at comparable levels to primary neurons (Kitazume et al., 2010). APP has three major alternatively spliced isoforms: 770, 751 and 695 residues in length which show cell-specific expression in the brain. Neurons solely express APP_{695} (Wertkin et al., 1993, Kitazume et al., 2010) while APP_{770} and APP_{751} exhibit a more ubiquitous expression pattern and contain a Kunitz Protease Inhibitor (KPI) domain, which favours the amyloidogenic processing of APP (Ho et al., 1996). Kitazume et al. (2010) showed that BMECs express APP_{770} and detected both sAPPα and sAPPβ in media from cultured BMECs, providing evidence for α- and β-secretase activity. However, Aβ40 and Aβ42 were only detectable in the media upon overexpression of APP_{770} in BMECs, suggesting that while the capability to produce Aβ is present in BMECs, production of Aβ from endogenous APP is limited and highlights the difficulty in detecting Aβ in non-transfected cells.

Platelets also represent a substantial peripheral source of APP at a concentration comparable to that found in the brain (Bush et al., 1990) and this may contribute to Aβ accumulation in the brain and cerebral vasculature in AD. Indeed, peripherally applied Aβ was shown to result in plaque formation in the brain (Eisele et al., 2010). As BMECs possess the capacity for amyloidogenic processing of APP, it is plausible that BMECs may contribute to Aβ deposits in the brain and cerebral vessel walls by utilise platelet-derived APP.

A recent study investigated the expression of BACE1 in BMECs of human, mouse and bovine origin, showing strong expression of the full-length active isoform in bovine microvessels (Devraj et al., 2016). BACE1 expression showed a predominant basolateral distribution with a 2.5-fold higher concentration compared to the luminal membrane, suggesting that Aβ generation within the endothelium may considerably contribute to amyloid formation in the walls of the blood vessels. Upon inhibition of BACE1 in mouse BMECs, an increase in mature APP and sAPPα was observed, indicating that in the absence of BACE1, the majority of full-length APP was not cleaved and that when cleaved, α-secretase-mediated cleavage predominated (Devraj et al., 2016). In BBB microvessels of a transgenic AD mouse model over-expressing human APP_{751}, a 4-fold increase in BACE1 mRNA expression compared to age-matched wild-type mice was observed, suggesting an increase in APP processing activity by BACE1 (Devraj et al., 2016). In addition,

basolaterally-expressed LRP1 was upregulated. LRP-1 is known to be involved in the endocytosis of APP, therefore increased BACE1 activity coupled with increased endocytosis of neuronal-derived APP may result in increased Aβ production in BMECs. The apical Aβ influx transporter RAGE also showed increased transcript levels in this study while apically expressed Pgp, involved in Aβ efflux at the BBB, was downregulated. BMECs could therefore be contributing to brain Aβ by increased APP processing, enhanced influx of blood-derived Aβ and/or decreased efflux of Aβ into circulation.

4.1.2 Investigating BIN1 Protein Function *in vitro*

With endocytic trafficking central to the proteolysis of APP, the identification of several AD risk genes implicated in CME has stimulated research into the function of these genes in the brain and how they may affect APP processing. As the second most associated AD susceptibility loci after *APOE*, the genetic evidence associating *BIN1* with AD pathogenesis (Chapter 1, Section 1.3) has resulted in many follow-up studies using cellular models (Glennon et al., 2013, Chapuis et al., 2013, Miyagawa et al., 2016, Ubelmann et al., 2017).

A widely-used method of investigating protein function *in vitro* involves the use of RNA interference. This is the process by which RNA molecules inhibit gene expression by inactivating the corresponding mRNA using double-stranded RNA. The phenomenon is based on the endogenously induced gene silencing effects of micro RNAs and the machinery involved can be exploited for downregulation of target genes by foreign double-stranded RNA (dsRNA) (Valencia-Sanchez et al., 2006). Short interfering RNAs (siRNAs) and dsRNAs target a specific mRNA for degradation, resulting in depletion of the corresponding protein, and are therefore a useful tool for studying protein function. As siRNAs carry a net negative charge, in order to enter the cell, they can be packaged into liposomes containing cationic lipids that mimic the natural phospholipids present in the plasma membrane. Lipid based-transfection is a highly efficient and reproducible method of siRNA delivery that can be used in many different cell types. Once inside the cell, the siRNA binds with the RNA-induced silencing complex (RISC) and unwinds to become single stranded (Valencia-Sanchez et al., 2006). It is then capable of binding to its complementary mRNA which induces mRNA cleavage by RNase activity within the RISC complex and targets it for degradation. While siRNAs are relatively resistant to

degradation, the level and duration of knockdown depends on the rate of cell growth and the dilution of siRNAs below a crucial threshold that is necessary to maintain inhibition of gene expression. Gene knockdown by siRNA is therefore a transient mechanism, with significant protein depletion usually achieved between 48-72 hours post-transfection (Moore, 2007).

In order to investigate the role of BIN1 in APP processing at the BBB, depletion of BIN1 protein followed by analysis of intracellular and extracellular products of APP proteolysis, may yield useful clues to inform future studies. This methodology does not require the development of a stable knockdown and therefore siRNA-mediated depletion offers a time-sensitive approach to the research question. It is also more representative of the parent cells which express endogenous levels of BIN1 prior to transfection and therefore it can give more information on the normal function of BIN1 in these cells. RNA interference has been used by many recent studies to investigate BIN1 function *in vitro* (Glennon et al., 2013, Meinecke et al., 2013, Ubelmann et al., 2017, Nakajo et al., 2016, Miyagawa et al., 2016) but the use of BIN1 siRNA in BMECs remains to be explored.

4.1.3 BIN1 and APP Processing

One of the first studies post-GWAS to investigate BIN1 protein expression in AD was conducted by Glennon et al. (2013), who found that BIN1 was reduced by 87% ($p=0.007$) in sporadic AD frontal cortex compared to non-dementia controls. With the hypothesised role of BIN1 in APP processing, they investigated whether there was a correlation between BIN1 and the levels of soluble and insoluble Aβ and Aβ plaque load. None of these parameters correlated with BIN1 expression, suggesting that decreased BIN1 is unlikely to affect the generation or degradation of Aβ. This was corroborated, in the same study, *in vitro* by siRNA-mediated depletion of BIN1 in a human neuroblastoma cell line (SH-SY5Y). No change in APP expression in cell lysate was observed nor in the production of Aβ and the soluble ectodomain resulting from α (sAPPα) or β (sAPPβ) cleavage in conditioned media (Glennon et al., 2013), suggesting that BIN1 may not be involved in the processing of APP.

These findings were recently supported by Ubelmann et al. (2017) who investigated the effects of Bin1 depletion in both mouse primary cortical neurons and N2a mouse neuroblastoma cells. The authors showed that siRNA-mediated depletion of Bin1 in N2a

cells did not affect cell surface APP or its endocytosis and its rate of trafficking to the lysosome was comparable to control cells, suggesting Bin1 does not control APP endocytic trafficking (Ubelmann et al., 2017). Similarly, BACE1, the β-secretase involved in APP cleavage, showed no change in surface expression or internalisation with Bin1 depletion. However, a reduction in the amount of BACE1 recycled back to the plasma membrane was detected, suggesting Bin1 is important for the endocytic recycling of BACE1 but not APP. The accumulated BACE1 that failed to recycle in Bin1-depleted N2a cells was found to associate with early endosomes. Furthermore, no change in BACE1 degradation was observed, suggesting that BACE1 accumulated in the early endosomes because of defective recycling mechanisms, rather than impaired lysosomal degradation.

The same defects were observed in Bin1-depleted mouse primary cortical neurons where increased intracellular Aβ42 was reported, suggesting BACE1 accumulation increased the amyloidogenic processing of APP (Ubelmann et al., 2017). A significant decrease in extracellular Aβ40 was observed with Bin1 depletion although no change in extracellular Aβ42 was reported. These findings suggest that Bin1 depletion may enhance the production of intracellular but not secreted Aβ. This was further supported by increased APP-CTFs, suggesting that BACE1 early endosome accumulation increases the amyloidogenic processing of APP. It was proposed that this is due to the increase in encounters between BACE1 and APP in early endosomes with Bin1 depletion, as an increase in APP and BACE1 colocalisation was observed in Bin1-depleted neurons. The retention of BACE1 in early endosomes was therefore sufficient to increase the encounter of BACE1 with APP contained within early endosomes.

Interestingly, the increase in Aβ42 in neurons and impairment of BACE1 recycling in N2a cells was rescued by re-expressing neuronal Bin1 but not ubiquitous Bin1, suggesting a specific function of the neuronal isoform. However, the impairment of BACE1 recycling with BIN1 depletion has also been demonstrated by Miyagawa et al. (2016) in both N2a cells and non-neuronal HeLa cells. This suggests that regulation of intracellular trafficking by BACE1 can be regulated by other ubiquitous isoforms of BIN1 and is not just a neuron-specific function. With an involvement in APP processing identified in both neuronal and non-neuronal cell lines and the aforementioned plausibility of the involvement of BMECS in amyloidosis, it brings into question whether BIN1 is involved in APP processing at the blood-brain barrier.

4.1.4 The hCMEC/D3 Cell Line as a Model of the BBB

Endothelial cells lining the CNS microvasculature possess unique morphological and functional properties involved in regulating exchanges between the circulating blood and brain parenchyma, distinguishing them from other vascular endothelia. The requirement for an *in vitro* culture system that accurately mimics the BBB has been recognised since brain capillaries were first isolated in the early 1970s (Brendel et al., 1974). It is difficult to investigate these properties *in vivo* as brain capillaries represent such a small proportion of total brain tissue. While utilisation of primary human brain endothelial cells represents an ideal model, the paucity of fresh human brain tissue makes this an impractical solution for large-scale studies.

The hCMEC/D3 cell line represents the first extensively characterised human brain endothelial cell line recapitulating most of the unique properties of the BBB (Weksler et al., 2005). Cells were derived from human temporal lobe microvessels isolated from a female epilepsy patient by surgical excision and transduced sequentially with the human telomerase reverse transcriptase (hTERT) and SV40 large T antigen lentiviral vectors. The clonal population of hCMEC/D3 cells was then selected which exhibited a normal diploid karyotype and elongated morphology in a tightly packed monolayer with contact inhibition at confluence, similar to primary brain endothelial cultures (Weksler et al., 2005). The cell line was extensively characterised for appropriate expression and localisation of endothelial and BBB-specific markers, including von Willebrand factor and junctional proteins VE-cadherin, β- and γ-catenins, ZO-1, JAM-1 and claudin-5, suggesting maintenance of both tight junction and adherens junction organization (Weksler et al., 2005). Immunological characteristics included expression of leukocyte adhesion molecules and chemokine receptors, such as CXCR-1 to CXCR-5 and CCR-3 to -CCR-6 (Weksler et al., 2005). However, only low to medium TEER levels of 30-50 Ω/cm^2 were achieved in hCMEC/D3 monolayers, compared to *in vivo* mammalian levels of 1000 Ω/cm^2, indicating suboptimal formation of tight junctions (Butt et al., 1990). Nevertheless, highly restricted permeability to drugs at a range of hydrophobicity was demonstrated in line with *in vivo* values (Weksler et al., 2005). Stable cell growth and endothelial characteristics were maintained at least until the 35th passage (Weksler et al., 2013).

The hCMEC/D3 brain endothelial cell line is widely utilised in BBB studies and the best-characterised human BMEC line. It displays a close phenotype and APP expression level to

human primary BMECs (Urich et al., 2012), therefore presents a good predictive human BBB model to study APP processing and endocytic processes.

4.1.5 Aims of this Chapter

The aim of this chapter was to achieve depletion of total BIN1 (all isoforms) in a human brain endothelial cell line in order to provide an *in vitro* model to investigate BIN1 function at the BBB. This was then to be used for the characterization of the role of BIN1 in APP processing in BMECs. Specifically, the level and localisation of intracellular APP was determined with BIN1 depletion, in addition to an analysis of the products of APP proteolysis: Aβ40, β-CTF, sAPPα and sAPPβ. Components of the secretases that mediated APP cleavage were also analysed for expression levels in BIN1 depleted cells, including BACE1, PSEN1 and ADAM10. The immortalised human hCMEC/D3 cell line was chosen for this study as it displays characteristics of the BBB in a species-relevant cell line for the study of BIN1 in AD.

4.2 Experimental Design

4.2.1 Optimisation of siRNA-mediated BIN1 Depletion

Cells were transfected in 6-well plates as described in Chapter 2, Section 2.2. An optimisation experiment was carried out using two different BIN1 siRNA oligonucleotides, sequence 'a' binds within exon 9 of the BIN1 mRNA while sequence 'b' targets a region spanning the exon 8/9 junction. Both these regions are common to all BIN1 isoforms in order to target total BIN1 depletion. For each treatment with BIN1 siRNA, two controls were run alongside; cells in OptiMEM without Oligofectamine or oligonucleotide and cells transfected with siRNA targeting green fluorescent protein (GFP), which is not expressed in mammalian cells. Non-transfected and GFP siRNA-treated cells were used as controls in all further experiments, with quantitative comparisons made between BIN1-depleted and GFP siRNA-treated cells as this control allows the transfection procedure and off-target effects to be accounted for. A sample size (n) of at least 3 replicates was used for all quantified experiments, with n defined as a biological replicate performed on one passage of cells with separate reagents to any other replicates.

Table 4.1: siRNA sequences used to analyse BIN1 depletion

siRNA target	**Sequence**	**Reference**
Total BIN1 'a'	CCAGAACCUCAAUGAUGUG	Custom designed (Eurofins)
Total BIN1 'b'	GGAGAUGAGCAAGCUCAAC	Custom designed (Eurofins)
GFP	GGCUACGUCCAGGAGCGCA	(Moody et al., 2015)

4.2.2 Western Blotting

Western blotting was performed as described in Chapter 2, Section 2.3 using the primary antibodies detailed in Table 4.2. For each sample, 10-20 μg protein was used per well and samples were electrophoresed on a 10% acrylamide gel. Some of the blots were carried out by Catherine Matheson and Robert Greening as part of a final year undergraduate project, co-supervised by myself. All densitometry analysis was re-analysed by myself. Quantification of protein was calculated by densitometry analysis normalizing to GAPDH expression, previously described in Chapter 2, Section 2.3.6. A sample size (n) of at least 3 replicates was used for all quantified experiments, as previously described.

4.2.3 Immunocytochemistry Conditions

Immunoctochemistry was carried out on a sample size of 3 per experiment as described in Chapter 2, Section 2.4 with cells fixed in 4% PFA according to Chapter 2, Section 2.4.1. For surface labelling of APP, triton X-100 was omitted from all wash buffers and antibody diluent. Alexa Fluor 488 Phalloidin (ThermoFisher Scientific) was used to stain filamentous actin (F-actin) at a 1/40 dilution for 20 min at RT, according to the manufacturer's instructions. For colocalisation experiments, cells were stained sequentially with each antibody one at a time and controls were carried out alongside using each antibody alone. Details of the antibodies used in this chapter can be found in Table 4.2

Table 4.2: Primary Antibodies used in Chapter 4

Antibody	Host	Supplier	Dilution	
			WB	ICC
BIN1	Mouse	Abcam	0.48 μg/ml	0.48 μg/ml
APP A4 (N-terminal, amino acids 66-81 of APP, clone 22C11)	Mouse	Millipore	N/A	1.33 μg/ ml
BACE1 (C-terminal, amino acids 485-501 of BACE1)	Rabbit	Millipore	N/A	1 μg/ ml
PSEN1	Rabbit	Abcam	1 μg/ml	N/A
ADAM10	Rabbit	Abcam	0.2 μg/ml	N/A

WB = Western blotting, ICC = Immunocytochemistry

4.2.4 Cell Viability

Cell viability following siRNA treatment was assessed using the CellTiter 96® AQueous One Solution Cell Proliferation Assay (Promega) according to manufacturer's instructions, as described in Chapter 2, Section 2.5.

4.2.5 Enzyme-linked Immunosorbent Assays (ELISAs)

ELISAs were used to quantify APP and products of its proteolysis in cell lysate and media from BIN1-depleted cells. For each assay, an initial optimisation was carried out to determine the appropriate amount of sample to be used. A four-point standard curve was used for optimisation, with the aim of reaching sufficient detection levels to fall within the exponential phase of the curve. For all assays, absorbance readings were converted to protein concentration values per ml of sample using a standard curve and then expressed as

a concentration per mg of total cell protein, according to protein concentration values calculated by BCA assay, described in Chapter 2, Section 2.3.2. These values were finally presented as a mean percentage of the non-transfected control for GFP siRNA-treated and BIN1-depleted cells.

4.2.5.1 Quantification of APP

For quantification of intracellular APP, the Human APP DuoSet ELISA kit (R&D Systems, Minneapolis, Minnesota, USA) and was used according to manufacturer's guidelines (Thomas et al., 2011). Briefly, the capture antibody (4 μg/ml) was adsorbed to a 96-well plate in PBS at RT overnight. Unbound sites were blocked with 1% BSA and 5% sucrose in PBS for 1 hour at RT. Samples were diluted 1/10 in PBS supplemented with 1% BSA quantified in duplicate using a six-point standard curve (0-20 ng/ml). The biotinylated detection antibody was used at 300 ng/ml and detected using streptavidin-HRP and *o*-Phenylenediamine dihydochloride (Sigma). The reaction was stopped after 35 min by the addition of 2.5M H_2SO_4 and the plate was then read at 492nm on a uQuant plate reader.

4.2.5.2 Quantification of APP fragments (Aβ40, sAPPa, sAPPβ and βCTF) and BACE1

For analysis of extracellular Aβ40, sAPPα and sAPPβ and intracellular β-CTF and BACE1, ELISA kits (IBL, Hamburg, Germany) were used according to manufacturer's instructions. Briefly, 48 hours post-transfection, cell media from siRNA-treated samples was quantified in duplicate using a standard curve on plates pre-coated with the capture antibody. Lysate samples for intracellular proteins (β-CTF and BACE1) were quantified singularly in order to use sufficient sample for detection with a limited stock volume while the extracellular proteins (Aβ40, sAPPα and sAPPβ) were quantified in duplicate. After adsorbing samples to pre-coated plates, an enzyme conjugate was added at 4°C for 60 minutes and detected using TMB substrate solution for 30 minutes at RT. TMB stop solution was added to stop the reaction and the plate read at 450nm on a uQuant plate reader.

4.3 Results

4.3.1 Optimisation of siRNA-mediated BIN1 Depletion

4.3.1.1 Level of knockdown

In order to deplete BIN1 protein levels in the hCMEC/D3 cell line, two siRNA oligonucleotides targeting full-length BIN1 protein were independently tested. Both siRNAs significantly decreased BIN1 expression by >73% compared to non-transfected cells (Figure 4.1) while siRNA targeting GFP did not affect BIN1 protein expression compared to non-transfected cells and was therefore used as a control for siRNA treatment. While both siRNAs significantly reduced the protein levels of BIN1 (siRNA 'a': 74% reduction $p = 0.02$, siRNA 'b': 90% reduction $p = 0.003$), the results of using siRNA 'a' were less consistent than the 90% BIN1 protein depletion of siRNA 'b' (Figure 4.1) therefore siRNA 'b' was chosen for use in all future studies. The level of BIN1 depletion was quantified by Western blotting and further visualised by immunocytochemistry, which confirmed the depletion of BIN1 protein Figure 4.2. BIN1 depletion did not cause any gross changes in cell morphology or apparent cytoskeletal defects, as visualised with F-actin staining (Figure 4.2). All three conditions show a similar filamentous distribution of actin throughout the cytoplasm and peripheral staining, most likely representing the plasma membrane, suggesting that the overall cell structure and cytoskeleton was not affected by BIN1 depletion.

4.3.1.2 Cell viability

To assess any effect of the siRNA treatment on cell viability, a colorimetric cell proliferation assay was used which measures the reduction of MTS (3-(4,5-dimethylthiazol-2-yl)-5-(3-carboxymethoxyphenyl)-2-(4-sulfophenyl)-2H-tetrazolium) to formazan by viable cells, allowing for quantification of cell viability in culture. There was no significant difference in the absorption measurements between non-transfected, GFP siRNA and BIN1-depleted cells suggesting no effect of siRNA treatment or BIN1 depletion on cell viability ($p > 0.05$ using a two-tailed unpaired Student's *t* test, Figure 4.3).

A)

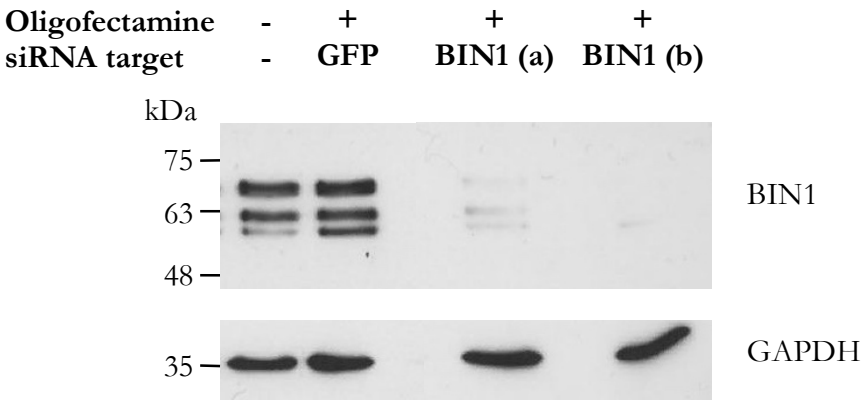

B)

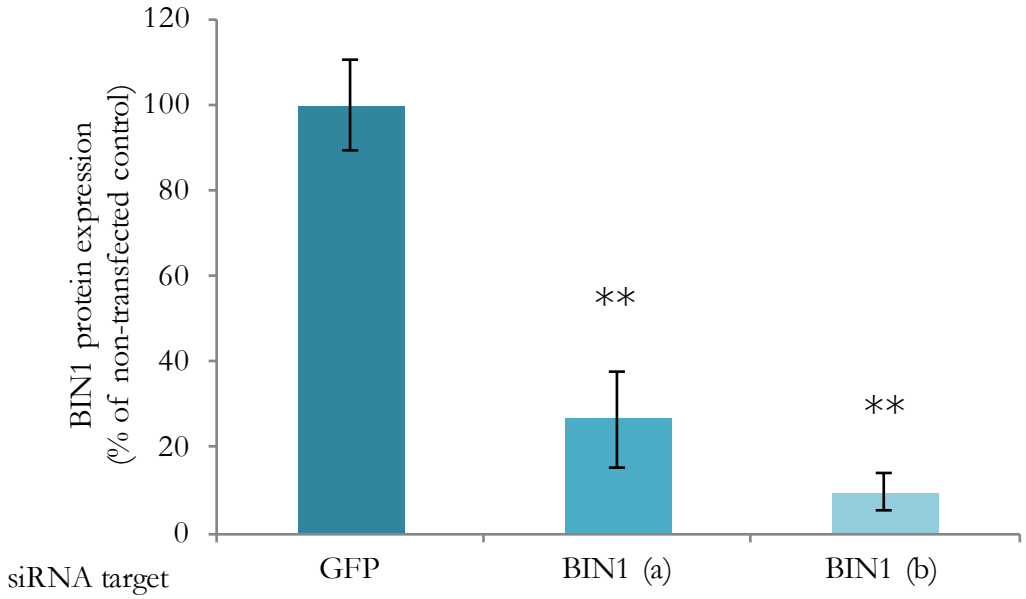

Figure 4.1: Optimisation of siRNA-mediated BIN1 depletion

A) A representative Western blot demonstrating successful knockdown of BIN1 protein 48 hours after exposure to separate siRNAs targeting BIN1 (a and b) in hCMEC/D3 cells.

B) Quantification of BIN1 depletion 48 hours post-transfection shows significant knockdown using each siRNA expressed as a mean percentage of non-transfected cells (n = 3, ** = $p<0.01$ using a two-tailed unpaired Student's *t* test, error bars = standard error of the mean (SEM).

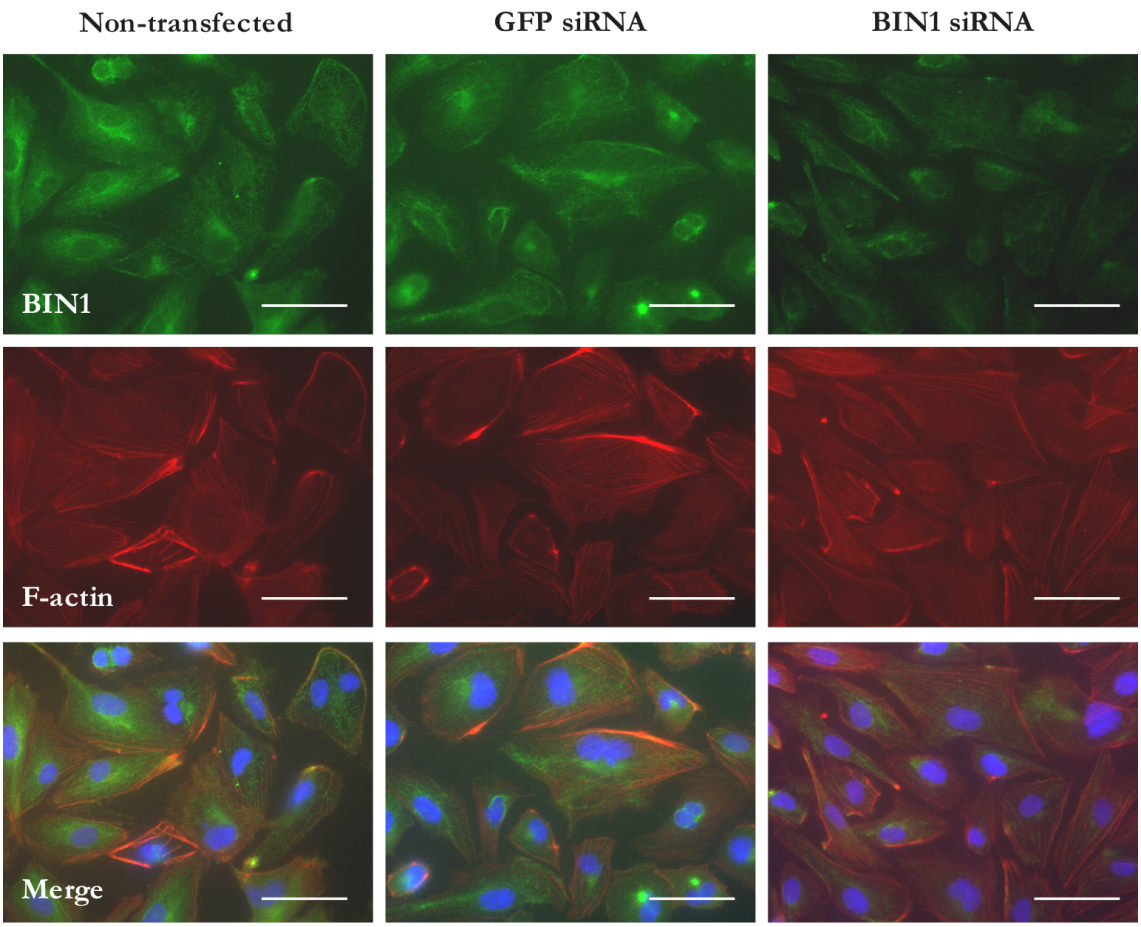

Figure 4.2: Visualisation of BIN1 depletion using siRNA b

Representative images of immunocytochemical staining of BIN1 (green) and F-actin (red) in non-transfected, GFP siRNA-treated and BIN1-depleted hCMEC/D3 cells. Nuclei are stained for DAPI, scale bar = 50 μm.

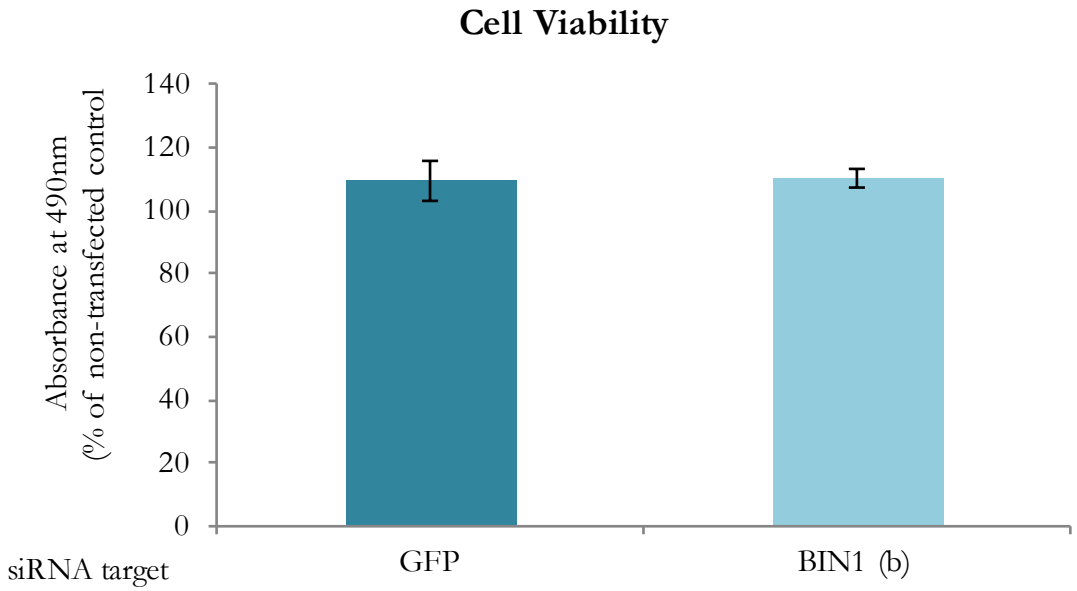

Figure 4.3: Quantification of cell viability upon treatment with GFP and BIN1 siRNA

Absorbance readings following an MTS colorimetric cell proliferation assay expressed as a percentage of non-transfected cells (100%). Values represent the mean, n = 3, error bars = SEM, $p > 0.05$ using a two-tailed unpaired Student's *t* test.

4.3.2 Levels of APP Components with BIN1 Depletion

4.3.2.1 Extracellular Aβ40

To investigate whether BIN1 may affect the proteolytic cleavage of APP to produce Aβ, levels of Aβ40 were analysed in the extracellular media of non-transfected, GFP siRNA-treated and BIN1-depleted cells by ELISA. The levels of extracellular Aβ40 indicated a 30% decrease for BIN1-depleted cells compared to non-transfected, however this did not reach significance when compared to GFP siRNA-treated cells (Figure 4.4, $p > 0.05$ using a two-tailed unpaired Student's *t* test). It should be noted that the levels of Aβ40 in the conditioned media ranged from 0.576 – 4.476 pg/ml which was at the low end of the detection limit of 1.56 pg/ml for the ELISA. Due to the low levels of Aβ40, it was anticipated that the level of Aβ42 produced would be beyond the limits of reliable detection for these cells as Aβ40 is produced at considerably higher levels than Aβ42 *in vivo* and in cultured BMECs (Mawuenyega et al., 2010, Kitazume et al., 2010). Aβ42 levels were therefore not analysed.

4.3.2.2 β-CTF

To further scrutinise the effect of BIN1 depletion on Aβ40 production, levels of the intracellular β-CTF, which undergoes β-cleavage to produce Aβ, were analysed. As it remains membrane-associated, intracellular β-CTF levels may allow a more detectable proxy for Aβ production. Indeed, β-CTF levels for all samples ranged from 1.680 – 2.982 pmol/L, well within the detection range of 0.19 – 12 pmol/L for the assay. Interestingly, in contrast to Aβ40 levels, a 40% increase in the intracellular β-CTF was observed with BIN1 depletion compared to GFP siRNA-treated cells ($p < 0.05$ using a two-tailed unpaired Student's *t* test,

Figure 4.5).

4.3.2.3 APP

The increase in β-CTF may be a result of increased internalisation of APP into the cell, therefore levels of intracellular APP were then quantified. APP levels in diluted samples ranged from 5.169 – 15.259 ng/ml, allowing for accurate readings within the detectable limit of 0.625 – 20 ng/ml. Total APP levels within the cell lysates were calculated at 55.262 – 194.870 ng/mg total protein. This large variation was observed between rather than within experiments and this was therefore overcome by expressing concentrations as a percentage of the non-transfected control. No significant difference was observed in total intracellular APP levels between BIN1-depleted and GFP siRNA-treated cells ($p > 0.05$ using a two-tailed unpaired Student's *t* test, (Figure 4.6). This was further supported by immunocytochemistry which was used to observe total APP and cell surface APP alone, in the absence of cell permeabilisation (Figure 4.12Figure 4.13). Overall levels of staining, although not quantitative, looked similar across conditions further suggesting there was no change in the levels of APP within the cell or on the cell surface. The observed localisation of APP is further described in Section 4.3.4.

4.3.2.4 sAPPa and *APPβ*

To further elucidate whether the increase in β-CTF was a result of a change at the β-cleavage stage of APP processing, the amount of sAPPβ in the extracellular media was quantified. However, levels ranged from 0 – 0.262 ng/ml which fell outside the detectable range of the assay (0.78 – 50 ng/ml) therefore reliable quantification of sAPPβ levels could not be established. Levels of sAPPα, on the other hand, ranged from 0.458 – 11.261 ng/ml, within the detectable range of the assay but showed large variation between samples and no significant difference with BIN1 depletion ($p > 0.05$ using a two-tailed Mann-Whitney test, Figure 4.7). These results suggest that the amyloidogenic processing of APP is perturbed by BIN1 depletion as an increase in β-CTF levels was observed. However,

increased β-cleavage of APP cannot be determined from these results due to the low levels of sAPPβ detected and lack of change in extracellular Aβ40 levels. With no change in extracellular sAPPα levels, a change in the non-amyloidogenic processing of APP is not suggested. Collectively, these findings do show a change in the amyloid pathway as a result of BIN1 depletion. Due to the established involvement of BIN1 in endocytic trafficking, this may be suggestive of perturbation in this mechanism.

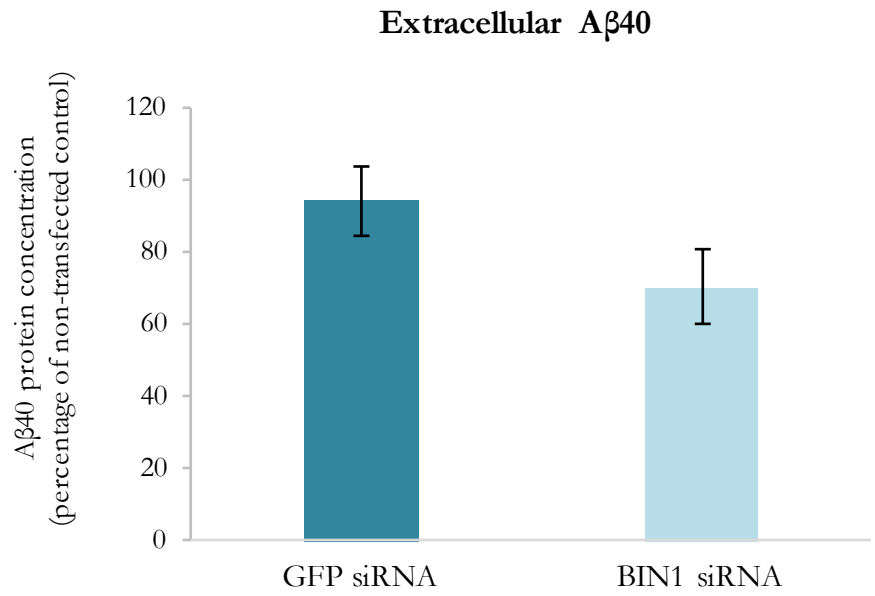

Figure 4.4: Quantification of extracellular Aβ40 upon BIN1 depletion

Aβ40 protein levels in the conditioned media of GFP and BIN1-depleted cells, detected by ELISA and expressed as a percentage of non-transfected cells (100%). The mean level of Aβ40 in non-transfected cells was 2.44 pg/mg total protein. Values represent the mean of six biological replicates, error bars = SEM, $p > 0.05$ using a two-tailed unpaired Student's *t* test.

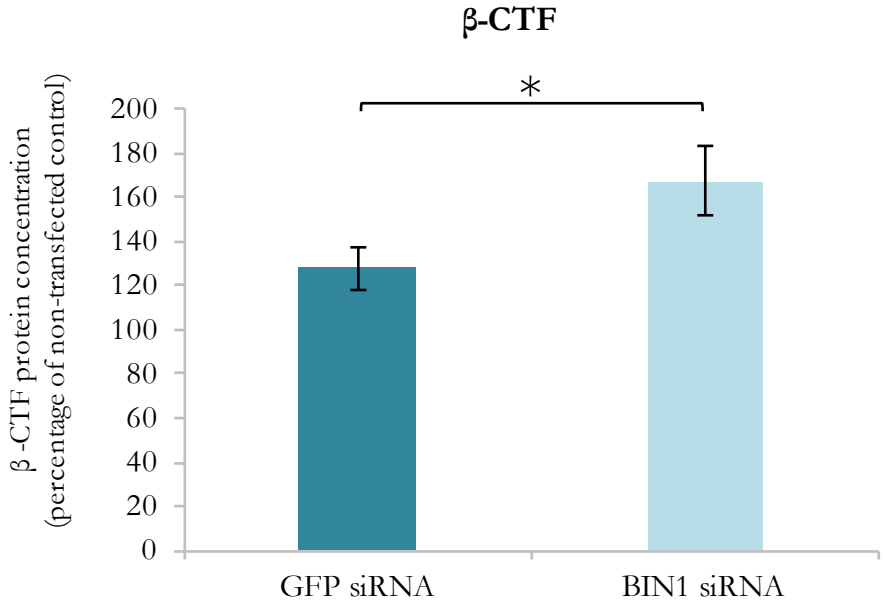

Figure 4.5: Quantification of intracellular β-CTF upon BIN1 depletion

β-CTF protein levels in GFP and BIN1-depleted cells, detected by ELISA and expressed as a percentage of non-transfected cells (100%). The mean level of β-CTF in non-transfected cells was 1.27 pg/mg total protein. Values represent the mean of nine biological replicates, error bars = SEM, * = $p<0.05$ using a two-tailed unpaired Student's *t* test.

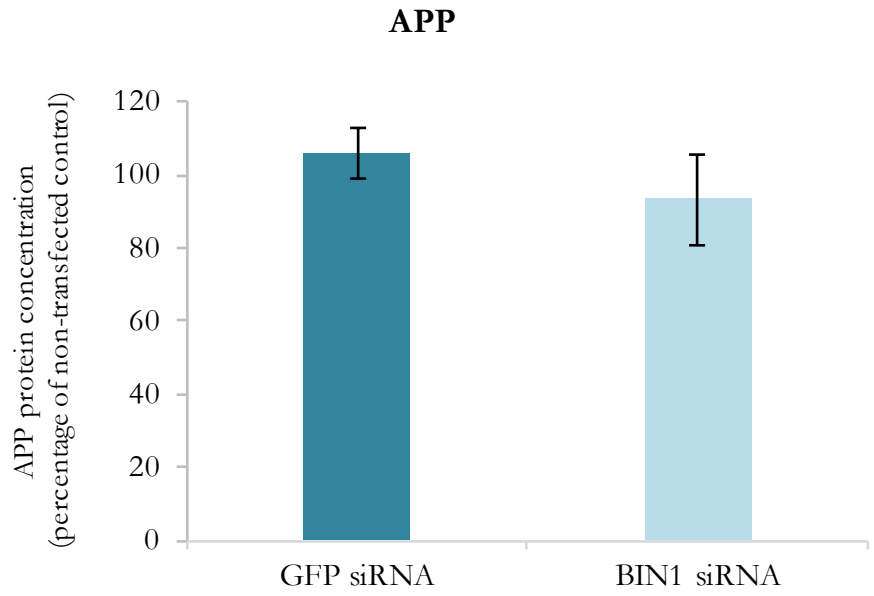

Figure 4.6: Quantification of total cellular APP upon BIN1 depletion

Total APP protein levels in GFP and BIN1-depleted cells, detected by ELISA and expressed as a percentage of non-transfected cells. Values represent the mean of nine biological replicates, error bars = SEM, $p > 0.05$ using a two-tailed unpaired Student's *t* test.

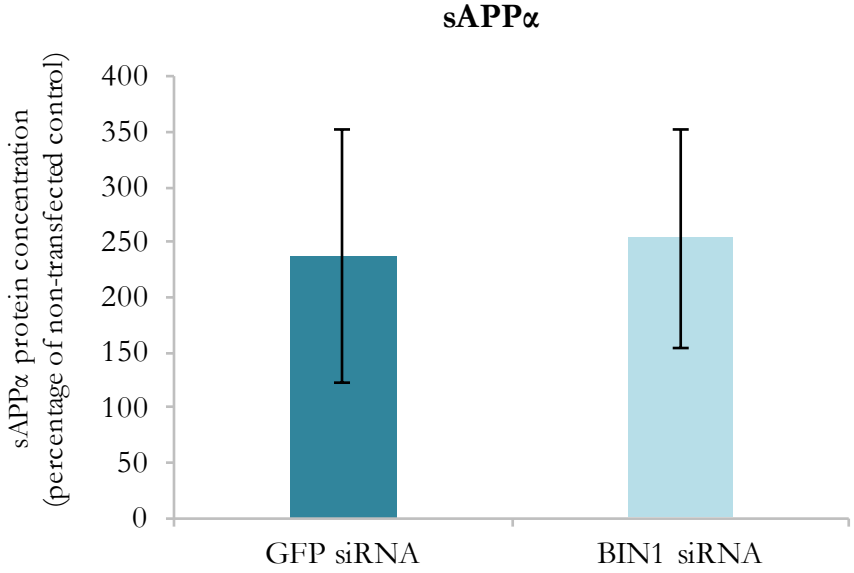

Figure 4.7: Quantification of extracellular sAPPα upon BIN1 depletion

Levels of sAPPα in the conditioned media of GFP and BIN1-depleted cells, detected by ELISA and expressed as a percentage of non-transfected cells. Values represent the mean of ten biological replicates, error bars = SEM, $p > 0.05$ using a two-tailed Mann-Whitney test.

4.3.3 APP Proteolytic Enzymes

4.3.3.1 BACE1

With previous studies indicating that depletion of BIN1 *in vitro* impairs the endosomal trafficking of BACE1, leading to intracellular accumulation, it was important to examine BACE1 levels with BIN1 depletion in the hCMEC/D3 cells. The level of cellular BACE1 showed no significant difference in BIN1-depleted cells compared to GFP siRNA-treated cells ($p > 0.05$ using a two-tailed unpaired Student's *t* test, Figure 4.8), suggesting that the increase in β-CTF may not be a result of increased β-secretase cleavage of APP by BACE1.

Next the intracellular localisation of BACE1 was examined. BACE1 largely showed a punctate, likely vesicular, distribution in the majority of cells with some cells exhibiting accumulation in the perinuclear region (Figure 4.9). In support of the ELISA data, although not quantitative, no gross differences in BACE1 levels were apparent with BIN1 depletion and its localisation was also unaffected, showing a similar distribution across conditions (Figure 4.9).

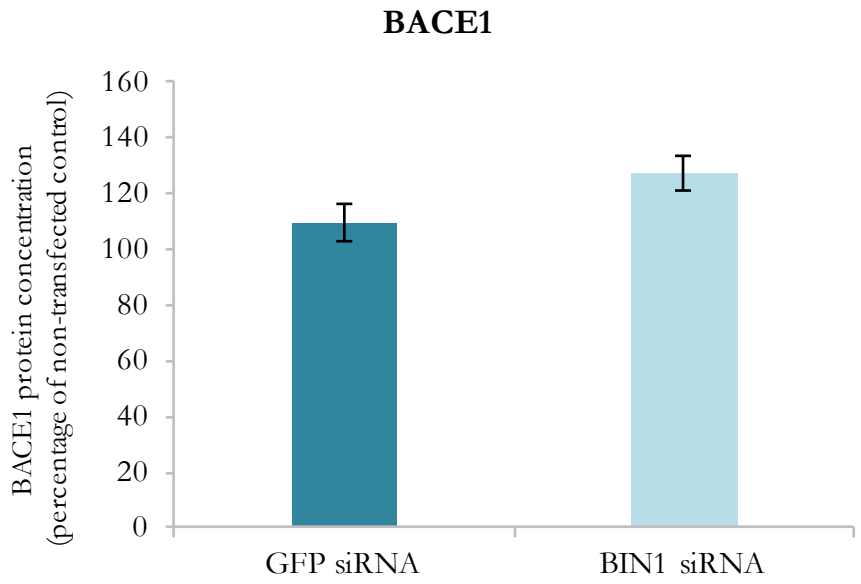

Figure 4.8: Quantification of cellular BACE1 upon BIN1 depletion

Total BACE1 protein levels in GFP and BIN1-depleted cells, detected by ELISA and expressed as a percentage of non-transfected cells. Values represent the mean of eight biological replicates, error bars = SEM, $p > 0.05$ using a two-tailed unpaired Student's *t* test.

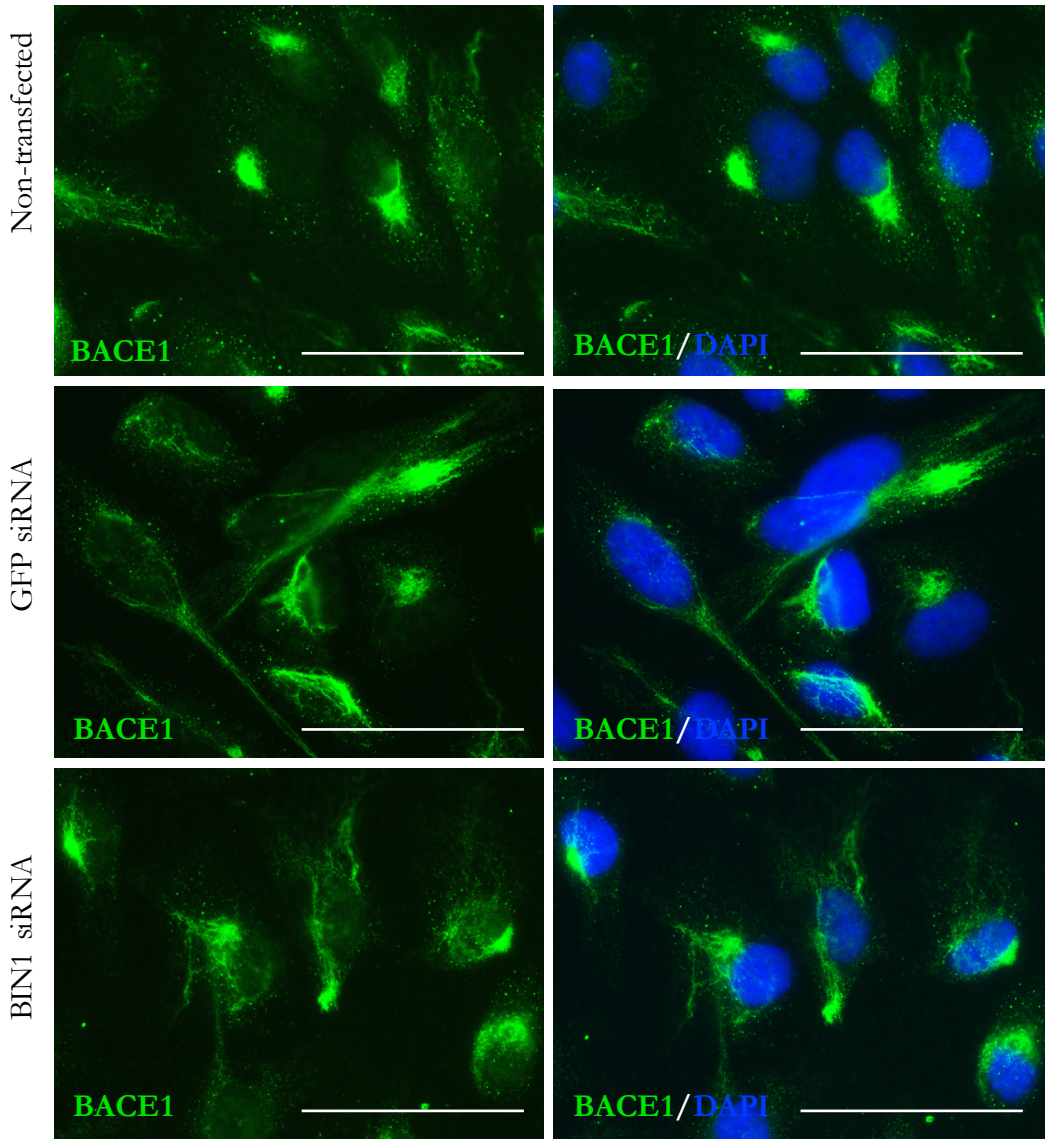

Figure 4.9: BACE1 expression with BIN1 depletion

Representative immunofluorescence images of BACE1 expression in non-transfected, GFP siRNA-treated and BIN1-depleted hCMEC/D3 cells. Images were taken at x40 magnification with DAPI used to stain the nuclei, scale bar = 50 μm.

4.3.3.2 Presenilin 1

PSEN1 encodes the catalytic subunit of the γ-secretase complex and has over 200 identified mutations that cause fAD through altered γ-secretase function resulting in increased production of longer Aβ oligomers such as Aβ42 (Borchelt et al., 1996, Scheuner et al., 1996). As an increase in β-CTF was observed, with no obvious signs of increased internalisation of APP, it is possible that alteration of γ-secretase cleavage occurs with BIN1 depletion resulting in an accumulation of β-CTF due to less proteolysis into Aβ. PSEN1 protein levels were therefore examined in hCMEC/D3 cells with BIN1 depletion by Western blotting. Two bands were produced when blots were probed for PSEN1, the first at 58 kDa corresponding to the full-length protein whereas the much smaller band at 25 kDa may represent the N-terminal fragment (Figure 4.10A). Indeed, PSEN1 is proteolytically cleaved at its large hydrophilic loop domain and is detected predominantly as stable N- and C-terminal fragments at 28 and 18 kDa, respectively (Thinakaran et al., 1996). This endoproteolysis is thought to remove the loop domain that otherwise inhibits substrate binding and therefore activates PSEN1 (Knappenberger et al., 2004). The images of full-length and N-terminal PSEN1 presented in Figure 4.10A were derived from separate blots, as sufficiently quantifiable bands for the full-length protein were only obtained on a gel that had been run too far for the N-terminal fragment to remain. For this reason, the full-length protein required normalization to α-tubulin rather than GAPDH as this larger protein remained on the gel. Further optimisation would ensure both fragments could be detected on the same blot for more accurate quantification.

There was no significant difference in PSEN1 holoprotein (58 kDa) expression with BIN1 depletion compared to GFP siRNA-treated cells ($p > 0.05$ using a two-tailed unpaired Student's *t* test, Figure 4.10B). The third replicate blot for the PSEN1 N-terminal fragment (25 kDa) was unreliable and was therefore excluded from analysis. This left only two blots for densitometry analysis. According to the GraphPad statistical software used, both SEM and *t* test calculations are valid with a sample of 2 (http://www.graphpad.com). Therefore, statistical analysis was carried out and showed no significant change in PSEN N-terminal fragment levels with BIN1 depletion compared to GFP siRNA-treated cells ($p > 0.05$ using a two-tailed unpaired Student's *t* test, Figure 4.10C). This suggests that BIN1 depletion did not affect levels of PSEN1, therefore it is unlikely that a change in γ-secretase cleavage was driving the changes observed in the amyloidogenic pathway with BIN1 depletion.

4.3.3.3 ADAM10

ADAM10 (A disintegrin and metalloproteinase domain-containing protein 10) is a membrane-bound protease and is one of the major APP α-secretases, cleaving APP within the Aβ domain, thus preventing Aβ generation (Asai et al., 2003). In order to explore whether the increase in β-CTF with BIN1 depletion may have been associated with a change in the α-cleavage of APP, levels of ADAM10 protein were measured by Western blot. As ADAM10 is subject to intramembrane proteolysis (Tousseyn et al., 2009), multiple bands were detected, with a strong band appearing at ~99 kDa followed by two bands at ~75 kDa and ~69 kDa and the lowest bands at ~59 and ~55 kDa (Figure 4.11A). All bands were produced across all conditions with no apparent difference observed in total ADAM10 protein levels upon BIN1 depletion. Unfortunately, clear bands for the housekeeping gene GAPDH were unable to be achieved in two of the four blots generated. Figure 4.11B shows densitometry analysis of total ADAM10 expression from the two blots that successfully produced GAPDH bands, showing no significant difference between BIN1-depleted and GFP siRNA-treated cells ($p > 0.05$ using a two-tailed unpaired Student's *t* test). Collectively these findings suggest that BIN1 depletion does not affect the amyloidogenic processing of APP by influencing secretase expression and therefore β-CTF may be increased in BIN1-depleted cells by an alternative method.

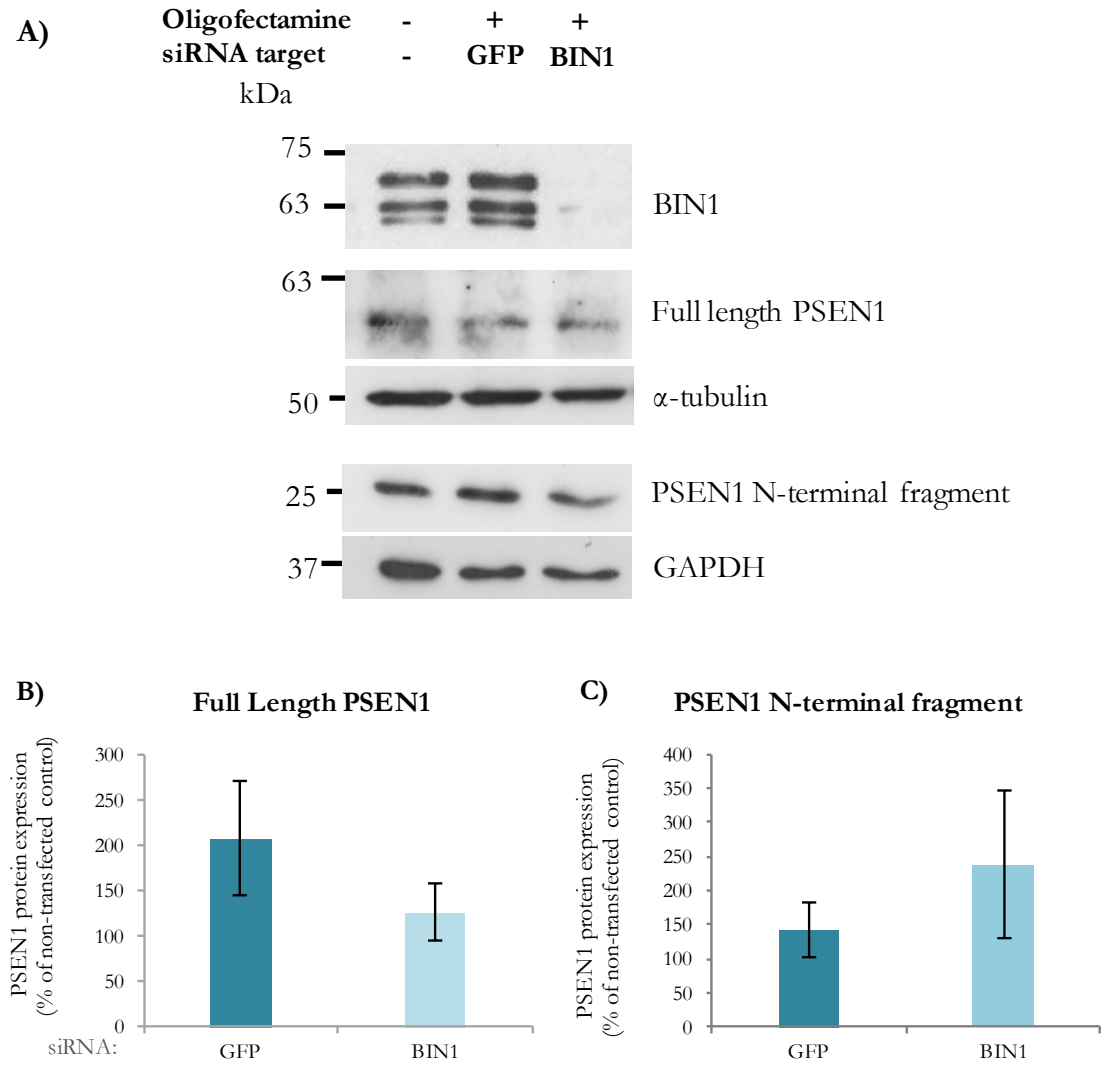

Figure 4.10: PSEN1 expression with BIN1 depletion

A) Representative Western blots showing expression of the PSEN1 holoprotein (full length) and N-terminal fragment.

B) Densitometry analysis of full length PSEN1 expression, normalised to GAPDH expression and expressed as a percentage of non-transfected cells, n = 3, error bars = SEM, $p > 0.05$ using a two-tailed unpaired Student's *t* test.

C) Densitometry analysis of PSEN1 C-terminal fragment expression, normalised to α-tubulin expression and expressed as a percentage of non-transfected cells, n = 2, error bars = SEM, $p > 0.05$ using a two-tailed unpaired Student's *t* test.

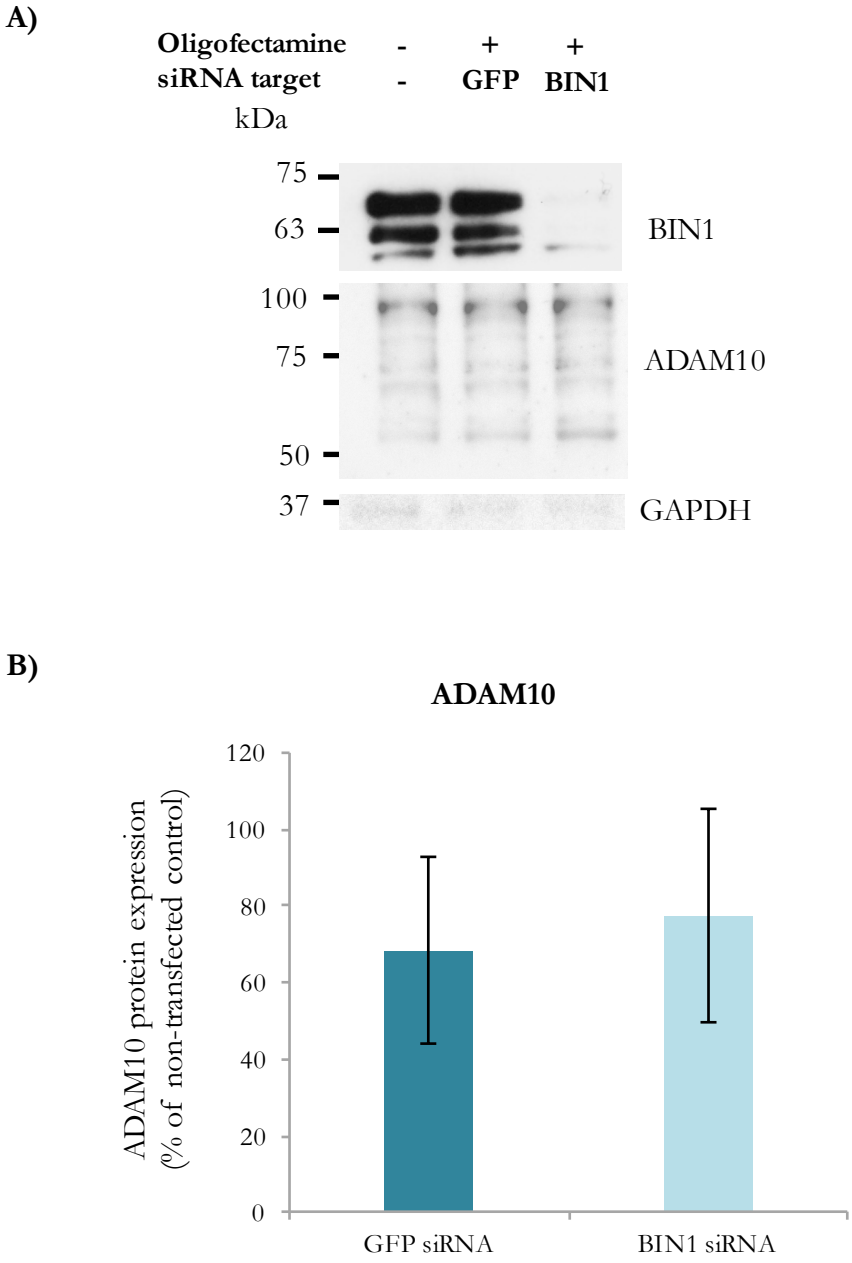

Figure 4.11: ADAM10 expression with BIN1 depletion

A) Representative Western blots showing expression of all detected ADAM10 protein domains in non-transfected, GFP siRNA-treated and BIN1 depleted hCMEC/D3 cells.

B) Densitometry analysis of total ADAM10 expression, normalised to GAPDH expression and expressed as a percentage of non-transfected cells, n = 2, error bars = SEM, $p > 0.05$ using a two-tailed unpaired Student's *t* test.

4.3.4 Localisation of APP and BACE1

With no gross changes in levels of key components of the APP proteolytic enzymes, the localisation of APP with BIN1 depletion was then investigated to see if this gave any mechanistic insights into the increase in βCTF. Immunocytochemistry was used to observe total APP and cell surface APP alone, in the absence of cell permeabilisation. Intracellular APP showed a strong uniform pattern of cytoplasmic staining which was filamentous in nature, appearing to follow a similar pattern to the actin cytoskeleton, previously observed with F-actin staining (Figure 4.2). This localisation pattern did not differ between conditions and was therefore not affected by GFP or BIN1 siRNA treatment (Figure 4.12) Extracellular APP staining, however, revealed a patchy, discontinuous distribution of APP in all conditions, suggesting low levels of expression in the plasma membrane (Figure 4.13). Immunoreactivity was high in the perinuclear region of some cells with the area overlying the nucleus, identified by DAPI staining, most frequently devoid of staining. Some cells (approximately 60%) were devoid of extracellular staining altogether. Across each coverslip, areas of enhanced filamentous staining were observed, much like those in the permeabilised condition, suggesting intracellular staining had occurred but the degree of this staining was not affected by siRNA treatment.

The colocalisation of APP with BACE1 was also analysed to investigate whether the increase in β-CTF levels with BIN1 depletion was related to increased intracellular encounters between APP and BACE1. APP and BACE1 showed a strong degree of colocalisation in the cytoplasm of non-transfected hCMEC/D3 cells (Figure 4.14). This staining was considered specific to APP and BACE1 as it did not differ from control conditions where each antibody was used in isolation (Figure 4.15). With BIN1 depletion, however there was no observable change in the localisation pattern of BACE1 and APP and they remained both expressed abundantly in the cytoplasm (Figure 4.14).

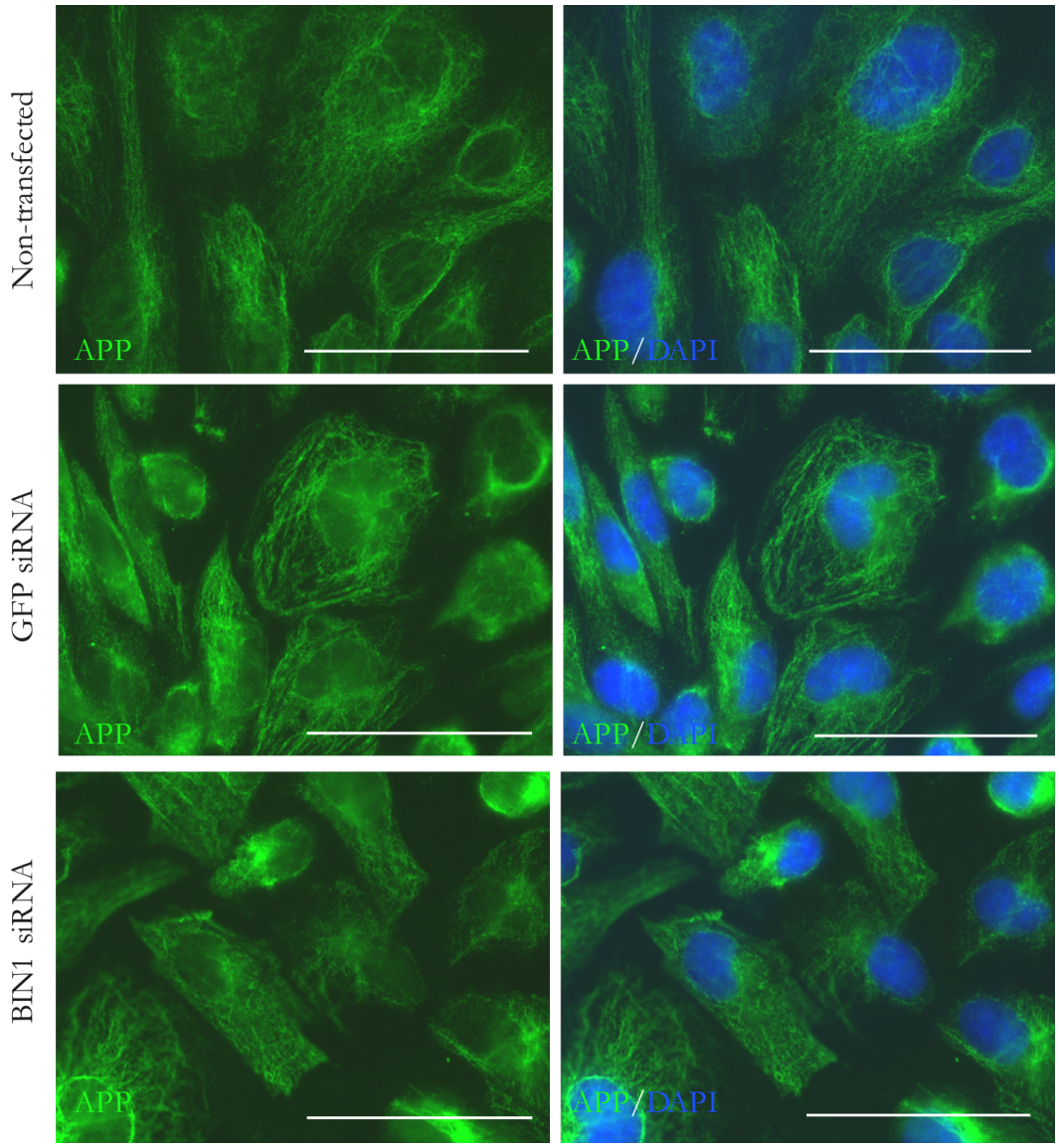

Figure 4.12: APP expression with BIN1 depletion

Representative immunofluorescence images of APP expression in non-transfected, GFP siRNA-treated and BIN1-depleted hCMEC/D3 cells. Images were taken at x40 magnification with DAPI used to stain the nuclei, scale bar = 50 μm.

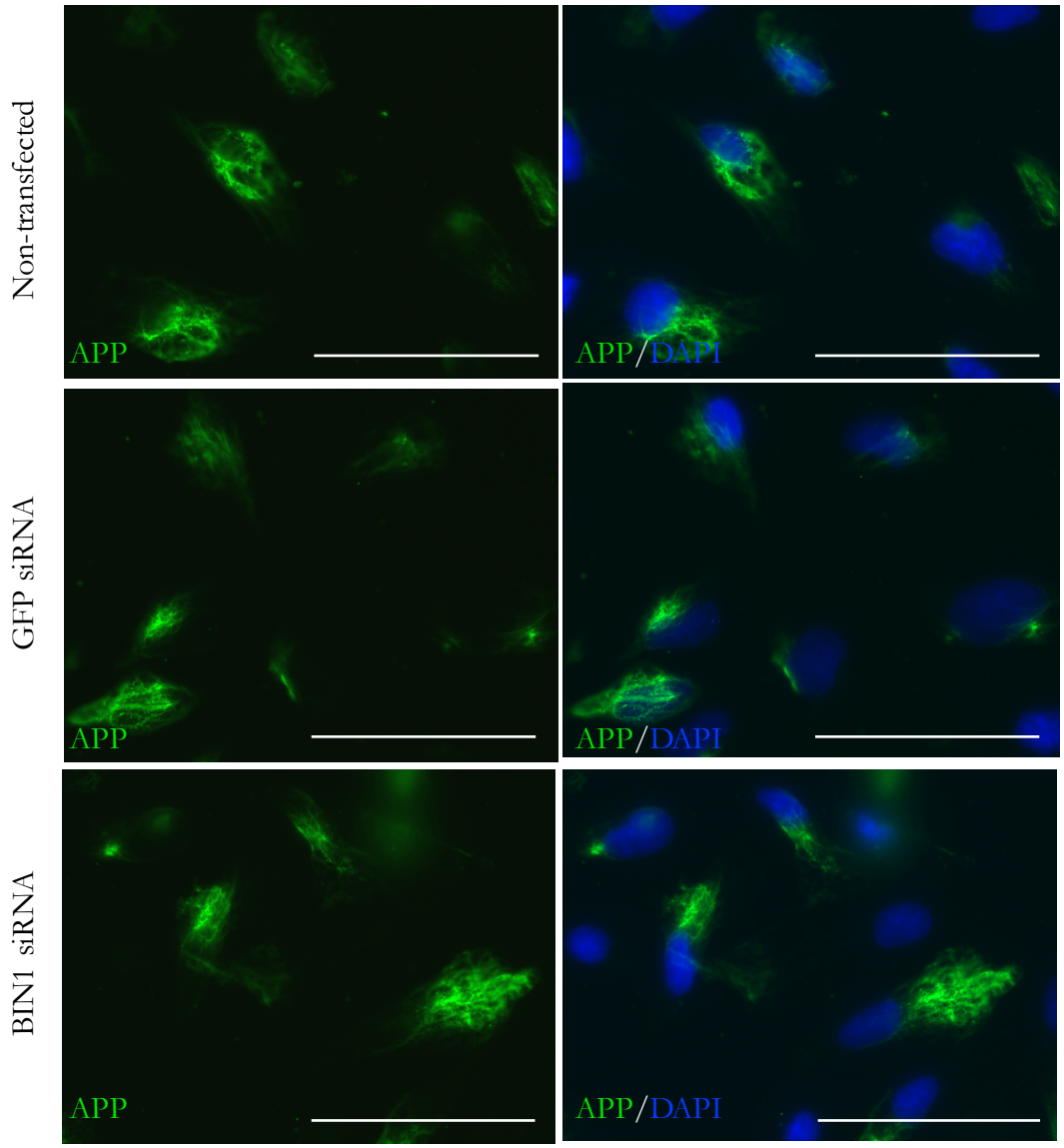

Figure 4.13: Extracellular APP expression with BIN1 depletion

Representative immunofluorescence images of APP expression without permeabilisation in non-transfected, GFP siRNA-treated and BIN1-depleted hCMEC/D3 cells. Images were taken at x40 magnification with DAPI used to stain the nuclei, scale bar = 50 μm.

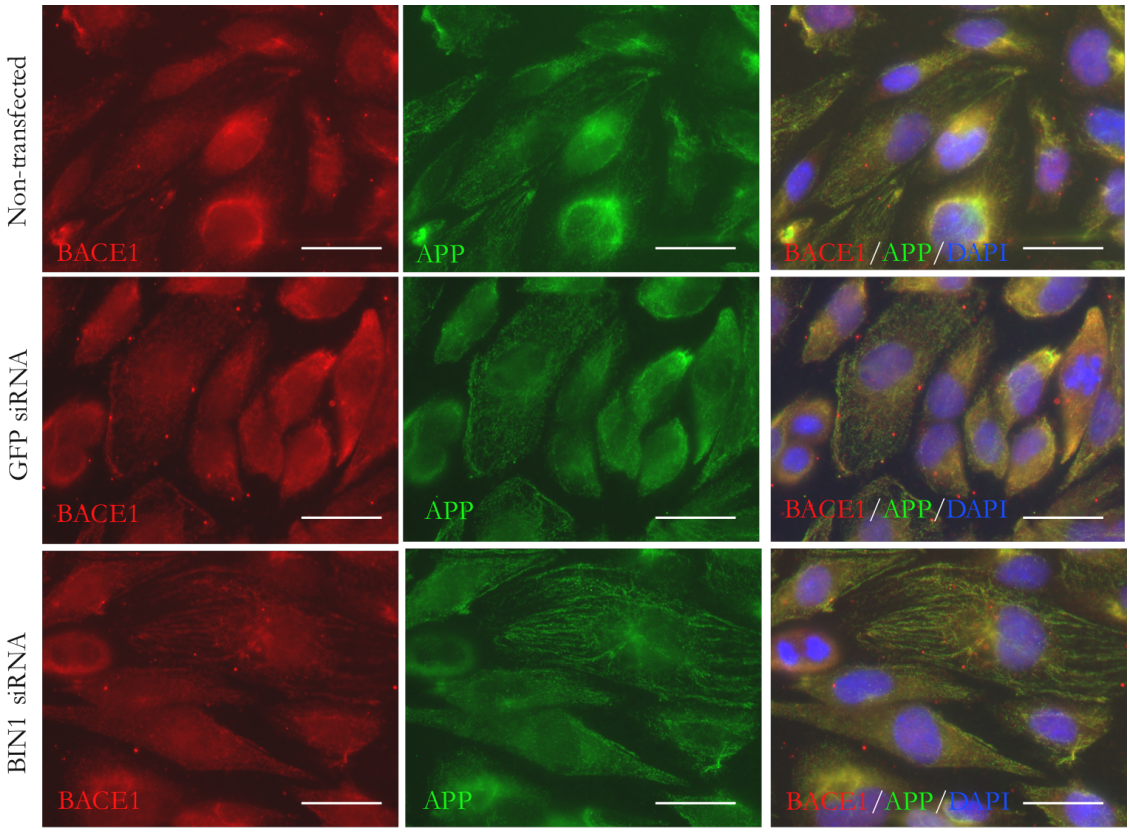

Figure 4.14: Colocalisation of BACE1 and APP with BIN1 depletion

Representative immunofluorescence images of BACE1 and APP expression in non-transfected, GFP siRNA-treated and BIN1-depleted hCMEC/D3 cells. Both antibodies were also used in isolation to confirm specificity. Images were taken at x40 magnification with DAPI used to stain the nuclei, scale bar = 25 μm

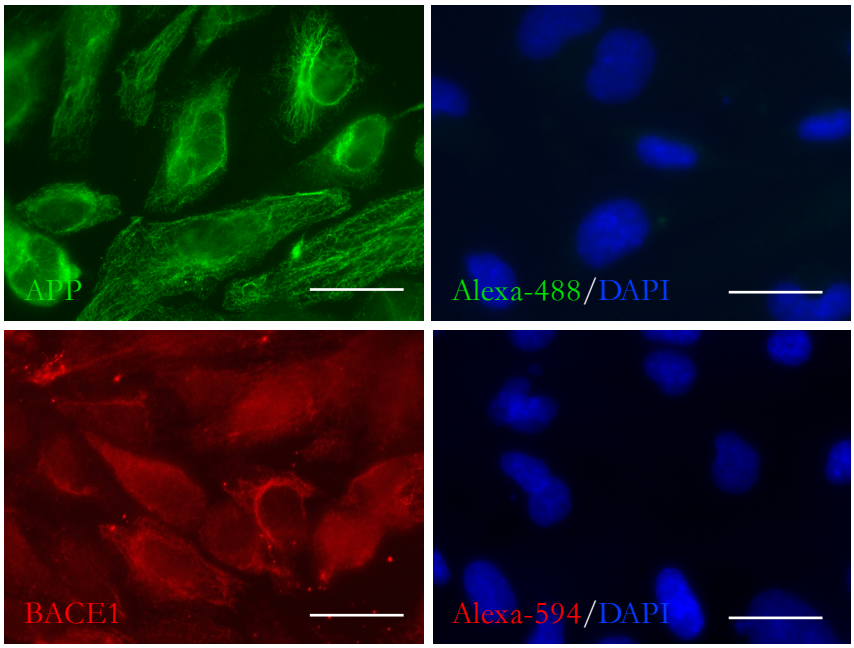

Figure 4.15: Staining of APP, BACE1 and secondary antibodies in isolation

Representative images of hCMEC/D3 cells stained with APP (top left, green) and BACE1 (bottom left, red) in isolation to illustrate that the same localisation pattern was observed compared to when the antibodies were used sequentially in the colocalisation experiment. The secondary antibodies used in this chapter did not confer background staining as illustrated in these representative images for Alexa-488 mouse (top right, green) and Alexa-594 Rabbit (bottom right, red). DAPI was used to stain the nuclei, scale bar = 25 μm.

4.4 Discussion

In this chapter, significant depletion of BIN1 by 90% has been demonstrated in hCMEC/D3 cells to create a model by which to assess the role of BIN1 in APP processing at the BBB. It has been demonstrated that depletion of BIN1 does not affect the proliferation of cells, suggesting it is not an essential component for cell viability, consistent with previous findings from a *Bin1* null mouse model (Muller et al., 2003). While no significant differences in the levels of APP and Aβ40 were observed, a significant increase in the C-terminal fragment of APP as a result of β-cleavage, β-CTF, was found with BIN1 depletion, suggesting the amyloidogenic processing of APP is affected by BIN1 depletion. Analysis of sAPPα and sAPPβ fragments, however, did not further elucidate this mechanism due to high variability between samples and levels falling beyond the detectability limit of the assay, respectively. Key components of the APP proteolytic enzymes, ADAM10, BACE1 and PSEN1 suggested there was no change in the levels of α, β and γ-secretases, respectively. This is indicative that the alteration in amyoidogenic processing of APP with BIN1 depletion is not the result of a change in levels of APP proteolytic enzymes.

4.4.1 BIN1 has a Role in the Amyloidogenic Processing of APP

With no apparent effect on intracellular APP following BIN1 depletion, it is suggestive that BIN1 is not involved in the internalisation of APP and this cannot account for the increase in β-CTF observed. This is consistent with previous work by Glennon et al. (2013), where siRNA-mediated knockdown of BIN1 in the human neuroblastoma SH-SY5Y cell line had no significant effect on intracellular APP expression. In addition, no change was detected in Aβ40, Aβ42 or sAPPα levels in the conditioned media, providing further support for the present study which reports no change in sAPPα and Aβ40 with BIN1 depletion compared to GFP siRNA-treated cells. Very low levels of Aβ40 were detected in the media of hCMEC/D3 cells therefore any small change in levels may not have been detected. Indeed, undetectable levels of endogenous Aβ have previously been reported in human BMECs where only upon overexpression of APP_{770} were Aβ40 and Aβ42 detectable in the culture media (Kitazume et al., 2010). Intracellular Aβ levels were not analysed in the present

study. Intracellular Aβ is often difficult to quantify as evidence suggests that Aβ40 is rapidly shipped out of cells (Koo and Squazzo, 1994) and is drastically diluted once in media. While sAPPβ levels were undetectable in the hCMEC/D3 cell media, Glennon et al. (2013) reported no change with BIN1 depletion in SH-SY5Y cells, further suggesting that BIN1 depletion does not affect the amyloidogenic processing of APP. The authors also reported that while BIN1 protein levels were decreased in sAD frontal cortex compared to age-matched controls, this did not correlate with soluble Aβ, insoluble Aβ or Aβ load, suggesting that depletion of BIN1 does not impact on the generation of Aβ peptides in the brain (Glennon et al., 2013). The authors suggested that the BIN1 homologue, AMPH1, could be involved in a compensatory mechanism when BIN1 is depleted, however this is yet to be investigated.

The present findings do suggest an enhancement of the amyloidogenic pathway with BIN1 depletion as indicated by increased βCTF, either in terms of increased production or decreased clearance. In support of this, a recent study reported that siRNA-mediated depletion of Bin1 in mouse neuroblastoma N2a cells and non-neuronal HeLa cells enhanced the amyloidogenic processing of APP (Miyagawa et al., 2016). Western blotting showed that BACE1 levels increased by approximately 50% and 30% with Bin1 depletion in N2a and HeLa cells, respectively, compared to non-targeting siRNA-treated cells while secreted Aβ40 and Aβ42 also showed a significant increase in both cell lines. Furthermore, a BACE1 activity assay in the membrane fractions of N2a cells revealed that the increase in BACE1 expression corresponded to increased activity with BIN1 depletion. While the present findings indicate no significant difference in secreted Aβ40 or BACE1 expression, Miyagawa et al. (2016) reported no effect on intracellular APP levels, consistent with our findings. Both studies therefore suggest an enhancement of the amyloidogenic pathway with BIN1 depletion, without affecting the levels of intracellular APP. The lack of change in BACE1 expression in the present study does not rule out a change in BACE1 activity levels and this remains to be quantified through an *in vitro* activity assay.

Miyagawa et al. (2016) attributed the increase in BACE1 levels and activity to impaired intracellular trafficking of BACE1. This was based on evidence that labelled BACE1 was remained in early endosomes of HeLa cells 120 minutes after labelling in BIN1-depleted cells, whereas a large fraction had disappeared from control cells by this time point. In addition, a significant reduction of BACE1 in late endosome/lysosome compartments was observed in Bin1-depleted N2a cells, suggesting defective endocytic trafficking of BACE1

beyond the early endosomes. The present study did not observe any gross changes in the localisation of BACE1 with BIN1 depletion, while enhanced BACE1 staining in the perinuclear region was clearly apparent with BIN1 depletion in the study by Miyagawa et al. (2016). Unfortunately, time did not allow for an analysis of BACE1 colocalisation with early endocytic markers, such as early endosome antigen 1 (EEA1) and while BACE1 accumulation was not apparent, it would be interesting to investigate whether enhanced localisation in early endosomes is observed with BIN1 depletion in the hCMEC/D3 cell line. BACE1 did show a strong pattern of colocalisation with APP in the present study, supporting previous evidence that BACE1 is involved in APP processing in BMECs (Devraj et al., 2016), however this distribution was not affected by BIN1 depletion. APP localisation also remained the same across conditions, showing strong filamentous staining throughout the cytoplasm, consistent with that previously reported in astrocytes (Young et al., 1999) while cortical neurons display a vesicular-like distribution with multiple fine fluorescent puncta (Allinquant et al., 1994). In the absence of detergent, staining was patchy and approximately 60% of cells showed a lack of staining altogether, consistent with that previously reported in embryonic cortical neurons (Allinquant et al., 1994). This suggests that APP may be poorly expressed in hCMEC/D3 cell membranes or resides within vesicular structures near the cell surface or membrane invaginations.

It is interesting that, despite BIN1 depletion previously resulting in increased Aβ production in both a neuronal and non-neuronal cell line (Miyagawa et al., 2016), the present study does not show this effect in a brain endothelial cell line. The increase in β-CTF without an increase in intracellular APP may suggest upregulation of the amyloidogenic processing of APP, however changes in any of the products of its proteolysis could not be detected to support this. This may suggest that levels are below detection to observe small changes or that β-CTF accumulation has occurred as a result of a change in β- and/or γ-secretase activity or impaired clearance/degradation of β-CTF.

The data presented are not suggestive of a change in β-secretase activity as a result of BIN1 depletion, contrary to aforementioned studies (Miyagawa et al., 2016, Ubelmann et al., 2017). Firstly, while an increase in β-secretase cleavage is likely to result in an increase in β-CTF, this would also be expected to increase the amount of sAPPβ produced by the same cleavage event. Unfortunately, levels of sAPPβ were too low to detect in the conditioned media therefore this could not be measured reliably. Secondly, an increase in Aβ40 would also be expected if an increase in β-secretase cleavage had occurred, as previously reported

(Miyagawa et al., 2016, Ubelmann et al., 2017) whereas no change in Aβ40 was observed. Finally, no change in BACE1 expression levels or cellular localisation was found in BIN1-depleted hCMEC/D3 cells, suggesting that in this cell line BIN1 depletion does not affect the processing of APP by β-secretase cleavage.

The presence of at least five separate protein bands for the α-secretase ADAM10 was expected given the known existence of an unprocessed pro-form as well as the mature enzyme (Anders et al., 2001), the proteolytic shedding known to occur in this protein (Tousseyn et al., 2009) and the possibility of ADAM10 splice variants or degradative products. However, there was no observable difference in expression across all detected bands between non-transfected, GFP siRNA-treated and BIN1 depleted cells. Coupled with the lack of change in sAPPα levels detected with BIN1 depletion, these results suggest that α-secretase expression was not affected by BIN1 depletion. However, it should be noted that ADAM10 is not the only putative α-secretase and other members of the ADAM family, in addition to several signaling cascades, can activate/increase α-secretase processing of APP. An *in vitro* α-secretase activity assay would be required to elucidate whether the α-cleavage of APP was affected by BIN1 depletion.

Although an increase in β-CTF was observed, no corresponding change in Aβ40 was detected with BIN1 depletion. It is possible that a change in γ-secretase activity occurred with BIN1 depletion resulting in increased β-CTF but the effect was too minor to be detectable in the Aβ40 ELISA, due to the low endogenous Aβ40 levels in these cells. The levels of PSEN1 were therefore examined with BIN1 depletion as an indicator of γ-secretase activity. The lack of significant change in PSEN1 expression suggests that there was no change in the amount of γ-secretase available to alter proteolytic activity. However, protein levels of enzyme components cannot be considered an accurate measure of enzymatic activity as changes in γ-secretase activity have previously been reported in the absence of a change in PSEN1 levels (Burns et al., 2003). It would therefore be necessary to carry out a γ-secretase activity assay to determine this. Furthermore, the intracellular localisation of components of the γ-secretase complex were not examined. This is highly relevant to the production of Aβ as PSEN1 and PSEN2 have been demonstrated to have very different subcellular locations in wild-type MEFs, with PSEN2 showing strong enrichment in late endosomes and lysosome compartments while PSEN1 was broadly distributed in the cell (Sannerud et al., 2016). The restricted compartmentalisation of PSEN2 in late endosomes/lysosomes results in selective cleaving of substrates within these

vesicles, such as APP, generating a pool of intracellular Aβ. In the context of the present study, it would be interesting to explore the cellular distribution of both PSEN1 and PSEN2 with BIN1 depletion, given that this mediates the substrates they interact with and the ultimate production of Aβ. Moreover, while the levels of extracellular Aβ are often considered an indicator of intracellular Aβ levels, there is evidence suggesting the levels of these Aβ pools can independently vary. For example, when PSEN1 knockout MNT-1 human melanoma cells were transduced with β-CTF, less Aβ40 and Aβ42 was secreted compared to control cells but a significant increase in intracellular Aβ levels was recorded (Sannerud et al., 2016). The low levels of extracellular Aβ40 in the present study suggest that detection of intracellular Aβ may be challenging, however this analysis may provide further mechanistic insights on the consequences of BIN1 depletion on intracellular amyloidogenic processing and clearance.

4.4.2 Does BIN1 have a Cell Type-specific Role in BMECs?

Due to considerable alternative slicing, it is well documented that BIN1 is involved in multiple functional roles (Tan et al., 2013) and perhaps the role of BIN1 in BMECs of the BBB differs considerably from both neurons and other somatic cell types. Indeed, Ubelmann et al. (2017) reported that depletion of Bin1 in mouse primary cortical neurons resulted in a major reduction in BACE1 recycling to the plasma membrane in neuronal axons. However, only a minor reduction in BACE1 recycling was detected in the cell bodies and dendrites, suggesting Bin1 has a compartmentalised role within neuronal axons. The endocytic recycling defect as a result of Bin1 depletion was rescued by expression of siRNA-resistant neuronal Bin1, demonstrating a role for neuronal Bin1 in BACE1 recycling. While neurons can be considered to exhibit polarity in terms of signals propagating in one direction from dendrites to axons, endothelial and epithelial cells exhibit apical-basolateral polarity. In addition to a compartmentalised role in the axonal domain of neurons, BIN1 has recently been implicated in the regulation of endocytic transport of apical, but not basolateral, proteins in polarised mouse mammary epithelial cells (Nakajo et al., 2016). It is possible that BIN1 may also have a similar role specific to the apical domain in BMECs which may not become apparent in the present experimental design due to a lack of established polarity in culture. This is an important aspect to consider in BBB models and therefore presents an avenue for future research, which will be further discussed in Chapter 7.

4.4.3 β-CTF Toxicity Independent of Aβ

The increase in β-CTF with BIN1 depletion, in the absence of significant changes in Aβ production are particularly interesting in light of emerging evidence that β-CTF may contribute to sAD pathogenesis, independent of Aβ (Kim et al., 2016). Endosomal abnormalities, in the form of enlarged Rab5-positive vesicles, are among the earliest neuropathological features of AD (Cataldo et al., 2000) and induction of AD-like endosomal pathology has been observed in fibroblasts by overexpressing β-CTF (Jiang et al., 2010). In this study, pharmacologically inhibition of γ-secretase reduced Aβ40 and Aβ42 production but increased β-CTF levels and led to AD-like endosome dysfunction. Expression of a mutant form of APP that cannot undergo beta-cleavage, however, had no effect on endosomes (Jiang et al., 2010). These findings suggest that β-CTF but not Aβ or α-CTF is implicated in endocytic dysfunction in AD.

β-CTF has also been implicated in endosomal dysfunction in transgenic mouse models. Accumulation of β-CTF was observed in the hippocampus of triple-transgenic mice overexpressing mutant APP, Tau and physiological levels of mutant PSEN1 (Lauritzen et al., 2012). Accumulation of β-CTF was reported from 3 months of age in enlarged structures expressing the lysosomal enzyme cathepsin B and lysosomal associated membrane protein-1 (Lamp1). This accumulation further increased by the pharmacological blockade of γ-secretase. While extracellular Aβ deposits and tau tangles were observed, intracellular Aβ was only detectable several months after β-CTF, also in enlarged cathepsin B-positive structures, and extracellular Aβ deposits were detected from 12 months of age onwards. Double-transgenic mice lacking the PSEN1 mutation also showed β-CTF accumulation, demonstrating it cannot be accounted for by loss of PSEN1 function preventing γ-cleavage. Aged double transgenic mice also showed very few extracellular Aβ plaques and both Aβ40 and Aβ42 levels were very low suggesting that β-CTF accumulation did not correlate with Aβ load. Much like the present study, increased β-CTF did not correspond with increased Aβ production, suggesting a mechanism of impaired β-CTF clearance instead of increased production. Furthermore, the findings by Lauritzen et al. (2012) suggested that β-CTF was the earliest detectable amyloidogenic catabolite. It is possible that accumulation of β-CTF may precede further pathological changes that would not be detectable *in vitro*, such as the present study, as the time courses studied *in vitro* are too short to develop all of the pathologies that would be seen in AD.

The accumulation of β-CTF in enlarged structures positive for the lysosomal markers cathepsin B and Lamp1 in the triple transgenic mouse model suggested a link between β-CTF and endosomal-autophagic-lysosomal (EAL) pathology (Lauritzen et al., 2012). Kim et al. (2016) extended these findings to elucidate a novel mechanism by which accumulation of β-CTF is both an effect, and a cause of EAL dysfunction. Of particular interest in this study was the GTPase rab5 which regulates early endosomes and has previously shown upregulation in individuals with MCI and sAD (Ginsberg et al., 2010). Kim et al. (2016) showed that rab5 activation was significantly decreased when β-CTF levels were increased in N2a cells, either by overexpressing wild-type APP or inhibiting γ-secretase cleavage, compared to control cells expressing endogenous levels of β-CTF. The authors further showed that β-CTF recruits the rab5 effector APPL1 (adaptor protein containing pleckstrin homology domain, phosphotyrosine binding domain and leucine zipper motif) to rab5 endosomes. Here, it stabilises active GTP-rab5, leading to accelerated endocytosis, endosome enlargement and impaired axonal transport of endosomes (Kim et al., 2016). This was consistent with their findings that β-CTF levels were elevated in sAD cerebral cortex samples whereas APP and α-CTF levels were unaltered compared to age-matched controls (Kim et al., 2016). Collectively, these findings suggest the involvement of a pathological loop whereby β-CTF accumulation can occur as a result of impaired endocytic trafficking but can also be the cause of it, further exacerbating the impairment. This could indeed be the case with BIN1 depletion and it is therefore important to explore endocytic function in this cell model.

4.4.4 Conclusions

This chapter presents evidence on the role of BIN1 in APP processing within the novel context of the BBB. BIN1 depletion results in a significant increase in intracellular β-CTF levels, without impacting intracellular APP levels or secreted Aβ40 or sAPPα. Furthermore, protein levels of key α- β- and γ-secretases were unchanged with BIN1 depletion, indicative of no alteration in enzymatic activity, however activity levels were not measured. Collectively, the data do not compliment the literature which has described the involvement of BIN1 in regulating BACE1 intracellular trafficking. However, this work presents a novel context for examining the role of BIN1 in APP processing and such experiments have not previously been reported in BMECs. While it is possible that cell-type specificity may account for the disparity between the present results and the literature,

the polarised nature of BMECs *in vivo* may be involved in BIN1 function therefore future work would include the establishment of polarity in culture. This will be further discussed in Chapter 7. Enzyme activity assays have also been cited as an important aspect of future work in order to elucidate any change in secretase activity levels with BIN1 depletion. Moreover, the increase in β-CTF in the absence of increased secretion of Aβ40 is suggestive of altered endosomal trafficking resulting in impaired degradation of β-CTF and possibly not an overall increase in the amyloidogenic processing of APP. With the well-established role of BIN1 in CME and downstream endocytic trafficking, the following chapter will examine CME function in this BIN1-depleted cell model.

Chapter 5

The Role of BIN1 in Clathrin-Mediated Endocytosis at the BBB

5.1 Introduction

Chapter 5 furthers investigations into the role of BIN1 in APP processing at the BBB by exploring its previously recognised role in CME. Much research into BIN1 function within the context of AD to date has focused on its involvement in endocytic recycling in neurons (See Chapter 1, Section 1.4). However, CME is also an important mechanism for transcytosis at the BBB and defects in transcytosis have been implicated in impaired clearance of Aβ from the brain (Erickson and Banks, 2013). With mounting evidence implicating BIN1 in endocytic trafficking in both neuronal and non-neuronal cells (Tan et al., 2013), it brings into question whether BIN1 may provide an important endocytic function in endothelial cells at the BBB. This chapter utilises siRNA-mediated depletion of BIN1 in hCMEC/D3 cells to examine the effect on key CME-related proteins, endocytic uptake and recycling.

5.1.1 Endocytosis at the BBB

The crucial function of the BBB in regulating the flux of molecules between the circulating blood in the brain microvasculature and the CNS relies heavily on different vesicular transport pathways. Molecules can enter the cell by a variety of endocytic mechanisms and are shuttled through an internal membrane system for metabolic utilisation or degradation via the lysosomes (Smith and Gumbleton, 2006). This highly regulated internal membrane system is also involved in the transport of newly synthesised proteins from the ER through the Golgi to the plasma membrane where they may be exocytosed or replace those proteins and membrane components captured by endocytosis. In polarised cells, such as BMECs, both apical and basolateral membranes partake in endocytosis with each possessing their own endosomal compartments (Shivas et al., 2010). This allows endocytosed receptors to return to their original membrane, maintaining the receptor composition at these separate domains. Three major types of endocytosis have been definitively identified and defined in BMECs: non-specific fluid-phase endocytosis (Guillot et al., 1990), adsorptive-mediated endocytosis (Raub and Audus, 1990) and receptor-mediated endocytosis (Fishman et al., 1987), encompassing the most common CME.

5.1.1.1 Fluid-phase endocytosis

Fluid-phase endocytosis is the non-specific uptake of solutes from the immediate extracellular environment by inward budding of the plasma membrane. It is ubiquitous throughout tissue cell types but its low level in BMECs is considered a defining feature of the BBB (Keaney and Campbell, 2015). Horseradish peroxidase (HRP) is a 40 kDa plant glycoprotein that does not bind the plasma membrane or undergo transcytosis at the BBB and is instead sequestered into endocytic vesicles for degradation in the lysosome (Noble et al., 1994). Early studies used HRP internalisation in mouse BMECs as a measure of fluid-phase endocytosis, noting that its rate of uptake was 10-fold less than the absorptive-mediated endocytic marker wheat germ agglutinin (WGA) (Banks and Broadwell, 1994). Morphological studies of the BBB using transmission electron microscopy (TEM) showed poor internalisation of HRP within mouse BMECs (Reese and Karnovsky, 1967). Dextrans are another example of fluid-phase endocytic markers. They are hydrophilic polysaccharides that when conjugated to a fluorescent tag, have been used extensively as an index of fluid-phase endocytosis in BBB transport studies. Dextran uptake studies have

also shown low levels of fluid phase endocytosis to be present in BMECs. A comparison between endothelial cells of the brain and the periphery estimated that rates of fluid-phase endocytosis of fluorescently-labelled dextran were 30-40-fold less in BMECs than in aortic vascular endothelial cells (Mizuguchi et al., 1994).

5.1.1.2 Adsorptive-mediated endocytosis

Adsorptive-mediated endocytosis (AME) is also a non-specific process but occurs to a greater extent and rate than fluid-phase endocytosis at the BBB. It requires an excess positive charge on the molecule, which allows it to bind to the cell surface through electrostatic interactions with the negatively-charged plasma membrane. WGA is a member of the lectin family and an example of cargo internalised by AME through its interactions with negatively-charged oligosaccharides on the cell surface. AME occurs to a greater extent than fluid-phase endocytosis at the BBB. Banks and Broadwell (1994) traced HRP-labelled WGA through mouse and rat brain capillary endothelium *in vivo* showing a 10-fold increase in uptake compared to HRP alone. The HRP-WGA showed accumulation both in endosomes and lysosomes and was detected in cells and processes of the neuropil four hours after intravenous injection, illustrating the adsorptive transcytosis of WGA across the BBB.

5.1.1.3 Receptor-mediated endocytosis

Two main pathways have been identified for receptor-mediated endocytosis: the clathrin-dependent and the caveolar/lipid raft-dependent endocytic pathways (Doherty and McMahon, 2009). CME is the best characterised mechanism for mediating the internalisation of ligand-bound membrane receptors into cells. As previously described in Chapter 1, Section 1.4.1, CME is a ubiquitous cellular mechanism involving the binding of a specific ligand to its cell surface receptor facilitating uptake of the receptor-ligand complex. The receptor and bound ligand may be recycled back to the plasma membrane from which it originally budded. An example of a complex that is trafficked in this manner is the transferrin receptor (TfR) and its iron-binding ligand transferrin (Tf) (Iacopetta and Morgan, 1983). Alternatively, both receptor and ligand may be trafficked via early endosomes to lysosomes for degradation. In polarised cells, such as BMECS, ligand-bound receptors may bypass the lysosomal system and enter the transcytotic pathway, resulting in

the ultimate delivery of the ligand to a different plasma membrane domain (Descamps et al., 1996). This is evident in apical to basolateral transport across BMECs. In order for this to occur, the endocytosed material must be selectively retrieved from the early endosomes or it will continue onto MVBs, late endosomes and lysosomes for degradation (Preston et al., 2014).

At the BBB, up to 20 receptors have been identified that are involved in receptor-mediated endocytosis, with the majority using CCVs to commence transcytosis between the apical and basolateral membranes (Preston et al., 2014). Despite the importance and complexity of receptor-mediated endocytic mechanisms at the BBB, low endocytic activity relative to peripheral endothelial cells is one of the key properties of BMECs with only 15% of the number of endocytic vesicles of an equivalently-sized skeletal muscle capillary endothelial cell (Coomber and Stewart, 1986). The technical challenge of visualising such infrequent events may in part account for our limited knowledge of how cargo destined for transcytosis is trafficked through BMECs.

5.1.2 Transcytosis

From the recycling endosome, cargo can either be recycled directly back to the plasma membrane or progress further down the transcytotic pathway, fusing with late endosomes, mostly found in the perinuclear region. While cargo destined for degradation is sorted into endocytic carrier vesicles to the lysosome, MVBs can arise from the inward budding of the late endosome which creates intraluminal vesicles. These are then released as exosomes at the plasma membrane. Extracellular microvesicles from BMECs have been successfully isolated and characterised, containing in excess of 1000 proteins, among which were receptors known to undergo CME such as the TfR and LRP1 (Haqqani et al., 2013).

For successful transcytosis to occur through BMECs, internalised cargo and/or receptors from one membrane must traverse the cell for exocytosis on the opposite membrane. The relative composition at these respective domains is therefore crucial to BMEC function and the ultimate homeostasis of the brain (Shivas et al., 2010). Differences in lipid composition between the two membranes have been identified, showing that the basolateral membrane contains more caveolae, flask-shaped membrane invaginations which form at microdomains rich in glycosphingolipids and sphingomyelin (Bendayan et al., 2006). The

distribution of target receptors is specific to apical or basolateral domains and is an important determinant of the direction of transcytosis. The receptor for Tf, for example, is found on the apical side of BMECs, largely limiting its transport in the direction of blood-to-brain (Roberts et al., 1993). Bidirectional transport of molecules may utilise specific basolateral and apical receptors. For example, the efflux of Aβ, implicated in AD pathogenesis, involves the efflux transporter LRP1 while Aβ influx is mediated by RAGE, as described in Chapter 1, Section 1.6.4.

The mechanisms controlling transcytosis in BMECs are still poorly understood, but evidence has been gathered from studies in other polarised cell types. With both membranes internalising cargo-bound receptors through to recycling endosomes, cargo must bypass the lysosome system and be directed for exocytosis at the appropriate membrane, while proteins and lipids must be correctly recycled back to their membrane of origin to maintain polarity (Shivas et al., 2010). In epithelial cells, separate early endosome compartments exist such that apically endocytosed and basolaterally endocytosed cargo are segregated (Bomsel et al., 1990). Thompson et al. (2007) found that apical and basolateral proteins were pre-sorted into separate membrane subdomains within the same recycling endosome in Madin-Darby Canine Kidney (MDCK) epithelial cells, but only once polarisation had been achieved by growing at confluency. This sorting was not observed in non-polarised Chinese hamster ovary (CHO) cells (Thompson et al., 2007).

5.1.3 Transferrin Transport at the BBB

Tf is the principal iron-carrying protein in plasma (Bradbury, 1997) and is an archetypal substrate for CME. Tf and its receptor are ubiquitously expressed, providing researchers with an accessible system for measuring CME using fluorescently-labelled Tf which can be traced into the cell. The TfR is a 90kDa homodimer which spans the plasma membrane and mediates the entry of two molecules of iron-bound Tf (holotransferrin) at a time by CME. Within the N- and C- terminal domain of the transferrin protein are hydrophilic binding clefts for oxidised iron (Fe^{3+}) (MacGillivray et al., 1983). Upon iron binding, a conformational change in the protein is induced which enhances affinity for the TfR present on the cell surface (Young et al., 1984).

The TfR complex is endocytosed via CCVs and trafficked to the early endosome where Tf-bound iron dissociates in the acidic environment and is reduced from Fe^{3+} to Fe^{2+} (Dautry-

Varsat et al., 1983). This releases Fe^{2+} into the endosome for active transport into the cytoplasm by a divalent metal transporter. Within BMECs, Fe^{2+} can then cross the basolateral membrane by active transporters such as ferroportin (Wu et al., 2004). Once iron is released from Tf, it is termed apotransferrin and remains bound to the TfR within the acidic endosome. Apotransferrin is then recycled back to the plasma membrane, where it was initially internalised, for release into the extracellular fluid at physiological pH, allowing it to bind iron once more.

Tf transport at the BBB has been extensively investigated as it not only enters via CME but also crosses the BBB by transcytosis (Descamps et al., 1996), providing an attractive target for drug transport studies. Descamps et al. (1996) showed that iron crosses bovine BMECs bound to Tf with approximately 75% being trafficked for release at the basolateral side (Descamps et al., 1996). Furthermore, the TfR transcytotic pathway has been successfully manipulated to deliver therapeutic antibodies to the brain. Yu et al. (2011) showed that a bispecific antibody targeting TfR and BACE1 successfully accumulated in the mouse brain leading to a greater reduction in brain Aβ than treatment with a monospecific BACE1 antibody. Although a full understanding of the precise cellular mechanisms associated with TfR trafficking at the BBB remains unclear, the extensive literature available suggests that transferrin proposes a useful and reliable substrate for the demonstration of clathrin-mediated endocytosis and recycling in BMECs.

5.1.4 CME at the BBB with Relevance to AD

In the context of AD, CME is crucial to APP processing. As previously described in Chapter 1, Section 1.4.3, alterations in the internalisation of APP via CME can influence whether APP enters the non-amyloidogenic or amyloidogenic pathway, therefore affecting the production of Aβ. CME at the BBB is also important for the transcytosis of exogenous Aβ across BMECs as LRP1, which mediates Aβ clearance, is internalised via CCPs (Zhao et al., 2015).

The molecular mechanisms involved in LRP1-mediated Aβ clearance across the BBB have recently been analysed in more detail, implicating PICALM in regulating this process (Zhao et al., 2015). Decreased levels of PICALM were reported in AD brain endothelium and this was associated with ~50% diminished basolateral-to-apical transcytosis of Aβ *in* vitro, compared to age-matched controls. Using human brain endothelial monolayers, binding of

Aβ to the ectodomain of LRP1 was shown to initiate CME of the Aβ-LRP1 complex. PICALM, clathrin heavy chain (CHC) and AP2 bound to LRP1 within 30s of Aβ40 addition, however, while CHC and AP2 dissociated rapidly, consistent with uncoating of the CCV, PICALM remained associated with LRP1 for up to 4 min. PICALM and the Aβ40-LRP1 complex trafficked to Rab5-positive early endosomes, but not late endosomes or lysosomes, and were found to associate with the ERC marker Rab11. Depletion of PICALM by siRNA inhibited Aβ40 basolateral-to-apical transendothelial transport, suggesting it is critical for maintaining the endosomal trafficking of Aβ throughout the basolateral-to-apical transcytotic pathway (Zhao et al., 2015). These findings are of particular interest to the present study as the association of *PICALM* with sAD was initially established through genome-wide association studies, much like *BIN1* (Harold et al., 2009, Lambert et al., 2009, Seshadri et al., 2010, Lambert et al., 2013). Furthermore, the associated variants are not within the coding region of *PICALM* but ~88kb 5' of the gene itself (Harold et al., 2009, Lambert et al., 2013), suggesting the variant may mediate sAD risk by affecting *PICALM* gene expression. Indeed, the sAD-associated *PICALM* SNP rs659023^{G} was significantly associated with decreased expression of PICALM in PBMCs, demonstrating a *cis*-regulatory effect (Raj et al., 2012). AD risk loci upstream of the *BIN1* gene have also been implicated in transcriptional regulation of *BIN1* (Chapuis et al., 2013, Raj et al., 2012). This was demonstrated in SH-SY5Y, HEK and PBMCs, suggesting that AD-associated genetic variants upstream of the *BIN1* gene may confer expression changes in *BIN1* in both neuronal and non-neuronal cell types.

Zhao and colleagues concluded their findings by using CRISPR/Cas9 genome editing to generate isogenic iPSC lines for the two homozygous allelic variants of the highly validated and replicated rs3851179 *PICALM* SNP, whose rs3851179^{A} allele is associated with a reduced risk of AD compared to the rs3851179^{G} allele (Harold et al., 2009, Lambert et al., 2009, Lambert et al., 2013). Upon differentiation into endothelial cells, they found that the rs3851179^{A}-expressing lines had 72–78% higher expression levels of PICALM mRNA and protein, with 120% higher Aβ clearance than the rs3851179^{G} allele (Zhao et al., 2015).

Given that both *PICALM* and *BIN1* have been identified as sAD susceptibility loci and are implicated in CME pathways, these findings bring to question whether they may both be implicated in AD pathogenesis through defective endocytic mechanisms. While the involvement of PICALM in endocytic trafficking at the BBB has been demonstrated (Zhao

et al., 2015), the potential role that BIN1 might play in endocytic trafficking at the BBB is yet to be explored.

5.1.5 Aims of this Chapter

Within the context of the aforementioned literature, the increase in β-CTF levels following BIN1-depletion in hCMEC/D3 cells demonstrated in Chapter 4 may be indicative of perturbed endocytic mechanisms in this cell line. The aim of this chapter therefore was to investigate whether BIN1 depletion affects CME and recycling in the hCMEC/D3 cell line, as an *in vitro* model of the BBB. To address this research question, BIN1 protein was depleted using siRNA and compared to cells treated with GFP siRNA as a non-targeting control. Analysis of endocytic protein expression was carried out by Western blotting while CME itself was measured by Alexa-488-conjugated transferrin uptake. Endocytic recycling was analysed by chasing transferrin-pulsed cells with unlabeled transferrin and measuring its depletion over time. An analysis of the BIN1 isoforms expressed in hCMEC/D3 cells allowed for further interpretation of the data, shedding new light on the role of BIN1 in non-neuronal cell types.

5.2 Experimental Design

5.2.1 BIN1 Depletion in hCMEC/D3 cells

Cell plating and depletion of BIN1 protein was performed as previously described in Chapter 2, Section 2.2 and confirmed by Western blotting as described in Chapter 2, Section 2.3.

5.2.2 Western Blotting

Western blotting was performed as described in Chapter 2, Section 2.3 using the primary antibodies detailed in Table 5.1 with 10-20 μg protein used per sample, run on a 10% acrylamide gel. Some of the blots investigating AP2, CHC and PICALM with BIN1 depletion were carried out by Catherine Matheson and Robert Greening as part of a final year project, co-supervised by myself. All densitometry analysis was independently analysed by the students and myself. Due to the large size of the AMPH1 protein, a 7% acrylamide gel was prepared. Mouse whole brain lysate was used as a positive control for AMPH1 expression, with 2 μg protein loaded per well. Samples were prepared, as previously described, by Lelos et al., (2011) from 22-month-old Tg2576 (TG) and wild-type mice. Briefly, following dissection, tissue was homogenised at 75 mg/ml in 2% wt/vol SDS and supplemented with 1× protease inhibitor cocktail III (Calbiochem, Nottingham, England). Tissue was incubated with agitation overnight and centrifuged at 100,000 x g for 1 hour and the soluble supernatant fraction diluted 1:40 in EC buffer (20 mM Na_2HPO_4/NaH_2PO_4, 0.2 mM EDTA, 0.4 M NaCl, 0.2% BSA, 0.05% CHAPS, 0.05% NaN_3, pH 7) for use. Quantification of protein was calculated by densitometry analysis normalising to GAPDH expression, previously described in Chapter 2, Section 2.3.6. A sample size (n) of at least 3 replicates was used for all quantified experiments, with n defined as a biological replicate performed on one passage of cells with separate reagents to any other replicates.

Table 5.1: Primary antibodies used for Western blotting in Chapter 5

Protein	Species	Supplier	Working concentration
BIN1	Mouse	Abcam	0.48 µg/ml
AP2µ2	Mouse	BD Biosciences	0.5 µg/ml
CHC	Mouse	BD Biosciences	0.25 µg/ml
PICALM	Rabbit	Millipore (See Appendix II)	0.66 µg/ml
AMPH1	Rabbit	Abcam	0.133 µg/ml
GAPDH	Mouse	Abcam	0.13 µg/ml

5.2.3 AP2 depletion

Depletion of AP2µ2 was performed as described for BIN1 depletion in Chapter 4, Section 4.2.1 using the siRNA sequence 5'-AAGUGGAUGCCUUUCGGGUCA-3' (Eurofins) previously demonstrating successful knockdown (Moody et al., 2015). An optimisation experiment was performed to determine the concentration of oligonucleotide that would achieve consistent AP2µ2 depletion for future experiments. Final concentrations ranging from 25-75 nM were used for optimisation alongside matching concentrations of GFP siRNA as controls. The concentration of oligofectamine and length of transfection and all other methods were kept consistent throughout, as previously described in Chapter 4, Section 4.2.1. AP2µ2 depletion was confirmed by Western blotting, as described in Section 5.2.2.

5.2.4 Transferrin Uptake

Uptake of Alexa-488-conjugated transferrin (Alexa-48-Tf) was performed according to previously published methods (Thomas et al., 2016, Al Soraj et al., 2012). Cells were cultured in 6-well or 12-well plates and transfected with GFP siRNA or BIN1 siRNA, as

described in Chapter 4, Section 4.2.1. As a measure of endocytosis, uptake of Alexa-488-Tf was quantified 48 hours post-transfection. Firstly, cells were washed twice with OptiMEM and serum-starved with OptiMEM with 0.2% BSA for 30 min at 37°C. After a further two washes with OptiMEM, cells were incubated with 7.8 μg/ml (100 nM) Alexa-488-Tf diluted in OptiMEM for 5, 15, 30 and 60 minutes. An optimisation experiment was carried out with non-transfected cells to determine the maximum time point to be used, when Alexa-488-Tf levels plateaued. Cells without the addition of ligand were incubated at 37°C for the duration of the assay to act as a time 0 control. Cells were harvested on ice by washing twice with ice-cold PBS, once with ice-cold acid wash (0.2 M acetic acid, 0.2 M NaCl, pH 2.0) and a further three times with RT PBS. Trypsin (0.05%, ThermoFisher Scientific) was added to cells and incubated at RT until the cells were in suspension before adding the same volume of trypsin inhibitor solution (500 μg/ml trypsin inhibitor, 75 μg/ml DNase, 1% BSA in PBS). The cell suspension was then centrifuged at 325 x g at 4°C for 3 min, the pellet washed twice with ice-cold PBS, resuspended in 500 μl 75 μg/ml DNAse, 1% BSA in PBS and transferred to fluorescence-activated cell sorting (FACS) tubes via 30 μm filters (Sysmex, Milton Keynes, England). The geometric mean of fluorescent intensity for at least 10,000 events was measured by flow cytometry using the BD FACSverse (BD Biosciences, Oxford, England) with debris and doublets gated out.

5.2.5 Alexa-488-Tf Recycling

Cells were cultured in 12-well plates and transfected with GFP siRNA or BIN1 siRNA, as described in Chapter 4, Section 4.2.1. Following two washes with OptiMEM, cells were pulsed with 7.8 μg/ml Alexa-488-Tf for 60 min at 37°C. Cells were washed 6 times with RT PBS and chased with 100 μg/ml unlabelled holotransferrin (Sigma) in OptiMEM for 7.5, 15, 30 and 60 min at 37°C. For each time point, a control sample was washed 6 times in ice-cold PBS and chased with 100 μg/ml unlabelled holotransferrin at 4°C for 7.5, 15, 30 and 60 min to inhibit endocytic pathways. For the time 0 controls, cells were harvested immediately after the pulse as follows. Plates were placed on ice and washed three times with ice-cold PBS, once with ice-cold acid wash (0.2 M acetic acid, 0.2 M NaCl, pH 2.0) and a further three times with ice-cold PBS. Cells were trypsinised on ice with 0.05% trypsin until in suspension before adding the same volume of trypsin inhibitor solution. Cell suspension was then centrifuged at 325 x g at 4°C for 3 min, the pellet washed once

with ice-cold 75 μg/ml DNAse, 1% BSA in PBS and, resuspended in 500μl before transferring to FACs tubes via 30 μm filters. Fluorescent intensity of at least 10,000 events, with debris and doublets gated out, was measured by FACS using the BD FACSverse.

5.2.6 Immunocytochemistry Conditions

Cells were fixed in 100% methanol and immunocytochemistry was carried out as described in Chapter 2, Section 2.4 with three replicates per experiment and representative images shown. The early endosome marker EEA1 (rabbit polyclonal antibody, Abcam) was used at 1.67 μg/ml.

5.2.7 Identification of BIN1 mRNA Isoforms

In order to determine which BIN1 isoforms are expressed in the hCMEC/D3 cell line, total RNA was extracted from cultures, the region of interest amplified by polymerase chain reaction (PCR), cloned and sequenced.

5.2.7.1 Total RNA extraction and quantification

Cells were harvested by treatment with Trypsin/EDTA as described in Chapter 2, Section 2.1.2 and counted using by trypan blue exclusion method (Chapter 2, Section 2.1.5) to ensure no more than 1 x 10^7 cells were used. Cells were transferred to an RNase-free polypropylene centrifuge tube (ThermoFisher Scientific) and centrifuged at 455 x g for 5 min. Supernatant was completely removed and the total RNA prepared from the cell pellet immediately using the RNeasy® Mini Kit (Qiagen, Hilden, Germany) according to the manufacturer's instructions. RNA was eluted in 30 μl RNase-free water and concentration and absorption ratios determined using a Nanodrop 800 (ThermoFisher Scientific). A ratio of A_{260nm} to A_{280nm} above a value of 2.0 indicated a suitable level of RNA and the absence of contaminating protein.

5.2.7.2 cDNA synthesis from total RNA

A QuantiTect Reverse Transcription Kit (Qiagen) was used for the elimination of genomic DNA and creation of cDNA from 1 µg RNA according to manufacturer's instructions. The cDNA was stored at -20°C.

5.2.7.3 Polymerase Chain Reaction (PCR) primer design

While the entire BIN1 mRNA was too large a fragment for standard PCR amplification, the area containing the CLAP domain, with the most potential for variability due to alternative splicing events, was targeted for PCR amplification. Primer sequences (Eurofins) were designed to amplify the region between exon 11 and exon 15, neither of which are subject to alternative splicing. The sequences were as follows: 5'-TGTCAGTGGCCGTGTAGTC-3', 5'-CCCGAGATCAGAGTCAACCA-3'. PCR primers were designed *in silico* using the Primer 3 web resource (www.http://bioinfo.ut.ee/primer3) with default settings and an average length of 20 base pairs and GC content less than 80%.

5.2.7.4 PCR primer optimisation

For optimisation, each PCR reaction contained 6.67 ng/µl cDNA or equivalent volume of nuclease-free water as a negative control, 1.6 mM deoxynucleotides (dNTPs), 0.23 µM of each primer, 1.2 µl 10x PCR buffer (Qiagen) and 0.06 µl Hot Start Taq polymerase (Qiagen) made up to a total volume of 12 µl with nuclease-free water. A gradient PCR was carried out, with a melting temperature (T_m) range of 52 – 60 ºC, incorporating the T_m specified by the manufacturer for each primer. Samples were incubated under the following conditions in thermocyclers (Bio-Rad): 95°C for 15 min, 35 cycles of 95°C for 40 s, T_m for 40 s and 72°C for 1 min followed by a final incubation at 72°C for 10 min. The T_m of 57 ºC was considered to give the strongest band for each isoform and was therefore chosen for amplification. In order to generate enough PCR product for cloning, the reaction was scaled up to 25 µl in volume. Following amplification, samples were cooled to 4°C before further use or frozen for long-term storage at -20 °C.

5.2.7.5 Agarose Gel Electrophoresis

Post-PCR samples were analysed using a 2% (w/v) agarose gel in 0.5X Tris/Borate/EDTA buffer (ThermoFisher Scientific) containing 0.1 µg/ml Ethidium Bromide (Sigma). Agarose solution was heated until clear and cooled slightly before pouring into a gel mould with appropriate gel comb and left to cool until solid. PCR products were diluted in 6x purple gel loading dye (New England Biolabs, Ipswich, Massachusetts, USA) and run at 100 V alongside 10 µl Quick-Load 100 bp DNA ladder (New England BioLabs) until sufficient separation of bands was achieved.

5.2.7.6 DNA Clean-up

Amplified DNA was purified using the QIAquick PCR Purification Kit (Qiagen), according to manufacturer's instructions and quantified using a Nanodrop 800.

5.2.7.7 Ligation

The pGEM®-T Vector (Promega) was used to insert amplified cDNA fragments for molecular cloning according to the manufacturer's instructions. The ligation reaction combined 50 ng pGEM®-T vector, 5 µl 2X rapid ligation buffer, 8.3 ng PCR product and 3 Weiss units T4 DNA Ligase made up to a final volume of 10 µl in nuclease-free water and was incubated at 4°C overnight to produce the maximum number of transformants. A negative control ligation reaction was set up alongside using an equal volume nuclease-free water in place of the PCR product.

5.2.7.8 Transformation

High-efficiency DH5α™ competent cells (ThermoFisher Scientific) were thawed on ice and gently mixed before combining 50 µl with 2 µl ligation reaction (separate reactions for the positive and negative ligations). The tubes were gently mixed and incubated on ice for 20 min before heat-shocking the cells in a 42°C water bath for 30 s and immediately returning to the ice for 2 min. Cells were incubated with 920 µl RT SOC medium, added directly to tubes, for 1 hour at 37°C. Meanwhile, growth plates were prepared using lysogeny broth (LB) agar (Sigma) containing 100 µg/ml ampicillin (Sigma) and left to

solidify before spreading 200 µl cell culture per plate and incubating overnight at 37°C to allow colony formation. Plates could then be stored at 4°C before colonies were picked for screening.

5.2.7.9 PCR Screening

A total of 48 samples were picked at random from individual colonies using a P10 pipette tip and added to the following PCR mix: 0.24 mM dNTPs, 0.234 mM of each primer, 2.5 µl 10x PCR buffer and 0.125 µl Hot Start Taq polymerase made up to a total volume of 12 µl with nuclease-free water. The remainder of cells on the same tip were added to a corresponding growth plate containing 50 µl LB broth and 100 µg/ml ampicillin and incubated for 6 hours at 37°C. A total of 48 colonies were picked for screening and incubated in thermocyclers alongside a negative control without any DNA and a positive control with 4 µl cDNA substituted with 4 µl water according to the aforementioned incubation times in section 5.2.7.3. Samples were electrophoresed as previously described in section 5.2.7.5 and 18 colonies were selected that represented the full range of fragment sizes observed from the screen, including at least 3 samples of each size.

5.2.7.10 Isolation of plasmid DNA

Cultures from the selected colonies were expanded at 37°C with shaking at 225 rpm overnight in 3 ml LB broth with 100 µg/ml ampicillin. One third of the culture was mixed with 100 µl DMSO and snap-frozen on dry ice before storing at -80°C. Plasmid DNA was isolated from the remaining 2 ml culture using the QIAprep Spin Miniprep Kit (Qiagen) according to the manufacturer's instructions and quantified using a Nanodrop 800.

5.2.7.11 DNA sequencing

Isolated plasmid DNA was sent for Sanger sequencing via Source Bioscience (Nottingham, England) and the results visualised using UCSC Genome Browser (www.genome.ucsc.edu).

5.3 Results

5.3.1 BIN1 Depletion and CME-related Protein Expression

To explore any indicator of CME disturbance, expression levels of key endocytic proteins were analysed by Western blotting following BIN1 depletion.

5.1.1.1 AP2 expression

As the most important adaptor protein involved in the linking cargo to nucleating clathrin at the plasma membrane during CME, AP2 is a major hub of protein-protein interactions at the CCP and a change in its expression would be highly indicative of alterations in this process. Depletion of the μ2 subunit of the AP2 complex has been shown to severely inhibit receptor-mediated endocytosis of transferrin (Motley et al., 2003), therefore an analysis of AP2μ2 expression levels following BIN1 depletion was carried out. AP2μ2 was detected as a single band at ~50 kDa (Figure 5.1A). Using a two-tailed unpaired Student's *t* test, it was determined that there was no significant difference in AP2μ2 expression between BIN1-depleted and GFP siRNA-treated cells ($p > 0.05$, two-tailed unpaired Student's *t* test, Figure 5.1B).

5.3.1.1 Clathrin Heavy Chain

The clathrin protein functions as a heterohexamer, formed of three light chains and three heavy chains. Depletion of clathrin heavy chain has been shown to inhibit CME, with no CCPs or CCVs detected (Motley et al., 2003). Any change in protein levels of clathrin heavy chain (CHC) may be indicative of a change in the frequency of CCP/CCV formation and this was therefore analysed upon BIN1 depletion. A single band at ~169 kDa was observed for CHC (Figure 5.2A). There was no significant different between CHC protein levels in BIN1-depleted cells and GFP siRNA-treated cells ($p > 0.05$, two-tailed unpaired Student's *t* test, Figure 5.2B).

5.3.1.2 PICALM

PICALM levels were of particular interest in this cell line due to the aforementioned study implicating PICALM in the regulation of Aβ transcytosis at the BBB (Zhao et al., 2015). It would therefore be interesting to investigate whether depletion of BIN1 protein has an impact on PICALM expression which may implicate a potential role for BIN1 in this process. PICALM is known to express multiple isoforms (Parikh et al., 2014). While only a single band was readily detectable at ~ 64 kDa, evidence of a larger band at ~ 76 kDa was apparent in some blots but this did not reach measurable levels in all replicates (Figure 5.3A). No significant difference in levels of the strongest PICALM isoform was detected with BIN1 depletion compared to GFP siRNA-treated cells ($p > 0.05$ using a two-tailed unpaired Student's *t* test), suggesting BIN1 does not impact levels of this key CME-related protein, in addition to AP2 and CHC (Figure 5.3B). As the efflux of Aβ across the BBB is mediated by LRP1, which undergoes CME, LRP1 levels in hCMEC/D3 cells were analysed with a view to comparing these levels between BIN1-depleted and GFP siRNA-treated cells. However, unfortunately LRP1 protein was not reliably detectable in non-transfected hCMEC/D3 lysate by Western blotting (data not shown) therefore this analysis was not pursued.

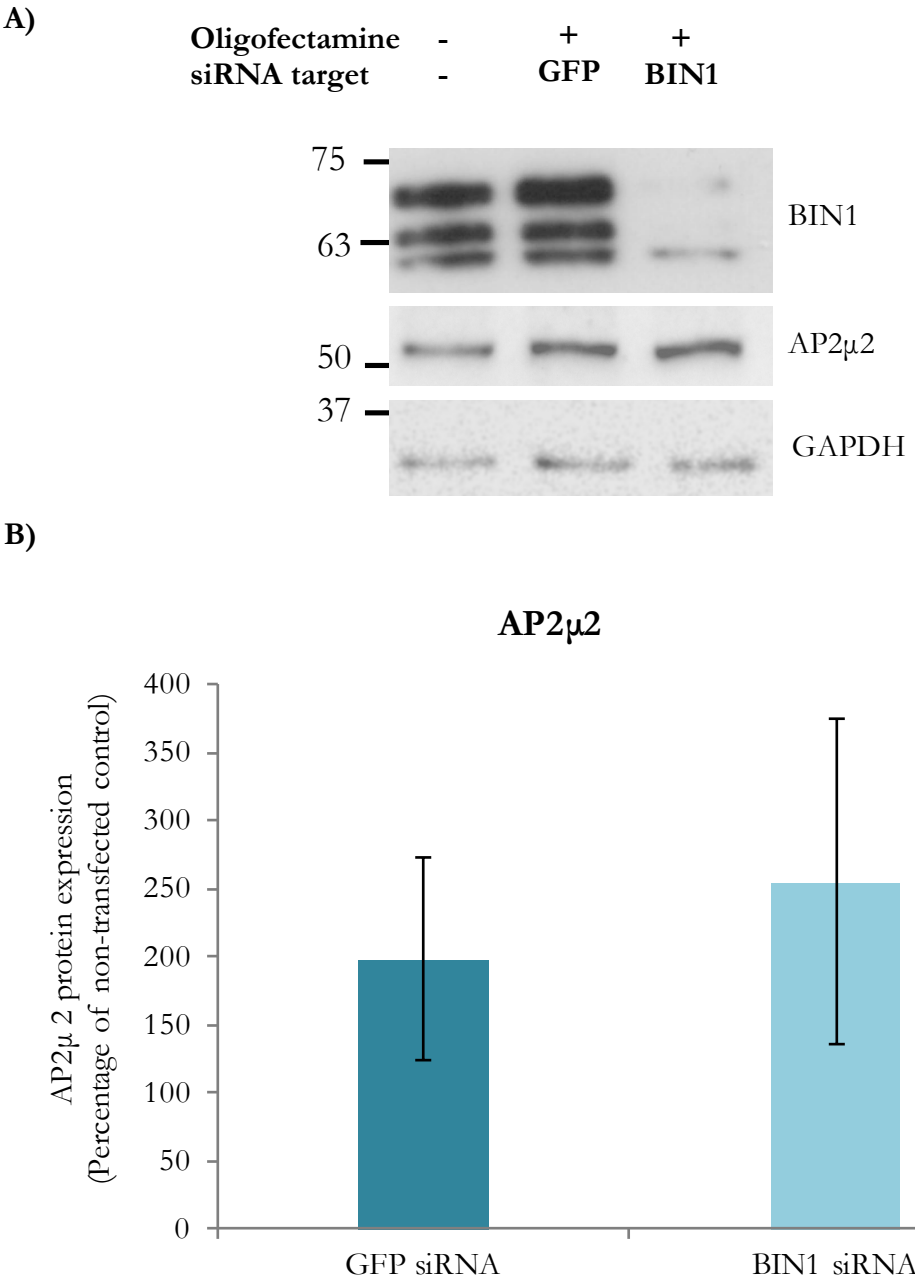

Figure 5.1: AP2µ2 protein levels in BIN1-depleted hCMEC/D3 cells

A) Representative Western blot showing levels of AP2µ2 protein in non-transfected, GFP siRNA and BIN1-depleted hCMEC/D3 cells.

B) Quantification of AP2µ2 expression based on densitometry analysis, expressed as mean percentage expression of non-transfected cells after normalisation to GAPDH, error bars = SEM, n = 4, $p > 0.05$ using a two-tailed unpaired Student's *t* test.

A)

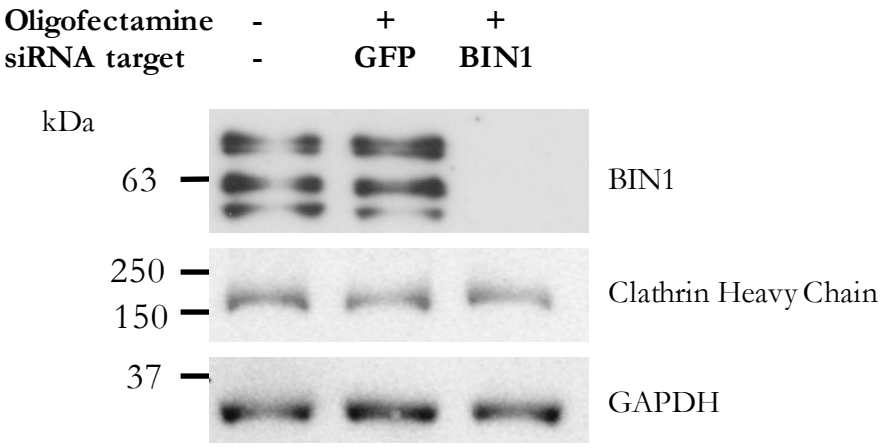

B)

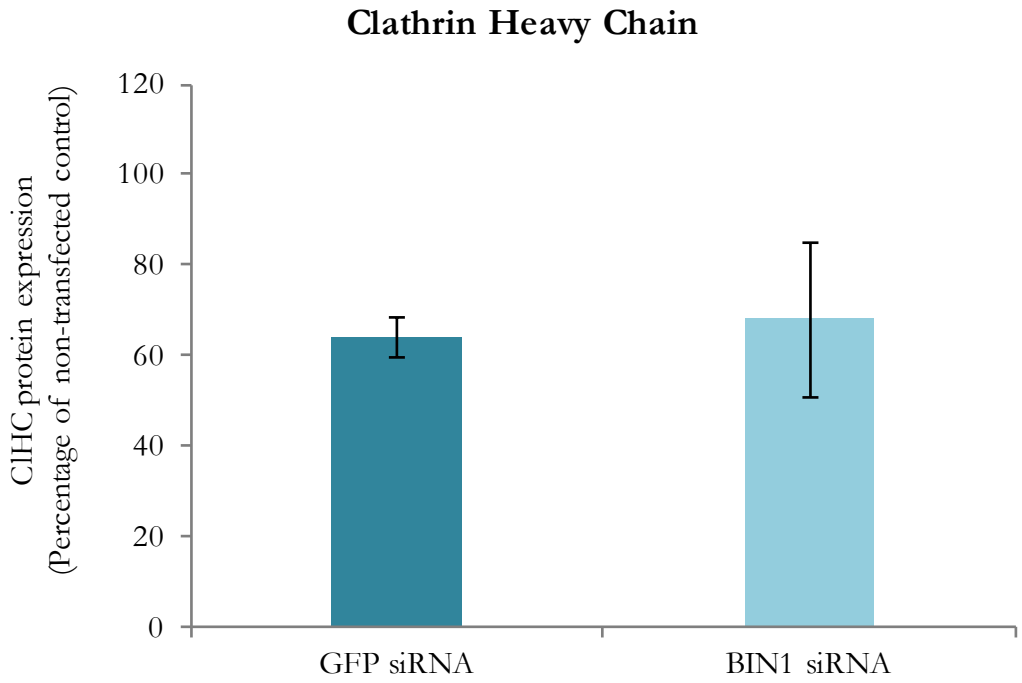

Figure 5.2: Clathrin heavy chain protein levels in BIN1-depleted hCMEC/D3 cells

A) A representative Western blot showing levels of CHC protein in non-transfected, GFP siRNA and BIN1-depleted hCMEC/D3 cells.

B) Quantification of CHC expression based on densitometry analysis, expressed as mean percentage expression of non-transfected cells after normalisation to GAPDH, error bars = SEM, n = 4, $p > 0.05$ using a two-tailed unpaired Student's *t* test.

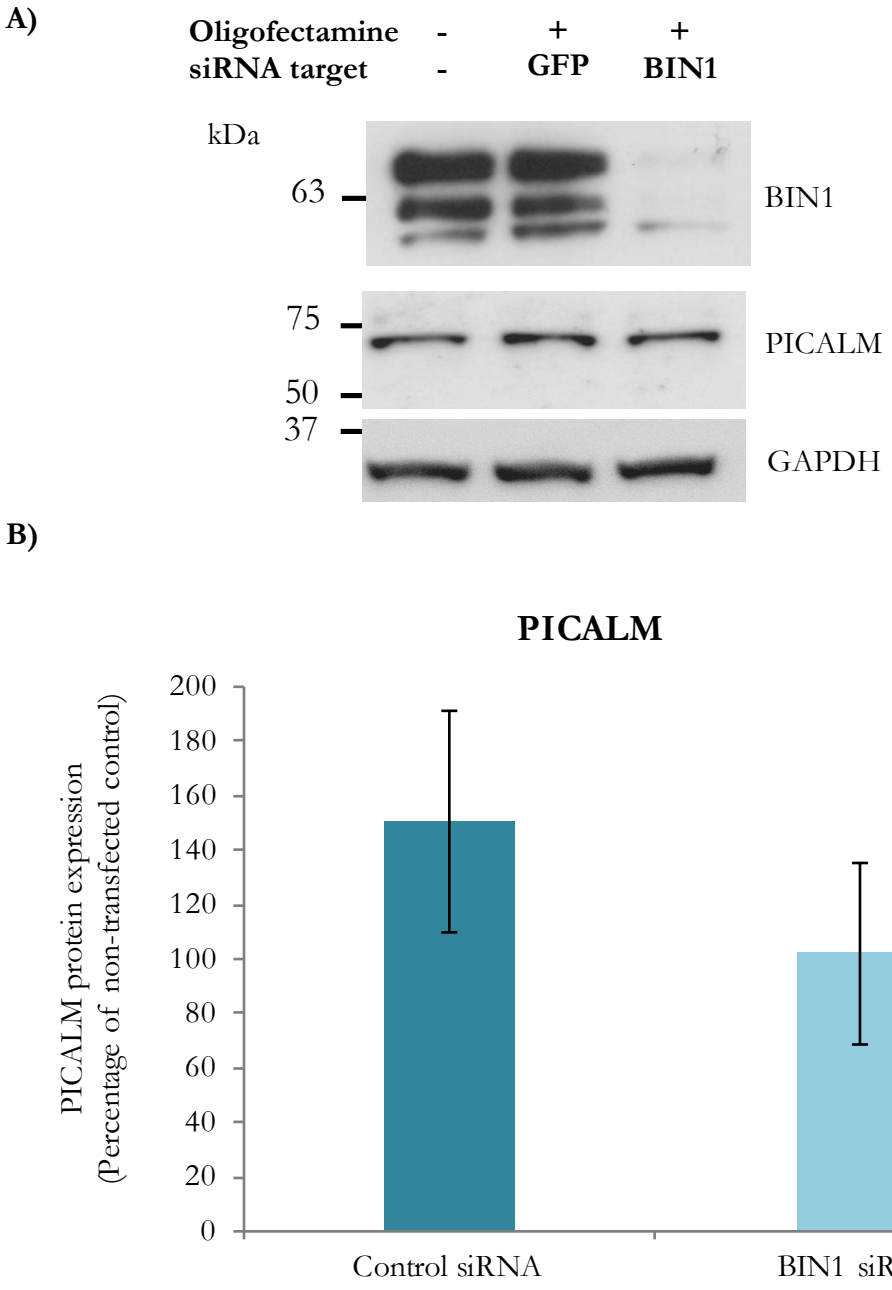

Figure 5.3: PICALM protein levels in BIN1-depleted hCMEC/D3 cells

A) A representative Western blot showing levels of PICALM protein in non-transfected, GFP siRNA and BIN1-depleted hCMEC/D3 cells.

B) Quantification of PICALM expression based on densitometry analysis of four biological replicates, expressed as mean percentage expression of non-transfected cells, error bars = SEM, $p > 0.05$ using a two-tailed unpaired Student's *t* test.

5.3.2 Alexa-488-Tf Uptake as a Measure of CME in hCMEC/D3 cells

5.3.2.1 Optimisation of Alexa-488-Tf Uptake in hCMEC/D3 cells

To further examine mechanistically whether the observed changes in APP processing were related to the involvement of BIN1 in CME in BMECs, the effect of BIN1 depletion on Tf internalisation was analysed. The TfR is expressed on the endothelium of brain capillaries (Jefferies et al., 1984) and is known to undergo CME on the luminal membrane with rapid recycling back to the cell surface (Roberts et al., 1993). Firstly, a time-course of transferrin exposure was carried out using flow cytometry to visualise the rate at which Alexa 488-conjugated transferrin was internalised into non-transfected hCMEC/D3 cells. This was used to determine the time points required to best compare transferrin levels for subsequent experiments.

Levels of transferrin uptake rose sharply from 0-30 minutes, increasing 3.5-fold in the first 5 minutes (Figure 5.4). The 5 minute time point has frequently been used in the literature for comparisons of transferrin uptake as the rapid uptake has been shown to saturate after this time (Muller et al., 2003, Xiao et al., 2012). While the rate of uptake in hCMEC/D3 cells slowed after 5 minutes, it still increased over 2.2-fold between 5-15 minutes and plateaued after 30 minutes, peaking between 60-90 minutes after Alexa-488-Tf exposure (Figure 5.4). A slight reduction in Alexa-488-Tf levels was evident at 90 minutes compared to 60 minutes, suggesting the rate of recycling back to the plasma membrane was higher than the rate of uptake. It was therefore decided that the maximum time point for subsequent studies should be 60 minutes as no further increase in Alexa-488-Tf levels was observed after this time. Further time points selected included 5 minutes, to make comparisons with the aforementioned literature, in addition to 15 and 30 mins so that a full time-course could be plotted.

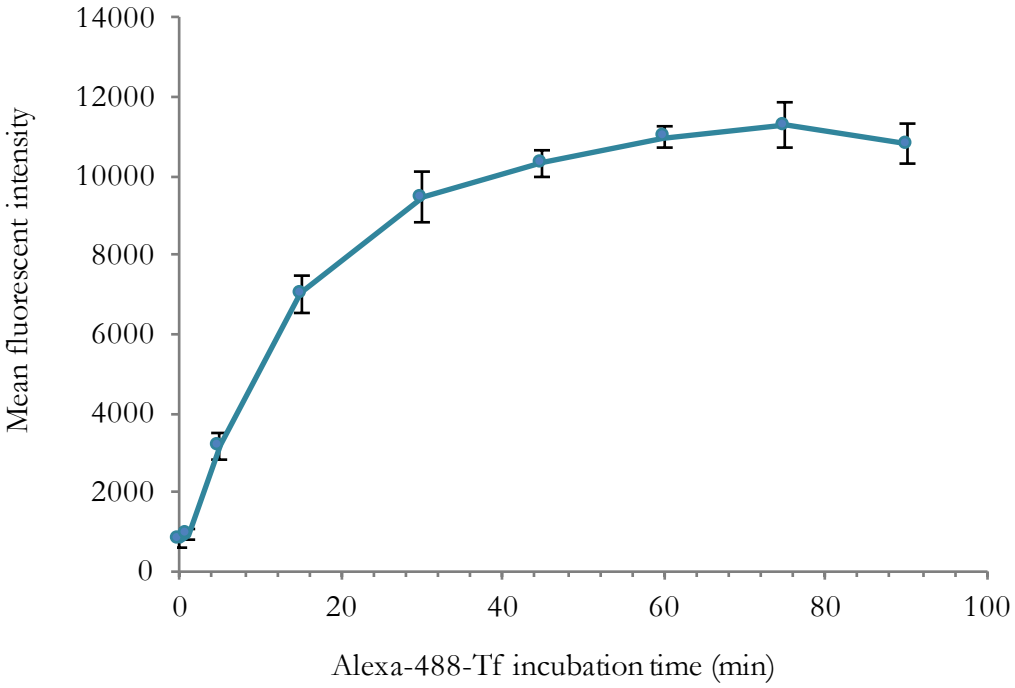

Figure 5.4: Alexa-488-Tf uptake in non-transfected hCMEC/D3 cells

Quantification of Alexa-488-Tf internalisation over a time course of 90 minutes. Values represent the geometric mean, n = 3, error bars = SEM.

5.3.2.2 Establishment of a positive control for CME inhibition

In order to make comparisons with a positive control for impaired Tf internalisation, siRNA-mediated depletion of the μ2 subunit of the AP2 complex was used, as previously demonstrated (Moody et al., 2015). The aim of depleting AP2μ2 was to induce defects specific to early endocytic events, where AP2 is involved, rather than targeting other endocytic machinery, such as clathrin which also mediates post-Golgi vesicular transport and would therefore not be specific to CME (Motley et al., 2003). The TfR associates, via tyrosine-based motifs, with the phosphorylated μ2 subunit of AP2 (Olusanya et al., 2001) therefore depletion of this subunit impairs transferrin uptake (Motley et al., 2003). The concentration of AP2μ2 siRNA was optimised at 25, 50 and 75 nM in order to determine the lowest concentration necessary for significant protein depletion. Two distinct bands were detected for AP2μ2 at sizes 47 and 50 kDa (Figure 5.5A), whereas only one band was detectable in earlier analysis of AP2μ2 level with BIN1 depletion (Figure 5.1). Both bands were measured for densitometry analysis and all three siRNA concentrations showed consistent AP2 depletion, however a significant 62% reduction in protein was only confirmed by using 25 nM siRNA ($p<0.05$, two-tailed unpaired Student's t test Figure 5.5B). This gave the highest level of knockdown and allowed the use of the lowest concentration of siRNA.

To determine the effectiveness of the assay, Alexa-488-Tf uptake was analysed over a time-course of 60 minutes in AP2μ2-depleted cells. After 5 minutes, a significant 48% reduction in Alexa-488-Tf uptake was evident compared to GFP siRNA-treated cells ($p<0.01$, two-tailed unpaired Student's *t* test) with Alexa-488-Tf levels increasing 1.4-fold in AP2μ2-depleted cells compared to 2.7-fold in GFP siRNA-treated cells (Figure 5.6A). While the level of Alexa-488-Tf in AP2μ2-depleted cells remained significantly lower than GFP siRNA-treated cells across all time points, the rate of uptake remained similar after the initial 5 minute incubation with a 1.8-fold increase in AP2-depleted cells and a 1.9-fold increase in GFP siRNA-treated cells between 5-15 minutes.

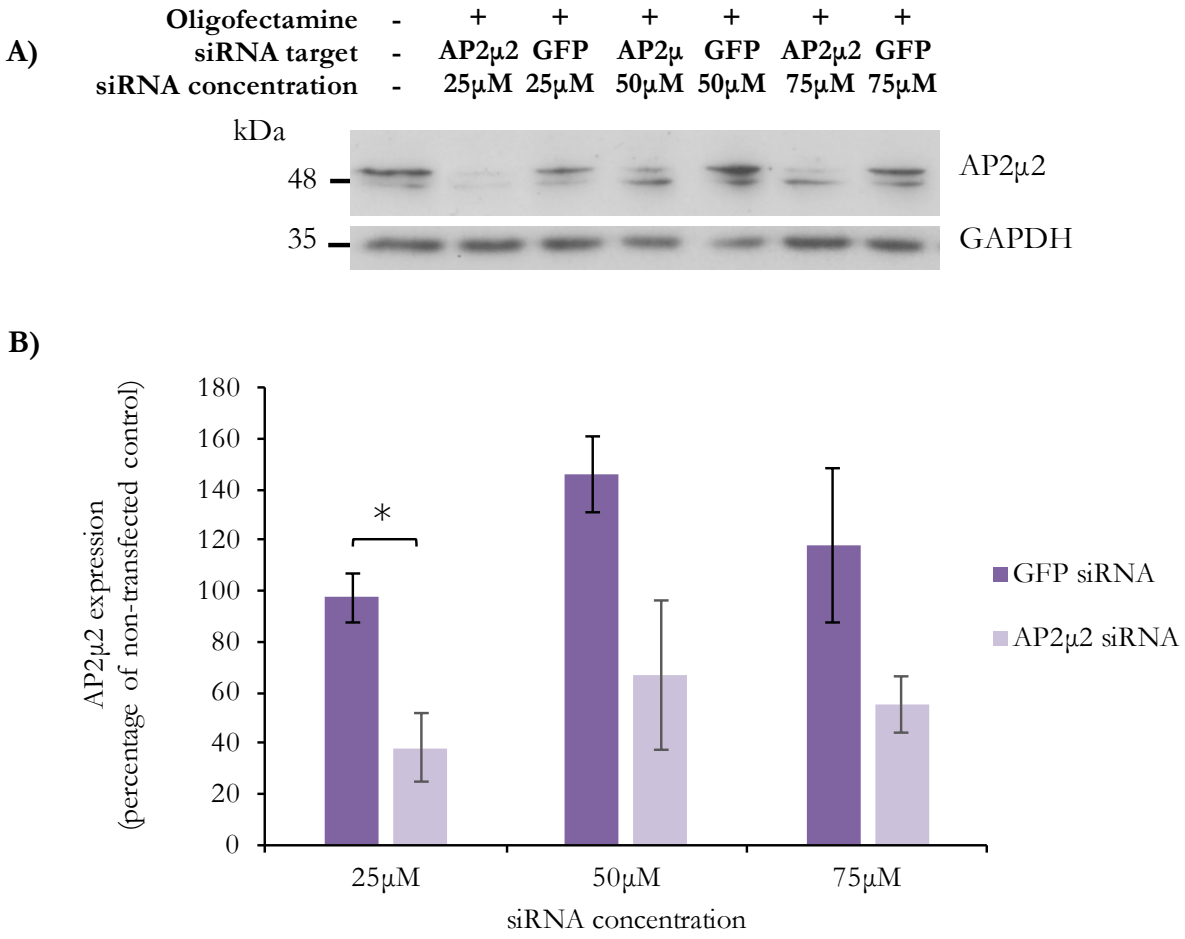

Figure 5.5: Optimisation of siRNA-mediated AP2µ2 depletion

A) A representative Western blot demonstrating successful knockdown of AP2µ2 protein with the treatment of 3 different concentrations of siRNA in hCMEC/D3 cells.

B) Quantification of both AP2µ2 bands shows significant depletion using 25µM siRNA expressed as a mean percentage of non-transfected cells, n = 3, * = $p<0.05$ using a two-tailed unpaired Student's *t* test, error bars = SEM.

5.3.3 The Effect of BIN1 Depletion on Alexa-488-Tf Uptake

The same assay was then used to determine if BIN1 depletion affected Alexa-488-Tf uptake. There was no significant difference in Alexa-488-Tf levels between BIN1-depleted and GFP siRNA-treated cells across all time points (Figure 5.6B). Alexa-488-Tf levels increased by 2.9 and 2.6-fold for GFP siRNA-treated and BIN1-depleted cells, respectively. At all subsequent time points, very little difference was observed in Alexa-488-Tf uptake between the two conditions with a 1.9-fold rate of increase between 5-15 min. The rate of uptake began to plateau after 15 mins, reaching the highest level of fluorescence at 60 minutes. Overall, a slower rate of uptake was observed compared to the optimisation experiment using untreated cells, suggesting that the siRNA treatment process in itself may have affected the rate of endocytic uptake.

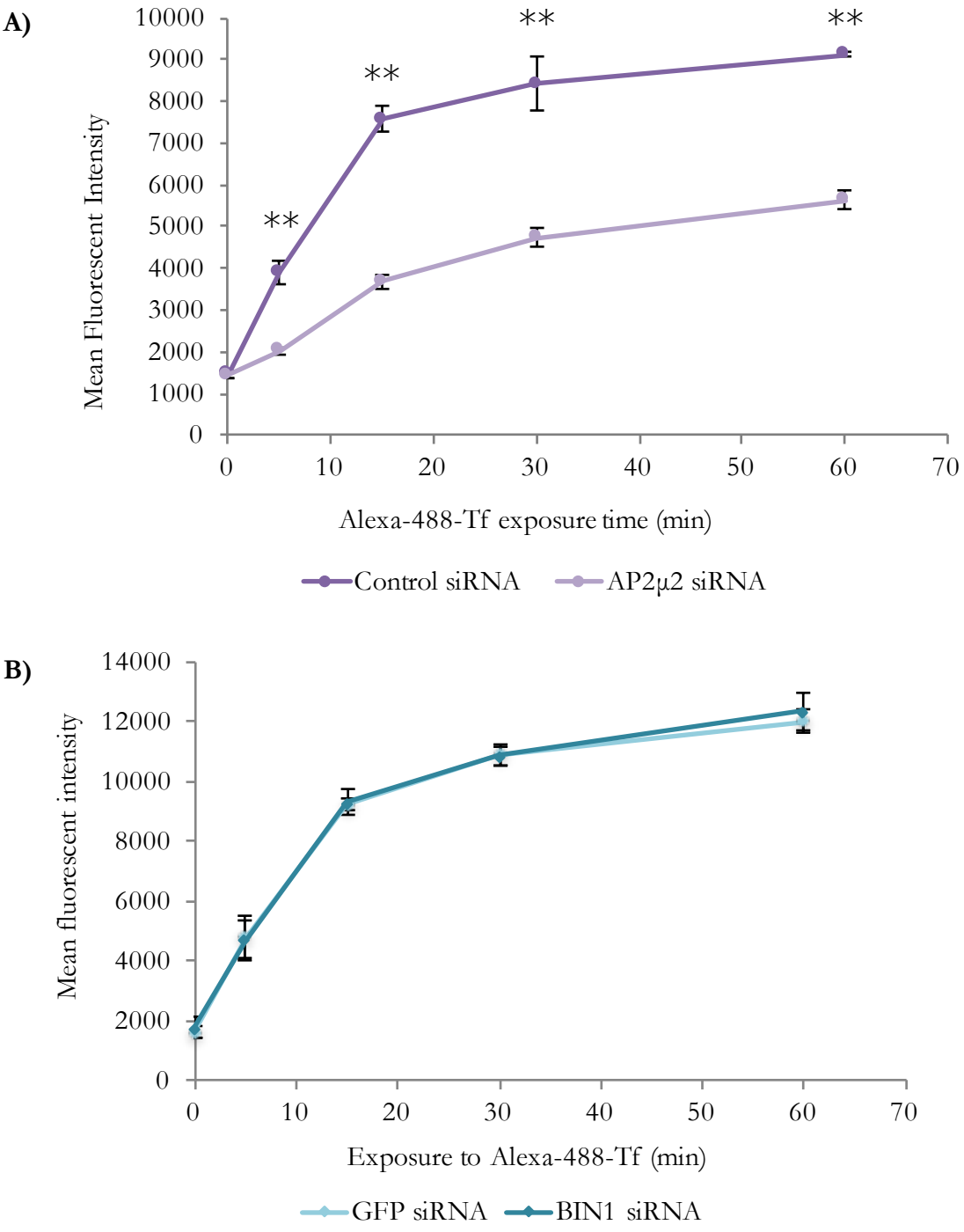

Figure 5.6: The effect of AP2µ2 or BIN1 depletion on Alexa-488-Tf uptake

A) Quantification of Alexa-488-Tf internalisation with AP2µ2 depletion in comparison to GFP siRNA-treated cells over a time course of 60 minutes. Values represent the geometric mean, ** = $p<0.01$, two-tailed unpaired Student's *t* test, error bars = SEM.

B) Quantification of Alexa-488-Tf internalisation with BIN1 depletion in comparison to GFP siRNA-treated cells over a time course of 60 minutes. Values represent the geometric mean, n = 3, error bars = SEM.

5.3.4 The Effect of BIN1 Depletion on Alexa-488-Tf Recycling

While BIN1 depletion did not affect Alexa-488-Tf uptake in hCMEC/D3 cells, BIN1 has been implicated in endocytic recycling (Pant et al., 2009, Miyagawa et al., 2016), therefore a pulse-chase assay was used to examine the recycling of Alexa-488-Tf back to the plasma membrane. Following transfection, cells were pulsed with Alexa 488-Tf for 60 minutes to saturation, before chasing with unlabeled holotransferrin for 0-60 minutes. In GFP siRNA-treated cells, Alexa-488-Tf was rapidly recycled out of the cells during the chase phase at 37°C, reaching a mean fluorescent intensity of 4458 by 60 minutes, near the mean background fluorescence level of 3338 (Figure 5.7). In contrast, cells maintained at 4ºC during the chase phase did not show a significant decrease across any time points, with 92% of the fluorescence at time point 0 still remaining after 60 minutes in GFP siRNA-treated cells. This suggests that the decrease in Alexa-488-Tf observed during the 37ºC chase was due to active endocytic recycling as endocytic pathways are inhibited at 4°C.

With BIN1 depletion, Alexa-488-Tf followed the same pattern of recycling, with mean fluorescent intensity decreasing at the same rate as GFP siRNA-treated cells. A two-tailed unpaired Student's *t* test confirmed there was no significant difference in Alexa-488-Tf levels between GFP siRNA-treated and BIN1-depleted cells across 7.5, 15, 30 and 60 minutes ($p>0.05$). However, a significant difference was detected at the 0 time point ($p < 0.05$) suggesting there was a difference in the level of Alexa-488-Tf uptake across the 60 minute pulse (Figure 5.7). This brought into question the difference in methodology between the Alexa-488-Tf uptake and recycling experiments, particularly the temperature at which trypsinisation was carried out. In the uptake experiments, cells were trypsinised at RT to ensure the reaction would take place within the time-constraints of the experiment. However, it was observed that the cells could be trypsinised at 4°C within 15 minutes, therefore cells were trypsinised on ice in the recycling experiments to inhibit endocytic trafficking during this time. In light of this apparent difference in intracellular Alexa-488-Tf levels following the pulse period of the recycling experiment, the Alexa-488-Tf uptake experiment was repeated once more, but trypsinising on ice (results not shown). This showed no difference in fluorescence levels between GFP siRNA-treated and BIN1-depleted cells across all time points, and replicated the results of the previous 3 uptake experiments where cells had been trypsinised at RT. This therefore assured confidence in the data.

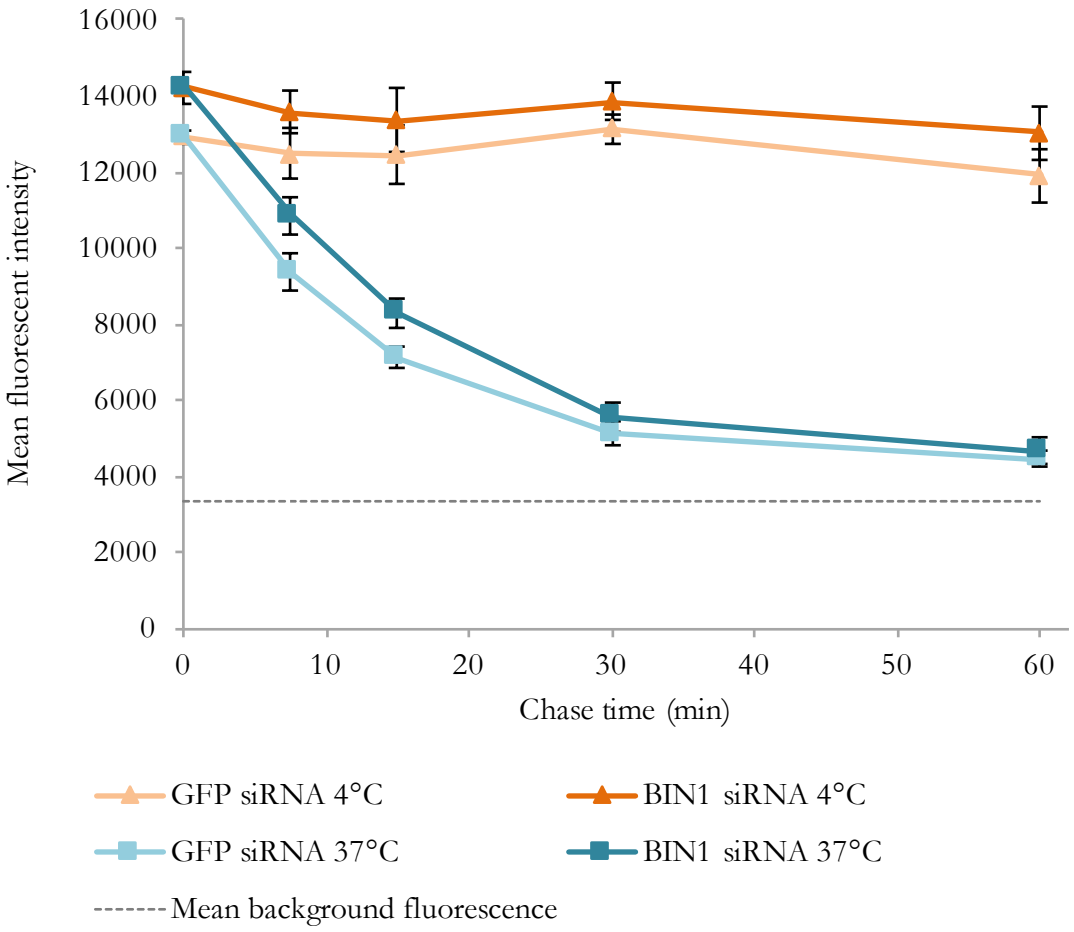

Figure 5.7: The effect of BIN1 depletion of Alexa-488-Tf recycling

Quantification of Alexa-488-Tf recycling with BIN1 depletion in comparison to GFP siRNA-treated cells after a 60 minute pulse at 37°C followed by chasing with unlabeled holotransferrin over a time course of 60 minutes. To illustrate inhibition of endocytic recycling, the chase was also performed at 4°C for each siRNA condition. Values represent the geometric mean, n = 3-4, error bars = SEM.

5.3.5 Early Endosome Morphology with BIN1 depletion

Several recent studies, showing defective endocytic trafficking as a result of BIN1 depletion, have also shown recapitulation of the enlarged endosome morphology that is an early feature of AD pathology (Cataldo et al., 2000, Miyagawa et al., 2016, Ubelmann et al., 2017). Therefore, the early endosome marker, EEA1, was used to observe early endosome localisation and size in BIN1-depleted cells. EEA1 showed punctate cytoplasmic staining, suggestive of a vesicular distribution in the early endosomes (Figure 5.8). Consistent with a lack of impairment in Alexa-488-Tf recycling, the distribution and observed intensity of EEA1 staining was not altered by BIN1 depletion suggesting that early endosome abnormalities, often indicative of endocytic recycling dysfunction, did not occur.

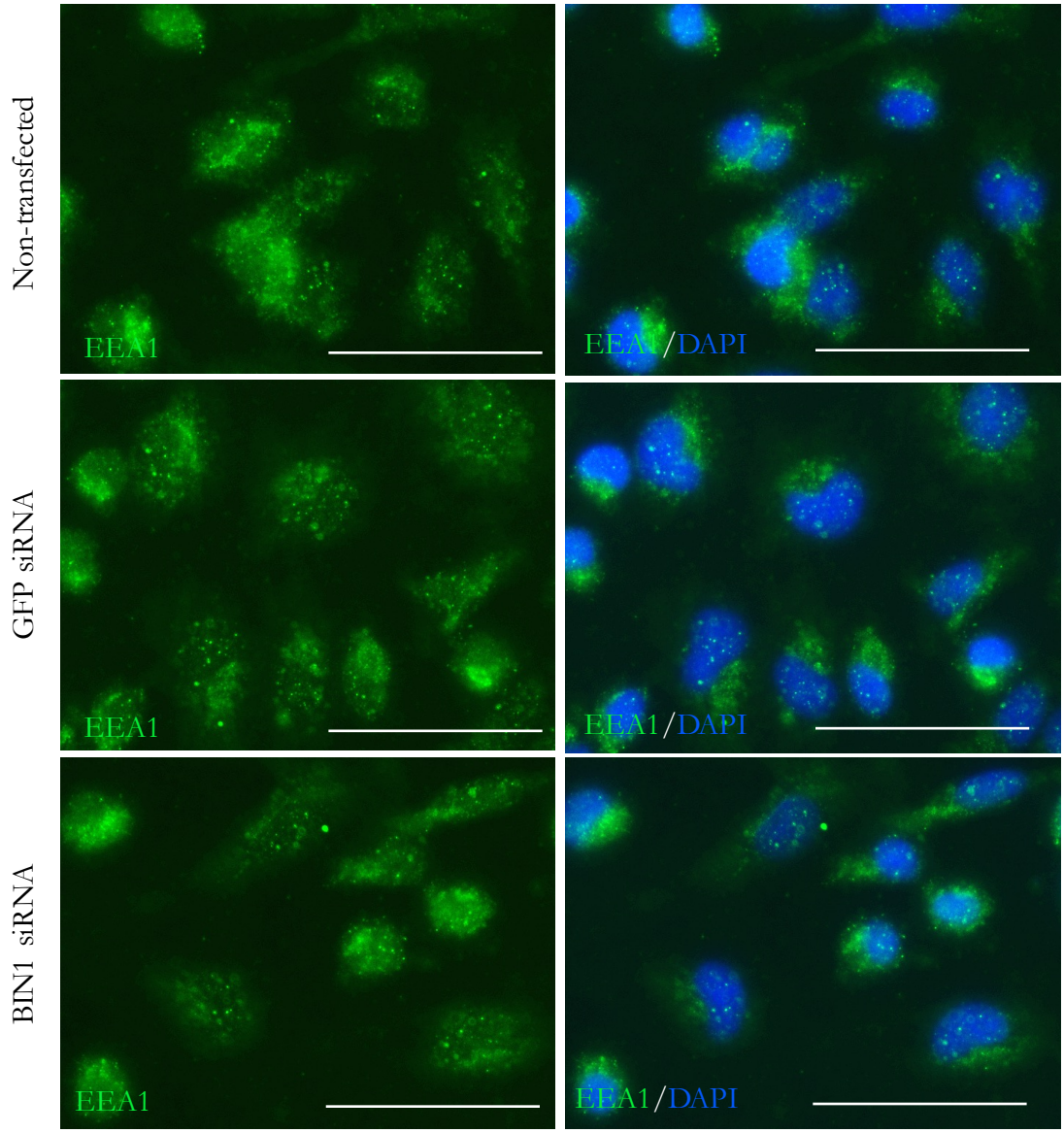

Figure 5.8: EEA1 staining of Early Endosomes with BIN1 depletion

Representative immunofluorescence images of EEA1 expression, a marker of early endosomes, in non-transfected, GFP siRNA-treated and BIN1-depleted hCMEC/D3 cells. Images were taken at x40 magnification with DAPI used to stain the nuclei, scale bar = 25 μm.

5.3.6 Amphiphysin I Expression in hCMEC/D3 cells

Amphiphysin 1 (AMPH1) is a BIN1 homologue which forms heterodimers with BIN1 to aid in endocytic uptake through interactions with dynamin (Wigge et al., 1997a). While no effect on Tf uptake was observed with BIN1 depletion, it is possible that AMPH1 may have compensated for the loss of BIN1 therefore Tf uptake was unaffected. As AMPH1 is considered to be brain-specific, its expression in the hCMEC/D3 cell line was investigated by Western blotting with a view to analysing any expression changes with BIN1 depletion. AMPH1 protein was not detectable in hCMEC/D3 cells lysates, despite exhibiting strong expression in mouse whole brain lysate (Figure 5.9). However, analysis of AMPH1 expression with BIN1 depletion was not carried out and it therefore cannot be ruled out that these levels may have become detectable with BIN1 depletion.

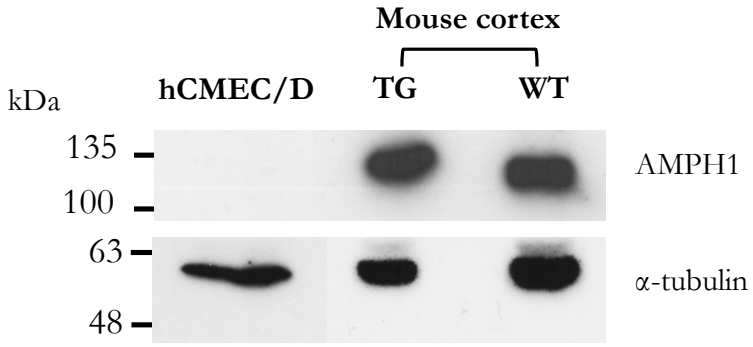

Figure 5.9: AMPH1 expression in hCMEC/D3 cells

Western blot showing undetectable AMPH1 expression in hCMEC/D3 cell lysate compared to transgenic (TG) and wild-type (WT) mouse whole cortex lysate. Irrelevant bands have been removed for the purpose of figure readability.

5.3.7 BIN1 Isoform Expression in hCMEC/D3 cells

All BIN1 isoforms contain an N-terminal domain which senses and generates membrane curvature and a C-terminal SH3 domain which mediates interactions with CME-related proteins such as dynamin and adaptor proteins (Wechsler-Reya et al., 1997). The CLAP domain, encoded by the alternatively-spliced exons 12a-d, is only found in brain-specific isoforms and is predicted to be critical for the recruitment of dynamin and its self-assembly at the CCP (Owen et al., 1998). Western blot analysis of BIN1 in hCMEC/D3 cells showed the presence of at least three different size bands at approximately 68, 58 and 55 kDa (Figure 5.1), suggesting multiple isoforms are expressed in these cells. The brain-specific isoform containing the CLAP domain has been shown to migrate at 90 kDa (De Rossi et al., 2016) therefore these results suggest the CLAP domain is not expressed in these cells, possibly explaining why there was no effect of BIN1 depletion on CME or recycling.

In order to characterise the BIN1 isoforms expressed in hCMEC/D3 cells, total RNA was extracted from the cells and primers designed to specifically target the region containing the CLAP domain. The amplified region incorporated exons 11-15, of which exons 12a, 12b, 12c, 12d and 13 are subject to alternative splicing. A sample of the PCR product was subject to gel electrophoresis to confirm amplification and 5 distinct bands were observed at approximately 455, 353, 311, 219 and 113 kb, representing considerable alternative splicing of this region (Figure 5.10). Taq DNA polymerase preferentially adds an adenine to the 3' end of the PCR product which allowed ligation of the PCR product to a pGEM®-T Vector by complementary base pairing to the thymine residues on both 3' ends of this open vector. The PCR products were transformed into DH5α™ cells and grown on agar containing ampicillin; the ampicillin resistance gene within the vector allowed the selective growth of colonies only from cells that had taken up the vector. In total, 48 colonies were selected for PCR screening which showed PCR products of varying lengths had been successfully cloned (Figure 5.10). Clones with more than one band were excluded and those showing a single band were selected for sequencing, incorporating at least three samples from each sized band.

A total of 18 PCR products were sequenced, 3 of which returned without any recognisable coding DNA and were therefore excluded from analysis (Figure 5.10). As expected, all 15 PCR products contained exons 11, 14 and 15 which are expressed in all BIN1 isoforms. Of the alternatively spliced exons (12a, 12b, 12c, 12d and 13), the sequences either contained both exons 12a and 13, exon 12a alone, exon 13 alone or none at all (Figure 5.11). The isoforms that these can be attributed to include brain-specific and ubiquitous isoforms. The precise signature isoforms expressed cannot be determined as the presence of two further alternatively spliced exons (6a and 10) was not investigated. However, none of the isoforms sequenced contained the full complement of exons (12a-d) that encode the CLAP domain, suggesting this region is not expressed in hCMEC/D3 cells.

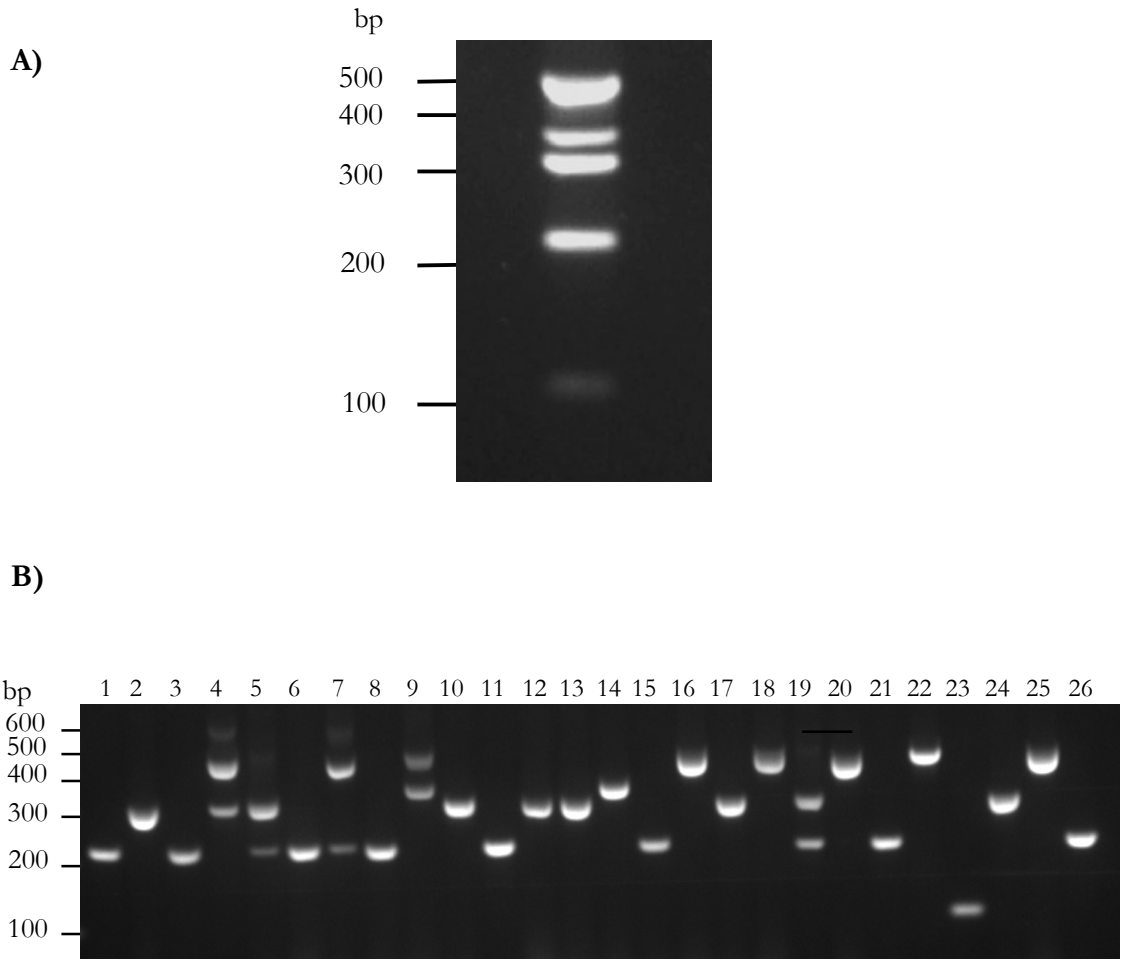

Figure 5.10 PCR amplification and cloning of BIN1 exons 11-15 in hCMEC/D3 cells

A) A gel electrophoresis image of the PCR product amplified from hCMEC/D3 cDNA targeting exons 11-15 of the BIN1 gene. Distinct bands represent the different isoforms due to alternative splicing within this region.

B) A representative PCR screen from 26 DH5α™colonies showing the variation in size within the amplified region (exons 11-15) of the BIN1 gene. Each well has been amplified from a single colony and therefore represents the PCR products ligated into the pGEM®-T Vector that they contain.

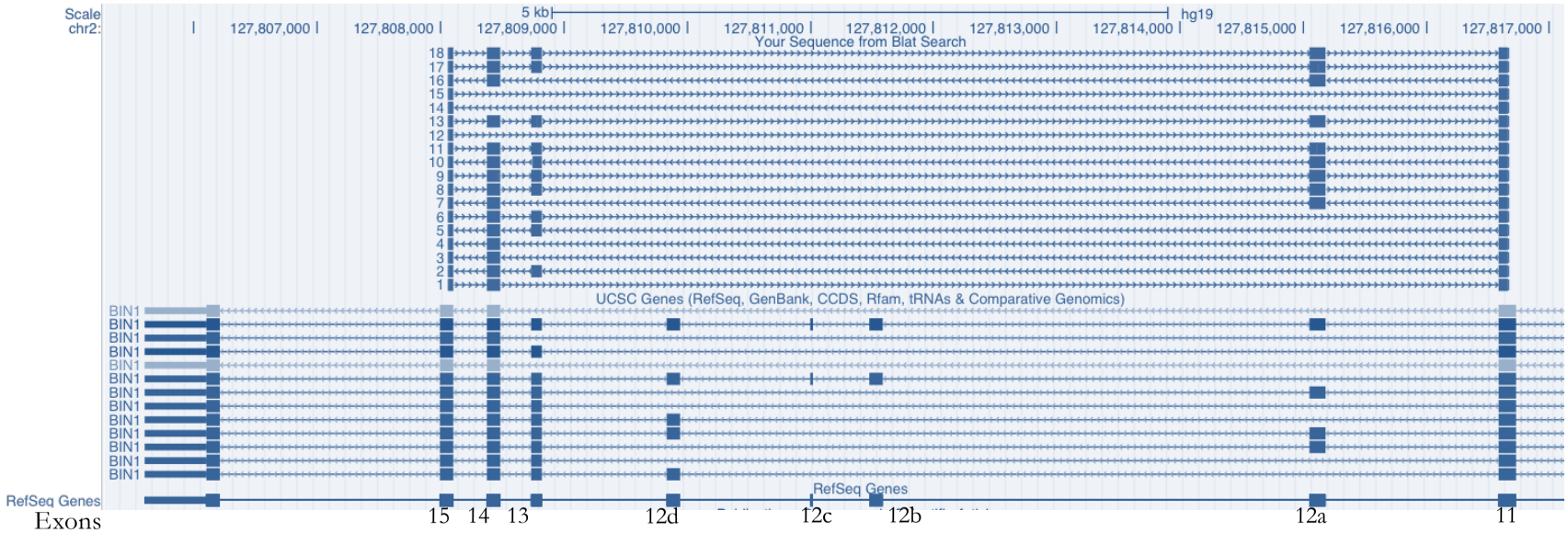

Figure 5.11: Alignment of exons 11-15 of the BIN1 gene showing the isoforms expressed in hCMEC/D3 cells

An alignment of all PCR products against the *BIN1* gene in UCSC Genome Browser, used to determine the isoforms expressed in hCMEC/D3 cells. PCR products 12, 14 and 15 did not align with any coding regions and were therefore excluded from analysis.

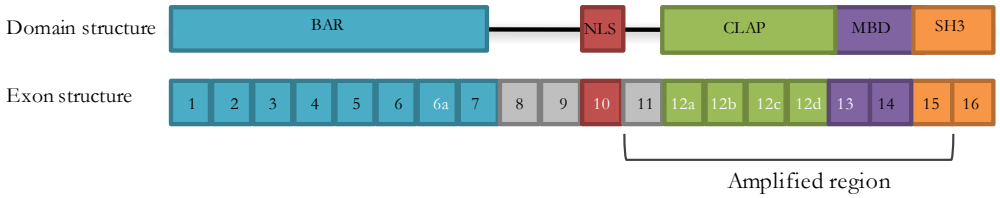

Number of PCR products (15 in total)	Correspond to which isoform(s)	Tissue expression	Alternatively spliced exons expressed
7	Isoform 4	Brain	 Exons 12a and 13
	Isoform 6	Brain	
2	Melanoma isoform	Cancer	 Exon 12a
3	Isoform 8	Muscle	 Exon 13
	Isoform 9	Ubiquitous	
3	Isoform 10	Ubiquitous	 None

Figure 5.12: Potential BIN1 isoforms expressed in hCMEC/D3 cells

A schematic illustrating the full length BIN1 protein domain structure with corresponding exon structure and the target region for amplification between exons 11-15 for RNA cloning and sequencing. The table shows the number of PCR products sequenced and which isoforms these correspond to, with schematics of the exon structure of each isoform(s) for clarity. The isoforms are depicted in full in Chapter 1, Figure 1.2. BAR, BAR domain; SH3, SH3 domain; MBD, Myc binding domain; CLAP, clathrin-associated protein binding region; PI, phosphoinositide binding region. Exons are numbered by reference to Wechsler-Reya et al. (1997).

5.4 Discussion

In this chapter, the role of BIN1 in CME in the hCMEC/D3 human brain endothelial cell line has been investigated, in light of the previously observed increase in β-CTF levels, reported in Chapter 4. BIN1 depletion in hCMEC/D3 cells did not significantly affect the expression of key CME-related proteins AP2, CHC and PICALM or the uptake/recycling of Tf, a marker of CME. An analysis of the BIN1 isoforms expressed in hCMEC/D3 cells revealed that isoforms containing the full-length CLAP domain are not expressed in this cell line, collectively suggesting that BIN1 is not important for CME in hCMEC/D3 cells.

5.4.1 BIN1 is not Crucial for CME in hCMEC/D3 cells

The findings presented in this chapter suggest that BIN1 is not a crucial player in CME in BMECs. Firstly, analysis of AP2 expression upon BIN1 depletion showed no change in protein levels suggesting that early endocytic events were not perturbed in BIN1-depleted cells as AP2 function is specific to this early stage (Motley et al., 2003). Furthermore, unaltered levels of CHC with BIN1 depletion suggested there was not a change in the number of CME events occurring at the plasma membrane or within the cells, as clathrin is known to also be involved in intracellular membrane trafficking (Motley et al., 2003). PICALM expression was also unaffected by BIN1 depletion, further supporting the notion that BIN1 is not important for CME or endocytic trafficking mechanisms, such as the intracellular transcytosis of Aβ that PICALM has been shown to regulate in BMECs (Zhao et al., 2015).

These results were further supported by measuring Tf uptake in AP2μ2-depleted cells which showed significant inhibition of Alexa-488-Tf uptake after just 5 minutes. This not only validates the assay as an effective measure of CME, but also demonstrates the importance of AP2 in this mechanism. In BIN1-depleted cells, however, Alexa-488-Tf uptake remained unaffected, further suggesting that BIN1 does not have a crucial role in CME in the hCMEC/D3 cell line. This is somewhat unexpected due to previous studies implicating BIN1 in CME based on two key lines of evidence. Firstly, the binding of certain isoforms with key endocytic machinery such as clathrin, AP2 and dynamin in neuronal cells (Butler et al., 1997, Ramjaun and McPherson, 1998) and macrophages (Gold et al., 2000). Secondly, the demonstration that Bin1 dominant negative mutants, lacking the

dynamin-binding SH3 domain, severely impaired CME in macrophages (Gold et al., 2000). Collectively, these studies suggest that BIN1 is involved in CME in both neuronal and non-neuronal cells and depletion of BIN1 may therefore result in CME dysfunction. However, the results from the present study do not support this hypothesis and suggest that BIN1 is not universally important for CME. Indeed, it has been shown that *Bin1* knockout MEFs and BIN1-depleted HeLa cells are not defective in Tf uptake (Muller et al., 2003, Pant et al., 2009). However, both *Bin1* knockout MEFs and BIN1-depleted HeLa cells showed an approximately 3-fold and 2-fold increase in Tf uptake compared to controls, respectively (Muller et al., 2003, Pant et al., 2009). Pant and colleagues reported that this was a result of Tf accumulating in the juxtanuclear compartment of BIN1-depleted HeLa cells due to delayed recycling back to the plasma membrane, suggesting that BIN1 may not be crucial for endocytic uptake, but may be important for intracellular endocytic trafficking.

Indeed, clathrin-mediated endocytic mechanisms are not only limited to the plasma membrane. The presence of clathrin coats has been demonstrated in endosomes where they appear to mediate the sorting of ubiquitinated cargo towards degradation (Raiborg et al., 2002) and the recycling of proteins to the plasma membrane (Sachse et al., 2002). While BIN1 may not be involved in CME *per se* in BMECs, it may have a function in clathrin-dependent intracellular endocytic sorting. Consistent with a role in endocytic recycling, BIN1 was found to be enriched on tubules of the ERC and important for the maintenance and correct functioning of these structures in mouse primary cortical neurons (Ubelmann et al., 2017). In this study, Bin1 was reported to regulate BACE1 trafficking as BACE1 accumulated in early endosomes with Bin1 siRNA-mediated depletion, suggesting that the exit of BACE1 from early endosomes for recycling was impaired. Indeed, a greater number of neurons showed evidence of tubular carriers containing BACE1 with Bin1-depletion compared to controls (Ubelmann et al., 2017). Tubular endocytic carriers play an important role in mediating transport within the endocytic pathways and, upon scission, transport their cargo from the early endosomes/ERC to the plasma membrane. While the number and length of BACE1 tubular carriers also increased in Bin1-depleted axons, live imaging revealed that scission events, following tubule formation, were not observed. Instead, tubules remained stably associated with early endosomes, suggesting that Bin1 controls the scission, but not formation, of tubules in axons. In this manner, BACE1 tubule exit from axonal-early endosomes was inhibited by Bin1 depletion, leading to impaired BACE1

recycling, accumulation in early endosomes and increased Aβ generation (Ubelmann et al., 2017). Collectively, the aforementioned findings by Pant et al. (2009) and Ubelmann et al. (2017) suggest that Bin1 does not have a necessary functional role in CME but is important for endocytic trafficking downstream of CME.

In the hCMEC/D3 cell line used in the present study, however, there was no difference in the rate of Tf recycling with BIN1 depletion compared to GFP siRNA-treated cells suggesting, in these cells, it is not pivotal in the endocytic recycling process. Furthermore, several recent studies that have implicated BIN1 in regulating endocytic recycling have also demonstrated enlargement of EEA1-positive early endosomes with BIN1 depletion (Miyagawa et al., 2016, Ubelmann et al., 2017), recapitulating an early pathological feature of AD (Cataldo et al., 2000). Early endosome morphology was therefore investigated in the present study but no difference was observed between conditions, suggesting that accumulation of cargo in the early endosomes did not occur with BIN1 depletion and therefore supporting the notion that BIN1 is not crucial for endocytic recycling in hCMEC/D3 cells.

5.4.2 Asymmetry of Endocytic Processes

The endosomal trafficking route of Tf in BMECs, unlike other non-neuronal cell types used in BIN1-depletion studies, involves the apical to basolateral transcytosis of the receptor-bound Tf due to the establishment of polarity at the BBB (Descamps et al., 1996). While the Tf recycling assay can be used as an indicator of transcytotic function, it does not represent an accurate measure of transport across polar domains and it therefore still remains to be investigated whether BIN1 has a role in transcytosis at the BBB. BMECs are known to be well polarised *in vivo*, with distinct apical and basolateral domains, segregated by tight junctions (Shivas et al., 2010). While the hCMEC/D3 cell line has been shown to express the Par/aPKC planar cell polarity complex, which contributes to the regulation of tight junction integrity and apical-basolateral polarity (Artus et al., 2014), the tightness of the monolayers formed in this cell line is relatively low compared to *in vivo* levels (Weksler et al., 2005). Many drug transport studies that have used the hCMEC/D3 cell line, culture the cells on transwell filters which allow cells to feed both apically and basolaterally and thereby carry out metabolic activities in a more natural fashion. This aids polarisation; hCMEC/D3 monolayers display five-fold higher concentrations of TJ proteins on

transwell filters than on plastic coverslips (Weksler et al., 2013). In the present study, cells were cultured on fibronectin-coated culture vessels. With the aim of the study to investigate basic endocytic function with BIN1 depletion, rather than transcytotic activity, it was not deemed necessary to establish polarity in the culture system. However, an effect on CME and recycling cannot be ruled out, had the culture system been designed to grow cells in a polarised fashion, with the establishment of apical and basolateral domains. Since the cells used in this study may lack the polarisation seen *in vivo*, it is possible that BIN1 may have a role in the trafficking of cargo to a particular domain, which could not be detected by the Tf recycling study. Indeed, BIN1 has recently been implicated in the transport of apical-directed proteins in polarised epithelial cells of the small intestine (Nakajo et al., 2016). Depletion of Bin1 in mouse small intestine organoids resulted in altered localisation of apical proteins but not basolateral proteins, suggesting Bin1 is involved in apical protein transport through generation of membrane tubules at the ERC (Nakajo et al., 2016). This is of particular interest due to the similar structural nature of intestinal epithelial cells and brain endothelial cells, with both possessing apical-basolateral polarity and intercellular tight junctions. It would therefore be interesting to investigate BIN1 depletion in polarised BMECs and to analyse the trafficking of specific apical and basolateral proteins in this culture system.

5.4.3 Is BIN1 Acting Alone?

It was thought to be a possibility that AMPH1 may be acting in compensation for the loss of BIN1 in the hCMEC/D3 cells. Indeed, *in vitro* analysis of both AMPH1 and BIN1 simultaneous knockdown resulted in a significant decrease in Tf uptake after 7 minutes incubation in human retinal pigment epithelial cells (Meinecke et al., 2013). Furthermore, overexpression of either Amph1 or Bin1 blocked CME in COS cells and this defect was rescued by their coexpression, illustrating the important role of the heterodimer in endocytic function (Wigge et al., 1997a). The expression of either protein alone, however, had a dominant-negative effect. Nevertheless, in the hCMEC/D3 cell line AMPH1 failed to reach detectable levels by Western blot. AMPH1 protein expression with BIN1 depletion was not investigated therefore it cannot be ruled out that AMPH1 may reach detectable levels with BIN1 depletion.

5.4.4 Endocytic Cargo Specificity

As a positive control for inhibition of CME, AP2μ2 was depleted in hCMEC/D3 cells. While depletion to undetectable levels was not achieved by siRNA transfection, significant impairment of transferrin uptake was successfully demonstrated at the level of AP2μ2 depletion achieved, supporting previous findings in HeLa cells (Moody et al., 2015). Interestingly, however, AP2–depleted HeLaM cells were capable of internalising EGF and an LDL receptor chimera, but were defective in Tf uptake (Motley et al., 2003), suggesting that AP2 is not essential for CCV formation but has a cargo-selective requirement in CME and that alternative adaptors may facilitate EGF and LDL uptake. While Tf was used in the present study as a universal marker of CME, given the selectivity displayed by AP2, it is possible that BIN1 also has a cargo-specific role in CME. While BIN1 depletion does not affect transferrin uptake in hCMEC/D3 cells, suggesting BIN1 is not essential for CME, it cannot be ruled out that it plays a role in the specific endocytic uptake of other cargo. In the future, it would be interesting to trace APP through endosomal trafficking with BIN1 depletion in order to further investigate the increase observed in β-CTF and whether perturbed endocytic trafficking of APP may be involved.

5.4.5 Tissue-specific Isoform Expression

With BIN1 subject to extensive alternative splicing, displaying a tissue-specific pattern of isoform expression, it remained to be investigated which BIN1 isoforms were expressed in human BMECs. The region of interest in this study focused on BIN1 exons 12a-d, which collectively encode the CLAP, involved in interactions with the endocytic mediators clathrin and AP2 (Ramjaun and McPherson, 1998). The presence of an isoform containing exon 12a but not 12b-d of the CLAP domain or 13 was found in hCMEC/D3 cells. While the functional relevance of the individual exons that comprise the CLAP domain has not been elucidated, this isoform has previously been attributed to an aberrant splicing event that relieves MYC inhibition by BIN1 (Ge et al., 1999). This melanoma-specific isoform is thought to be associated with the loss of the tumour suppressor activity of BIN1(Ge et al., 1999). Its expression has previously been reported in human cell lines: WI-38, HeLa, and Rh-30 but not normal non-neuronal murine tissues, suggesting it may be functionally redundant but is expressed in cell lines to promote immortalisation or establishment (Wechsler-Reya et al., 1997).

Of the 18 DNA fragments sequenced from extracted hCMEC/D3 RNA, none contained the full complement of exons required to encode the CLAP domain, supporting the findings that BIN1 does not have a pivotal role in CME in these cells. These findings are supported by RNAseq analysis of the mouse cerebral cortex, where only exon 12a of the CLAP domain was detected in sequenced transcripts from BMECs (Zhang et al., 2014). The importance of the CLAP domain to the function of BIN1 in CME is unclear. Several studies have demonstrated its involvement, including (Slepnev et al., 1998) who demonstrated that overexpression of the central domain of Amph1 (amino acids 250-588), incorporating the CLAP domain between amino acids 378-422 (Ramjaun and McPherson, 1998), blocks Tf uptake. This is of relevance to BIN1 as the sequence of amino acids within this region is conserved between Amph1 and Bin1 (Slepnev et al., 1998), suggesting that the CLAP domain of BIN1 may also be important for Tf uptake. Interestingly, overexpression of the human BIN1 neuronal isoform 1 in rat hippocampal neurons has been shown to significantly decrease Tf uptake, while overexpression of the human BIN1 ubiquitous isoform 9, which lacks the CLAP domain, did not affect Tf uptake (Calafate et al., 2016). This suggests that isoforms lacking the CLAP domain, such as those expressed in hCMEC/D3 cells, are not important for CME and supports the lack of effect on Tf uptake in the present study. Collectively, these studies suggest that the CLAP domain may be required for CME and therefore may explain the lack of effect on Tf uptake with BIN1 depletion in hCMEC/D3 cells.

However, all BIN1 isoforms still contain the BAR domain, involved in inducing membrane curvature, and the SH3 domain, which binds dynamin (Casal et al., 2006), therefore BIN1 may still have a role in endocytosis in these cells, independent of clathrin. Indeed, despite non-neuronal BIN1 isoforms lacking the CLAP domain, BIN1 depletion has been shown by different groups to have an effect on endocytic processes in HeLa cells, a non-neuronal cell line (Pant et al., 2009, Miyagawa et al., 2016). Specifically, depletion of BIN1 in these studies resulted in intracellular accumulation of internalised cargo, suggesting that the general function of BIN1 is to regulate intracellular trafficking of cargo from the early endosome to the degradation pathway. The specific cargo Miyagawa and colleagues investigated was BACE1. By expressing BIN1 mutants lacking either the BAR domain or the SH3 domain, pulldown assays revealed that it was the BAR domain that was required for the binding of BIN1 with BACE1. Therefore, while the CLAP domain may be important in CME processes that take place at the plasma membrane in neurons, such as

synaptic vesicle endocytosis, it is the BAR domain, common to all BIN1 isoforms, that is involved in intracellular trafficking of cargo. This notion, however, is not in agreement with the findings of the present study where no accumulation of Tf was detected with BIN1 depletion, nor was BACE1 accumulation observed in Chapter 4. Should BIN1 have the same role in intracellular trafficking in hCMEC/D3 cells that is observed in HeLa cells, higher levels of Tf, and BACE1, would be expected in the BIN1-depleted cells as its recycling back to the plasma membrane is impaired.

The CLAP domain is not the only alternatively spliced region within BIN1 of interest in the context of CME. Exon 6a (often referred to as exon 7 in the literature) is present only in 3 of the brain-specific isoforms (Chapter 1, Figure 1.2) and has been shown to promote an interaction between dynamin 2 and Bin1 (Ellis et al., 2012). N2a cells transiently expressing Bin1 isoforms including or lacking exon 6a were used to analyse the uptake of Tf. Inclusion of exon 6a did not affect Bin1 protein levels but resulted in a significant increase in Tf uptake whereas overexpression of Bin1 lacking exon 6a inhibited Tf uptake (Ellis et al., 2012). As Bin1 can homodimerise and heterodimerise with Amph1, the overexpression of an isoform lacking exon 6a may have sequestered endogenous exon 6a-containing Bin1 and Amph1, thus preventing functional interactions with dynamin 2. This suggests that BIN1 exon 6a strongly promotes interactions with dynamin 2 and is therefore important for efficient endocytosis in neuronal cells. Furthermore, in COS-7 cells, fibroblast-like cells derived from monkey kidney tissue, plasma membrane targeting was shown to be dependent on the presence of Bin1 exon 6a while the CLAP domain was not required for Bin1 membrane localisation (Ramjaun et al., 1999). In both COS-7 cells and rat brain extracts, the presence of exon 6a also resulted in a greater degree of Bin1 dimerisation (Ramjaun et al., 1999). Taken together, these studies support a role for BIN1 exon 6a in dynamin interactions, membrane targeting and dimerisation during endocytosis. While the expression of isoforms containing exon 6a in the hCMEC/D3 cell line was not directly addressed, none of the exon combinations that were sequenced correspond to exon 6a-containing isoforms, suggesting they are not expressed in BMECs. In support of this, a recent study quantified *BIN1* transcript levels in human anterior cingulate brain tissue samples and showed that exon 6a-containing BIN1 transcript levels were positively associated with synaptophysin expression (a neuronal marker) but not with von Willebrand Factor (*VWF*) and CD31, markers of endothelial cells (De Rossi et al., 2016). Therefore,

the lack of isoforms expressing the CLAP domain or exon 6a supports our findings suggesting that BIN1 may not participate in CME in hCMEC/D3 cells.

This recent study by De Rossi et al. (2016) explored BIN1 expression and isoform diversity in the human brain, providing novel insights into a possible non-neuronal role for BIN1. They reported that, unlike AMPH1, the majority of BIN1 immunoreactivity is not associated with neurons in the human brain and that its isoform distribution greatly differs between white and grey matter. The majority of BIN1 isoforms expressed in the brain corresponded to ~65-75 kDa (De Rossi et al., 2016), the reported size of the ubiquitous BIN1 isoforms and of similar size to those shown in the present study in hCMEC/D3 cells. While De Rossi et al. (2016) reported these smaller isoforms were present in both the grey matter and white matter, the ~90 kDa isoform, containing the CLAP domain, was only expressed in grey matter at lower levels. This suggests that the expression of BIN1 isoforms in the brain is diverse and this may reflect diverse functions in different cell types. Furthermore, RT-PCR analysis of human brain samples showed the expression of 7 different BIN1 isoforms that lacked the full CLAP domain, of which, 6 did not contain exon 6a, further supporting the suggestion that a large proportion of BIN1 expressed in the brain may not participate in CME (De Rossi et al., 2016).

5.4.6 Conclusions

Collectively, the findings presented in this chapter suggest that BIN1 isoforms expressed in hCMEC/D3 cells do not function in CME and BIN1 is therefore not a requirement for this mechanism. This is consistent with the findings from Chapter 4, where no difference was observed in intracellular APP levels with BIN1 depletion, suggesting the increase in β-CTF is not attributed to an increase in total APP uptake. It is important to acknowledge that only one siRNA was used throughout this analysis and it would be beneficial to replicate the results using a different siRNA sequence to validate the findings. Furthermore, the hCMEC/D3 cells used in the present study were not cultured in such a way to represent the polarised nature of the brain endothelial cells *in vivo*. While the uptake and recycling studies can be considered an indicator of transport mechanisms at the BBB, it would be interesting to repeat these assays in a culture system that established apical and basolateral domains in the cells. This would also allow an assay of transcytosis mechanisms across the endothelial layer, should the cells be cultured on transwell filters rather than an

adherent monolayer on tissue culture vessels. Had time allowed, investigating AMPH1 expression with BIN1 depletion would have shed light on the possibility of a compensatory mechanism with BIN1 depletion, while optimisation of LRP1 antibodies may have permitted analyses of LRP1 expression.

While no change in the endocytic recycling of transferrin was observed, it is possible that β-CTF accumulation occurred with BIN1 depletion due to impaired trafficking to the lysosome. As transferrin is rapidly recycled back to the plasma membrane, this assay does not allow for an assessment of trafficking to the lysosome for degradation. However, Miyagawa et al. (2016) have shown impaired lysosomal trafficking of BACE1 in BIN1-depleted N2A cells whereby BACE1 protein levels were significantly reduced in late endosomes/lysosomes compared with the control cells. Therefore, it seems plausible that Bin1 may have a role in endocytic trafficking to the lysosome and this presents a further avenue for research. In addition, while clathrin-dependent mechanisms may not be affected, the dynamin-binding and membrane curvature function of ubiquitous BIN1 may be involved in clathrin-independent endocytic mechanisms and this is yet to be investigated.

Chapter 6

BIN1: Endocytic Function Beyond Clathrin-associated Mechanisms

6.1 Introduction

This chapter aims to further explore the mechanism by which BIN1 depletion increases intracellular β-CTF levels in hCMEC/D3 cells through exploring the role of BIN1 in a clathrin-independent context. Despite the absence of the CLAP domain in hCMEC/D3 BIN1 isoforms, the N-terminal BAR domain is still capable of inducing the curvature of membranes (Peter et al., 2004, Picas et al., 2014) while the C-terminal SH3 domain binds to dynamin (Picas et al., 2014), which is involved in other forms of endocytosis. Therefore, it was expected that these mechanisms would be important in terms of their contribution towards CME in hCMEC/D3 cells. With no evidence of this, the function of BIN1 in membrane curvature and dynamin recruitment may be more apparent in other clathrin-independent forms of endocytosis. The plasma membrane is involved in the lateral compartmentalisation of molecules destined for internalisation at the cell surface. Microdomains of the plasma membrane are enriched in cholesterol and sphingolipids that assist this compartmentalisation role. Endocytosis of ligands and receptors at these microdomains occurs via clathrin-independent lipid raft endocytosis. Caveolae are caveolin-1 (CAV1)-enriched smooth invaginations of the plasma membrane that form a subdomain of lipid rafts. Clathrin-independent methods of endocytosis are explored in the present chapter in addition to the trafficking of these lipid raft-mediated vesicles to the

lysosomal system. Hypothesising that the increase in β-CTF levels could be attributed to impaired lysosomal clearance with BIN1 depletion, indicators of lysosomal function are analysed within the chapter to further scrutinise the role of BIN1 at the BBB.

6.1.1 Clathrin-independent Endocytosis

There are many mechanisms of endocytosis at the BBB that take place independent of CME, including non-specific processes such as fluid-phase and adsorptive endocytosis, as previously described in Chapter 5. Clathrin, CAV1 and flotillin-1 define three separate types of region within the plasma membrane that can all undergo internalization (Glebov et al., 2006). Flotillin and caveolar endocytosis are both clathrin-independent and will be further described in Section 6.1.2.

6.1.2 Trafficking via Lipid Rafts

Whereas the plasma membrane is mostly composed of phospholipids, lipid rafts exist as distinct lipid-ordered regions with a high concentration of sphingolipids and cholesterol that can coalesce to serve as a signaling platform or function in membrane trafficking (Simons and Sampaio, 2011). These lipid microdomains were first described in epithelial cells in the early 1990s as membrane structures that are insoluble to detergents such as Triton X-100 and therefore float in low density fractions (Brown and Rose, 1992). While much is now known about the mechanistic details of CME and its structural component clathrin, far less is known about clathrin-independent endocytosis (CIE). While CME is dependent on dynamin for vesicle scission (Wigge et al., 1997b, Owen et al., 1998), CIE can be dynamin-dependent, such as caveolar endocytosis (Oh et al., 1998) while flotillin-dependent endocytosis may be dependent (Meister et al., 2014) or independent of dynamin (Glebov et al., 2006), depending on the cargo or cellular context.

6.1.2.1 Flotillin-mediated endocytosis

The flotillin proteins were first thought to associate with caveolae, flask shape invaginations at the membrane surface involved in caveolar endocytosis (Bickel et al., 1997). However, flotillin-1 has since been shown to reside in punctate plasma membrane structures and specific endocytic compartments distinct from CCPs and CAV1-positive

caveolae (Glebov et al., 2006). Although functionally distinct, flotillin-1 and flotillin-2 are both ubiquitously expressed and share 47% homology (Edgar and Polak, 2001). Functionally, flotillins have been implicated in signal transduction and cellular migration and adhesion in addition to membrane trafficking (Meister et al., 2014). The idea that flotillins establish an endocytic pathway independent of clathrin and caveolin was based on findings that flotillin-1 levels increased in early endocytic vesicles following fluid-phase uptake of magnetic nanoparticles but flotillin-1 did not colocalise with the CME marker Tf or with clathrin (Glebov et al., 2006). Furthermore, co-overexpression of flotillin-1 and 2 in HeLa cells was sufficient to generate flotillin-positive membrane invaginations that did not colocalise or disrupt CAV1 distribution (Frick et al., 2007). In this study, flotillin-1 and 2 were shown to coassemble into microdomains, distinct from CAV1-positive caveolae. This induced membrane curvature, the formation of invaginations morphologically similar to caveolae and resulted in the accumulation of intracellular vesicles (Frick et al., 2007).

Flotillin-mediated endocytosis has been implicated in APP trafficking and Aβ production. Flotillin-1 was identified to directly interact with the intracellular domain of APP, AICD, in a screen of human brain cDNA, suggesting flotillin-1 may be involved in the recruitment of APP to lipid rafts (Chen et al., 1999). Schneider et al. reported that flotillin-2 depletion impaired APP endocytosis in mouse N2a neuroblastoma cells and primary hippocampal neurons, resulting in reduced production of Aβ (Schneider et al., 2008). This was shown to be due to a significant reduction in APP clustering at the plasma membrane, suggesting that flotillin-2 promotes the clustering of APP which enhances its endocytosis rate via CME. While this effect was not found for flotillin-1 depletion (Schneider et al., 2008), Bitsikas et al. (2014) reported that MEFs from *Flotillin-1* knockout mice ectopically expressing human *APP* and *PSEN1* showed a small reduction in APP endocytosis. However, no difference in APP clustering was observed with *Flotillin-1* knockout in this study. Collectively, these studies suggest that flotillin-1 and -2 may be involved in the endocytic uptake of APP.

6.1.2.2 Caveolar endocytosis

One of the most researched methods of clathrin-independent endocytosis is that involving caveolae. Caveolae are a specific form of lipid raft defined by 50-100nm pits in the plasma membrane, rich in the transmembrane caveolin proteins and with a characteristic flask

shape. Caveolae form at lipid raft domains and are capable of mediating non-specific adsorptive-mediated endocytosis, the trafficking of some membrane receptors and are important in cell signalling (Razani and Lisanti, 2001).

Caveolins are cholesterol-binding membrane proteins that exist in three related forms: CAV1, -2, and -3. Whole mouse brain tissue analysis initially indicated a lack of caveolin proteins and corresponding mRNA in the brain, however it was later established that both CAV1 and -2 are expressed in the endothelium of the brain microvasculature (Schlachetzki and Pardridge, 2003). Within the brain, CAV1 and 2 are primarily expressed in endothelial cells whereas CAV3 is expressed in astrocytes (Ikezu et al., 1998b). While flotillins are the major markers of lipid rafts in neurons (Lang et al., 1998), expression of caveolin proteins has been identified in neurons (Galbiati et al., 1998). CAV1 is the main protein component of caveolae and its overexpression in caveolae-deficient cells induces the formation of plasma membrane invaginations indistinguishable from normal caveolae, suggesting that CAV1 is necessary for this process (Lipardi et al., 1998). CAV1 binds cholesterol and sphingolipids (Murata et al., 1995, Fra et al., 1995), the two primary components of lipid rafts, and its association with cholesterol is important for caveolae biogenesis (Rothberg et al., 1992). The ability of CAV1 to self-oligomerise into higher order complexes (Schlegel and Lisanti, 2000) allows a meshwork to form which is thought to act synergistically with cholesterol and distort the plasma membrane, driving the invagination of caveolae (Hoop et al., 2012).

Later, CAV2 was isolated through microsequencing of adipocyte-derived caveolin-enriched membranes and identified as a CAV1-related protein, sharing 38% sequence identity to CAV1 (Scherer et al., 1996). CAV2 was coexpressed with CAV1 in all analysed tissues, however, unlike CAV1, CAV2 was found to exist mainly as a monomer. CAV2 is not required for caveolae formation, with the caveolar membrane system remaining intact in cav2-deficient mice (Razani et al., 2002). However, CAV2 has been shown to undergo phosphorylation which allows it to positively regulate CAV1-dependent caveolae formation (Sowa et al., 2003). CAV3 is a muscle-specific protein, sharing 60% homology with CAV1, and is associated with T-tubules during development, which are thought to form by the repeated budding of caveolae (Parton et al., 1997). In addition to caveolins, scaffolding proteins such as cavins are found within caveolae and are thought to be the major structural component (Parton and Collins, 2016). Cavin was shown to colocalise with

CAV1 in lipid rafts and was important for maintaining the expression level of CAV1 in adipocytes (Liu and Pilch, 2008).

Although diverse functions have been identified for caveolae, their physiological role in different cell types and tissues is not fully understood. CAV1 is expressed in many different cell types but shows particularly high expression in peripheral endothelial cells (Lisanti et al., 1994), which indeed contain a large number of caveolae (Sowa, 2011). The transcytosis of macromolecules was the first proposed function for caveolae (Palade and Bruns, 1968) and the caveolae-mediated intracellular and transcellular transport of insulin and albumin has since been demonstrated in cultured lung and aortic endothelial cells (Schnitzer et al., 1994). SV40 and cholera toxin subunit B (ctxB) have been extensively studied as potential caveolar cargoes as both ligands bind the ganglioside GM1, which is found in caveolae (Neu et al., 2008). However, internalization of ctxB has also been demonstrated to also take place via both clathrin-dependent and clathrin-independent mechanisms with caveolae contributing to ctxB uptake (Torgersen et al., 2001). Initially caveolar endocytosis was thought to mirror CME with the caveolae pinching off into a caveosome. The caveosome was described as an immobile intermediate compartment, rich in CAV1 and distinct from normal endosomes, involved in the trafficking from caveolae to the ER and was not labelled by fluid-phase markers or ligands of CME (Pelkmans et al., 2001). The neutral pH and lack of LysoTracker accumulation in the caveosome made it distinct from existing endocytic compartments and it was thought to be a means of cell entry for some viruses/toxins to avoid the lysosomal pathway (Pelkmans et al., 2001). However, more recently this has been questioned and it is now thought that caveolae internalise and fuse with the early endosome as endogenous CAV1 has been observed in early endosomes but not late endosomes and lysosomes (Hayer et al., 2010). Under normal conditions, endogenous CAV1 is found in early endosomes but when highly overexpressed, CAV1 accumulated in late endocytic compartments positive for Rab7 and Lamp1, markers of late endosomes and lysosomes respectively which were not tested in the original study. The neutral pH of CAV1-containing organelles recorded in the original study has since been revised by the authors as it was determined using SV40 as a probe at a time point when the virus may have reached the neutral environment of the ER (Hayer et al., 2010).

With regards to caveolar endocytosis at the BBB, an unusually low rate of transcytosis has been identified as one of the unique properties of BMECs, relative to peripheral

endothelial cells. Recently, a mechanism has been described through which the unique lipid composition of BMECs is maintained in order to specifically inhibit caveolae-mediated transcytosis and maintain BBB integrity (Andreone et al., 2017). Lipidomic analysis showed that the lipid signature of mouse BMECs differs from that of lung endothelial cells, which do not possess the restrictive barrier properties of BMECs, by a significant enrichment in lipids containing the omega-3 fatty acid docosahexaenoic acid (DHA) (Andreone et al., 2017). DHA is a highly unsaturated fatty acid that disrupts liquid-ordered caveolae domains. This suggests that the lipid composition and corresponding suppression of caveolae-mediated transcytosis in BMECs may be crucial to maintain the relative impermeability of the BBB. Furthermore, changes in caveolar-endocytic mechanisms are therefore likely to impact on the barrier properties of BMECs.

6.1.3 Lipids Rafts and the Amyloidogenic Processing of APP

In addition to the aforementioned interaction between flotillin and APP in Section 6.1.2.1, there is strong evidence implicating lipid rafts in the processing of APP but the precise mechanism is still to be elucidated and there are contradictions in the literature. Numerous studies have suggested that the amyloidogenic processing of APP occurs at lipid rafts as APP, BACE1 and γ-secretase have been found to localise in these regions (Wahrle et al., 2002, Ehehalt et al., 2003). Lipid rafts have also demonstrated critical involvement in regulating Aβ generation through the association of BACE1 and APP with detergent-resistant membranes in a cholesterol-dependent manner (Simons et al., 1998, Riddell et al., 2001). Cholesterol plays a crucial role in maintaining lipid rafts in a functional state and the demonstration that cholesterol ablation disrupts lipid rafts, resulting in inhibition of Aβ production without affecting sAPPα levels in hippocampal neurons, implicates lipid rafts in the amyloidogenic processing of APP (Simons et al., 1998). Furthermore, BACE1 has been found within a unique raft population distinct from caveolae and this association was perturbed with cholesterol depletion, suggesting that the partitioning of BACE1 into lipid rafts may underlie the cholesterol sensitivity of Aβ production (Riddell et al., 2001). Indeed, the majority of β-CTF in CHO cells cofractionated with BACE1 in lipid raft fractions (Riddell et al., 2001).

The cytoplasmic domain of APP has been shown to physically associate with CAV1, the depletion of which prevented α-secretase processing of APP suggesting that caveolae play a

pivotal role in the α-cleavage of APP (Ikezu et al., 1998a). However, this colocalisation is not sufficient to prove true caveolar compartmentalization as in CHO cells, BACE1, APP and Psen1 did not show colocalisation with Cav1 (Riddell et al., 2001). Nevertheless, while only a minor proportion of APP was shown to cofractionate with BACE1 in lipid rafts (Riddell et al., 2001), it is only a small percentage of total cell APP that is processed via the β-secretase cleavage pathway under normal physiological conditions (Selkoe, 1994). Cordy *et al.* showed that relatively little BACE1 is found in lipid rafts of the SH-SY5Y neuroblastoma cell line but when BACE1 was targeted exclusively to lipid raft domains by a glycosylphosphatidylinositol anchor, secretion of sAPPβ and Aβ was significantly increased (Cordy et al., 2003). This effect was reversed when lipid rafts were disrupted by depleting cholesterol, suggesting that the amyloidogenic processing of APP occurs predominantly in lipid rafts and BACE1 is the rate-limiting enzyme.

Inflated levels of cholesterol have been linked to increased levels of βCTFs and amyloid load in the CNS (Refolo et al., 2000), suggesting APP is more readily processed by β-secretase under these conditions. Altered cholesterol levels may therefore alter the distribution of APP and BACE1 in lipid rafts or affect enzymatic activity. Cholesterol accumulation is a key hallmark of Niemann-Pick type C (NPC) disease and much research in this field has provided information regarding the relationship between cholesterol and Aβ. NPC is a lysosomal storage disease caused by mutations in the *NPC1* or *NPC2* genes resulting in impaired trafficking and accumulation of free cholesterol in the late endosomal/lysosomal compartments leading to increased β-CTF and Aβ formation (Yamazaki et al., 2001). Using an NPC *in vitro* model (CHO $NPC1^{-/-}$ cells), which shows accumulation of free cholesterol, Kosicek et al. (2010) showed that APP and CTFs redistributed to lipid raft fractions compared to wild-type cells. Furthermore, increased distribution of APP and CTFs were found in lipid raft fractions upon γ-secretase inhibition in NPC cells compared to wild-type, suggesting that lipid rafts are the likely site of APP amyloidogenic processing upon NPC1 dysfunction.

6.1.4 Lysosomal Dysfunction and β-CTF Accumulation

Increasing evidence suggests that NPC and AD are likely to share a common underlying feature; dysfunctional clearance of cargo via the secretory-endocytic-autophagic-lysosomal-exocytic network (Boland and Platt, 2015). Figure 6.1 shows a schematic of the endo-

lysosomal portion of this network and in particular, illustrates the trafficking of APP and the products of its amyloidogenic proteolysis. APP is endocytosed from the plasma membrane into endocytic vesicles which fuse with early endosomes. Here, β-cleavage of APP releases sAPPβ and β-CTF, which remains membrane-bound. Aβ is then released by γ-cleavage and the components are either trafficked to the lysosome via the late endosome for degradation or exocytosed at the plasma membrane.

In addition to enlarged rab5-positive early endosomes, upregulation of lysosomal processes and accumulation of lysosomes has been reported as an early feature of AD and implicates the lysosomal system in Aβ pathology (Cataldo et al., 1994). The increase in β-CTF levels with BIN1 depletion in the present study may be indicative of β-CTF accumulation due to impaired lysosomal degradation. Indeed, in the brains of NPC mouse models, cholesterol accumulation has been associated with a large accumulation of β-CTF (Burns et al., 2003). The levels and activity of β -secretase and α-secretase remained unaffected but the activity of γ-secretase was increased by over 50% in NPC mice compared with wild type littermate controls. The accumulation of β-CTF in NPC mice compared to controls suggests that the increase in γ-secretase activity was not sufficient to clear all of the β-CTF and that β-CTF clearance mechanisms may be defective in NPC mice (Burns et al., 2003). Boland et al. (2010) also reported the accumulation of β-CTFs in three mouse models of lysosomal storage diseases, suggesting that defective lysosomal flux causes impaired lysosomal proteolysis of β-CTFs. Furthermore, Rab proteins are involved in the regulation of compartmentalised membrane trafficking and can be perturbed in lysosomal storage diseases (Choudhury et al., 2004). This is of particular interest to the present study as recently, Rab8 was shown to form a complex involving Bin1 that regulates transport of apical-directed proteins from the endocytic recycling complex in polarised intestinal epithelial cells (Nakajo et al., 2016). The authors further showed enlargement of lysosomes after Bin1 depletion in mouse intestinal organoids, suggestive of defective lysosomal degradation. Therefore, it seems plausible that BIN1 may have a role in normal functioning of the lysosome.

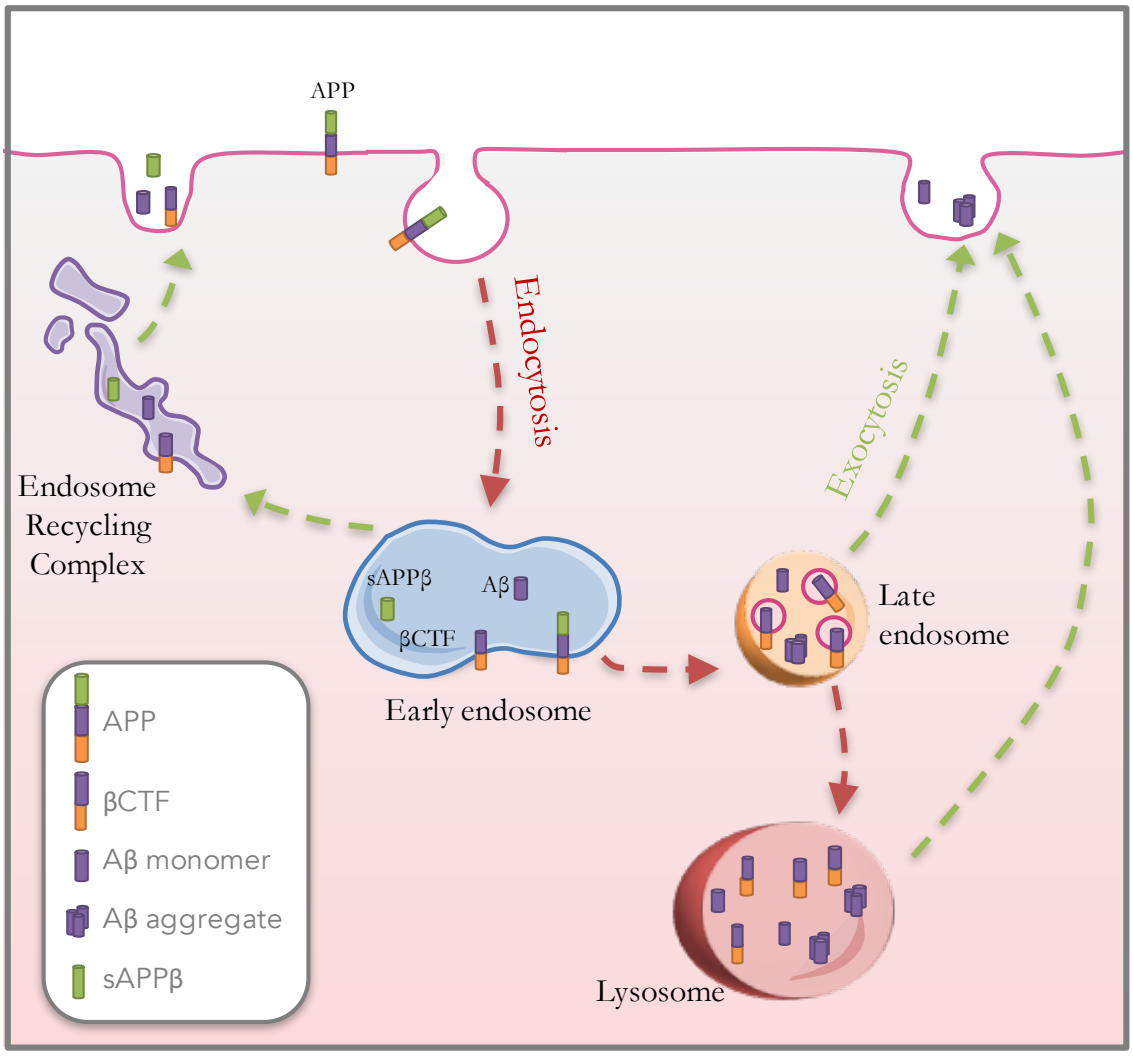

Figure 6.1: The Endo-Lysosomal trafficking of APP and Products of its Amyloidogenic Processing

A schematic depicting the endo-lysosomal trafficking of APP, Aβ, β-CTF and sAPPβ. Newly synthesised APP is transported from the Golgi to the plasma membrane where it is rapidly endocytosed into endocytic vesicles which fuse with early endosomes. Here, β-cleavage of APP releases sAPPβ and β-CTF which remains membrane-bound. Aβ is then released by γ-cleavage and the components are either trafficked to the lysosome via the late endosome for degradation or exocytosed at the plasma membrane. Adapted from Boland and Platt (2015)

6.1.5 Aims of this Chapter

This chapter aims to investigate whether BIN1 is involved in endo-lysosomal trafficking, hypothesising that depletion of BIN1 expression in human brain endothelial cells impairs lysosome function and alters the amyloidogenic pathway. Furthermore, while BIN1 does not appear to have a crucial role in CME in the hCMEC/D3 cell line, CIE can also be dynamin-dependent and involves curvature of the plasma membrane. Therefore, the dynamin-recruiting and membrane-bending properties of BIN1 may have a role in CIE. This hypothesis will be analysed through protein expression of key CIE-related proteins in addition to trafficking of lipid raft markers.

6.2 Experimental Design

6.2.1 BIN1 Depletion in hCMEC/D3 cells

Cell culture and depletion of BIN1 protein was performed as previously described in Chapter 4, Section 4.2.1 and confirmed by Western blotting as described in Chapter 2, Section 2.3.

6.2.2 Immunofluorescent Staining

Immunocytochemistry was used to observe lysosome morphology using lysosomal associated membrane protein-2 (LAMP2) (mouse monoclonal antibody, 0.32 μg/ml, Developmental Studies Hybridoma Bank, Iowa, US) and CAV2 expression (0.25 μg/ml, BD Biosciences) and was carried out as described in Chapter 2, Section 2.4 with three replicates per experiment and representative images shown. Cells were fixed in 100% methanol as described in Chapter 2, Section 2.4.2.

6.2.3 LysoTracker Staining

In order to label acidic organelles within cells, a live cell stain using LysoTracker was performed. Cells were plated and transfected as previously described in Chapter 2, Section 2.2 in 8-well glass bottom chamber slides (Ibidi, Martinsried, Germany). Forty-eight hours post-transfection, cells were washed 3x in RT PBS before adding 200 μl/well of 200 nM LysoTracker Green (ThermoFisher Scientific) in PBS and incubating at 37°C for 5 min, protected from light. Cells were washed 3x in RT PBS before incubating with 4 μg/ml Hoechst® dye (Sigma) in PBS for 10 min at RT, protected from light, to stain the nuclei. Cells were immediately live imaged on the Axio Observer A1 microscope with three replicates per experiment and representative images shown.

6.2.4 Western Blotting

Western blotting was performed as described in Chapter 2, Section 2.3 using the primary antibodies detailed in Table 6.1, 10-20 μg protein was used per well and run on a 10%

acrylamide gel. Some of the blots investigating CAV1, Caveolin-2, flotillin-1 and flotillin-2 with BIN1 depletion were carried out by Catherine Matheson and Robert Greening as part of their final year undergraduate (BSc Pharmacy) projects, co-supervised by myself. All densitometry analysis was independently analysed by the students and myself. Quantification of protein was calculated by densitometry analysis normalising to GAPDH expression, previously described in Chapter 2, Section 2.3.6.

Table 6.1: Primary antibodies used for Western blotting in Chapter 6

Protein	**Host Species**	**Supplier**	**Working concentration**
CAV1	Rabbit	Cell Signalling	0.08 µ/ml
CAV2	Mouse	BD Biosciences	0.5 µg/ml
Flotillin-1	Mouse	BD Biosciences	0.5 µg/ml
Flotillin-2	Rabbit	Novus	0.98 µg/ml
GAPDH	Mouse	Abcam	0.13 µg/ml

6.2.5 Fluorescence Staining of Free Cholesterol

Filipin can bind to complexes of cholesterol and other lipids (Arthur et al., 2011) and was therefore used to observe cholesterol localisation in cells. Cells were fixed in 4% PFA on pre-sterilised coverslips, as previously described in Chapter 2, Section 2.4.1, washed three times with PBS and incubated with 150 µg/ml filipin complex (Sigma) in EGM-2 medium for 30 min at room temperature, protected from light. Cells were washed once with EGM-2 and twice with PBS and mounted on glass slides with SlowFade Gold antifade mountant. Cells were imaged on the Axio Observer A1 microscope with three replicates per experiment and representative images shown.

6.2.6 Cholera Toxin Subunit B Trafficking

CtxB binds ganglioside GM1 in the plasma membrane and has previously been used as a marker for lipid raft transport (Nichols et al., 2001). In order to optimise the analysis of CtxB trafficking, different chase times and CtxB concentrations were tested. Cells were seeded on pre-sterilised fibronectin-coated glass coverslips at a density of 84,000 cells per cm^2, as previously described in Chapter 2, Section 2.1.2 and allowed to adhere overnight. Medium was removed and cells pulsed with 2 μg/ml ffluorescein isothiocyanate-conjugated CtxB (FITC-CtxB) in chilled EGM-2 media for 30 min in a cool box to allow binding to plasma membrane GM1 without endocytosis proceeding. Cells were washed once with EGM-2 media at 37°C before chasing with EGM-2 media at 37°C for 45, 60, 75 or 90 min. This experiment was repeated, incorporating a 0 min chase control and increasing concentrations of CtxB (2, 5, 10 and 20μg/ml) over a time course of 0, 1, 2 or 3 hours. Following the chase, cells were backwashed three times for 10 min with 1% BSA and 0.1% heparin in chilled EGM2 medium to remove surface labelling, followed by two washes with RT PBS and fixed in 4% PFA at RT for 10 min, as described in Chapter 2, Section 2.4.1. Coverslips were mounted onto glass slides using SlowFade Gold Antifade Mountant (ThermoFisher). Slides were imaged on the Axio Observer A1 microscope.

6.2.7 CAV1 Depletion

Depletion of CAV1 was performed as described for BIN1 depletion in Chapter 2, section 2.2 using the siRNA sequence 5'-AGACGAGCUGAGCGAGAAG-3' (Eurofins). This siRNA was used at a final concentration of 50 nM, which has previously been used to demonstrate successful knockdown (Al Soraj et al., 2012). CAV1 depletion was confirmed by Western blotting, as described in Section 6.2.4.

6.2.8 Genistein Inhibitor Treatment

To selectively inhibit caveolar endocytosis, cells were pre-incubated for 30 min with 200 μM genistein in phenol red-free OptiMEM medium (ThermoFisher Scientific) before BODIPY- LacCer addition, as described in Section 6.2.9.

6.2.9 BODIPY-Lactosylceramide Trafficking

Fluorescent boron-dipyrromethene (BODIPY)-labelled lactosylceramide (LacCer, ThermoFisher Scientific) was used as a marker for caveolar endocytosis. Cells were washed twice with RT PBS before pulse labelling with 1 μM BODIPY-LacCer in HEPES/HBSS solution (10 μM HEPES in Hanks Buffered Salt Solution, both ThermoFisher Scientific) for 30 min at 10 °C to load the plasma membrane. For each condition, a sample without the addition of BODIPY-LacCer was included to measure background fluorescence levels. Cells were washed 3x with ice-cold phenol red-free OptiMEM medium (ThermoFisher Scientific) followed by chasing for 15 min at 4°C or 37°C in phenol red-free OptiMEM. Cells were then back exchanged to remove surface labelling by washing with 5% BSA in PBS 6 x 10 min on ice with gentle agitation. Cells were kept on ice, washed twice with ice-cold PBS and ice-cold trypsin (0.05%, ThermoFisher Scientific) was added to cells and the plate incubated on ice until the cells were in suspension. An equal volume of ice-cold trypsin inhibitor solution (500μg/ml trypsin inhibitor, 75μg/ml DNase, 1% BSA in PBS) was added to cells and the cell suspension centrifuged at 325 x g at 4°C for 3 min. The pellet was resuspended in 0.33 mM Trypan Blue (Sigma) in PBS and incubated at 4°C for 30 min. Cells were washed three times with ice-cold PBS by centrifugation as previously described, resuspended in 500μl ice-cold PBS and transferred to FACs tubes via 30μm filters. The geometric mean of fluorescent intensity for at least 10,000 events was measured by flow cytometry using the BD FACSverse with debris and doublets gated out.

6.3 Results

6.3.1 Assessing Lysosome Function with BIN1 depletion

6.3.1.1 Lysosomal morphology

In order to explore whether increased β-CTF with BIN1 depletion was a result of impaired lysosomal clearance, the morphology of lysosomes was examined by fluorescent microscopy. Expansion of the late endosome and lysosome compartments can be indicative of lysosomal dysfunction (Platt et al., 2012). LysoTracker is a fluorescent, cell permeable probe that selectively accumulates in acidic organelles and provides a means by which the morphology and relative fluorescence of the late endosome/lysosome compartments can be observed in live cells with BIN1 depletion. Fluorescently-labelled LysoTracker was observed in all hCMEC/D3 cells, showing strong punctate staining which was particularly prominent in the perinuclear region, as identified by its location relative to DAPI-stained nuclei (Figure 6.2). There was no observable difference in the strength of fluorescence or localisation of staining with BIN1 depletion compared to GFP siRNA-treated cells. As LysoTracker can label other acidic compartments and is therefore not limited to lysosomes, antibodies against lysosome-associated membrane proteins (LAMPs) present a more specific approach. LAMP2B has previously been used to demonstrate aberrant lysosome morphology in Bin1-depleted mouse intestinal organoids (Nakajo et al., 2016) and was therefore used to specifically label lysosomes in hCMEC/D3 cells. LAMP2B showed more diffuse punctate staining than LysoTracker, consistent with its more specific labelling pattern (Figure 6.3). All cells showed positive staining for LAMP2B and the puncta showed accumulation at the perinuclear region in the majority of cells, however distribution throughout the cytoplasm was also observed. The localisation and strength of fluorescence was not affected by GFP siRNA treatment compared to non-transfected cells and also remained consistent with BIN1 depletion compared to GFP siRNA treatment, suggesting that reduced levels of BIN1 do not cause gross morphological changes in lysosomes.

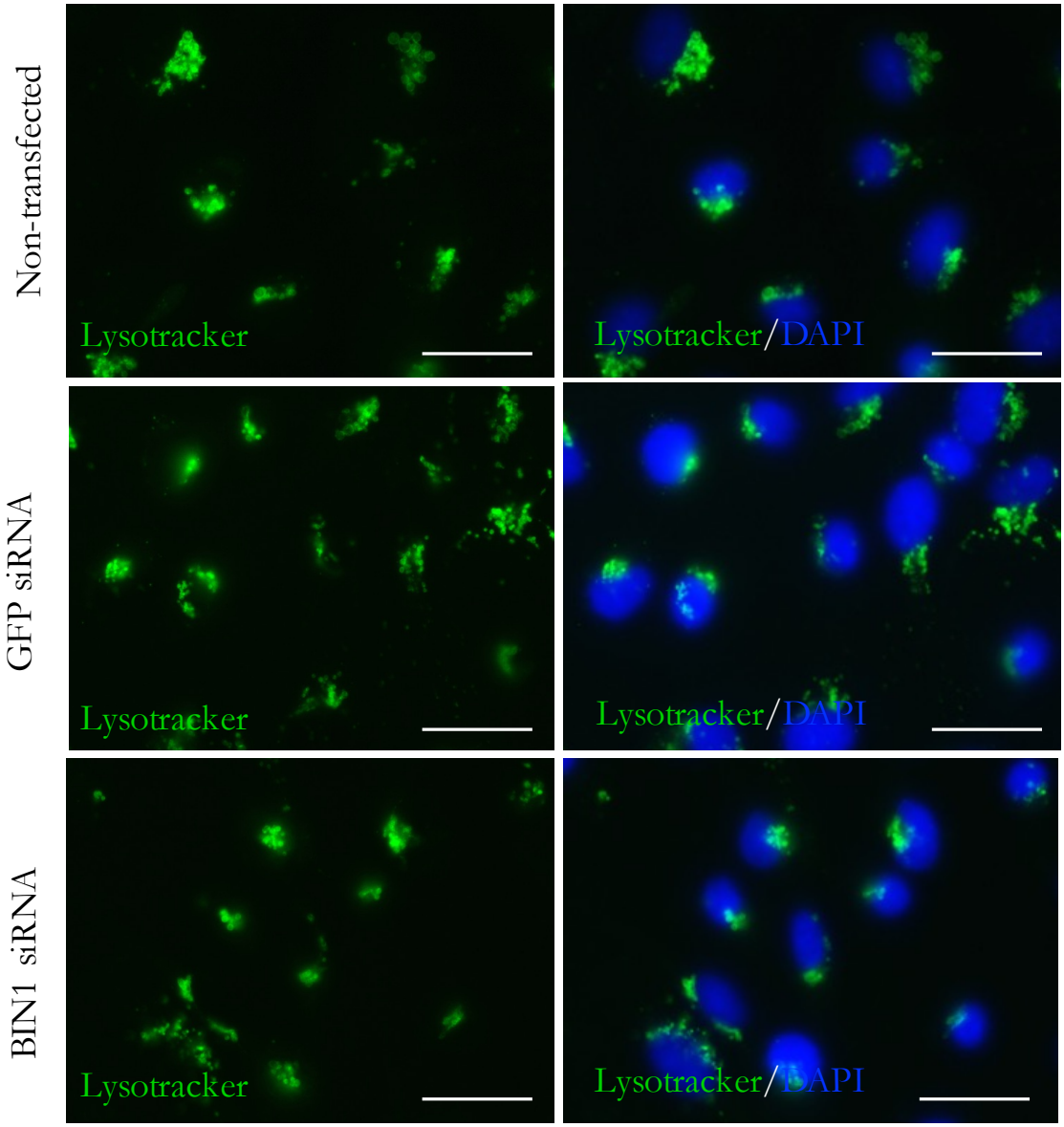

Figure 6.2: Live cell images of LysoTracker-stained acidic organelles

Representative images taken of live cells stained with LysoTracker Green which marks acidic organelles, such as lysosomes, in non-transfected, GFP siRNA-treated and BIN1-depleted hCMEC/D3 cells. Images taken at x40 magnification, scale bar = 25 μm.

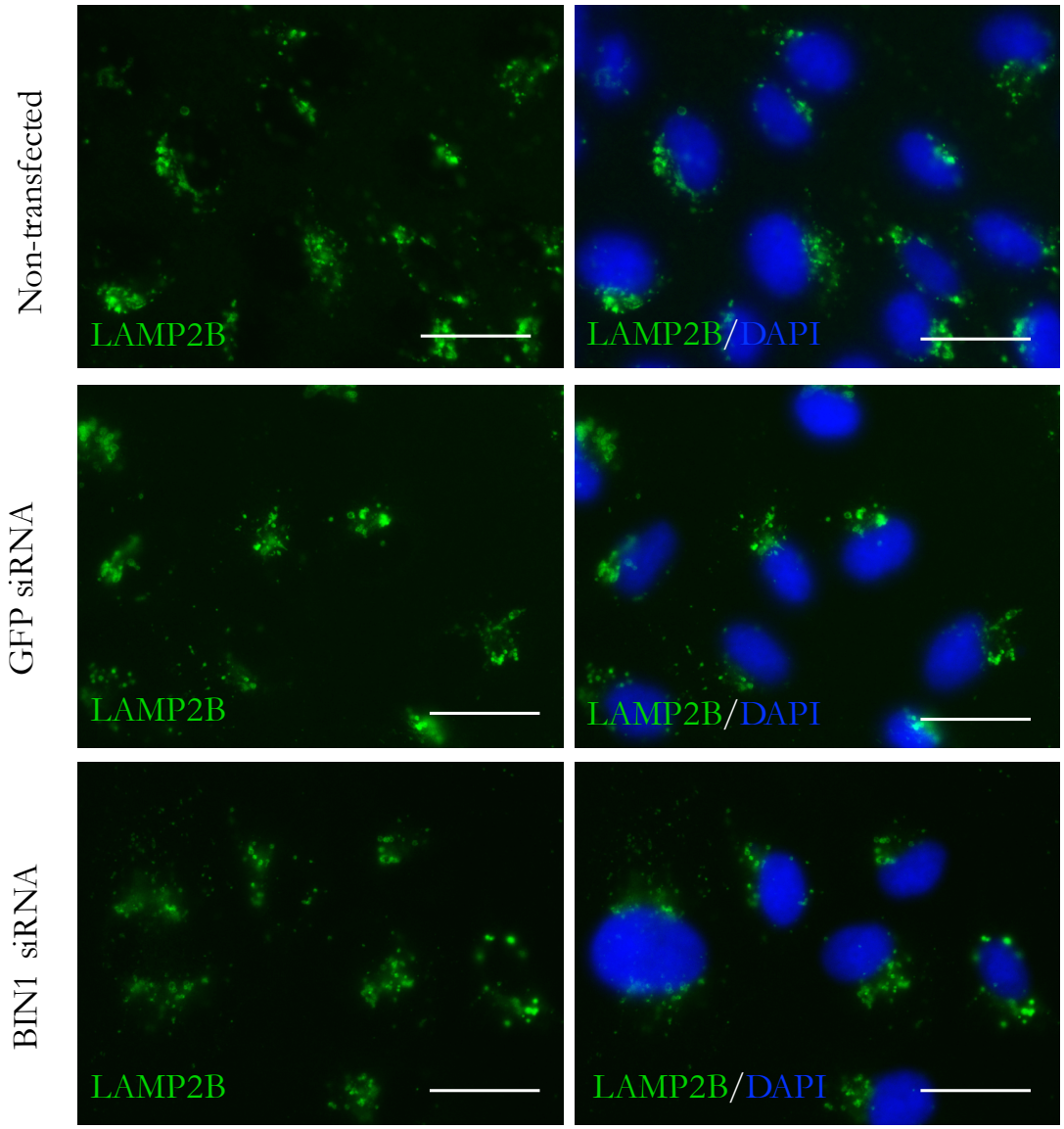

Figure 6.3: Fluorescent images of LAMP2B expression with BIN1 depletion

Representative images of lysosomal marker, LAMP2B, expression in non-transfected, GFP siRNA-treated and BIN1-depleted hCMEC/D3 cells. Images taken at x40 magnification, scale bar = 25 μm.

6.3.1.2 Cholesterol transport

While the gross morphology of lysosomes appeared unaffected by BIN1 depletion, impaired lysosome function may occur in the absence of morphological changes. Lysosome dysfunction often causes accumulation of cholesterol and glycosphingolipids (GSLs) in the lysosomes. This is a result of reduced breakdown, as cholesterol and GSLs should normally be found in the perinuclear ERC following internalisation in lipid rafts (te Vruchte et al., 2004). To analyse cholesterol localisation with BIN1 depletion, fixed cells were stained with filipin, a cytochemical probe specific for cholesterol. Cholesterol was found in small puncta, predominantly localised to the perinuclear region and there was significant plasma membrane staining with evidence of diffuse staining throughout the cytoplasm or underlying membrane (Figure 6.4). Crucially, no observable difference in cholesterol localisation or staining intensity was shown between non-transfected, GFP siRNA-treated and BIN1-depleted cells, suggesting a reduction in BIN1 does not impact on lysosome function.

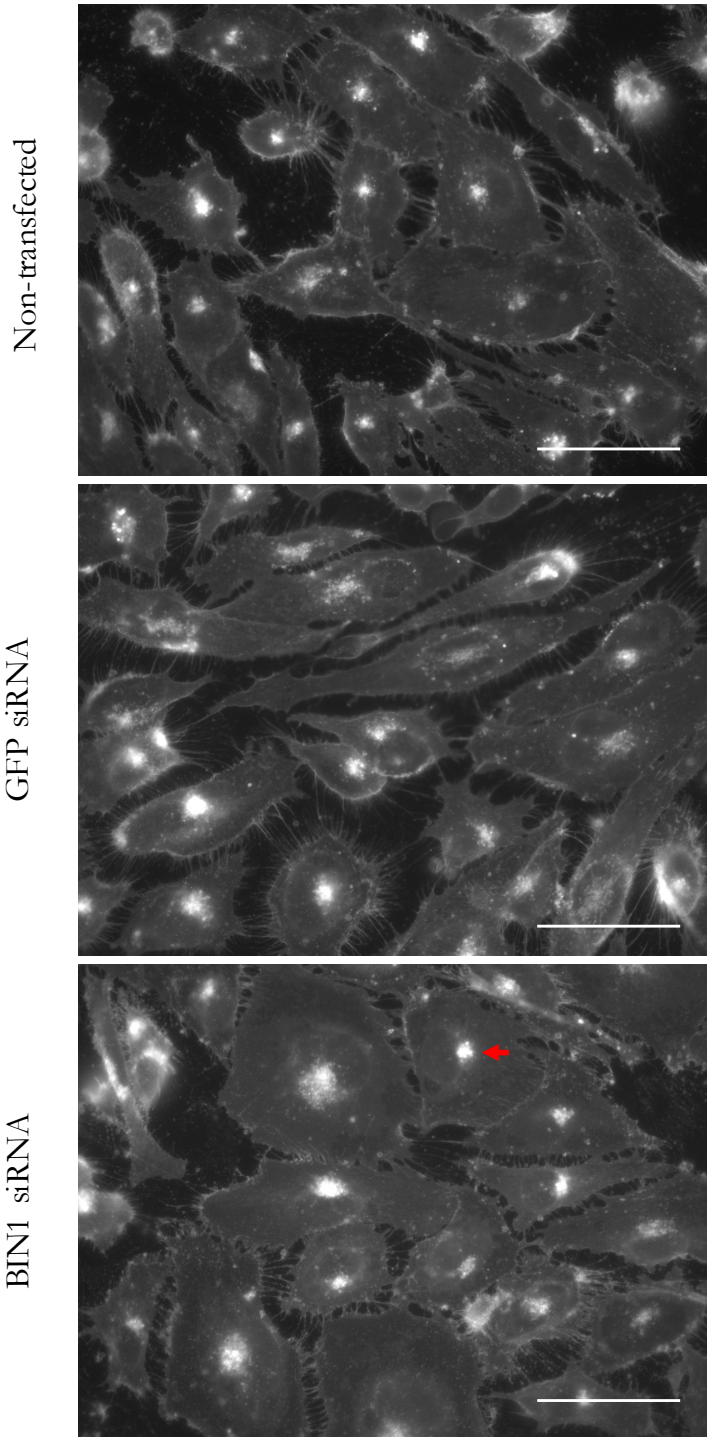

Figure 6.4: Cholesterol localisation in hCMEC/D3 cells with BIN1 depletion

Representative fluorescent images showing specific staining of free cholesterol with filipin in non-transfected, GFP siRNA treated and BIN1 depleted hCMEC/D3 cells. Cholesterol staining is present throughout the plasma membrane and shows particularly intense staining in the perinuclear region (example indicated by red arrow). Images were taken at x40 magnification, scale bar = 25 μm.

6.3.2 Clathrin-independent Endocytosis

While no clear indicators of lysosome function were observed, the secondary objective of this study was to investigate whether BIN1 has a role in clathrin-independent mechanisms of endocytosis in the hCMEC/D3 cell line. Indeed, several aforementioned lines of evidence have suggested that amyloidogenic processing of APP occurs in lipid raft fractions. The expression levels of key CIE proteins, flotillin-1, CAV1 and CAV2 were investigated with BIN1 depletion by Western blotting.

6.3.2.1 Flotillin-1 and 2 expression

Flotillin-1 and 2 associate with cholesterol-enriched lipid non-caveolar microdomains and are important for clathrin-independent endocytosis (Glebov et al., 2006) and APP processing (Schneider et al., 2008). Flotillin-1 and 2 expression was detected in hCMEC/D3 cells with a single band at approximately 45 kDa and 48 kDa, respectively (Figure 6.5). The level of expression of flotillin-1 was not affected by BIN1 depletion (Figure 6.6). Due to time constraints, only two replicates of flotillin-2 expression were possible with one suggesting a small increase in expression compared to GFP siRNA-treated cells and the other a small decrease. Overall, no significant change in level of flotillin-2 was observed with BIN1 depletion compared to GFP siRNA-treated cells (Figures 6.5 and 6.7), suggesting that the expression of flotillins was not affected by a reduction in BIN1 expression.

6.3.2.2 Expression of the caveolins

The caveolins are the major protein components of cholesterol- and GSL-rich flask-shaped invaginations of plasma membrane caveolae. Both CAV1 and CAV2 showed strong expression in hCMEC/D3 cells with single bands at approximately 21 kDa and 22 kDa respectively (Figure 6.5). CAV1 showed consistent expression which did not alter with BIN1 depletion in comparison to GFP siRNA-treated cells (Figure 6.8), however there was evidence of an 86% increase in CAV2 expression, compared to GFP siRNA-treated cells which was statistically significant upon densitometry analysis (Figure 6.9, $p = 0.03$ using a two-tailed unpaired Student's *t* test). The increase in CAV2 expression was further demonstrated by immunocytochemistry (Figure 6.10) which showed enhanced intensity of

fluorescence in BIN1-depleted cells compared to non-transfected and GFP siRNA-treated. In all conditions, CAV2 showed faint punctate expression throughout the cells with particularly enhanced expression in the perinuclear region in the majority of cells and at the lateral edges of some cells. Although not compared to other markers or CAV1 expression, the pattern of CAV2 expression did not observably differ with BIN1 depletion compared to GFP siRNA and non-transfected cells. Collectively, this data suggests that BIN1 depletion results in an increase in CAV2 expression but does not affect its localisation.

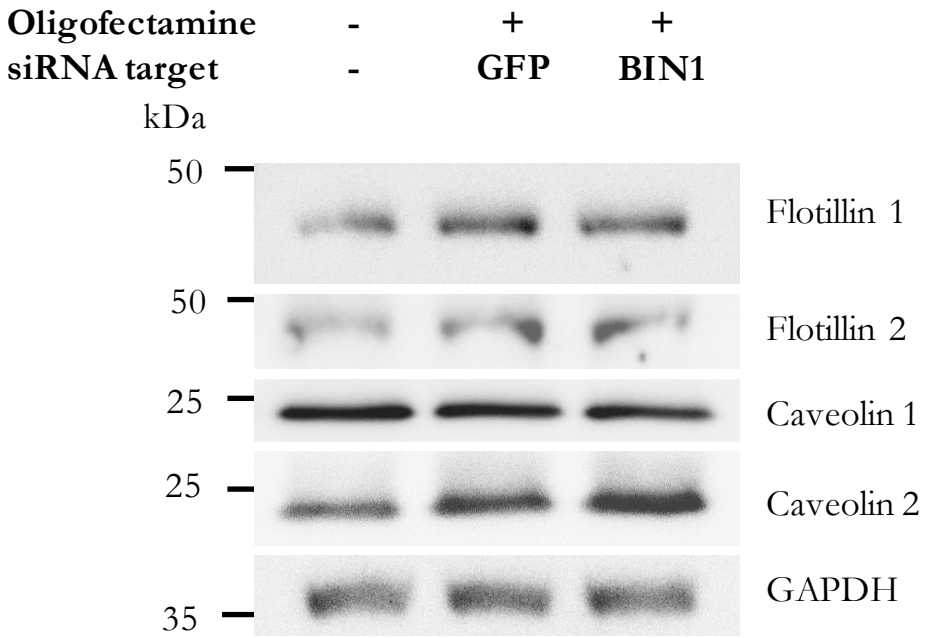

Figure 6.5: Expression of key clathrin-independent endocytic proteins with BIN1 depletion

Representative Western blots of Flotillin-1, Flotillin-2, CAV1 and Caveolin-2 expression in non-transfected, GFP siRNA treated and BIN1 depleted hCMEC/D3 cells. GAPDH was used as a housekeeping protein.

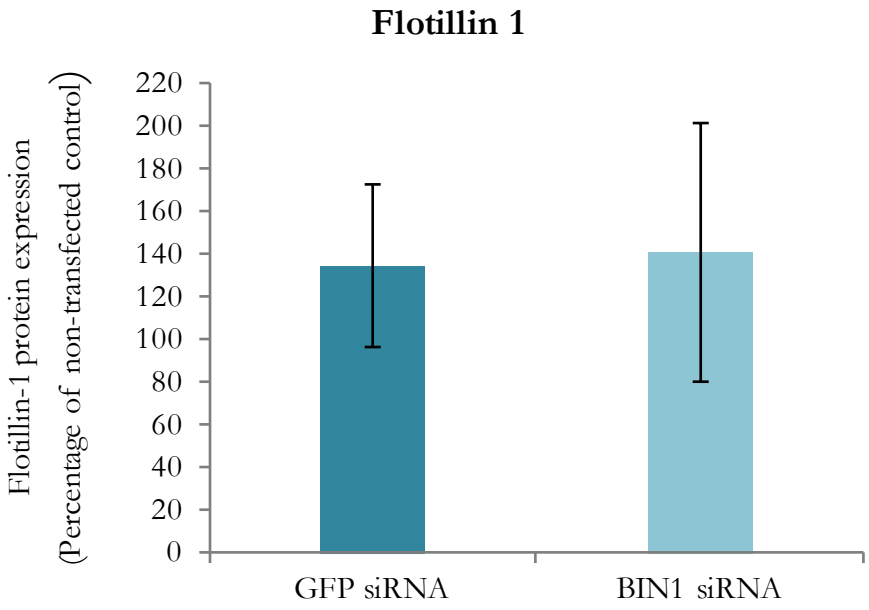

Figure 6.6: Quantification of Flotillin-1 expression with BIN1 depletion

Quantification of flotillin-1 expression based on densitometry analysis, expressed as mean percentage expression of non-transfected cells after normalisation to GAPDH, error bars = SEM, n = 4, $p > 0.05$ using a two-tailed unpaired Student's *t* test.

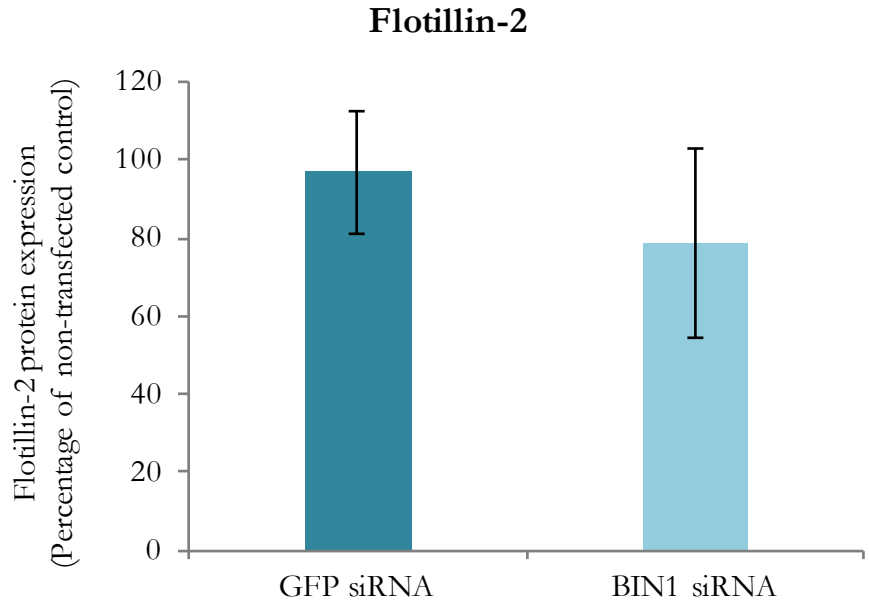

Figure 6.7: Quantification of Flotillin-2 expression with BIN1 depletion

Quantification of flotillin-2 expression based on densitometry analysis, expressed as mean percentage expression of non-transfected cells after normalisation to GAPDH, n = 2, $p > 0.05$ using a two-tailed unpaired Student's *t* test.

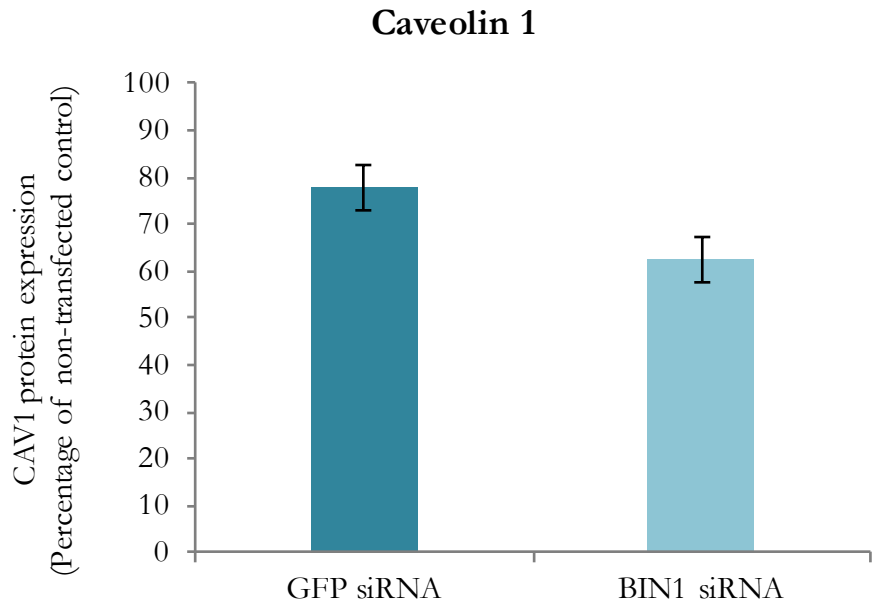

Figure 6.8: Quantification of CAV1 expression with BIN1 depletion

Quantification of CAV1 expression based on densitometry analysis, expressed as mean percentage expression of non-transfected cells after normalisation to GAPDH, error bars = SEM, n = 4, $p > 0.05$ using a two-tailed unpaired Student's *t* test.

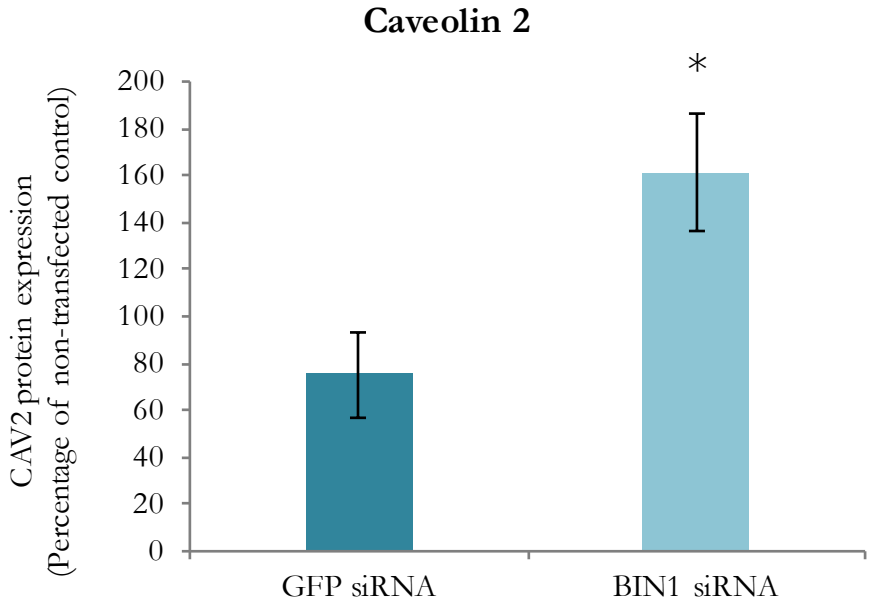

Figure 6.9: Quantification of CAV2 expression with BIN1 depletion

Quantification of CAV2 expression based on densitometry analysis, expressed as mean percentage expression of non-transfected cells after normalisation to GAPDH, error bars = SEM, n = 4, * = $p < 0.05$ using a two-tailed unpaired Student's *t* test.

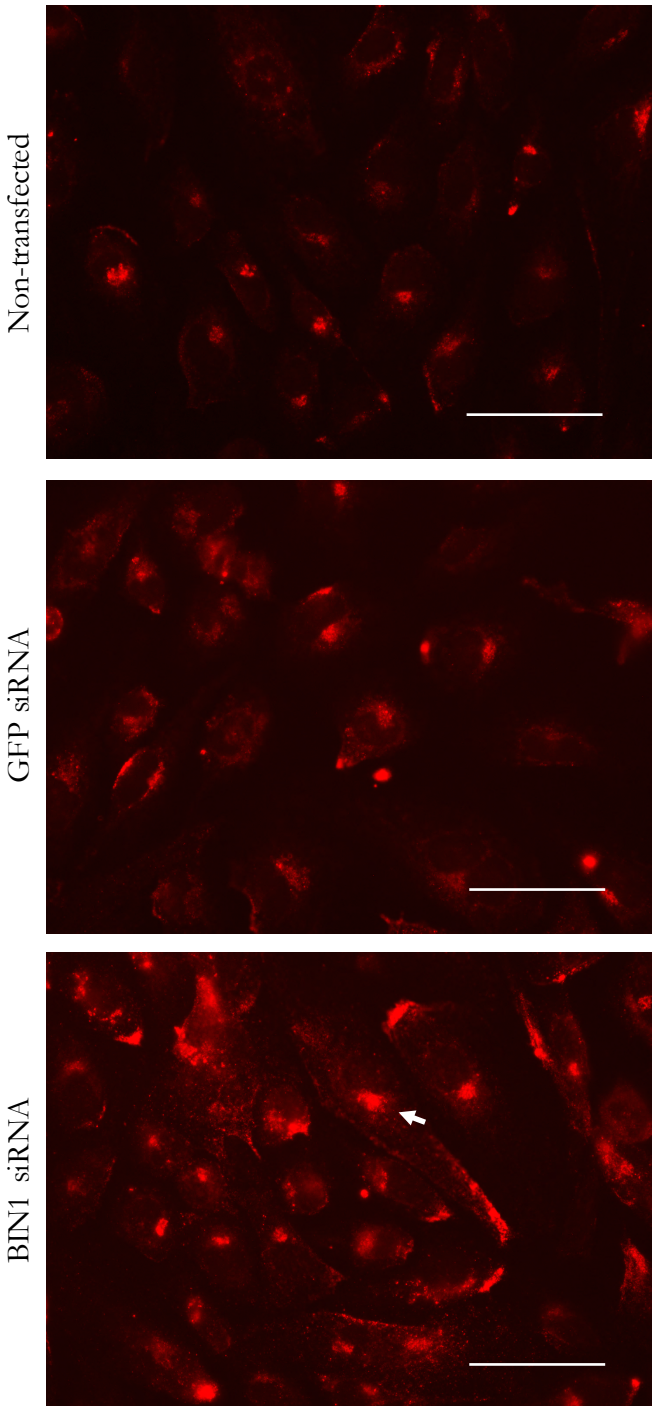

Figure 6.10: Caveolin-2 expression in hCMEC/D3 cells with BIN1 depletion

Representative fluorescent images showing CAV2 expression in non-transfected, GFP siRNA treated and BIN1-depleted hCMEC/D3 cells. CAV2 is expressed predominantly in the perinuclear region (example indicated with white arrow) and the intensity of staining is more pronounced in BIN1-depleted cells, suggesting increased expression. Images were taken at x40 magnification, scale bar = 25 μm.

6.3.3 Lipid Raft/Caveolar Endocytosis and Trafficking

CAV2 has previously been implicated in the regulation of caveolae (Sowa et al., 2003), therefore, the increase in CAV2 expression with BIN1 depletion provides rationale for investigating the function of caveolar endocytosis. Furthermore, impaired fusion of late endosomes to lysosomes results in the accumulation of glycosphingolipids in lysosomal storage diseases such as NPC, therefore analyzing the trafficking of lipids enriched within lipid rafts may also give an indication of lysosome function.

6.3.3.1 CtxB trafficking

CtxB binds the plasma membrane ganglioside GM1 which is found in cholesterol- and GSL-rich microdomains (lipid rafts) at the plasma membrane and is endocytosed via lipid raft/caveolar endocytosis (Orlandi and Fishman, 1998). FITC-labelled CtxB was used in this study as a marker of lipid raft transport from the plasma membrane to late endosomes/lysosomes by a pulse-chase assay (Lachmann et al., 2004). This assay would not only give an indication of altered lipid raft trafficking but also lysosome dysfunction that would be indicated by trapped lysosomal CtxB which cannot exit to the Golgi.

In order to optimise the assay in the hCMEC/D3 cell line, four different chase time points were used (0, 1, 2 and 3 hours) in non-transfected cells to determine the optimal time point to observe CtxB trafficking to the Golgi. Widespread faint punctate staining was observed in all conditions, including a non-stained control condition (Figure 6.11), which was therefore considered to be autofluorescence. Across all time points, a very small population (<1%) of cells exhibited positive staining, predominantly in the perinuclear region, suggestive of Golgi staining, as represented in Figure 6.11, with Hoechst staining the nuclei. Figure 6.12 shows representative comparisons of positive CtxB staining between the time points and also across different concentrations of CtxB, ranging from 2-20 μg/ml. The 0 min chase control was incorporated to visualise surface staining of CtxB which indeed showed diffuse plasma membrane staining on a small number of cells. After 1-3 hours chase, staining was more intense in the perinuclear region compared to 0 hours. However, no observable difference in the number of cells showing positive Golgi staining was noted between time points. Increasing concentrations of CtxB at 2, 5, 10 and 20 μg/ml were used in an attempt to optimise the number of positively-stained cells. While the

background punctate staining appeared to increase slightly with CtxB concentration, the number of positively-stained cells did not (Figure 6.12). This suggested that GM1 expression in the hCMEC/D3 cell line was not sufficient for CtxB to be used as a marker for lipid raft trafficking and an alternative method was sought to analyse this.

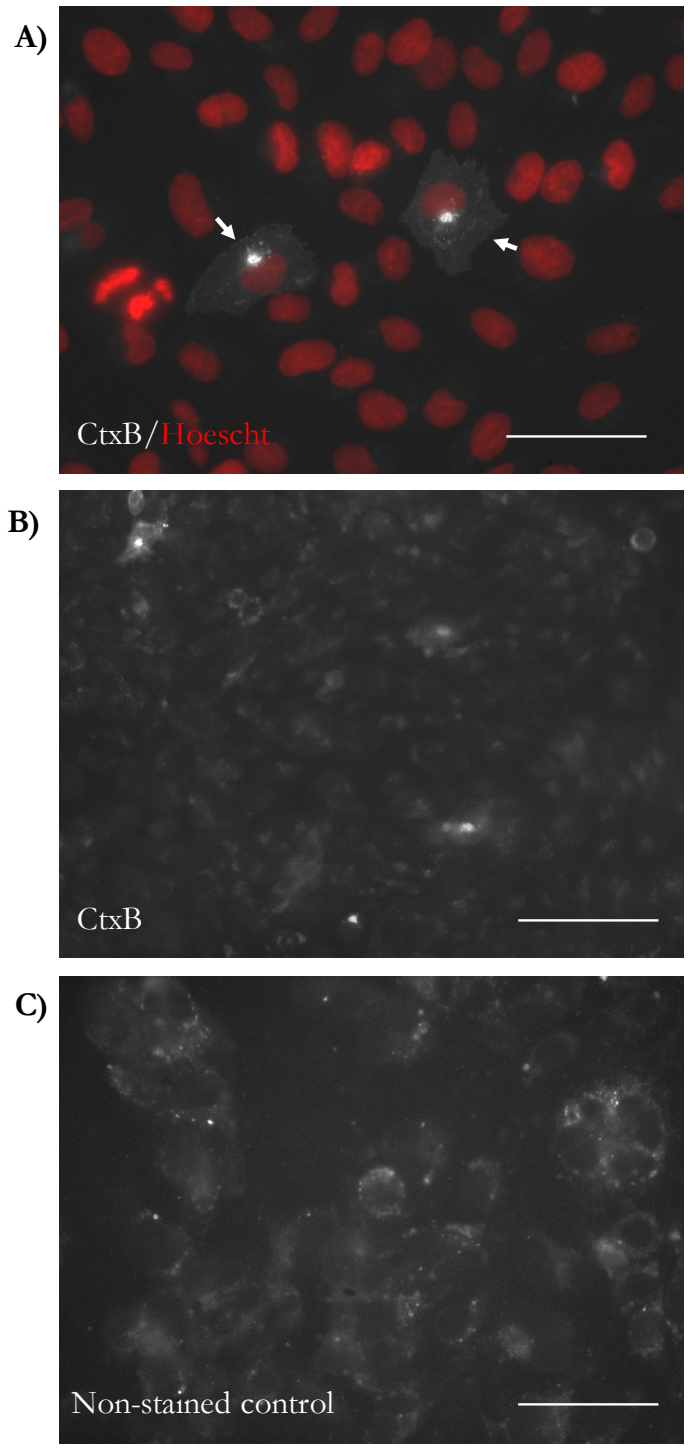

Figure 6.11: CtxB staining GM1 ganglioside in non-transfected hCMEC/D3 cells

Representative examples of FITC-CtxB (2 μg/ml) staining in hCMEC/D3 cells. A) Positive Golgi staining after a 1 hour chase is shown (white arrows), taken at x 40 magnification with Hoechst staining the nuclei. B) A representative image taken at x20 magnification to illustrate the low percentage (<1%) of cells showing positive FITC-CtxB staining in all conditions. C) The non-stained control had no CtxB applied yet showed diffuse punctate staining, confirming that this is a result of background fluorescence. Scale bar = 25 μm.

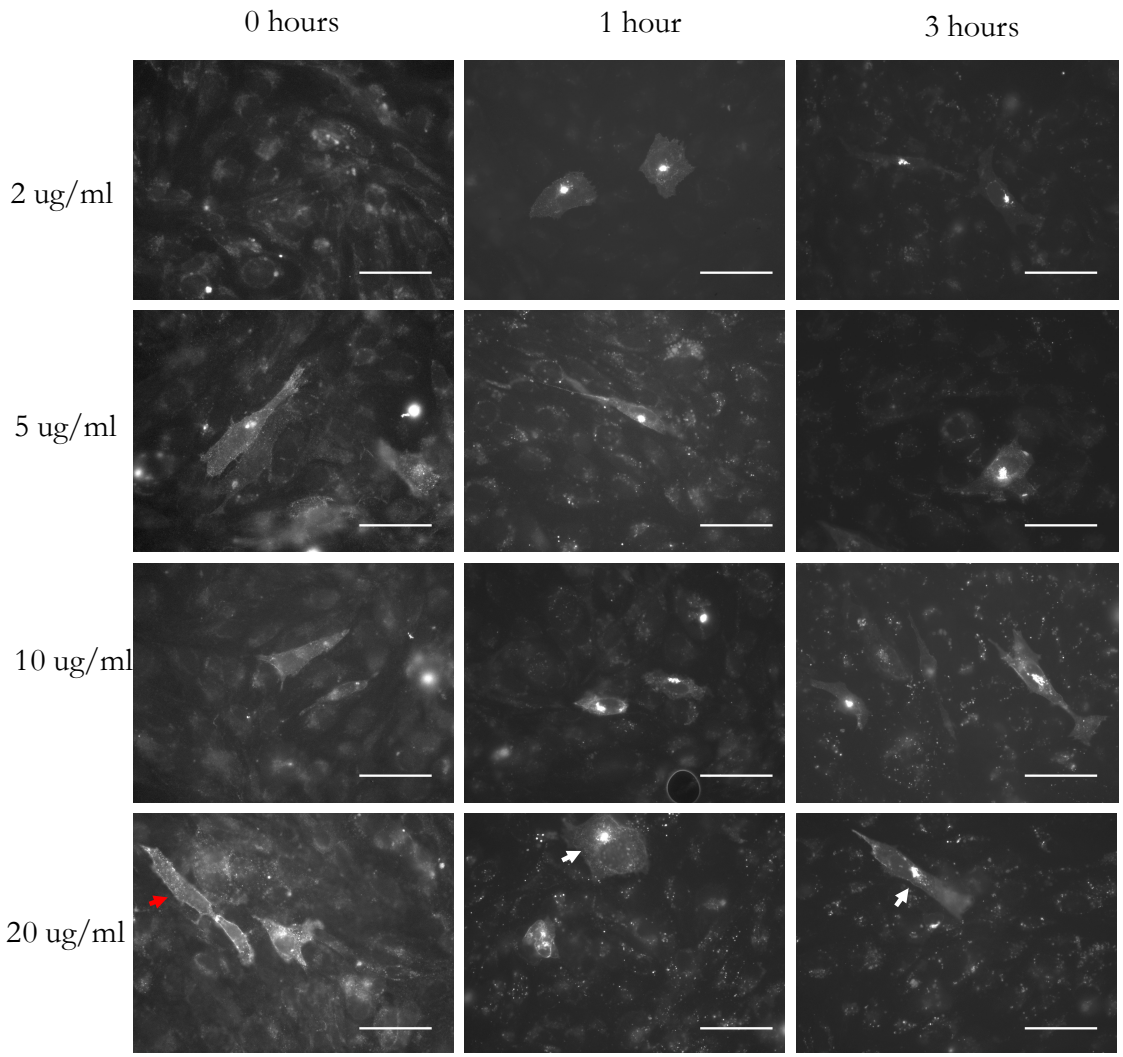

Figure 6.12: Optimisation of concentration and chase time for CtxB staining of hCMEC/D3 cells

Representative fluorescent images of hCMEC/D3 cells pulsed with 2 – 20 µg/ml FITC-CtxB and chased for 0-3 hours to optimise the number of cells showing positive staining. Increased background punctate staining was evident in the 20 µg/ml conditions compared to 2 µg/ml. With no chase (0 hours), CtxB showed plasma membrane staining (example indicated with red arrow) with perinuclear staining evident after 1-3 hours (examples identified with white arrows), suggestive of Golgi localisation. Images taken at x40 magnification, Scale bar = 25 µm.

6.3.3.2 BODIPY-LacCer trafficking

BODIPY-LacCer is a fluorescent analogue of the globoside lactosylceramide (Sharma et al., 2003) which is internalised from the plasma membrane by a caveolar-related mechanism and subsequently targeted to the Golgi apparatus (Singh et al., 2003). CAV1 is required for caveolar endocytosis and inhibition of LacCer uptake has previously been demonstrated upon CAV1 depletion (Al Soraj et al., 2012). Therefore, siRNA-mediated depletion of CAV1 was performed to establish a control for inhibition of LacCer uptake. CAV1 siRNA successfully depleted levels of CAV1 protein by 82%, which was confirmed by Western blotting (Figure 6.13). CAV1 expression was not affected by BIN1-depletion (Figure 6.13). When cells were chased at 37°C, considerable uptake of BODIPY-LacCer was apparent by the nearly 10-fold increase in fluorescence compared to those chased at 4°C, where inhibition of LacCer uptake was observed (Figure 6.13). A two-way ANOVA was used to determine the effect of temperature and siRNA treatment on LacCer uptake. There was a significant effect of temperature on LacCer uptake ($p<0.001$), demonstrating that uptake of LacCer in these cells is an active endocytic process as endocytic pathways are inhibited at 4°C. However, there was no significant effect of siRNA treatment on LacCer uptake after a 15 min chase at 37°C, suggesting that BIN1 is not central to the uptake of LacCer. Surprisingly, CAV1 depletion did not affect LacCer uptake, suggesting that CAV1 is not crucial for caveolar uptake in these cells. CAV1 depletion was intended as a positive control for inhibition of LacCer uptake, based on previous findings in other cell types (Al Soraj et al., 2012) and the well-documented role of CAV1 in caveolar uptake (Lisanti et al., 1994, Lipardi et al., 1998, Razani et al., 2001). The sensitivity of this assay for measuring caveolar uptake was therefore questioned and alternative means of inhibition sought in order to test this.

The internalisation of caveolae is facilitated by the actin cytoskeleton. Genistein is a tyrosine kinase inhibitor which causes local disruption of the actin cytoskeleton at endocytic sites and has been extensively used as an inhibitor of caveolar endocytosis (Singh et al., 2003, Vercauteren et al., 2010, Mougeolle et al., 2015). BODIPY-LacCer uptake was analysed in hCMEC/D3 cells with and without genistein treatment. Chasing cells at 4°C inhibited LacCer uptake to the same extent in both genistein-treated and non-treated cells. Unfortunately, time constraints only permitted the completion of two replicates, however, at 37°C, Genistein treatment resulted in a significant 30% reduction in LacCer uptake

compared to non-treated control cells ($p<0.01$ using a two-tailed unpaired Student's *t* test, Figure 6.14) suggesting successful inhibition of CIE.

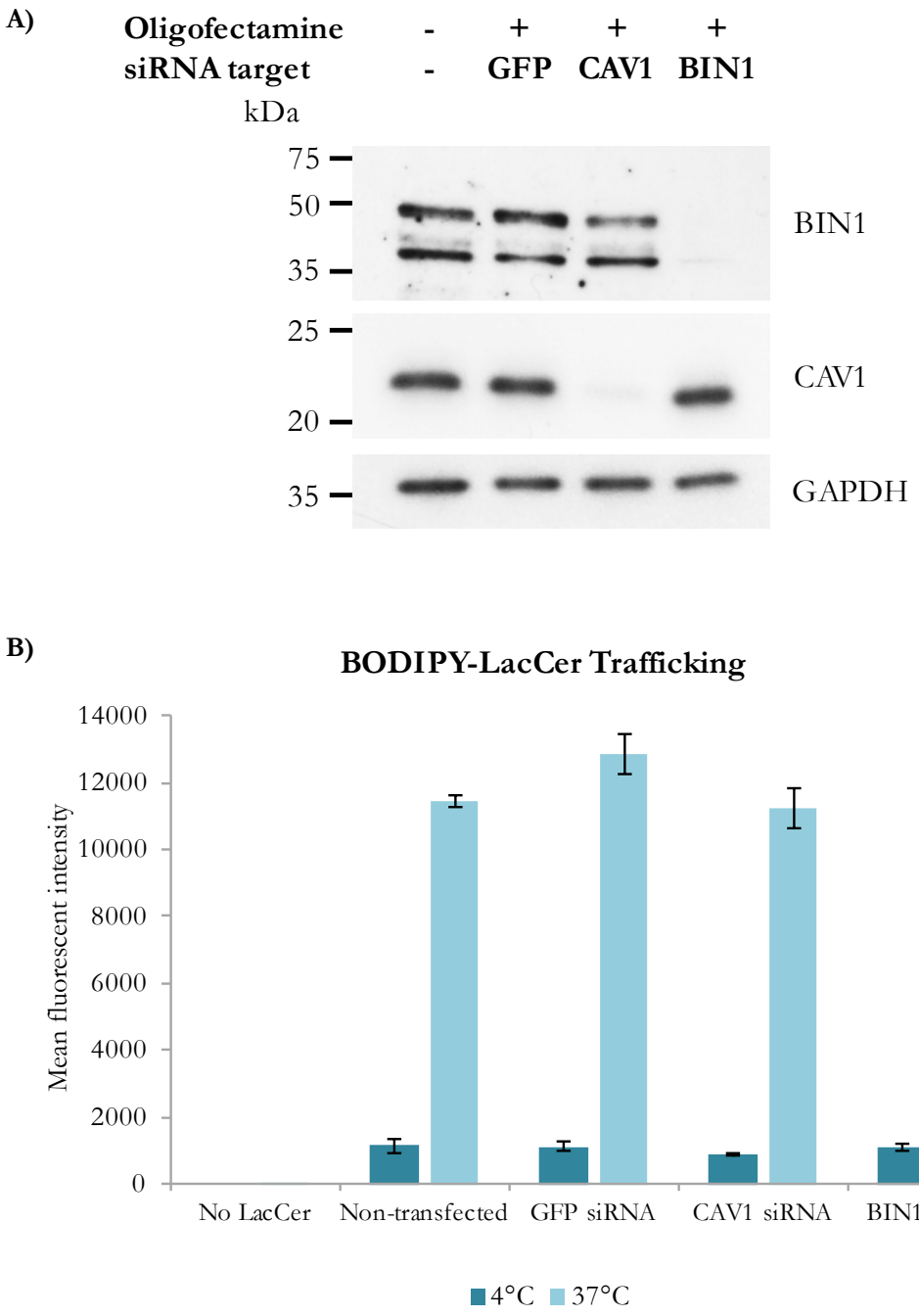

Figure 6.13: LacCer Uptake with BIN1 depletion to measure Caveolar Endocytosis

A) A representative Western blot showing successful siRNA-mediated depletion of CAV1 which did not affect BIN1 levels.

B) Quantification of BODIPY-LacCer trafficking in BIN1-depleted cells in comparison to CAV1-depleted, GFP siRNA-treated and non-transfected cells. BODIPY-LacCer was chased for 15 min at 4°C or 37°C before washing off surface-bound fluorescence and analysing intracellular fluorescence by FACs. There was no significant difference with CAV1 or BIN1 depletion compared to GFP siRNA-treated or non-transfected cells but a significant difference in mean fluorescent intensity between 4°C and 37°C ($p<0.001$, two-way ANOVA). Values represent the geometric mean, n= 3-4, error bars = SEM.

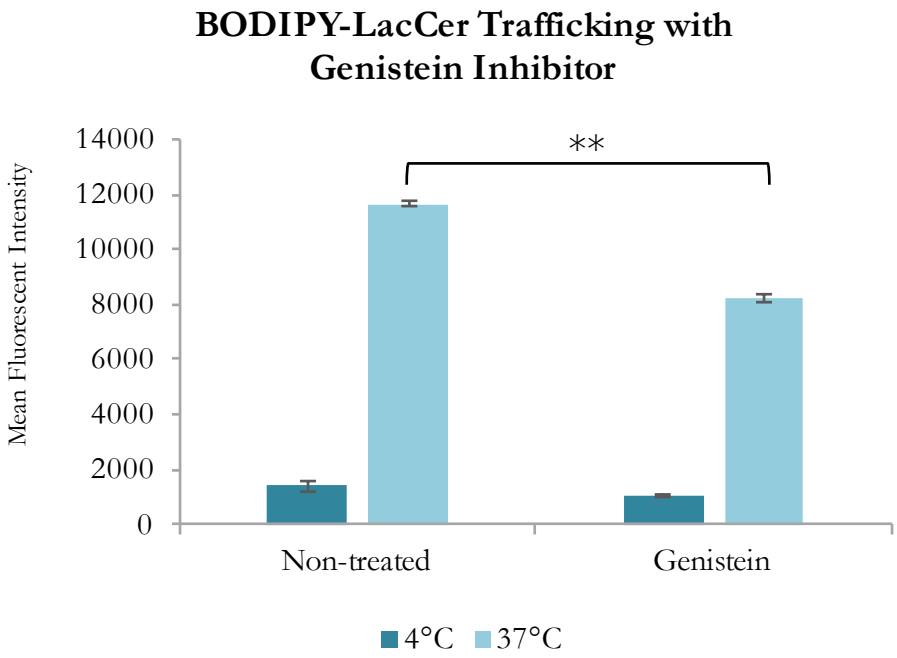

Figure 6.14: LacCer Uptake with Genistein Treatment to inhibit CIE

Quantification of BODIPY-LacCer trafficking in Genistein-treated cells in comparison to non-treated cells. BODIPY-LacCer was chased for 15 min at 4°C or 37°C before washing off surface-bound fluorescence and analysing intracellular fluorescence by FACs. Values represent the geometric mean, n = 2, ** = $p<0.01$ using a two-tailed unpaired Student's *t* test.

6.4 Discussion

This chapter aimed to investigate the relationship between BIN1 and endocytic trafficking to the lysosome, independent of clathrin-mediated mechanisms, in order to ascertain the involvement of BIN1 in the amyloidogenic processing of APP in BMECs. Firstly, morphological indicators of lysosome dysfunction were analysed, including lysosome morphology and cholesterol localisation. Both LysoTracker and, more specifically LAMP2B, were used as lysosome markers and a change in morphology or localisation of these with BIN1 depletion was not observed. Cholesterol localisation was also unaffected by BIN1 depletion, suggesting no impairment in lysosome function. Next, the expression of flotillin-1, flotillin-2, CAV1 and CAV2, key proteins involved in CIE, was analysed. While Ffotillin-1 and 2 and CAV1 showed no difference in levels, CAV2 showed a significant increase in expression with BIN1 depletion. In order to assess the function of caveolar endocytosis, markers of lipids found in lipid rafts were examined. CtxB, which binds GM1, did not show enough positive staining in the cells to reliably assess its trafficking. However, considerable uptake of BODIPY-LacCer was demonstrated in these cells, but this was not altered with BIN1 depletion therefore suggesting that BIN1 is not important for CIE in hCMEC/D3 cells.

6.4.1 Lysosome Morphology is not Affected by BIN1 depletion

Endolysosomal/autophagic alterations are well-recognised early neuropathological features of AD, including enlarged early endosomes, lysosome abnormalities and the progressive accumulation of autophagic vacuoles (Cataldo et al., 1994, Cataldo et al., 2000, Nixon et al., 2005). Impairment of autophagy has also been associated with some lysosomal storage diseases, caused by impaired degradation of some membrane lipids, such as NPC, which is associated with severe neurodegeneration in early life (Platt et al., 2012). Accumulation of sphingolipids, by the addition of exogenous GSLs to human H4, HeLa and HEK293 cells, has been shown to result in the marked accumulation of APP-CTFs due to decreased lysosome-dependent degradation of APP-CTFs (Tamboli et al., 2011). Prominent accumulation of APP-CTFs was also reported in primary human fibroblasts obtained from patients with lysosomal storage diseases (Tamboli et al., 2011). These findings suggested that sphingolipid accumulation affects autophagic flux and impairs the clearance of APP-

CTFs. Impaired lysosomal function has also previously been associated with β-CTF accumulation in neurons of 3-month-old triple transgenic AD mice, harbouring mutations in *PSEN1*, *APP*, and *MAPT* (Lauritzen et al., 2012). The β-CTF accumulation was found within enlarged cathepsin B and Lamp1-positive structures and was not associated with Aβ load. Furthermore, a small but significant increase in γ-secretase activity was reported, suggesting that the accumulation of β-CTF was unlikely to be accounted for by impaired γ-secretase function and may be due to defective lysosomal clearance (Lauritzen et al., 2016). This thesis therefore set out to investigate whether the increase in βCTF with BIN1 depletion, in the absence of changes in Aβ, is associated with lysosomal defects. The results have shown that BIN1 depletion in the hCMEC/D3 cell line did not inflict observable morphological changes on lysosomes, as assessed by LysoTracker and LAMP2B staining. LysoTracker showed a high intensity of staining which resided in the perinuclear region, with minimal, if any, LysoTracker accumulating in peripheral lysosomes. This was also supported by LAMP2B staining which showed a greater number of puncta in the perinuclear region, however these were more diffuse than LysoTracker and peripheral staining was more frequently observed in cells. This is consistent with previous reports of LysoTracker staining acidic organelles in human adipose microvascular endothelial cells where a greater accumulation of puncta was observed in the perinuclear region whereas dextran conjugated to Alexa- Fluor-647, a pH-insensitive lysosome marker, showed more widespread staining throughout the cell (Johnson et al., 2016). The authors concluded that the position of lysosomes within the cell determines their luminal pH as this pattern of heterogeneity in LysoTracker staining across the cell was due to peripheral lysosomes being less acidic than juxtanuclear ones. While the intensity of LysoTracker staining in the present study suggested there was no change in lysosome acidity with BIN1 depletion, pH is a crucial indicator of lysosome function and this was not explicitly measured in the present study. This could be investigated by examining the ratio of dextran-conjugated fluorescent reporters, one of which is pH-dependent, which would allow a comparison of lysosomal pH between non-transfected, GFP siRNA-treated and BIN1-depleted cells.

The lack of change in lysosome structure with BIN1 depletion suggests there was unlikely to be a gross impairment in lysosome function and that the increase in β-CTF observed may not be due to defective degradation and clearance via the lysosomal pathway. While very little is available in the literature regarding the relationship between BIN1 and lysosomal function, siRNA-mediated depletion of Bin1 in mouse intestinal organoids

resulted in the gross enlargement of lysosomes, using lamp2 as a marker (Nakajo et al., 2016). Furthermore, accumulation of dipeptidyl peptidase IV, a membrane glycoprotein predominantly expressed at the apical membrane of polarised cells (Alfalah et al., 2002), was found in the enlarged lamp2-positive structures of Bin1-depleted organoids. Collectively these findings suggest that Bin1 is involved in transporting cargo to the apical membrane in intestinal epithelial cells and with Bin1 depletion, apical proteins accumulated in lysosomes possibly due to the accumulation of unsorted apical proteins in the ERC which may fuse or mature into lysosomes (Nakajo et al., 2016). This was investigated in a polarised *in vitro* context and may therefore relate to a possible function in BMECs. However, in the present study, no effect of BIN1 depletion on lysosome morphology was observed, suggesting the function of BIN1 in endocytic trafficking may differ between cell types. Nevertheless, polarisation was not established in the hCMEC/D3 cells in the present study, therefore apical and basolateral cargo may not have been distinguished and any defect in trafficking of apical cargo could not be observed. This presents an avenue for future study that will be further discussed in Chapter 7.

6.4.2 Cholesterol Localisation with BIN1 Depletion

Cellular cholesterol is either stored as free cholesterol or cholesterol esters in the form of cytoplasmic droplets (Ikonen, 2008). Filipin selectively stains free cholesterol, which is an essential structural component of cell membranes. Within the cell, cholesterol is abundant in the endocytic recycling compartment (Mukherjee et al., 1998), a perinuclear compartment which is responsible for most of the recycling of plasma membrane receptors. Cholesterol is also enriched in lipid rafts on the plasma membrane (Ikonen, 2008). Lysosome dysfunction often causes accumulation of free cholesterol in the lysosomes which can inhibit Rab GTPases, which promote endocytic recycling (te Vruchte et al., 2004). Abnormal distribution and transport of cholesterol has been linked to many neurodegenerative diseases including Huntington's, NPC and AD (Vance, 2012). In NPC, filipin staining is often used as a diagnostic criteria to identify the accumulation of free cholesterol in the lysosomes of cultured skin fibroblasts (Hankey, 2008). Consistent with the lysosome morphology, no change in cholesterol localisation or membrane content was observed with BIN1 depletion in hCMEC/D3 cells, suggesting that lysosome function and cholesterol trafficking was not impaired. However, cholesterol levels were not quantified therefore this would be required to confirm these findings. In all conditions, cholesterol

was localised to the perinuclear region, suggestive of ERC staining, while diffuse cell-wide staining was consistent with its presence throughout the cell membrane. In support of the previous findings on lysosome morphology, the lack of change in cholesterol localisation with BIN1 depletion suggests that BIN1 is not crucial for normal lysosome function in hCMEC/D3 cells. Therefore, impaired lysosome function may not account for the increase in β-CTF observed with BIN1 depletion in these cells and BIN1 may affect the processing of APP through a different pathway.

6.4.3 The Role of BIN1 in Clathrin-independent Endocytosis

Cholesterol is highly enriched in lipid raft fractions, however, the utility of filipin in analysing lipid raft function is limited as when applied *in vitro,* it disrupts caveolae and inhibits lipid raft endocytosis by sequestering cholesterol (Orlandi and Fishman, 1998). In order to investigate clathrin-independent mechanisms of endocytosis with BIN1 depletion, firstly expression levels of key CIE proteins, flotillin-1, flotillin-2, CAV1 and CAV2, were measured. While the flotillins are thought to define a clathrin-independent pathway of endocytosis (Glebov et al., 2006), they have been implicated in the clathrin-mediated endocytosis of APP (Schneider et al., 2008). Furthermore, (John et al., 2014) reported that flotillins directly bind to the cytoplasmic tail of BACE1 and depletion of flotillin-1 or -2 in HeLa cells showed a significant increase in BACE1 levels, particularly in the perinuclear region. In the flotillin-2-depleted cells, an increase in β-CTF but not APP levels was observed, suggesting that flotillin-2 knockdown increased the expression and endosomal localization of BACE1, resulting in increased amyloidogenic processing of APP (John et al., 2014).

The aforementioned study by (John et al., 2014) draws many parallels with studies investigating BIN1 depletion and its involvement in BACE1 endocytic recycling (Miyagawa et al., 2016, Ubelmann et al., 2017). A possible relationship between BIN1 and flotillin-mediated endocytic trafficking remains to be investigated, therefore an analysis of flotillin levels with BIN1 depletion in the present study aimed to explore this. Both flotillin-1 and flotillin-2 expression were readily detectable in hCMEC/D3 cells, however levels did not appear to alter with BIN1 depletion. While APP processing has been shown to be altered by flotillin-2 depletion (John et al., 2014), BIN1 depletion did not affect levels of flotillin-1 or -2 in the present study, suggesting the increase in β-CTF with BIN1 depletion is unlikely

to have been brought about by flotillin-mediated mechanisms. However, flotillin-mediated internalisation was not explicitly measured in the present study due to the lack of change in flotillin levels. This would be an interesting further experiment in order to elucidate whether flotillin-mediated endocytosis is affected by BIN1 depletion.

6.4.3.1 The Effect of BIN1 Depletion on the Expression of Caveolins

The results presented in this chapter show that CAV1 levels were unaffected while CAV2 protein levels were increased with BIN1 depletion. The molecular mechanism of caveolae assembly is not fully understood, however CAV1 is known to be required for this process (Razani et al., 2001). Many studies have suggested that CAV1 is sufficient to drive caveolae biogenesis and CAV2 may modulate the actions of CAV1 in this process (Sowa et al., 2003). In polarised cells such as epithelial and endothelial cells, sorting of proteins destined for the two plasma membrane domains occurs in the Golgi where separate apical and basolateral vesicles form to deliver cargo to the required destinations (Mellman and Nelson, 2008). While CAV1 is present on both the apical and basolateral domains of MDCK polarised epithelial cells, CAV2 is strongly enriched on the basolateral membrane and vesicles (Scheiffele et al., 1998). CAV1/2 heteroligomers are incorporated into basolateral-directed vesicles in the Golgi whereas CAV1 homoligomers are incorporated into apical-directed vesicles (Scheiffele et al., 1998). LNCaP cells, human prostate adenocarcinoma cells which are devoid of caveolin expression and caveolae, were used to show that coexpression of CAV1 and CAV2 promote the formation of caveolae on the basolateral surface (Sowa et al., 2003). It should be noted, however, that inducing expression of a protein in cells which do not endogenously express that protein can often lead to the formation of non-specific and/or unnatural protein interactions (Park, 2008). The authors further demonstrated that CAV2 is phosphorylated by casein kinase 2 at serines 23 and 36 and that this is a crucial step in the formation of plasma membrane-attached caveolae (Sowa et al., 2003). However, expression of a mutant CAV2 which cannot be phosphorylated showed no detectable caveolae formation but a 3-fold increase in the number of smooth vesicles in close proximity to the plasma membrane compared to cells expressing wild-type CAV2 (Sowa et al., 2003). This suggests that the phosphorylation of CAV2 may regulate the exocytosis/endocytosis of CAV1-dependent vesicles, therefore emphasising the importance of CAV2 in caveolar endocytosis. The increase in CAV2 expression with BIN1 depletion in the present study may indicate alterations in caveolar-

related endocytic mechanisms. This is of particular significance to AD as CAV1 has been identified as an important regulator of γ-secretase activity by modulating the partitioning of γ-secretase between caveolar and non-caveolar membranes (Kapoor et al., 2010).

The increase in CAV2 expression with BIN1 depletion is particularly interesting in light of recent findings suggesting BIN1 is involved in the regulation of apical-directed transport in polarised epithelial cells. BIN1-depleted small intestine organoids showed a significant accumulation of apical-directed proteins in lysosomes, but not basolateral proteins (Nakajo et al., 2016). While Sowa et al. (2003) reported the involvement of CAV2 in the formation of caveolae at the basolateral surface of rat kidney epithelial cells, Cav-2 depletion in *Caenorhabditis elegans* was shown to cause a specific defect in the uptake of BODIPY-LacCer from the apical side of intestinal cells (Parker et al., 2009). Studies investigating CAV2 in endocytic trafficking in BMECs remain to be conducted, however it may be that depletion of BIN1 in the hCMEC/D3 cell line results in increased basolateral-directed transport and/or decreased apical-directed transport, hence showing an increase in CAV2 expression but no observable change in CAV1 expression. Indeed, caveolae have shown a polarised distribution in rat BMECs with 1.7-fold greater numbers at the basolateral compared to the apical membrane (Bendayan et al., 2006) therefore analysis of caveolar endocytosis in a polarised culture system with BIN1 depletion would be important for future work. With regards to AD pathogenesis, this could have consequences for clearance of Aβ or other toxins across BMECs or possibly affect the composition of apical/basolateral membranes which may impact the barrier properties BMECs. In order to investigate caveolar endocytosis, trafficking of CtxB was used as a marker of this mechanism.

6.4.3.2 The role of BIN1 in Lipid-raft Trafficking

GM1, the receptor for CtxB, is clustered in detergent-insoluble lipid rafts in the plasma membrane and its internalisation is dependent on and mediated by these cholesterol- and GSL-rich microdomains (Orlandi and Fishman, 1998). Trafficking of CtxB was optimised with the aim of visualising lipid raft endocytosis with BIN1 depletion. Unfortunately, insufficient positive CtxB staining was obtained with non-transfected cells to make reliable comparisons between conditions. This may be due to low expression levels of the GM1 ganglioside in the plasma membrane of hCMEC/D3 cells, which has not previously been reported, as sufficient expression is necessary for this to be a valid method. Indeed, GM1

ganglioside was shown to be readily detectable in cultured astrocytes, neuroblastoma cells (SH-SY5Y), and pheochromocytoma cells (PC12) cells but not brain-derived endothelial cells (Yamamoto et al., 2007). Furthermore, analysis of the GSL composition of the human BMEC line SV-HCECs showed that GM3 and GM2 were the major gangliosides present, with GM1 only representing 3% of the population (Duvar et al., 2000). LacCer, however, comprised 36% of the total neutral glycosphingolipids (Duvar et al., 2000) and has the benefit of a well-characterised fluorescent analogue available therefore presented a more quantifiable marker for lipid raft trafficking. Furthermore, the specificity of CtxB as a raft marker is controversial, since ctxB/GM1 have been found to be internalised not only by CIE, but also via CCPs and thus CME (Hansen and Nichols, 2009). Therefore, considerable rationale was presented for analysing lipid raft endocytosis by alternative means.

Glycosphingolipids, such as LacCer, are internalised from the plasma membrane via a clathrin-independent, caveolar-related mechanism (Singh et al., 2003). They are delivered to the early endosomes, where they are fractionated into two major pools, one that is transported via late endosomes to the Golgi apparatus and the other that is returned to the plasma membrane via the ERC (Sharma et al., 2003). Cells with lysosomal trafficking defects, such as cultured fibroblasts from patients with NPC, show abnormalities in the intracellular trafficking of lipids (Chen et al., 1999). In pulse-chase experiments, BODIPY-LacCer accumulates in endosomes and lysosomes rather than being targeted to the Golgi as it is in normal cells. While such gross changes observed in lipid storage diseases would not be expected with BIN1 depletion in hCMEC/D3 cells, given the subtle effects demonstrated in this thesis so far, quantification of internalization via CIE may suggest an effect on this mechanism. LacCer is internalised by a clathrin-independent, caveolar-related route and has been shown to colocalise with Cav1 in vesicular structures upon endocytosis in rat fibroblasts (Singh et al., 2003). Since it was shown to be one of the major GSLs found in the SV-HCEC cells, also a human BMEC cell line (Duvar et al., 2000), it was used as a marker to investigate the function of CIE with BIN1 depletion in hCMEC/D3 cells.

Despite an increase in CAV2 levels, the present study shows no significant difference in LacCer uptake with BIN1 depletion, suggesting that BIN1 is not important for CIE in hCMEC/D3 cells. While a positive control demonstrating LacCer uptake inhibition in this assay was not achieved using CAV1 siRNA, further discussed in Section 6.4.3.3, inhibition

of LacCer was achieved by genistein treatment. Despite the use of only two replicates in this assay, a preliminary conclusion can be reached suggesting that BIN1 depletion does not affect LacCer uptake in hCMEC/D3 cells and may not be crucial for caveolar endocytosis. This finding is important in the context of BMECs at the BBB as inhibition of caveolar endocytosis has recently been demonstrated as a mechanism by which the restrictive permeability of the BBB is maintained (Andreone et al., 2017). Should BIN1 depletion have resulted in a change in LacCer uptake in hCMEC/D3 cells, this may have implications for the permeability of BBB, which is often compromised in AD (Zipser et al., 2007).

6.4.3.3 CAV1 depletion did not affect LacCer uptake

Surprisingly, CAV1 depletion in the hCMEC/D3 cell line did not have a significant effect on BODIPY-LacCer uptake. This is in contrast to a previous study using the same siRNA for CAV1 in HeLa cells which showed a 50% reduction in BODIPY-LacCer uptake over a 15 min chase period (Al Soraj et al., 2012). Furthermore, when C2C12 mouse myoblast cells were subjected to oxidative stress, causing degradation of Cav1, a significant reduction in BODIPY-LacCer uptake was observed (Mougeolle et al., 2015). Other groups have successfully applied siRNA methods to deplete CAV1 in alternative caveolar endocytic assays. Albumin is predominantly transported through a caveolae-mediated pathway and impairment of albumin uptake has been demonstrated with siRNA-mediated-Cav1 depletion in mouse aortic endothelial cells (Gonzalez et al., 2004), human umbilical vein endothelial cells (HUVECs) (Pavlides et al., 2014) and in lung endothelial cells of *Cav1* knockout mice (Schubert et al., 2001). While siRNA-mediated CAV1 depletion has previously been investigated in the hCMEC/D3 cell line (Zhong et al., 2010), the effect on LacCer uptake is yet to be reported. However, Zhong et al. (2010) investigated siRNA-mediated CAV1 depletion in the hCMEC/D3 cell line in relation to the relationship between CAV1 and Pgp expression, reporting that Pgp expression was not affected by CAV1 depletion. This was inconsistent with previous findings in bovine BMECs, which proposed that Pgp activity may be modulated by Cav1, suggesting that the results of Cav1 depletion in these cells may be different to other cells. Furthermore, while the present results may suggest that CAV1 is not required for caveolar uptake in hCMEC/D3 cells, it is important to acknowledge evidence that sphingolipids can enter cells by multiple

mechanisms (Hansen and Nichols, 2009). Therefore, in the present study, LacCer was considered a marker for CIE and not specifically caveolae-mediated pathways. Furthermore, uptake of LacCer has been demonstrated in human colon carcinoma Caco-2 cells, with very low *CAV1* mRNA and undetectable CAV1 protein levels, suggesting other pathways are likely to be responsible for LacCer endocytosis in this cell line (Ilina et al., 2015). Alternative endocytic processes may have been responsible for LacCer internalization in the hCMEC/D3 cell line and/or these may have compensated for the lack of CAV1. Crucially, demonstration of the sensitivity of the BODIPY-LacCer uptake assay was not achieved through CAV1 depletion therefore an alternative means of CIE inhibition was used.

6.4.3.4 Genistein

Genistein is a tyrosine kinase inhibitor which causes local disruption of the actin cytoskeleton at endocytic sites and has previously been shown to inhibit LacCer uptake in a variety of cell lines (Vercauteren et al., 2010, Mougeolle et al., 2015). In the present study, treatment of hCMEC/D3 cells with genistein induced a 30% reduction in BODIPY-LacCer uptake that reached statistical significance based on two replicates. While further replications of this study will be necessary to confirm the validity of the findings, a small but significant level of inhibition of LacCer uptake by genistein is suggested. This level of inhibition, however, was not comparable to previous findings where genistein was shown to inhibit LacCer uptake by 65% in C2C12 mouse myoblasts (Mougeolle et al., 2015) and 70% in D407 retinal pigment epithelial cells(Vercauteren et al., 2010). However, the extent to which this inhibition occurs varies between cell lines. Vercauteren et al. (2010) highlighted the different sensitivities of cell lines for individual inhibitors or treatments, including genistein where the inhibition level of LacCer uptake ranged from 30-70% across five different cell lines. The level of inhibition in the present study was therefore comparable to one of the cells lines analysed, an African green monkey kidney epithelial cell line (Vercauteren et al., 2010). This suggests that the extent to which LacCer is internalised by CIE varies between cell types. Optimisation of this experiment may have resulted in a greater level of LacCer uptake inhibition as Vercauteren et al. (2010) reported that the optimal inhibitor conditions in the cell lines assessed were a pre-treatment with 400 μM genistein for 2 hours and continued incubation with the inhibitor during the

application of the BODIPY-LacCer. This is double the concentration of genistein used in the present study and the inhibitor was only applied for 30 min before LacCer incubation in the hCMEC/D3 cells, and not during, therefore an optimisation of these conditions may yield a greater degree of inhibition. Nevertheless, a significant reduction in LacCer uptake with genistein treatment in the present study suggests that the sensitivity of this assay may be sufficient for hCMEC/D3 cells and is therefore a reliable measure of CIE. In light of this, the present findings suggest that BIN1 may not be important for CIE in hCMEC/D3 cells.

As with the use of LacCer as a marker for CIE, the use of inhibitors in endocytic assays must be carefully interpreted as their specificity can often be questioned (Vercauteren et al., 2010). While LacCer internalization was inhibited by ~80% with genistein in rat fibroblasts without affecting Tf uptake (Singh et al., 2003), genistein treatment inhibited both LacCer uptake and Tf uptake in D407 human retinal pigment epithelial cells by ~70% and ~80%, respectively (Vercauteren et al., 2010). This suggests that endocytic mechanisms can vary greatly between cell types. The effect of genistein treatment on CME through analysis of Tf uptake was not examined in the present study. Caution must therefore be exercised when interpreting results from studies using single measures of endocytic uptake and future work for the present study would include the utilisation of additional methods of CIE inhibition and CIE markers in order to replicate findings.

6.4.4 Conclusions

In summary, the present study has demonstrated that BIN1 depletion does not impact lysosome morphology or cholesterol trafficking in hCMEC/D3 cells. While the levels of flotillins were unaffected, CAV2 showed a significant increase with BIN1 depletion, however CIE, as assessed by LacCer trafficking, was not affected. Further work would include investigating the intracellular localisation of LacCer after trafficking, as while levels may not have considerably changed, altered trafficking may have still occurred with BIN1 depletion. Furthermore, apical and basolateral trafficking cannot be segregated in this non-polarised culture system and the aforementioned literature suggests that this is important for CIE mechanisms in endothelial cells. The establishment of apical-basolateral polarity in hCMEC/D3 cell culture as a future direction for research in the role of BIN1 will be further discussed in Chapter 7.

Chapter 7

General Discussion

7.1 Summary of Aims and Key Findings

The overall aim of this study was to investigate the functional role of BIN1 in the context of endocytic mechanisms in the brain to gain insight into the molecular pathogenesis of AD. To achieve this aim, two major objectives were explored:

- Utilising novel advances in the development of induced pluripotent stem cells (iPSCs) in order to create a more accurate neuronal cell model to study the role of BIN1 and endocytic mechanisms in neurons.
- To generate a transient BIN1-depleted brain endothelial cell model to investigate the role of BIN1 in APP processing and endocytic function at the BBB.

BIN1 has been implicated in sAD by a number of GWAS (Seshadri et al., 2010, Naj et al., 2011, Hollingworth et al., 2011, Lambert et al., 2013) and is the second most significantly associated susceptibility locus for sAD after *APOE* (Lambert et al., 2013). With multiple tissue-specific isoforms, the functions of BIN1 are wide-ranging and its involvement in mediating sAD risk is not fully understood. BIN1 is thought to play a critical role in CME and was recently shown to regulate intracellular trafficking of BACE1 (Miyagawa et al., 2016). This finding in both neuronal and non-neuronal cell lines emphasises the need to investigate BIN1 function in multiple sAD-relevant cell types. Table 7.1 summarises the key findings of this study.

Table 7.1: Summary of the Key Aims and Findings of this Thesis

Chapter	Aims	Key findings
3	To characterise and successfully differentiate PBMC-derived iPSCs into cortical glutamatergic neurons.	iPSCs derived from PBMCs can be directed to differentiate into cortical neurons through dual SMAD inhibition.
4	To achieve depletion of total BIN1 in a human brain endothelial cell line and to characterise its role in APP processing in hCMEC/D3 BMECs.	BIN1 depletion results in a significant increase in intracellular β-CTF levels, without impacting intracellular APP levels or extracellular Aβ40 or sAPPα. Protein levels of key α- β- and γ-secretases were unchanged with BIN1 depletion. BIN1 depletion did not affect BACE1 or APP localisation.
5	To investigate whether BIN1 depletion affects CME and recycling in the hCMEC/D3 cell line.	BIN1 depletion does not affect Tf uptake or recycling in the hCMEC/D3 cell line. The BIN1 isoforms expressed in hCMEC/D3 cells are not required for CME or recycling.
6	To explore whether BIN1 is involved in endo-lysosomal trafficking and/or CIE in hCMEC/D3 cells.	BIN1 depletion does not impact lysosome morphology or cholesterol trafficking in hCMEC/D3 cells. BIN1-depleted cells show an increase in CAV2 protein expression but LacCer trafficking, a marker of CIE, is not affected.

In Chapter 3, a novel cortical neuronal model was created through the differentiation of an iPSC line derived from PBMCs. The limitations and wider applications of this work have been extensively discussed in Chapter 3, therefore the general discussion will focus on the main body of the thesis investigating BIN1 function in hCMEC/D3 cells and the wider context of this work within the field of AD research.

In Chapter 4, the involvement of BIN1 in APP processing in hCMEC/D3c cells was investigated using siRNA-mediated depletion of all BIN1 protein isoforms. While no significant differences in the levels of APP and Aβ40 were observed with BIN1 depletion, a significant increase in β-CTF was found, suggesting that BIN1 may be involved in the amyloidogenic processing of APP. The mechanism from which this increase originated could not be further elucidated from levels of sAPPα as no significant change was detected with BIN1 depletion and a high level of variability was shown between samples. Furthermore, levels of sAPPβ fell beyond the detectability limit of the assay. The present findings do suggest an enhancement of the amyloidogenic pathway with BIN1 depletion, indicated by increased βCTF, either in terms of increased production or decreased clearance. A change in levels of key α-, β- and γ- secretases was not detected, suggesting that the increase in β-CTF may not be due to altered secretase activity. However, only overall levels of ADAM10, BACE1 and PSEN1 were analysed and not the enzymatic activity levels.

It is possible that an increase in the amount of APP being directed down the amyloidogenic pathway may have occurred without a change in secretase activity. Indeed, this was demonstrated by Miyagawa et al. (2016) when BIN1 depletion resulted in enhanced cleavage of APP by increased encounters with BACE1 due to endocytic trafficking defects. Nevertheless, Chapter 5 showed no change in CME or recycling, measured by internalization and trafficking of Alexa-488-Tf, with BIN1 depletion. These findings were, however, consistent with the lack of change in APP levels reported in Chapter 4, suggesting the increase in β-CTF was not due to increased internalization of APP by CME, and therefore may be sure to increased colocalisation with cleavage enzymes. Furthermore, the absence of BIN1 isoforms expressing the CLAP domain indicate that BIN may not be necessary for the proper functioning of CME in hCMEC/D3 cells.

Chapter 6 investigated a potential role for BIN1 in endocytic trafficking to the lysosome, independent of clathrin-mediated mechanisms. LysoTracker, LAMP2B and cholesterol staining suggested that BIN1 depletion did not inflict observable morphological changes on lysosomes or gross abnormalities in lysosome function. This suggests that BIN1 is not vital for the proper functioning of these organelles, at least in terms of the parameters measured in this study. Flotillin-1, flotillin-2 and CAV1, key proteins involved in CIE, showed no change in levels, however, CAV2 showed a significant increase in protein levels, leading to analysis of the function of CIE with BIN1 depletion in hCMEC/D3 cells. BODIPY-LacCer was used as a marker for CIE and FACs analysis showed no change in fluorescence with BIN1 depletion, suggesting the internalization of LacCer was not affected. This suggests that BIN1 may not be necessary for CIE in hCMEC/D3 cells and supports the lack of change in flotillin-1, flotillin-2 and CAV1 levels, however this finding does not further elucidate the functional relevance of increased CAV2 levels with BIN1 depletion. The demonstration of decreased LacCer uptake with Genistein treatment suggests that the assay is an effective measure of caveolar endocytosis, however, as previously discussed in Chapter 6, the extent to which LacCer uptake was inhibited by Genistein was not comparable to the majority of studies in the literature (Vercauteren et al., 2010, Mougeolle et al., 2015). The sensitivity of this assay therefore requires further optimisation, however, initial results suggest that, despite increasing CAV2 expression levels, BIN1 depletion may not impact CIE.

CAV2 has shown strong enrichment on the basolateral membrane and in basolateral vesicles of MDCK polarised epithelial cells (Scheiffele et al., 1998) and involvement in the formation of caveolae at the basolateral surface of rat kidney epithelial cells (Sowa et al., 2003), suggesting it may be involved in CIE from the basolateral domain. However, in *Caenorhabditis elegans*, Cav2 was predominantly expressed in the apical membrane of intestinal cells and *Cav2* null mutants were defective in the uptake of BODIPY-LacCer suggesting Cav2 was involved in apical trafficking (Parker et al., 2009). Indeed, endocytosis of Fm4-64, a plasma membrane marker, was perturbed at the apical, but not the basolateral membrane (Parker et al., 2009). Collectively, these data suggest that CAV2 may have a domain-specific role in polarised cells. A change in caveolar endocytosis with BIN1 depletion could have crucial implications for BBB permeability. Recently, it has been demonstrated that the lipid composition of BMECs inhibits specifically caveolae-mediated transcytosis in order to maintain BBB integrity (Andreone et al., 2017). While no defect in

LacCer uptake was identified with BIN1 depletion in the present study, it is possible that BIN1 may have a polarised role in BMECs which the present non-polarised culture system was not capable of detecting. Therefore, a role for BIN1 in endocytic trafficking in BMECs cells cannot be ruled out based on the present findings.

7.2 Is an Increase in β-CTF Sufficient to be a Key Driver in AD Pathogenesis?

The increase in β-CTF with BIN1 depletion is a key indication of altered amyloidogenic processing of APP, despite no change being detected in Aβ40 levels. Indeed, there is much emerging evidence that β-CTF may contribute to sAD pathogenesis, independent of Aβ (Kim et al., 2016). In particular, that β-CTF accumulation may contribute to endocytic dysfunction in AD (Jiang et al., 2010). In APP-overexpressing fibroblasts, Jiang et al. (2010) showed that either depletion of APP by shRNA or decreasing β-CTF production by inhibiting BACE1 reversed the pathologic endocytic changes observed in these cells, including endosome enlargement and accelerated uptake. Crucially, inhibition of γ-secretase in these cells, which reduced Aβ40 and Aβ42 production but increased β-CTF levels, also lead to AD-like endosome dysfunction, highlighting the importance of Aβ-independent pathogenic roles of β-CTF in AD. While demonstrating a novel link between the generation of βCTF and pathological endosomal effects that are not mediated by Aβ, this study was conducted in APP-overexpressing cells which are not representative of physiological levels of APP in sAD.

In the context of the present study, BMECs express APP_{751} and APP_{770} and the expression of these isoforms is higher in endothelial cells of cerebral blood vessels compared with peripheral arteries (Kitazume et al., 2010). While the expression of specific APP isoforms was not analysed in the present study, hCMEC/D3 cells have shown comparable APP expression levels to primary human BMECs in culture (Urich et al., 2012). Therefore suggesting that the expression level of APP in hCMEC/D3 cells is physiologically representative. It has been demonstrated that BMECs are capable of proteolytically processing APP to produce Aβ (Kitazume et al., 2010). However, endogenous Aβ was not detectable in this study (Kitazume et al., 2010) and the overexpression of APP_{770} was required in order to demonstrate the amyloidogenic activity of BMECs. Furthermore, APP expression in BMECs was shown to be 53% of the expression levels in neurons (Forloni et

al., 1992), suggesting that the BBB may contribute to APP processing to a lesser extent than neurons in the brain. Therefore, it brings into question the extent to which the increase in β-CTF observed in this study could be a key driver in AD pathogenesis. Nevertheless, the increase in β-CTF in the present study may be indicative of perturbations in other cell mechanisms not directly measured. Indeed, BIN1 is thought to have multiple functions in different tissues (Tan et al., 2013) and the functional relevance of the BIN1 isoforms in different cell types is still poorly understood.

7.3 BIN1: a Protein of Multiple Functions

The mechanism(s) by which BIN1 protein contributes to AD risk are currently unknown. BIN1 is member of the BAR family of proteins, that regulate membrane dynamics in a variety of cellular functions (Ren et al., 2006), and has been shown to interact and recruit dynamin (Meinecke et al., 2013). Much research has therefore focused on the involvement of BIN1 in endocytosis when attempting to elucidate the mechanism by which BIN1 mediates AD risk. With 55% protein homology to AMPH1 (Butler et al., 1997), BIN1 has been proposed to function in synaptic vesicle endocytosis (Wigge and McMahon, 1998). However primary neurons from *Bin1* knockout mice failed to demonstrate a defect in this mechanism, suggesting that BIN1 and AMPH1 may have divergent functions in the brain and reflecting the broad expression of BIN1 isoforms across several tissues (Muller et al., 2003).

While endocytosis is central to the amyloidogenic processing of APP (Carey et al., 2005), the lack of correlation established between BIN1 and Aβ pathology has shed doubt on the role of BIN1 in amyloidogenesis (Glennon et al., 2013). With over 10 alternatively-spliced isoforms showing specific tissue distribution and cellular localization, BIN1 has wide-ranging functions that may be dependent on cell type. Within the human brain, BIN1 isoform diversity has been demonstrated (De Rossi et al., 2016) with the majority of BIN1 showing non-neuronal expression and predominantly localizing to mature oligodendrocytes. In this context, an association between BIN1 expression and oligodendrocyte myelination was identified (De Rossi et al., 2016). BIN1 has also been implicated in modulating the pathophysiological process involving tau by studies showing a direct interaction of BIN1 with the tau protein (Chapuis et al., 2013) in addition to the association of BIN1 expression with NFTs (Holler et al., 2014). Furthermore, neuronal

BIN1 isoform 1, containing the CLAP domain, has been proposed to control tau aggregate entry into the cell through negative regulation of CME (Calafate et al., 2016). Therefore, a decrease in neuronal BIN1 isoform 1, as has been demonstrated in AD brains (Holler et al., 2014), may promote the propagation of tau pathology by increasing CME, thus promoting tau aggregate internalisation. Clearly, there are multiple mechanisms by which BIN1 may mediate risk in sAD, in part due to its multiple functions in different tissues. The current BIN1 literature fails to fully investigate the functional relevance of the different isoforms. The present study shows, for the first time, that the absence of the CLAP domain in brain endothelial BIN1 isoforms may account for an alternative role in this cell type and the apparent lack of involvement in CME. For future studies, it is highly important to establish which BIN1 isoforms are expressed in the cell type of interest because different regions of the protein account for different functional roles.

It must be acknowledged that, although this study suggests that BIN1 does not function in CME in BMECs, further work is required to confirm this. Firstly, the possibility of a compensatory mechanism involving AMPH1 was not fully elucidated in this study due to low expression levels in control hCMEC/D3 cells. While levels may have become detectable with BIN1-depletion, this was not investigated as it was deemed unlikely. Furthermore, a cargo-specific role for BIN1 in endocytic trafficking is also a possibility as analysis was limited to Tf, a well-regarded CME marker. Indeed, it has been demonstrated that depletion of PICALM in N2a cells did not affect transferrin uptake but resulted in a significant decrease in APP internalization, suggesting that the effect of PICALM on endocytosis is cargo-specific (Xiao et al., 2012). BIN1 may also have cargo-specific properties that would not have been revealed through analysis of transferrin trafficking. Although the results presented indicated no change in levels or localisation of APP with BIN1 depletion, future studies would include analysing the trafficking of specific cargo, such as APP.

7.4 BIN1 and Barrier Function

Beyond a possible role in APP processing, it would be interesting to investigate whether BIN1 is involved in maintaining the barrier function of BMECs. Evidence indicates a critical role for cerebrovascular dysfunction in AD and impairment of the BBB is thought to contribute to disease pathogenesis. Post-mortem studies in AD patients have shown

accumulation of blood-derived proteins in the hippocampus and cortex due to BBB breakdown in these regions (Zipser et al., 2007). While BBB breakdown occurs during normal ageing, it was shown to be more pronounced in individuals with MCI compared to age-matched controls, suggesting loss of BBB integrity may contribute to early cognitive impairment (Montagne et al., 2015). In addition to faulty BBB clearance of Aβ through deregulated LRP1/RAGE-mediated transport, previously discussed in Chapter 1, other transport mechanisms such as that involving glucose transporter 1 (GLUT1) have been implicated in AD (Winkler et al., 2015). GLUT1 is expressed at the BBB, in BMECs and astrocytes, but not in neurons and mediates glucose transport into the brain. Reduced GLUT1 levels have been reported in the cerebral microvessels of AD patients (Simpson et al., 1994). GLUT1 deficiency in the endothelium of mice overexpressing APP generates multiple parallel pathogenic mechanisms including diminished glucose uptake, microvasculature leakage, accelerated brain Aβ deposition and progressive neuronal loss (Winkler et al., 2015). The reduction in BBB GLUT1 expression may therefore exacerbate Alzheimer's disease cerebrovascular degeneration.

GLUT1 is internalised into mammalian cells by CIE (Eyster et al., 2009) and recycles via the Arf6 pathway, requiring Rab GTPases and receptor mediated endocytosis/Eps15 homology-domain containing 1 (RME-1/EHD1) family proteins (Chen et al., 2010). RME-1/EHD1 proteins, as key components of the recycling endosome, are involved in endosome-to-plasma membrane transport and have been shown to colocalise with AMPH1, the only amphiphysin gene in *C. elegans*. It is therefore possible that BIN1 could be involved in the endocytic transport of other BBB transport proteins, such as GLUT1, and could contribute to BBB dysfunction in AD in ways that are yet to be investigated. Perturbed endocytic recycling mechanisms could be crucial for the functionality of the BBB, particularly in maintaining its polarisation by ensuring the appropriate distribution of receptors at the apical and basolateral domains.

Indeed, BIN1 has recently been implicated in polarised endocytic trafficking in intestinal epithelial cells. Nakajo et al. (2016) identified a novel Rab8-binding protein complex involving Bin1, dynamin and EH domain-binding protein 1-like protein 1 (Ehbp1l1) which localises to the ERC and generates membrane tubules containing apical cargo proteins. In mouse intestinal organoids, siRNA-mediated depletion of BIN1 resulted in the missorting of apical proteins and induced the accumulation of apical but not basolateral membrane proteins in lysosomes (Nakajo et al., 2016). This study demonstrated a mechanism whereby

BIN1 was involved in the regulation of apical-directed transport in polarised cells and therefore provides rationale for establishing polarity to enable distinction between apical and basolateral domains when investigating BIN1 function in the hCMEC/D3 cell line. It is possible that BIN1 could be involved in apical/basolateral-specific transport in BMECs, which could go undetected in the present experimental design due to lack of established polarisation in culture. This may have an impact on barrier function by altering the protein composition of each membrane domain. Bin1 has been implicated in gut-immune barrier function whereby *Bin1* -/- mice exhibit higher transendothelial electrical resistance and decreased paracellular transepithelial flux compared to wild-types, resulting in suppression of experimental colitis (Chang et al., 2012). Bin1 was subsequently followed up as an immunotherapy target with altered expression of tight junction proteins in mice treated with Bin1 monoclonal antibody following experimentally-induced colitis (Thomas et al., 2016). This presents an interesting area for investigation at the BBB; whether BIN1 depletion affects the expression of tight junction proteins and endothelial barrier properties. The culture method used in the current project may not have been suitable for such studies as the inability to detect LRP1 in these cells suggested that relevant proteins may not have been expressed at endogenous levels. Analysis of barrier function would have required culturing BMECs in a manner to develop TJs and polarisation, further discussed in Section 7.5, and was unfortunately beyond the timeframe of this thesis.

Endothelial cells are considered a specialised type of epithelial cell that line the interior of blood vessels whereas epithelial cells line the cavity of tissues throughout the body. While endothelial cells lining the brain microvasculature may carry out a different function to peripheral endothelial/epithelial cells, both have defined basolateral and apical domains and are involved in barrier formation. When making comparisons between barriers of the CNS and the periphery, it is important to establish which BIN1 isoforms are expressed in each cell type as this can determine their function. Although very few studies detail the BIN1 isoforms expressed in the cells they are examining, DuHadaway et al. (2003) reported that rat intestinal epithelial cells appear to express the ubiquitous isoforms 9 and 10 in addition to the aberrant cancer isoform containing exon 12a. In the present study, these isoforms were also suggested to be expressed in the hCMEC/D3 cell line therefore the role of BIN1 polarised trafficking and/or barrier function in intestinal epithelial cells may also apply to BMECs and other tissues. Furthermore, in the study by Nakajo et al. (2016), the association between Bin1 and the Ehbp1l1 was mediated by the SH3 domain, which is

common to all BIN1 isoforms. Therefore, this involvement in apical-directed cargo transport may be a mechanism common to all BIN1 isoforms in polarised cells. This could have relevance for the BBB in AD as defective apical-directed transport in BMECs may alter the composition of receptors at the apical membrane which could impact transcytosis and barrier function of the BBB.

7.5 The hCMEC/D3 Cell Line as a BBB Model

The hCMEC/D3 cell line was used in the present study as it offers a well characterised, easy to use *in vitro* model of the human BBB. As the initial aim of this study was to investigate APP processing and basic endocytic function with BIN1 depletion, the cells were cultured as a monolayer on fibronectin-coated plates without the establishment of apical and basolateral domains. Many studies, however, have cultured hCMEC/D3 cells on semipermeable transwell filter inserts which mimic the blood (apical) side, whereas the well in which the insert sits mimics the brain (basolateral) side. The microporous membrane (0.4 μm) allows the exchange of small molecules and secreted growth factors between the two compartments. When cultured in this manner, endothelial cells are able to form a tight barrier, which is often measured by TEER and their permeability to hydrophilic molecules as paracellular permeability markers (Weksler et al., 2005). While the endocytic and recycling assays used in the present study can be considered an initial indicator of transcytosis in BMECs, adapting the culture method by utilising transwell inserts would offer the opportunity to investigate endocytic trafficking and transcytosis in a polarised context with BIN1 depletion. This adaptation was beyond the timeframe of the current project but is an important avenue for future research, investigating the potential role of BIN1 in barrier function of BMECs.

While the hCMEC/D3 cell line provides an easily accessible model for BBB studies, it has been suggested that BMECs are particularly affected by culturing in isolation, possibly due to the loss of their native environment within the NVU. A global transcriptome analysis which compared the hCMEC/D3 cell line with human primary BMECs and published analysis of freshly isolated mouse BECs identified a large proportion of probe sets showing different expression levels in hCMEC/D3 cells compared to human primary BMECs, with 2% probe sets exhibiting at least a 10-fold change (Daneman et al., 2010a). Most of the genes showing higher expression in hCMEC/D3 were involved in DNA repair, RNA

processing, mitosis and the immune/virus response, likely a consequence of the immortalization procedure. This transcriptomic analysis also revealed that TJ proteins, including Claudin-5, Occludin and JAM2 are expressed at low levels in comparison to freshly isolated mouse BMECs data while cell surface receptors LRP1 and RAGE are expressed at low levels in hCMEC/D3 cells, human primary BMECs and the freshly prepared mouse BMECs. Furthermore, the cultured cells in this study failed to maintain high levels of key BBB transporters such as SLC family members and ABC transporters. This data therefore suggests that BMECs lose their unique protein expression pattern outside of their native environment and display a more generic endothelial cell phenotype.

7.6 Alternative *in vitro* Models of the BBB

Many *in vitro* models of the BBB have been implemented to investigate drug permeation mechanisms however, to date, no unified method has been described for establishing a blood-brain barrier model. Many *in vitro* animal BBB models using primary or low passage porcine, bovine, rat or mouse cells generally report relatively high TEER values and low paracellular permeability (Helms et al., 2016). However, the isolation and purification procedure is time-consuming and produces minimal yields with a poor lifespan. Furthermore, differences in the expression of transporters and efflux pumps have been reported in animal BMECs compared to human (Uchida et al., 2011), rendering their relevance for the study of human disease uncertain. While some of the BBB-specific transporters and enzymes are expressed at much lower levels in immortalised cell lines, they have the advantage of an enhanced ability to proliferate in culture over primary models. For these reasons, an immortalised human cell line was used in the present study.

To better mimic the anatomic structure of the *in vivo* BBB, BMECs are often co-cultured with other cells, such as astrocytes and pericytes, that directly contribute to the barrier properties of BBB. A co-culture model whereby astrocytes were seeded to the underside of transwell filters and BMECs seeded on top, mimicking the structure of the NVU, resulted in significantly higher TEER than BMECs alone, directly reflecting increased structural integrity of the BBB (Wang et al., 2015). Another method by which improved barrier tightness has been achieved in culture is by subjecting hCMEC/D3 monolayers to physiological shear stress to mimic blood flow in a microfluidic device, which increased TEER approximately three-fold (Griep et al., 2013). This is because shear stress positively

affects endothelial cell physiology and tight junction formation (van der Meer et al., 2010). This has been extended with tissue engineering technology to develop *in vitro* 3D human vessels composed of a scaffold mesh with primary HUVECs, smooth muscle cells and astrocytes in a semi-pulsatile flow bioreactor system which have been used to model the BBB (Robert et al., 2017).

BBB models based on stem cell-derived endothelial cells have also started to emerge in the literature. Human ESC and iPSC-derived endothelial cells have demonstrated many BBB attributes including organised tight junctions, polarised transporter activity and TEER and molecular permeability that correlates well with *in vivo* brain uptake (Lippmann et al., 2012). Recently, Yamamizu et al. (2017) have designed a co-culture system with the four cell populations of the NVU, BMECS, pericytes, neurons and astrocytes, derived from human iPSCs. This not only provides a robust and reproducible human BBB model, expressing specific transporters and receptors and showing low permeability properties, but also allows the investigation of cell-cell interactions at the NVU which has so far been limited in *in vitro* studies.

7.7 Conclusions and Future Work

This thesis has investigated the role of BIN1, a sAD risk gene, in the novel context of brain endothelial cells that comprise the BBB. The findings that BIN1 depletion in hCMEC/D3 cells affects the amyloidogenic processing of APP but does not appear to impact on CME or recycling suggests an alternative role for BIN1 at the BBB to its role in endocytic trafficking previously reported in the literature in other cell types. Elucidation of the role of BIN1 in BMECs requires further investigation, particularly in light of an increase in CAV2 with BIN1 depletion but no apparent effect on CIE. Figure 7.1 summarises the working hypotheses as a result of this thesis which remain to be elucidated, including a role in CME that may have been compensated for in the present study. Although there is strong evidence for a role of BIN1 in endocytosis, other functions must be considered in the context of other brain cell types that may be involved in sAD pathogenesis. Of particular note is the predominant expression of BIN1 in oligodendrocytes and white matter in the brain (De Rossi et al., 2016). BIN1 cellular expression did not associate with neurofibrillary tangle pathology or senile plaques in AD brains, nor did it fit the overall distribution profiles of microglia, activated microglia, and astrocytes (De Rossi et al., 2017). Together

with evidence of differential expression of different BIN1 isoforms in the AD brain (Holler et al., 2014), these findings suggest that future research in the BIN1 field should involve elucidating isoform-specific functions in non-neuronal cell types in the brain. With regards to the present study, extending the experimental design to hCMEC/D3 cells cultured in a transwell assay for establishment of polarity has been cited as a future objective. Furthermore, this would allow an investigation of the role of BIN1 in barrier function of BMECs and this could be extended to the aforementioned alternative BBB models. It also remains to be elucidated whether the identified sAD risk variants 30kb upstream of the *BIN1* gene affect BIN1 isoform expression and a thorough analysis of this in different brain cell types would be important given the apparent varied function of BIN1 in the brain.

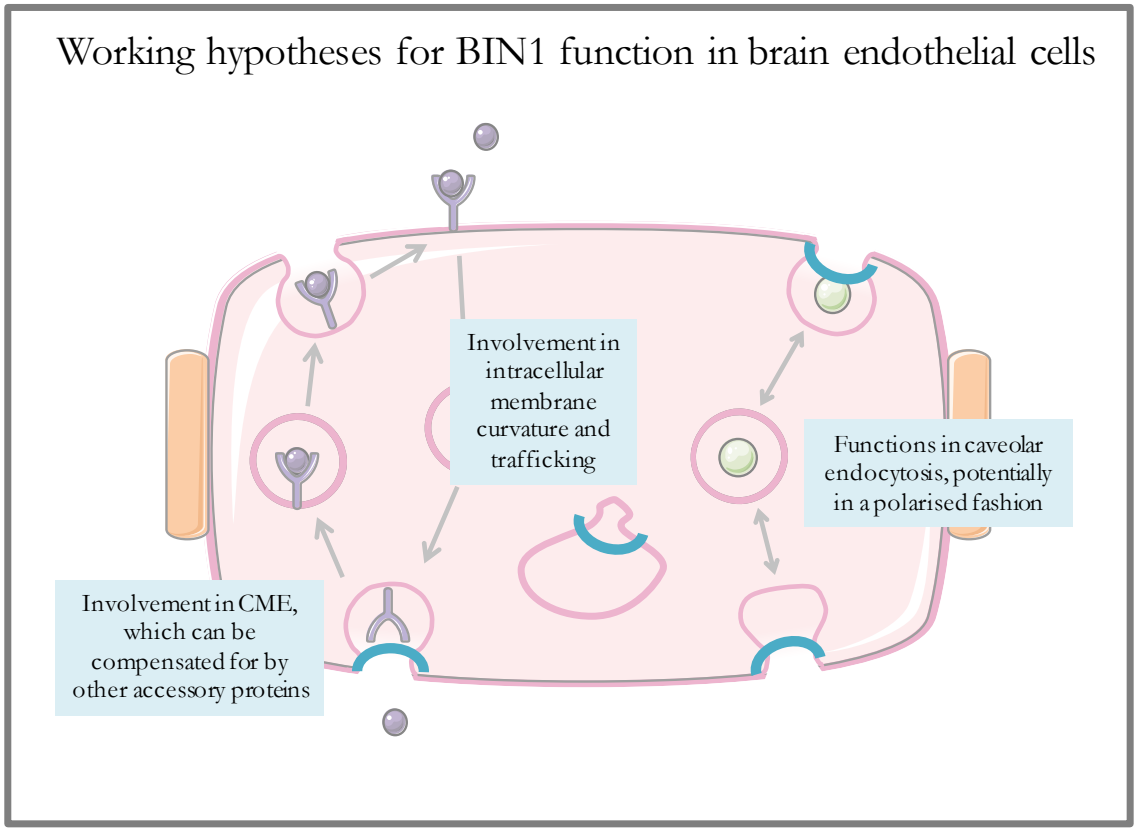

Figure 7.1: Working hypotheses on the potential role for BIN1 in brain endothelial cells as a result of the findings from this thesis

In conclusion, this thesis has shed new light on the possible role of BIN1 in APP processing and associated endocytic mechanisms in a novel *in vitro* context. The demonstration that BIN1 is not important for the normal functioning of CME suggests there may be other mechanisms by which it mediates sAD risk. AD is likely to be a multifactorial disease and BIN1 may act in combination with other risk factors to induce greater pathological effects than might be seen than in the present model. In the context of the currently available literature, it is clear that BIN1 is involved in diverse mechanisms within the brain, dependent on the cellular context, and much work still remains to identify the mechanisms by which BIN1 mediates its risk on sAD.

References

Abbott, N. J., Ronnback, L. and Hansson, E. 2006. Astrocyte-endothelial interactions at the blood-brain barrier. *Nat Rev Neurosci,* 7**,** 41-53.

Adams, S. L., Tilton, K., Kozubek, J. A., Seshadri, S. and Delalle, I. 2016. Subcellular Changes in Bridging Integrator 1 Protein Expression in the Cerebral Cortex During the Progression of Alzheimer Disease Pathology. *J Neuropathol Exp Neurol.* 75, 779-790.

Agosta, F., Vossel, K. A., Miller, B. L., Migliaccio, R., Bonasera, S. J., Filippi, M., et al. 2009. Apolipoprotein E epsilon4 is associated with disease-specific effects on brain atrophy in Alzheimer's disease and frontotemporal dementia. *Proc Natl Acad Sci USA,* 106**,** 2018-22.

Agu, C., Soares, F., Alderton, A., Patel, M., Ansari, R., Patel, S., et al. 2015. Successful Generation of Human Induced Pluripotent Stem Cell Lines from Blood Samples Held at Room Temperature for up to 48 hr. *Stem Cell Rep,* 5**,** 660-71.

Al Soraj, M., He, L., Peynshaert, K., Cousaert, J., Vercauteren, D., Braeckmans, K., et al. 2012. siRNA and pharmacological inhibition of endocytic pathways to characterize the differential role of macropinocytosis and the actin cytoskeleton on cellular uptake of dextran and cationic cell penetrating peptides octaarginine (R8) and HIV-Tat. *J Control Release,* 161**,** 132-41.

Alfalah, M., Jacob, R. and Naim, H. Y. 2002. Intestinal Dipeptidyl Peptidase IV Is Efficiently Sorted to the Apical Membrane through the Concerted Action of N- andO-Glycans as Well as Association with Lipid Microdomains. *J Bio Chem*, 277, 10683-90.

Allinquant, B., Moya, K., Bouillot, C. and Prochiantz, A. 1994. Amyloid precursor protein in cortical neurons: coexistence of two pools differentially distributed in axons and dendrites and association with cytoskeleton. *J Neurosci,* 14, 6842-54.

Alonso, A. D., Grundke-Iqbal, I., Barra, H. S. and Iqbal, K. 1997. Abnormal phosphorylation of tau and the mechanism of Alzheimer neurofibrillary degeneration: sequestration of microtubule-associated proteins 1 and 2 and the disassembly of microtubules by the abnormal tau. *Proc Natl Acad Sci USA,* 94**,** 298-303.

Alvarez, J. K., T. Prat, A. 2013. Glial influence on the blood brain barrier. *Glia,* 61**,** 1939-1958.

Alzheimer, A. 1907. Über eine eigenartige. Erkrankung der Hirnrinde. *Allgemeine Zeitschrift für Psychiatrie und Psychisch-Gerichtliche Medizin,* 64**,** 146-148.

Anders, A., Gilbert, S., Garten, W., Postina, R. and Fahrenholz, F. 2001. Regulation of the alpha-secretase ADAM10 by its prodomain and proprotein convertases. *FASEB J,* 15**,** 1837-9.

Andersen, O. M., Reiche, J., Schmidt, V., Gotthardt, M., Spoelgen, R., Behlke, J., et al. 2005. Neuronal sorting protein-related receptor sorLA/LR11 regulates processing of the amyloid precursor protein. *Proc Natl Acad Sci USA,* 102**,** 13461-6.

Andreone, B. J., Chow, B. W., Tata, A., Lacoste, B., Ben-Zvi, A., Bullock, K., et al. 2017. Blood-Brain Barrier Permeability Is Regulated by Lipid Transport-Dependent Suppression of Caveolae-Mediated Transcytosis. *Neuron,* 94**,** 581-94.

Arthur, J. R., Heinecke, K. A. and Seyfried, T. N. 2011. Filipin recognizes both GM1 and cholesterol in GM1 gangliosidosis mouse brain. *J Lipid Res*, 52, 1345-51.

Artus, C., Glacial, F., Ganeshamoorthy, K., Ziegler, N., Godet, M., Guilbert, T., et al. 2014. The Wnt/planar cell polarity signaling pathway contributes to the integrity of tight junctions in brain endothelial cells. *J Cereb Blood Flow Metab*, 34, 433-40.

Asai, M., Hattori, C., Szabo, B., Sasagawa, N., Maruyama, K., Tanuma, S., et al. 2003. Putative function of ADAM9, ADAM10, and ADAM17 as APP alpha-secretase. *Biochem Biophys Res Commun,* 301**,** 231-5.

Attems, J. and Jellinger, K. A. 2004. Only cerebral capillary amyloid angiopathy correlates with Alzheimer pathology--a pilot study. *Acta Neuropathol,* 107**,** 83-90.

Avilion, A. A., Nicolis, S. K., Pevny, L. H., Perez, L., Vivian, N. and Lovell-Badge, R. 2003. Multipotent cell lineages in early mouse development depend on SOX2 function. *Genes Dev,* 17**,** 126-40.

Baghbaderani, B. A., Syama, A., Sivapatham, R., Pei, Y., Mukherjee, O., Fellner, T., et al. 2016. Detailed Characterization of Human Induced Pluripotent Stem Cells Manufactured for Therapeutic Applications. *Stem Cell Rev,* 12**,** 394-420.

Balda, M. S., Whitney, J. A., Flores, C., Gonzalez, S., Cereijido, M. and Matter, K. 1996. Functional dissociation of paracellular permeability and transepithelial electrical resistance and disruption of the apical-basolateral intramembrane diffusion barrier by expression of a mutant tight junction membrane protein. *J Cell Biol,* 134**,** 1031-49.

Banks, W. A. and Broadwell, R. D. 1994. Blood to brain and brain to blood passage of native horseradish peroxidase, wheat germ agglutinin, and albumin: pharmacokinetic and morphological assessments. *J Neurochem*, 62, 2404-19.

Banks, W. A., Robinson, S. M., Verma, S. and Morley, J. E. 2003. Efflux of human and mouse amyloid beta proteins 1-40 and 1-42 from brain: impairment in a mouse model of Alzheimer's disease. *Neuroscience,* 121**,** 487-92.

Barrett, R., Ornelas, L., Yeager, N., Mandefro, B., Sahabian, A., Lenaeus, L., et al. 2014. Reliable generation of induced pluripotent stem cells from human lymphoblastoid cell lines. *Stem Cells Transl Med,* 3**,** 1429-34.

Bateman, R. J., Xiong, C., Benzinger, T. L., Fagan, A. M., Goate, A., Fox, N. C., et al. 2012. Clinical and biomarker changes in dominantly inherited Alzheimer's disease. *N Engl J Med,* 367**,** 795-804.

Beaulieu, E., Demeule, M., Ghitescu, L. and Béliveau, R. 1997. P-glycoprotein is strongly expressed in the luminal membranes of the endothelium of blood vessels in the brain. *Biochem J,* 326**,** 539-44.

Begley, D. J. 2007. Structure and function of the blood–brain barrier. *In:* Touitou, E., Barry, B.W. (ed.) *Enhancement in Drug Delivery*. Boca Raton: CRC Press.

Bendayan, R., Ronaldson, P. T., Gingras, D. and Bendayan, M. 2006. In situ localization of P-glycoprotein (ABCB1) in human and rat brain. *J Histochem Cytochem,* 54**,** 1159-67.

Bentahir, M., Nyabi, O., Verhamme, J., Tolia, A., Horre, K., Wiltfang, J., et al. 2006. Presenilin clinical mutations can affect gamma-secretase activity by different mechanisms. *J Neurochem,* 96**,** 732-42.

Bickel, P. E., Scherer, P. E., Schnitzer, J. E., Oh, P., Lisanti, M. P. and Lodish, H. F. 1997. Flotillin and epidermal surface antigen define a new family of caveolae-associated integral membrane proteins. *J Biol Chem*, 272, 13793-802.

Bitsikas, V., Riento, K., Howe, J. D., Barry, N. P. and Nichols, B. J. 2014. The role of flotillins in regulating abeta production, investigated using flotillin 1-/-, flotillin 2-/- double knockout mice. *PLoS One*, 9, e85217.

Boland, B. and Platt, F. M. 2015. Bridging the age spectrum of neurodegenerative storage diseases. *Best Pract Res Clin Endocrinol Metab*, 29, 127-43.

Boland, B., Smith, D. A., Mooney, D., Jung, S. S., Walsh, D. M. and Platt, F. M. 2010. Macroautophagy is not directly involved in the metabolism of amyloid precursor protein. *J Biol Chem*, 285, 37415-26.

Bomsel, M., Parton, R., Kuznetsov, S. A., Schroer, T. A. and Gruenberg, J. 1990. Microtubule- and motor-dependent fusion in vitro between apical and basolateral endocytic vesicles from MDCK cells. *Cell*, 62, 719-31.

Bonda, D. J., Mailankot, M., Stone, J. G., Garrett, M. R., Staniszewska, M., Castellani, R. J., et al. 2010. Indoleamine 2,3-dioxygenase and 3-hydroxykynurenine modifications are found in the neuropathology of Alzheimer's disease. *Redox Rep,* 15**,** 161-8.

Borchelt, D. R., Thinakaran, G., Eckman, C. B., Lee, M. K., Davenport, F., Ratovitsky, T., et al. 1996. Familial Alzheimer's disease-linked presenilin 1 variants elevate Abeta1-42/1-40 ratio in vitro and in vivo. *Neuron,* 17**,** 1005-13.

Boucrot, E., Saffarian, S., Zhang, R. and Kirchhausen, T. 2010. Roles of AP-2 in clathrin-mediated endocytosis. *PLoS One,* 5**,** e10597.

Braak, H. and Braak, E. 1991. Neuropathological stageing of Alzheimer-related changes. *Acta Neuropathol,* 82**,** 239-59.

Bradbury, M. W. 1997. Transport of iron in the blood-brain-cerebrospinal fluid system. *J Neurochem*, 69, 443-54.

Brendel, K., Meezan, E. and Carlson, E. C. 1974. Isolated brain microvessels: a purified, metabolically active preparation from bovine cerebral cortex. *Science,* 185**,** 953-5.

Brkic, M., Balusu, S., Van Wonterghem, E., Gorle, N., Benilova, I., Kremer, A., et al. 2015. Amyloid beta Oligomers Disrupt Blood-CSF Barrier Integrity by Activating Matrix Metalloproteinases. *J Neurosci,* 35**,** 12766-78.

Broeckhoven, C. V., Backhovens, H., Cruts, M., Winter, G. D., Bruyland, M., Cras, P., et al. 1992. Mapping of a gene predisposing to early|[ndash]|onset Alzheimer's disease to chromosome 14q24.3. *Nature Genet,* 2**,** 335-339.

Brown, D. A. and Rose, J. K. 1992. Sorting of GPI-anchored proteins to glycolipid-enriched membrane subdomains during transport to the apical cell surface. *Cell*, 68, 533-44.

Buerger, K., Ewers, M., Pirttila, T., Zinkowski, R., Alafuzoff, I., Teipel, S. J., et al. 2006. CSF phosphorylated tau protein correlates with neocortical neurofibrillary pathology in Alzheimer's disease. *Brain,* 129**,** 3035-41.

Buerger, K., Teipel, S. J., Zinkowski, R., Blennow, K., Arai, H., Engel, R., et al. 2002. CSF tau protein phosphorylated at threonine 231 correlates with cognitive decline in MCI subjects. *Neurology,* 59**,** 627-9.

Bungenberg, J., Surano, N., Grote, A., Surges, R., Pernhorst, K., Hofmann, A., et al. 2016. Gene expression variance in hippocampal tissue of temporal lobe epilepsy patients corresponds to differential memory performance. *Neurobiol Dis,* 86**,** 121-30.

Burns, M., Gaynor, K., Olm, V., Mercken, M., Lafrancois, J., Wang, L., et al. 2003. Presenilin redistribution associated with aberrant cholesterol transport enhances beta-amyloid production in vivo. *J Neurosci,* 23**,** 5645-9.

Bush, A. I., Martins, R. N., Rumble, B., Moir, R., Fuller, S., Milward, E., et al. 1990. The amyloid precursor protein of Alzheimer's disease is released by human platelets. *J Biol Chem,* 265**,** 15977-83.

Butler, M. H., David, C., Ochoa, G. C., Freyberg, Z., Daniell, L., Grabs, D., et al. 1997. Amphiphysin II (SH3P9; BIN1), a member of the amphiphysin/Rvs family, is concentrated in the cortical cytomatrix of axon initial segments and nodes of ranvier in brain and around T tubules in skeletal muscle. *J Cell Biol,* 137**,** 1355-67.

Butt, A. M., Jones, H. C. and Abbott, N. J. 1990. Electrical resistance across the blood-brain barrier in anaesthetized rats: a developmental study. *J Physiol,* 429**,** 47-62.

Buxbaum, J. D., Liu, K. N., Luo, Y., Slack, J. L., Stocking, K. L., Peschon, J. J., et al. 1998. Evidence that tumor necrosis factor alpha converting enzyme is involved in regulated alpha-secretase cleavage of the Alzheimer amyloid protein precursor. *J Biol Chem,* 273**,** 27765-7.

Bystron, I., Blakemore, C. and Rakic, P. 2008. Development of the human cerebral cortex: Boulder Committee revisited. *Nat Rev Neurosci,* 9**,** 110-22.

Cacace, R., Sleegers, K. and Van Broeckhoven, C. 2016. Molecular genetics of early-onset Alzheimer's disease revisited. *Alzheimers Dement,* 12**,** 733-48.

Calafate, S., Flavin, W., Verstreken, P. and Moechars, D. 2016. Loss of Bin1 Promotes the Propagation of Tau Pathology. *Cell Rep,* 17**,** 931-40.

Carey, R. M., Balcz, B. A., Lopez-Coviella, I. and Slack, B. E. 2005. Inhibition of dynamin-dependent endocytosis increases shedding of the amyloid precursor protein ectodomain and reduces generation of amyloid beta protein. *BMC Cell Biol,* 6**,** 30.

Casal, E., Federici, L., Zhang, W., Fernandez-Recio, J., Priego, E. M., Miguel, R. N., et al. 2006. The crystal structure of the BAR domain from human BIN1/ AMPHIPHYSIN II and its implications for molecular recognition†. *Biochemistry,* 45**,** 12917-28.

Castellano, J. M., Kim, J., Stewart, F. R., Jiang, H., Demattos, R. B., Patterson, B. W., et al. 2011. Human apoE isoforms differentially regulate brain amyloid-β peptide clearance. *Sci Transl Med,* 3**,** 89ra57.

Cataldo, A. M., Hamilton, D. J. and Nixon, R. A. 1994. Lysosomal abnormalities in degenerating neurons link neuronal compromise to senile plaque development in Alzheimer disease. *Brain Res*, 640, 68-80.

Cataldo, A. M., Peterhoff, C. M., Troncoso, J. C., Gomez-Isla, T., Hyman, B. T. and Nixon, R. A. 2000. Endocytic pathway abnormalities precede amyloid beta deposition in sporadic Alzheimer's disease and Down syndrome: differential effects of APOE genotype and presenilin mutations. *Am J Pathol,* 157**,** 277-86.

Caviness, V. S., Jr., Takahashi, T. and Nowakowski, R. S. 1995. Numbers, time and neocortical neuronogenesis: a general developmental and evolutionary model. *Trends Neurosci,* 18**,** 379-83.

Chambers, S. M., Fasano, C. A., Papapetrou, E. P., Tomishima, M., Sadelain, M. and Studer, L. 2009. Highly efficient neural conversion of human ES and iPS cells by dual inhibition of SMAD signaling. *Nat Biotechnology,* 27**,** 275-80.

Chandrasekaran, A., Varga, E., Nemes, C., Tancos, Z., Kobolak, J. and Dinnyes, A. 2016. Establishment of induced pluripotent stem cell (iPSC) line from a 63-year old patient with late onset Alzheimer's disease (LOAD). *Stem Cell Res,* 17**,** 78-80.

Chang, M. Y., Boulden, J., Katz, J. B., Wang, L., Meyer, T. J., Soler, A. P., et al. 2007. Bin1 ablation increases susceptibility to cancer during aging, particularly lung cancer. *Cancer Res,* 67**,** 7605-12.

Chang, M. Y., Boulden, J., Valenzano, M. C., Soler, A. P., Muller, A. J., Mullin, J. M., et al. 2012. Bin1 attenuation suppresses experimental colitis by enforcing intestinal barrier function. *Dig Dis Sci,* 57**,** 1813-21.

Chapuis, J., Hansmannel, F., Gistelinck, M., Mounier, A., Van Cauwenberghe, C., Kolen, K. V., et al. 2013. Increased expression of BIN1 mediates Alzheimer genetic risk by modulating tau pathology. *Mol Psychiatry,* 18**,** 1225-34.

Chavez-Gutierrez, L. 2013. Dissecting gamma-secretase function. *J Neurochem,* 125**,** 1-3.

Chen, B., Jiang, Y., Zeng, S., Yan, J., Li, X., Zhang, Y., et al. 2010. Endocytic sorting and recycling require membrane phosphatidylserine asymmetry maintained by TAT-1/CHAT-1. *PLoS Genet,* 6**,** e1001235.

Chen, C. S., Patterson, M. C., Wheatley, C. L., O'brien, J. F. and Pagano, R. E. 1999. Broad screening test for sphingolipid-storage diseases. *Lancet*, 354, 901-5.

Chen, I. P., Fukuda, K., Fusaki, N., Iida, A., Hasegawa, M., Lichtler, A., et al. 2013. Induced Pluripotent Stem Cell Reprogramming by Integration-Free Sendai Virus Vectors from Peripheral Blood of Patients with Craniometaphyseal Dysplasia. *Cell Reprogram,* 15**,** 503-13.

Choi, S. M., Liu, H., Chaudhari, P., Kim, Y., Cheng, L. Z., Feng, J., et al. 2011. Reprogramming of EBV-immortalized B-lymphocyte cell lines into induced pluripotent stem cells. *Blood,* 118**,** 1801-1805.

Choudhury, A., Sharma, D. K., Marks, D. L. and Pagano, R. E. 2004. Elevated endosomal cholesterol levels in Niemann-Pick cells inhibit rab4 and perturb membrane recycling. *Mol Biol Cell*, 15, 4500-11.

Cirrito, J. R., Deane, R., Fagan, A. M., Spinner, M. L., Parsadanian, M., Finn, M. B., et al. 2005. P-glycoprotein deficiency at the blood-brain barrier increases amyloid-beta deposition in an Alzheimer disease mouse model. *J Clin Invest,* 115**,** 3285-90.

Citron, M., Oltersdorf, T., Haass, C., Mcconlogue, L., Hung, A. Y., Seubert, P., et al. 1992. Mutation of the beta-amyloid precursor protein in familial Alzheimer's disease increases beta-protein production. *Nature,* 360**,** 672-4.

Coomber, B. L. and Stewart, P. A. 1986. Three-dimensional reconstruction of vesicles in endothelium of blood-brain barrier versus highly permeable microvessels. *Anat Rec*, 215, 256-61.

Corbo, R. M. and Scacchi, R. 1999. Apolipoprotein E (APOE) allele distribution in the world. Is APOE*4 a 'thrifty' allele? *Ann Hum Genet,* 63**,** 301-10.

Cordy, J. M., Hussain, I., Dingwall, C., Hooper, N. M. and Turner, A. J. 2003. Exclusively targeting beta-secretase to lipid rafts by GPI-anchor addition up-regulates beta-site processing of the amyloid precursor protein. *Proc Natl Acad Sci USA*, 100, 11735-40.

Cruts, M. 2017. AD&FTD Mutation Database [Online]. Available: http://www.molgen.ua.ac.be/ADMutations/ [Accessed 20th June 2017].

Damke, H., Baba, T., Warnock, D. E. and Schmid, S. L. 1994. Induction of mutant dynamin specifically blocks endocytic coated vesicle formation. *J Cell Biol,* 127**,** 915-34.

Daneman, R., Zhou, L., Agalliu, D., Cahoy, J. D., Kaushal, A. and Barres, B. A. 2010a. The mouse blood-brain barrier transcriptome: a new resource for understanding the development and function of brain endothelial cells. *PLoS One,* 5**,** e13741.

Daneman, R., Zhou, L., Kebede, A. A. and Barres, B. A. 2010b. Pericytes are required for blood–brain barrier integrity during embryogenesis. *Nature,* 468**,** 562-6.

Darocha-Souto, B., Scotton, T. C., Coma, M., Serrano-Pozo, A., Hashimoto, T., Serenó, L., et al. 2011. Brain Oligomeric β-Amyloid but Not Total Amyloid Plaque Burden Correlates With Neuronal Loss and Astrocyte Inflammatory Response in Amyloid Precursor Protein/Tau Transgenic Mice. *J Neuropathol Exp Neurol,* 70**,** 360-76.

Dautry-Varsat, A., Ciechanover, A. and Lodish, H. F. 1983. pH and the recycling of transferrin during receptor-mediated endocytosis. *Proc Natl Acad Sci* U S A, 80, 2258-62.

David, C., Mcpherson, P. S., Mundigl, O. and De Camilli, P. 1996. A role of amphiphysin in synaptic vesicle endocytosis suggested by its binding to dynamin in nerve terminals. *Proc Natl Acad Sci U S A,* 93**,** 331-5.

De Felice, F. G., Wu, D., Lambert, M. P., Fernandez, S. J., Velasco, P. T., Lacor, P. N., et al. 2008. Alzheimer's disease-type neuronal tau hyperphosphorylation induced by A beta oligomers. *Neurobiol Aging,* 29**,** 1334-47.

De Jager, P. L., Srivastava, G., Lunnon, K., Burgess, J., Schalkwyk, L. C., Yu, L., et al. 2014. Alzheimer's disease: early alterations in brain DNA methylation at ANK1, BIN1, RHBDF2 and other loci. *Nat Neurosci,* 17**,** 1156-63.

De Jonghe, C., Esselens, C., Kumar-Singh, S., Craessaerts, K., Serneels, S., Checler, F., et al. 2001. Pathogenic APP mutations near the gamma-secretase cleavage site differentially affect Abeta secretion and APP C-terminal fragment stability. *Hum Mol Genet,* 10**,** 1665-71.

De Rossi, P., Buggia-Prevot, V., Andrew, R. J., Krause, S. V., Woo, E., Nelson, P. T., et al. 2017. BIN1 localization is distinct from Tau tangles in Alzheimer's disease. *Science Matters*.

De Rossi, P., Buggia-Prévot, V., Clayton, B. L. L., Vasquez, J. B., Van Sanford, C., Andrew, R. J., et al. 2016. Predominant expression of Alzheimer's disease-associated BIN1 in mature oligodendrocytes and localization to white matter tracts. *Mol Neurodegener,* 11.

De Strooper, B. 2003. Aph-1, Pen-2, and Nicastrin with Presenilin generate an active gamma-Secretase complex. *Neuron,* 38**,** 9-12.

Deane, R., Du Yan, S., Submamaryan, R. K., Larue, B., Jovanovic, S., Hogg, E., et al. 2003. RAGE mediates amyloid-beta peptide transport across the blood-brain barrier and accumulation in brain. *Nat Med,* 9**,** 907-13.

Deane, R., Singh, I., Sagare, A. P., Bell, R. D., Ross, N. T., Larue, B., et al. 2012. A multimodal RAGE-specific inhibitor reduces amyloid β–mediated brain disorder in a mouse model of Alzheimer disease. *J Clin Invest,* 122**,** 1377-92.

Derosa, B. A., Van Baaren, J. M., Dubey, G. K., Lee, J. M., Cuccaro, M. L., Vance, J. M., et al. 2012. Derivation of autism spectrum disorder-specific induced pluripotent stem cells from peripheral blood mononuclear cells. *Neurosci Lett,* 516**,** 9-14.

Desai, M. K., Mastrangelo, M. A., Ryan, D. A., Sudol, K. L., Narrow, W. C. and Bowers, W. J. 2010. Early Oligodendrocyte/Myelin Pathology in Alzheimer's Disease Mice Constitutes a Novel Therapeutic Target. *Am J Pathol,* 177**,** 1422-35.

Descamps, L., Dehouck, M. P., Torpier, G. and Cecchelli, R. 1996. Receptor-mediated transcytosis of transferrin through blood-brain barrier endothelial cells. *Am J Physiol*, 270, 1149-58.

Devraj, K., Poznanovic, S., Spahn, C., Schwall, G., Harter, P. N., Mittelbronn, M., et al. 2016. BACE-1 is expressed in the blood-brain barrier endothelium and is upregulated in a murine model of Alzheimer's disease. *J Cereb Blood Flow Metab,* 36**,** 1281-94.

Di Paolo, G., Sankaranarayanan, S., Wenk, M. R., Daniell, L., Perucco, E., Caldarone, B. J., et al. 2002. Decreased synaptic vesicle recycling efficiency and cognitive deficits in amphiphysin 1 knockout mice. *Neuron,* 33**,** 789-804.

Dickerson, B. C., Bakkour, A., Salat, D. H., Feczko, E., Pacheco, J., Greve, D. N., et al. 2009. The Cortical Signature of Alzheimer's Disease: Regionally Specific Cortical Thinning Relates to Symptom Severity in Very Mild to Mild AD Dementia and is Detectable in Asymptomatic Amyloid-Positive Individuals. *Cereb Cortex,* 19**,** 497-510.

Dickerson, B. C., Stoub, T. R., Shah, R. C., Sperling, R. A., Killiany, R. J., Albert, M. S., et al. 2011. Alzheimer-signature MRI biomarker predicts AD dementia in cognitively normal adults. *Neurology,* 76**,** 1395-402.

Doherty, G. J. and Mcmahon, H. T. 2009. Mechanisms of endocytosis. *Annu Rev Biochem*, 78, 857-902.

Duhadaway, J. B., Lynch, F. J., Brisbay, S., Bueso-Ramos, C., Troncoso, P., Mcdonnell, T., et al. 2003. Immunohistochemical analysis of Bin1/Amphiphysin II in human tissues: diverse sites of nuclear expression and losses in prostate cancer. *J Cell Biochem,* 88**,** 635-42.

Duvar, S., Suzuki, M., Muruganandam, A. and Yu, R. K. 2000. Glycosphingolipid composition of a new immortalized human cerebromicrovascular endothelial cell line. *J Neurochem*, 75, 1970-6.

Ebnet, K., Suzuki, A., Ohno, S. and Vestweber, D. 2004. Junctional adhesion molecules (JAMs): more molecules with dual functions? *J Cell Sci,* 117**,** 19-29.

Edgar, A. J. and Polak, J. M. 2001. Flotillin-1: gene structure: cDNA cloning from human lung and the identification of alternative polyadenylation signals. *Int J Biochem Cell Biol*, 33, 53-64.

Ehehalt, R., Keller, P., Haass, C., Thiele, C. and Simons, K. 2003. Amyloidogenic processing of the Alzheimer β-amyloid precursor protein depends on lipid rafts. *J Cell Biol,* 160**,** 113-23.

Ehrlich, M., Boll, W., Van Oijen, A., Hariharan, R., Chandran, K., Nibert, M. L., et al. 2004. Endocytosis by random initiation and stabilization of clathrin-coated pits. *Cell,* 118**,** 591-605.

Eisele, Y. S., Obermüller, U., Heilbronner, G., Baumann, F., Kaeser, S. A., Wolburg, H., et al. 2010. Peripherally Applied Aβ-Containing Inoculates Induce Cerebral β-Amyloidosis. *Science,* 330**,** 980-2.

Eker, P., Holm, P. K., Van Deurs, B. and Sandvig, K. 1994. Selective regulation of apical endocytosis in polarized Madin-Darby canine kidney cells by mastoparan and cAMP. *J Biol Chem,* 269**,** 18607-15.

El Hokayem, J., Cukier, H. N. and Dykxhoorn, D. M. 2016. Blood Derived Induced Pluripotent Stem Cells (iPSCs): Benefits, Challenges and the Road Ahead. *J Alzheimers Dis Parkinsonism,* 6.

Elliott, K., Sakamuro, D., Basu, A., Du, W., Wunner, W., Staller, P., et al. 1999. Bin1 functionally interacts with Myc and inhibits cell proliferation via multiple mechanisms. *Oncogene,* 18**,** 3564-73.

Ellis, J. D., Barrios-Rodiles, M., Colak, R., Irimia, M., Kim, T., Calarco, J. A., et al. 2012. Tissue-specific alternative splicing remodels protein-protein interaction networks. *Mol Cell,* 46**,** 884-92.

Erickson, M. A. and Banks, W. A. 2013. Blood-brain barrier dysfunction as a cause and consequence of Alzheimer's disease. *J Cereb Blood Flow Metab*, 33, 1500-13.

Erickson, M. A., Hansen, K. and Banks, W. A. 2012. Inflammation-induced dysfunction of the low-density lipoprotein receptor-related protein-1 at the blood-brain barrier: protection by the antioxidant N-acetylcysteine. *Brain Behav Immun,* 26**,** 1085-94.

Erten-Lyons, D., Woltjer, R. L., Dodge, H., Nixon, R., Vorobik, R., Calvert, J. F., et al. 2009. Factors associated with resistance to dementia despite high Alzheimer disease pathology. *Neurology,* 72**,** 354-60.

Escott-Price, V., Bellenguez, C., Wang, L. S., Choi, S. H., Harold, D., Jones, L., et al. 2014. Gene-Wide Analysis Detects Two New Susceptibility Genes for Alzheimer's Disease. *PLoS One,* 9.

Escott-Price, V., Sims, R., Bannister, C., Harold, D., Vronskaya, M., Majounie, E., et al. 2015. Common polygenic variation enhances risk prediction for Alzheimer's disease. *Brain,* 138**,** 3673-84.

Esparza, T. J., Zhao, H., Cirrito, J. R., Cairns, N. J., Bateman, R. J., Holtzman, D. M., et al. 2013. Amyloid-beta oligomerization in Alzheimer dementia versus high-pathology controls. *Ann Neurol,* 73**,** 104-19.

Espuny-Camacho, I., Michelsen, K. A., Gall, D., Linaro, D., Hasche, A., Bonnefont, J., et al. 2013. Pyramidal Neurons Derived from Human Pluripotent Stem Cells Integrate Efficiently into Mouse Brain Circuits In Vivo. *Neuron,* 77**,** 440-456.

Evans, M. J., Kaufman, M.H. 1981. Establishment in culture of pluripotential cells from mouse embryos. *Nature,* 292**,** 154-6.

Eyster, C. A., Higginson, J. D., Huebner, R., Porat-Shliom, N., Weigert, R., Wu, W. W., et al. 2009. Discovery of new cargo proteins that enter cells through clathrin-independent endocytosis. *Traffic,* 10**,** 590-9.

Fanning, A. S., Jameson, B. J., Jesaitis, L. A. and Anderson, J. M. 1998. The tight junction protein ZO-1 establishes a link between the transmembrane protein occludin and the actin cytoskeleton. *J Biol Chem,* 273**,** 29745-53.

Farrer, L. A., Cupples, L. A., Haines, J. L., Hyman, B., Kukull, W. A., Mayeux, R., et al. 1997. Effects of age, sex, and ethnicity on the association between apolipoprotein E genotype and Alzheimer disease. A meta-analysis. APOE and Alzheimer Disease Meta Analysis Consortium. *JAMA,* 278**,** 1349-56.

Fede, G. D., Catania, M., Morbin, M., Rossi, G., Suardi, S., Mazzoleni, G., et al. 2009. A Recessive Mutation in the APP Gene with Dominant-Negative Effect on Amyloidogenesis. *Science,* 323**,** 1473-1477.

Ferrer, I., Marti, E., Tortosa, A. and Blasi, J. 1998. Dystrophic neurites of senile plaques are defective in proteins involved in exocytosis and neurotransmission. *J Neuropathol Exp Neurol,* 57**,** 218-25.

Fishman, J. B., Rubin, J. B., Handrahan, J. V., Connor, J. R. and Fine, R. E. 1987. Receptor-mediated transcytosis of transferrin across the blood-brain barrier. *J Neurosci Res*, 18, 299-304.

Folstein, M. F., Folstein, S. E. and Mchugh, P. R. 1975. "Mini-mental state". A practical method for grading the cognitive state of patients for the clinician. *J Psychiatr Res,* 12**,** 189-98.

Forloni, G., Demicheli, F., Giorgi, S., Bendotti, C. and Angeretti, N. 1992. Expression of amyloid precursor protein mRNAs in endothelial, neuronal and glial cells: modulation by interleukin-1. *Brain Res Mol Brain Res,* 16**,** 128-34.

Fra, A. M., Masserini, M., Palestini, P., Sonnino, S. and Simons, K. 1995. A photo-reactive derivative of ganglioside GM1 specifically cross-links VIP21-caveolin on the cell surface. *FEBS Lett*, 375, 11-4.

Fraser, L., Karlsberg Schaffer, S., Sussex, J., O'neill, P. and Cockcroft, L. 2014. The Trajectory of Dementia in the UK - Making a Difference. Report for Alzheimer's Research UK by OHE Consulting. London: Office of Health Economics.

Francis, P. T., Sims, N. R., Procter, A. W. and Bowen, D. M. 1993. Cortical pyramidal neurone loss may cause glutamatergic hypoactivity and cognitive impairment in Alzheimer's disease: investigative and therapeutic perspectives. *J Neurochem,* 60**,** 1589-604.

Frick, M., Bright, N. A., Riento, K., Bray, A., Merrified, C. and Nichols, B. J. 2007. Coassembly of flotillins induces formation of membrane microdomains, membrane curvature, and vesicle budding. *Curr Biol*, 17, 1151-6.

Furukawa, K., Sopher, B. L., Rydel, R. E., Begley, J. G., Pham, D. G., Martin, G. M., et al. 1996. Increased activity-regulating and neuroprotective efficacy of alpha-secretase-derived secreted amyloid precursor protein conferred by a C-terminal heparin-binding domain. *J Neurochem,* 67**,** 1882-96.

Fusaki, N., Ban, H., Nishiyama, A., Saeki, K. and Hasegawa, M. 2009. Efficient induction of transgene-free human pluripotent stem cells using a vector based on Sendai virus, an RNA virus that does not integrate into the host genome. *Proc Jpn Acad Ser B Phys Biol Sci,* 85**,** 348-62.

Galbiati, F., Volonte, D., Gil, O., Zanazzi, G., Salzer, J. L., Sargiacomo, M., et al. 1998. Expression of caveolin-1 and -2 in differentiating PC12 cells and dorsal root ganglion neurons: caveolin-2 is up-regulated in response to cell injury. *Proc Natl Acad Sci USA*, 95, 10257-62.

Gandy, S., Simon, A. J., Steele, J. W., Lublin, A. L., Lah, J. J., Walker, L. C., et al. 2010. Days to criterion as an indicator of toxicity associated with human Alzheimer amyloid-beta oligomers. *Ann Neurol,* 68**,** 220-30.

Gatz, M., Reynolds, C. A., Fratiglioni, L., Johansson, B., Mortimer, J. A., Berg, S., et al. 2006. Role of Genes and Environments for Explaining Alzheimer Disease. *Archives of General Psychiatry,* 63**,** 168-174.

Ge, K., Duhadaway, J., Du, W., Herlyn, M., Rodeck, U. and Prendergast, G. C. 1999. Mechanism for elimination of a tumor suppressor: Aberrant splicing of a brain-specific exon causes loss of function of Bin1 in melanoma. *Proc Natl Acad Sci USA,* 96**,** 9689-94.

Genin, E., Hannequin, D., Wallon, D., Sleegers, K., Hiltunen, M., Combarros, O., et al. 2011. APOE and Alzheimer disease: a major gene with semi-dominant inheritance. *Mol Psychiatry,* 16**,** 903-7.

Ginsberg, S. D., Alldred, M. J., Counts, S. E., Cataldo, A. M., Neve, R. L., Jiang, Y., et al. 2010. Microarray analysis of hippocampal CA1 neurons implicates early endosomal dysfunction during Alzheimer's disease progression. *Biol Psychiatry,* 68**,** 885-93.

Glebov, O. O., Bright, N. A. and Nichols, B. J. 2006. Flotillin-1 defines a clathrin-independent endocytic pathway in mammalian cells. *Nat Cell Biol,* 8**,** 46-54.

Glennon, E. B., Whitehouse, I. J., Miners, J. S., Kehoe, P. G., Love, S., Kellett, K. A., et al. 2013. BIN1 is decreased in sporadic but not familial Alzheimer's disease or in aging. *PLoS One,* 8**,** e78806.

Goate, A., Chartier-Harlin, M.-C., Mullan, M., Brown, J., Crawford, F., Fidani, L., et al. 1991. Segregation of a missense mutation in the amyloid precursor protein gene with familial Alzheimer's disease. *Nature,* 349**,** 704-706.

Goedert, M., Jakes, R., Crowther, R. A., Cohen, P., Vanmechelen, E., Vandermeeren, M., et al. 1994. Epitope mapping of monoclonal antibodies to the paired helical filaments of Alzheimer's disease: identification of phosphorylation sites in tau protein. *Biochem J,* 301**,** 871-7.

Gold, E. S., Morrissette, N. S., Underhill, D. M., Guo, J., Bassetti, M. and Aderem, A. 2000. Amphiphysin IIm, a novel amphiphysin II isoform, is required for macrophage phagocytosis. *Immunity*, 12, 285-92.

Gonzalez, E., Nagiel, A., Lin, A. J., Golan, D. E. and Michel, T. 2004. Small interfering RNA-mediated down-regulation of caveolin-1 differentially modulates signaling pathways in endothelial cells. *J Biol Chem*, 279, 40659-69.

Gorvel, J. P., Chavrier, P., Zerial, M. and Gruenberg, J. 1991. rab5 controls early endosome fusion in vitro. *Cell,* 64**,** 915-25.

Grabs, D., Slepnev, V. I., Songyang, Z., David, C., Lynch, M., Cantley, L. C., et al. 1997. The SH3 domain of amphiphysin binds the proline-rich domain of dynamin at a single site that defines a new SH3 binding consensus sequence. *J Biol Chem,* 272**,** 13419-25.

Grant, B. D. and Donaldson, J. G. 2009. Pathways and mechanisms of endocytic recycling. *Nat Rev Mol Cell Biol,* 10**,** 597-608.

Grbovic, O. M., Mathews, P. M., Jiang, Y., Schmidt, S. D., Dinakar, R., Summers-Terio, N. B., et al. 2003. Rab5-stimulated up-regulation of the endocytic pathway increases intracellular beta-cleaved amyloid precursor protein carboxyl-terminal fragment levels and Abeta production. *J Biol Chem,* 278**,** 31261-8.

Greener, T., Zhao, X., Nojima, H., Eisenberg, E. and Greene, L. E. 2000. Role of cyclin G-associated kinase in uncoating clathrin-coated vesicles from non-neuronal cells. *J Biol Chem,* 275**,** 1365-70.

Griep, L. M., Wolbers, F., De Wagenaar, B., Ter Braak, P. M., Weksler, B. B., Romero, I. A., et al. 2013. BBB on chip: microfluidic platform to mechanically and biochemically modulate blood-brain barrier function. *Biomed Microdevices,* 15**,** 145-50.

Groppe, J., Greenwald, J., Wiater, E., Rodriguez-Leon, J., Economides, A. N., Kwiatkowski, W., et al. 2002. Structural basis of BMP signalling inhibition by the cystine knot protein Noggin. *Nature,* 420**,** 636-42.

Grundke-Iqbal, I., Iqbal, K., Tung, Y. C., Quinlan, M., Wisniewski, H. M. and Binder, L. I. 1986. Abnormal phosphorylation of the microtubule-associated protein tau (tau) in Alzheimer cytoskeletal pathology. *Proc Natl Acad Sci USA,* 83**,** 4913-7.

Guerreiro, R., Wojtas, A., Bras, J., Carrasquillo, M., Rogaeva, E., Majounie, E., et al. 2013. TREM2 Variants in Alzheimer's Disease. *New England Journal of Medicine,* 368**,** 117-127.

Guillot, F. L., Audus, K. L. and Raub, T. J. 1990. Fluid-phase endocytosis by primary cultures of bovine brain microvessel endothelial cell monolayers. *Microvasc Res*, 39, 1-14.

Guillozet, A. L., Weintraub, S., Mash, D. C. and Mesulam, M. M. 2003. Neurofibrillary tangles, amyloid, and memory in aging and mild cognitive impairment. *Arch Neurol,* 60**,** 729-36.

Hankey, G., Wardlaw, J. 2008. Clinical Neurology, Florida, USA, CRC Press.

Hansen, C. G. and Nichols, B. J. 2009. Molecular mechanisms of clathrin-independent endocytosis. *J Cell Sci*, 122, 1713-21.

Haqqani, A. S., Delaney, C. E., Tremblay, T. L., Sodja, C., Sandhu, J. K. and Stanimirovic, D. B. 2013. Method for isolation and molecular characterization of extracellular microvesicles released from brain endothelial cells. *Fluids Barriers CNS*, 10, 4.

Hardy, J. and Allsop, D. 1991. Amyloid deposition as the central event in the aetiology of Alzheimer's disease. *Trends Pharmacol Sci,* 12**,** 383-8.

Hardy, J., Higgins, G. A. 1992. Alzheimer's Disease: The Amyloid Cascade Hypothesis. *Science,* 256**,** 184-5.

Hardy, J., Duff, K., Hardy, K. G., Perez-Tur, J. and Hutton, M. 1998. Genetic dissection of Alzheimer's disease and related dementias: amyloid and its relationship to tau. *Nat Neurosci,* 1**,** 355-8.

Hardy, J. and Selkoe, D. J. 2002. The amyloid hypothesis of Alzheimer's disease: progress and problems on the road to therapeutics. *Science,* 297**,** 353-6.

Hardy, J. 2006. Alzheimer's disease: the amyloid cascade hypothesis: an update and reappraisal. *J Alzheimers Dis,* 9**,** 151-3.

Harold, D., Abraham, R., Hollingworth, P., Sims, R., Gerrish, A., Hamshere, M. L., et al. 2009. Genome-wide association study identifies variants at CLU and PICALM associated with Alzheimer's disease. *Nature Genetics,* 41**,** 1088-U61.

Hartz, A. M., Miller, D. S. and Bauer, B. 2010. Restoring blood-brain barrier P-glycoprotein reduces brain amyloid-beta in a mouse model of Alzheimer's disease. *Mol Pharmacol,* 77**,** 715-23.

Hayer, A., Stoeber, M., Ritz, D., Engel, S., Meyer, H. H. and Helenius, A. 2010. Caveolin-1 is ubiquitinated and targeted to intralumenal vesicles in endolysosomes for degradation. *J Cell Biol*, 191, 615-29.

Helms, H. C., Abbott, N. J., Burek, M., Cecchelli, R., Couraud, P. O., Deli, M. A., et al. 2016. In vitro models of the blood-brain barrier: An overview of commonly used brain endothelial cell culture models and guidelines for their use. *J Cereb Blood Flow Metab.* 36, 862-90

Hemmati-Brivanlou, A. and Melton, D. A. 1994. Inhibition of activin receptor signaling promotes neuralization in Xenopus. *Cell,* 77**,** 273-81.

Hendry, S. H., Schwark, H. D., Jones, E. G. and Yan, J. 1987. Numbers and proportions of GABA-immunoreactive neurons in different areas of monkey cerebral cortex. *J Neurosci,* 7**,** 1503-19.

Henne, W. M., Boucrot, E., Meinecke, M., Evergren, E., Vallis, Y., Mittal, R., et al. 2010. FCHo Proteins are Nucleators of Clathrin-Mediated Endocytosis. *Science,* 328**,** 1281-4.

Hentze, H., Soong, P. L., Wang, S. T., Phillips, B. W., Putti, T. C. and Dunn, N. R. 2009. Teratoma formation by human embryonic stem cells: evaluation of essential parameters for future safety studies. *Stem Cell Res,* 2**,** 198-210.

Herreman, A., Hartmann, D., Annaert, W., Saftig, P., Craessaerts, K., Serneels, L., et al. 1999. Presenilin 2 deficiency causes a mild pulmonary phenotype and no changes in amyloid precursor protein processing but enhances the embryonic lethal phenotype of presenilin 1 deficiency. *Proc Natl Acad Sci USA,* 96**,** 11872-7.

Hirst, J., Barlow, L. D., Francisco, G. C., Sahlender, D. A., Seaman, M. N., Dacks, J. B., et al. 2011. The fifth adaptor protein complex. *PLoS Biol,* 9**,** e1001170.

Ho, L., Fukuchi, K. and Younkin, S. G. 1996. The alternatively spliced Kunitz protease inhibitor domain alters amyloid beta protein precursor processing and amyloid beta protein production in cultured cells. *J Biol Chem,* 271**,** 30929-34.

Holler, C. J., Davis, P. R., Beckett, T. L., Platt, T. L., Webb, R. L., Head, E., et al. 2014. Bridging integrator 1 (BIN1) protein expression increases in the Alzheimer's disease brain and correlates with neurofibrillary tangle pathology. *J Alzheimers Dis,* 42**,** 1221-7.

Hollingworth, P., Harold, D., Sims, R., Gerrish, A., Lambert, J. C., Carrasquillo, M. M., et al. 2011. Common variants at ABCA7, MS4A6A/MS4A4E, EPHA1, CD33 and CD2AP are associated with Alzheimer's disease. *Nature Genet,* 43**,** 429-35.

Holtta, M., Hansson, O., Andreasson, U., Hertze, J., Minthon, L., Nagga, K., et al. 2013. Evaluating amyloid-beta oligomers in cerebrospinal fluid as a biomarker for Alzheimer's disease. *PLoS One,* 8**,** e66381.

Hoop, C. L., Sivanandam, V. N., Kodali, R., Srnec, M. N. and Van Der Wel, P. C. A. 2012. Structural Characterization of the Caveolin Scaffolding Domain in Association with Cholesterol-Rich Membranes. *Biochemistry*, 51, 90-9.

Hu, Y. B., Dammer, E. B., Ren, R. J. and Wang, G. 2015. The endosomal-lysosomal system: from acidification and cargo sorting to neurodegeneration. *Transl Neurodegener,* 4.

Iacopetta, B. J. and Morgan, E. H. 1983. The kinetics of transferrin endocytosis and iron uptake from transferrin in rabbit reticulocytes. *J Biol Chem*, 258, 9108-15.

Ikezu, T., Trapp, B. D., Song, K. S., Schlegel, A., Lisanti, M. P. and Okamoto, T. 1998a. Caveolae, plasma membrane microdomains for alpha-secretase-mediated processing of the amyloid precursor protein. *J Biol Chem*, 273, 10485-95.

Ikezu, T., Ueda, H., Trapp, B. D., Nishiyama, K., Sha, J. F., Volonte, D., et al. 1998b. Affinity-purification and characterization of caveolins from the brain: differential expression of caveolin-1, -2, and -3 in brain endothelial and astroglial cell types. *Brain Res*, 804, 177-92.

Ikonen, E. 2008. Cellular cholesterol trafficking and compartmentalization. *Nat Rev Mol Cell Biol*, 9, 125-38.

Ilina, P., Partti, S., Niklander, J., Ruponen, M., Lou, Y. R. and Yliperttula, M. 2015. Effect of differentiation on endocytic profiles of endothelial and epithelial cell culture models. *Exp Cell Res*, 332, 89-101.

Israel, M. A., Yuan, S. H., Bardy, C., Reyna, S. M., Mu, Y. L., Herrera, C., et al. 2012. Probing sporadic and familial Alzheimer's disease using induced pluripotent stem cells. *Nature,* 482**,** 216-U107.

Jack, C. R., Jr., Petersen, R. C., O'brien, P. C. and Tangalos, E. G. 1992. MR-based hippocampal volumetry in the diagnosis of Alzheimer's disease. *Neurology,* 42**,** 183-8.

Jaeger, L. B., Dohgu, S., Hwang, M. C., Farr, S. A., Murphy, M. P., Fleegal-Demotta, M. A., et al. 2009. Testing the neurovascular hypothesis of Alzheimer's disease: LRP-1 antisense reduces blood-brain barrier clearance, increases brain levels of amyloid-beta protein, and impairs cognition. *J Alzheimers Dis,* 17**,** 553-70.

Janzer, R.C. and Raff, M.C. 1987. Astrocytes induce blood-brain barrier properties in endothelial cells. *Nature,* 325**,** 253-7.

Jarrett, J. T., Berger, E. P. and Lansbury, P. T., Jr. 1993. The carboxy terminus of the beta amyloid protein is critical for the seeding of amyloid formation: implications for the pathogenesis of Alzheimer's disease. *Biochemistry,* 32**,** 4693-7.

Jefferies, W. A., Brandon, M. R., Hunt, S. V., Williams, A. F., Gatter, K. C. and Mason, D. Y. 1984. Transferrin receptor on endothelium of brain capillaries. *Nature* 312, 162-163.

Jiang, Y., Mullaney, K. A., Peterhoff, C. M., Che, S., Schmidt, S. D., Boyer-Boiteau, A., et al. 2010. Alzheimer's-related endosome dysfunction in Down syndrome is Abeta-independent but requires APP and is reversed by BACE-1 inhibition. *Proc Natl Acad Sci USA,* 107**,** 1630-5.

John, B. A., Meister, M., Banning, A. and Tikkanen, R. 2014. Flotillins bind to the dileucine sorting motif of beta-site amyloid precursor protein-cleaving enzyme 1 and influence its endosomal sorting. *FEBS J*, 281, 2074-87.

Johnson, D. E., Ostrowski, P., Jaumouillé, V. and Grinstein, S. 2016. The position of lysosomes within the cell determines their luminal pH. *J Cell Biol*, 212, 677-92.

Jones, L., Lambert, J., Wang, L., Choi, S., Harold, D., Vedernikov, A., et al. 2015. Convergent genetic and expression data implicate immunity in Alzheimer's disease. *Alzheimers Dement,* 11**,** 658-71.

Jones, V. C., Atkinson-Dell, R., Verkhratsky, A. and Mohamet, L. 2017. Aberrant iPSC-derived human astrocytes in Alzheimer's disease. *Cell Death Dis,* 8**,** e2696.

Jonsson, T., Atwal, J. K., Steinberg, S., Snaedal, J., Jonsson, P. V., Bjornsson, S., et al. 2012. A mutation in APP protects against Alzheimer's disease and age-related cognitive decline. *Nature,* 488**,** 96-9.

Jonsson, T., Stefansson, H., Steinberg, S., Jonsdottir, I., Jonsson, P. V., Snaedal, J., et al. 2013. Variant of TREM2 Associated with the Risk of Alzheimer's Disease. *New England Journal of Medicine,* 368**,** 107-116.

Jost, M., Simpson, F., Kavran, J. M., Lemmon, M. A. and Schmid, S. L. 1998. Phosphatidylinositol-4,5-bisphosphate is required for endocytic coated vesicle formation. *Curr Biol,* 8**,** 1399-402.

Juottonen, K., Laakso, M. P., Insausti, R., Lehtovirta, M., Pitkanen, A., Partanen, K., et al. 1998. Volumes of the entorhinal and perirhinal cortices in Alzheimer's disease. *Neurobiol Aging,* 19**,** 15-22.

Kandimalla, K. K., Curran, G. L., Holasek, S. S., Gilles, E. J., Wengenack, T. M. and Poduslo, J. F. 2005. Pharmacokinetic analysis of the blood-brain barrier transport of 125I-amyloid beta protein 40 in wild-type and Alzheimer's disease transgenic mice (APP,PS1) and its implications for amyloid plaque formation. *J Pharmacol Exp Ther,* 313**,** 1370-8.

Kang, J., Lemaire, H. G., Unterbeck, A., Salbaum, J. M., Masters, C. L., Grzeschik, K. H., et al. 1987. The precursor of Alzheimer's disease amyloid A4 protein resembles a cell-surface receptor. *Nature,* 325**,** 733-6.

Kapoor, A., Hsu, W. M., Wang, B. J., Wu, G. H., Lin, T. Y., Lee, S. J., et al. 2010. Caveolin-1 regulates gamma-secretase-mediated AbetaPP processing by modulating spatial distribution of gamma-secretase in membrane. *J Alzheimers Dis*, 22, 423-42.

Karch, C. M., Jeng, A. T., Nowotny, P., Cady, J., Cruchaga, C. and Goate, A. M. 2012. Expression of novel Alzheimer's disease risk genes in control and Alzheimer's disease brains. *PLoS One,* 7**,** e50976.

Keaney, J. and Campbell, M. 2015. The dynamic blood-brain barrier. *FEBS J,* 282**,** 4067-79.

Kim, S., Sato, Y., Mohan, P. S., Peterhoff, C., Pensalfini, A., Rigoglioso, A., et al. 2016. Evidence that the rab5 effector APPL1 mediates APP-betaCTF-induced dysfunction of endosomes in Down syndrome and Alzheimer's disease. *Mol Psychiatry,* 21**,** 707-16.

Kitazume, S., Tachida, Y., Kato, M., Yamaguchi, Y., Honda, T., Hashimoto, Y., et al. 2010. Brain endothelial cells produce amyloid {beta} from amyloid precursor protein 770 and preferentially secrete the O-glycosylated form. *J Biol Chem,* 285**,** 40097-103.

Klunk, W. E., Pittsburgh, U. O., Mathis, C. A., Pittsburgh, U. O., Price, J. C., Pittsburgh, U. O., et al. 2009. Amyloid Imaging with PET in Alzheimer's Disease, Mild Cognitive Impairment, and Clinically Unimpaired Subjects. *In:* Silverman, D. (ed.) *PET in the Evaluation of Alzheimer's Disease and Related Disorders.* New York: Springer.

Knappenberger, K. S., Tian, G., Ye, X., Sobotka-Briner, C., Ghanekar, S. V., Greenberg, B. D., et al. 2004. Mechanism of gamma-secretase cleavage activation: is gamma-secretase regulated through autoinhibition involving the presenilin-1 exon 9 loop? *Biochemistry,* 43**,** 6208-18.

Koike, H., Tomioka, S., Sorimachi, H., Saido, T. C., Maruyama, K., Okuyama, A., et al. 1999. Membrane-anchored metalloprotease MDC9 has an alpha-secretase activity responsible for processing the amyloid precursor protein. *Biochem J,* 343 Pt 2**,** 371-5.

Kondo, T., Asai, M., Tsukita, K., Kutoku, Y., Ohsawa, Y., Sunada, Y., et al. 2013. Modeling Alzheimer's Disease with iPSCs Reveals Stress Phenotypes Associated with Intracellular A beta and Differential Drug Responsiveness. *Cell Stem Cell,* 12**,** 487-96.

Koo, E. H. and Squazzo, S. L. 1994. Evidence that production and release of amyloid beta-protein involves the endocytic pathway. *J Biol Chem,* 269**,** 17386-9.

Kosicek, M., Malnar, M., Goate, A. and Hecimovic, S. 2010. Cholesterol accumulation in Niemann Pick type C (NPC) model cells causes a shift in APP localization to lipid rafts. *Biochem Biophys Res Commun*, 393, 404-9.

Kozler, P. and Pokorny, J. 2003. Altered blood-brain barrier permeability and its effect on the distribution of Evans blue and sodium fluorescein in the rat brain applied by intracarotid injection. *Physiol Res,* 52**,** 607-14.

Kraepelin, E. 1910. *Psychiatrie: Ein Lehrbuch für Studierende und Ärzte,* Leipzig, Barth.

Krishna, A., Biryukov, M., Trefois, C., Antony, P. M., Hussong, R., Lin, J., et al. 2014. Systems genomics evaluation of the SH-SY5Y neuroblastoma cell line as a model for Parkinson's disease. *BMC Genomics,* 15**,** 1154.

Kuleshov, V., Xie, D., Chen, R., Pushkarev, D., Ma, Z., Blauwkamp, T., et al. 2014. Whole-genome haplotyping using long reads and statistical methods. *Nat Biotechnol,* 32**,** 261-6.

Kumar-Singh, S., Theuns, J., Van Broeck, B., Pirici, D., Vennekens, K., Corsmit, E., et al. 2006. Mean age-of-onset of familial alzheimer disease caused by presenilin mutations correlates with both increased Abeta42 and decreased Abeta40. *Hum Mutat,* 27**,** 686-95.

Kumari, S., Mg, S. and Mayor, S. 2010. Endocytosis unplugged: multiple ways to enter the cell. *Cell Res,* 20**,** 256-75.

Lachmann, R. H., Te Vruchte, D., Lloyd-Evans, E., Reinkensmeier, G., Sillence, D. J., Fernandez-Guillen, L., et al. 2004. Treatment with miglustat reverses the lipid-trafficking defect in Niemann-Pick disease type C. *Neurobiol Dis*, 16, 654-8.

Lacor, P. N., Buniel, M. C., Chang, L., Fernandez, S. J., Gong, Y., Viola, K. L., et al. 2004. Synaptic targeting by Alzheimer's-related amyloid beta oligomers. *J Neurosci,* 24**,** 10191-200.

Lambert, J. C., Heath, S., Even, G., Campion, D., Sleegers, K., Hiltunen, M., et al. 2009. Genome-wide association study identifies variants at CLU and CR1 associated with Alzheimer's disease. *Nature Genet,* 41**,** 1094-9.

Lambert, J. C., Ibrahim-Verbaas, C. A., Harold, D., Naj, A. C., Sims, R., Bellenguez, C., et al. 2013. Meta-analysis of 74,046 individuals identifies 11 new susceptibility loci for Alzheimer's disease. *Nature Genet,* 45**,** 1452-8.

Lang, D. M., Lommel, S., Jung, M., Ankerhold, R., Petrausch, B., Laessing, U., et al. 1998. Identification of reggie-1 and reggie-2 as plasmamembrane-associated proteins which cocluster with activated GPI-anchored cell adhesion molecules in non-caveolar micropatches in neurons. *J Neurobiol*, 37, 502-23.

Lasagna-Reeves, C. A., Castillo-Carranza, D. L., Sengupta, U., Clos, A. L., Jackson, G. R. and Kayed, R. 2011. Tau oligomers impair memory and induce synaptic and mitochondrial dysfunction in wild-type mice. *Molecular Neurodegener,* 6**,** 39.

Laterra, J., Keep, R., Betz, L. A. and Goldstein, G. W. 1999. Blood—Brain Barrier. *In:* Siegel, G. J., Agranoff, B. W., Albers, R. W., Fisher, S. K. and Uhler, M. D. (eds.) *Basic Neurochemistry: Molecular, Cellular and Medical Aspects.* 6th ed. Philadelphia, USA: Lippincott-Raven.

Lauritzen, I., Pardossi-Piquard, R., Bauer, C., Brigham, E., Abraham, J. D., Ranaldi, S., et al. 2012. The beta-secretase-derived C-terminal fragment of betaAPP, C99, but not Abeta, is a key contributor to early intraneuronal lesions in triple-transgenic mouse hippocampus. *J Neurosci,* 32**,** 16243-55.

Lauritzen, I., Pardossi-Piquard, R., Bourgeois, A., Pagnotta, S., Biferi, M. G., Barkats, M., et al. 2016. Intraneuronal aggregation of the β-CTF fragment of APP (C99) induces Aβ-independent lysosomal-autophagic pathology. *Acta Neuropathol*, 132, 257-76.

Lee, E., Marcucci, M., Daniell, L., Pypaert, M., Weisz, O. A., Ochoa, G. C., et al. 2002. Amphiphysin 2 (Bin1) and T-tubule biogenesis in muscle. *Science,* 297**,** 1193-6.

Lelos, M. J., Thomas, R. S., Kidd, E. J. and Good, M. A. 2011. Outcome-specific satiety reveals a deficit in context-outcome, but not stimulus- or action-outcome, associations in aged Tg2576 mice. *Behav Neurosci*, 125, 412-25.

Leone, D. P., Srinivasan, K., Chen, B., Alcamo, E. and Mcconnell, S. K. 2008. The determination of projection neuron identity in the developing cerebral cortex. *Curr Opin Neurobiol,* 18**,** 28-35.

Lewis, J., Dickson, D. W., Lin, W. L., Chisholm, L., Corral, A., Jones, G., et al. 2001. Enhanced neurofibrillary degeneration in transgenic mice expressing mutant tau and APP. *Science,* 293**,** 1487-91.

Lewis, F., Karlsberg Schaffer, S., Sussex, J., O'Neill, P. and Cockcroft, L. 2014. The Trajectory of Dementia in the UK - Making a Difference, A Report for Alzheimer's Research UK by OHE Consulting.

Lipardi, C., Mora, R., Colomer, V., Paladino, S., Nitsch, L., Rodriguez-Boulan, E., et al. 1998. Caveolin transfection results in caveolae formation but not apical sorting of glycosylphosphatidylinositol (GPI)-anchored proteins in epithelial cells. *J Cell Biol*, 140, 617-26.

Lippa, C. F., Swearer, J. M., Kane, K. J., Nochlin, D., Bird, T. D., Ghetti, B., et al. 2000. Familial Alzheimer's disease: site of mutation influences clinical phenotype. *Ann Neurol,* 48**,** 376-9.

Lippmann, E. S., Azarin, S. M., Kay, J. E., Nessler, R. A., Wilson, H. K., Al-Ahmad, A., et al. 2012. Human Blood-Brain Barrier Endothelial Cells Derived from Pluripotent Stem Cells. *Nat Biotechnol,* 30**,** 783-91.

Lisanti, M. P., Scherer, P. E., Vidugiriene, J., Tang, Z., Hermanowski-Vosatka, A., Tu, Y. H., et al. 1994. Characterization of caveolin-rich membrane domains isolated from an endothelial-rich source: implications for human disease. *J Cell Biol*, 126, 111-26.

Liu, L. and Pilch, P. F. 2008. A critical role of cavin (polymerase I and transcript release factor) in caveolae formation and organization. *J Biol Chem*, 283, 4314-22.

Loh, Y. H., Wu, Q., Chew, J. L., Vega, V. B., Zhang, W., Chen, X., et al. 2006. The Oct4 and Nanog transcription network regulates pluripotency in mouse embryonic stem cells. *Nat Genet,* 38**,** 431-40.

Loh, Y. H., Hartung, O., Li, H., Guo, C., Sahalie, J. M., Manos, P. D., et al. 2010. Reprogramming of T cells from human peripheral blood. *Cell Stem Cell,* 7**,** 15-9.

Lopez-Perez, E., Zhang, Y., Frank, S. J., Creemers, J., Seidah, N. and Checler, F. 2001.

Constitutive alpha-secretase cleavage of the beta-amyloid precursor protein in the furin-deficient LoVo cell line: involvement of the pro-hormone convertase 7 and the disintegrin metalloprotease ADAM10. *J Neurochem,* 76**,** 1532-9.

Lorincz, M. C., Dickerson, D. R., Schmitt, M. and Groudine, M. 2004. Intragenic DNA methylation alters chromatin structure and elongation efficiency in mammalian cells. *Nat Struct Mol Biol,* 11**,** 1068-75.

Lyketsos, C. G., Carrillo, M. C., Ryan, J. M., Khachaturian, A. S., Trzepacz, P., Amatniek, J., et al. 2011. Neuropsychiatric symptoms in Alzheimer's disease. *Alzheimers Dement,* 7**,** 532-9.

Macgillivray, R., Mendez, E., Shewale, J., Sinha, S., Lineback-Zins, J. and Brew, K. 1983. The Primary Structure of Human Serum Transferrin. *J. Biol. Chem.*, 258, 3543-53.

Mack, A. A., Kroboth, S., Rajesh, D. and Wang, W. B. 2011. Generation of induced pluripotent stem cells from CD34+ cells across blood drawn from multiple donors with non-integrating episomal vectors. *PLoS One,* 6.

Mahairaki, V., Ryu, J., Peters, A., Chang, Q., Li, T., Park, T. S., et al. 2014. Induced Pluripotent Stem Cells from Familial Alzheimer's Disease Patients Differentiate into Mature Neurons with Amyloidogenic Properties. *Stem Cells and Development,* 23**,** 2996-3010.

Mahley, R. W. 2016. Apolipoprotein E: from cardiovascular disease to neurodegenerative disorders. *J Mol Med (Berl),* 94**,** 739-46.

Mandybur, T. I. 1975. The incidence of cerebral amyloid angiopathy in Alzheimer's disease. *Neurology,* 25**,** 120-6.

Maness, L. M., Banks, W. A., Podlisny, M. B., Selkoe, D. J. and Kastin, A. J. 1994. Passage of human amyloid beta-protein 1-40 across the murine blood-brain barrier. *Life Sci,* 55**,** 1643-50.

Mann, D. M., Yates, P. O. and Marcyniuk, B. 1985. Correlation between senile plaque and neurofibrillary tangle counts in cerebral cortex and neuronal counts in cortex and subcortical structures in Alzheimer's disease. *Neurosci Lett,* 56**,** 51-5.

Mariani, J., Simonini, M. V., Palejev, D., Tomasini, L., Coppola, G., Szekely, A. M., et al. 2012. Modeling human cortical development in vitro using induced pluripotent stem cells. *Proc Natl Acad Sci U S A,* 109**,** 12770-5.

Marks, B., Stowell, M. H., Vallis, Y., Mills, I. G., Gibson, A., Hopkins, C. R., et al. 2001. GTPase activity of dynamin and resulting conformation change are essential for endocytosis. *Nature,* 410**,** 231-5.

Martel, C. L., Mackic, J. B., Mccomb, J. G., Ghiso, J. and Zlokovic, B. V. 1996. Blood-brain barrier uptake of the 40 and 42 amino acid sequences of circulating Alzheimer's amyloid beta in guinea pigs. *Neurosci Lett,* 206**,** 157-60.

Masters, C. L., Simms, G., Weinman, N. A., Multhaup, G., Mcdonald, B. L. and Beyreuther, K. 1985. Amyloid plaque core protein in Alzheimer disease and Down syndrome. *Proc Natl Acad Sci USA,* 82**,** 4245-9.

Maurer, K., Volk, S. and Gerbaldo, H. 1997. Auguste D. and Alzheimer's disease. *Lancet,* 349**,** 1546-1549.

Mawuenyega, K. G., Sigurdson, W., Ovod, V., Munsell, L., Kasten, T., Morris, J. C., et al. 2010. Decreased Clearance of CNS Amyloid-β in Alzheimer's Disease. *Science,* 330**,** 1774.

Mckhann, G., Drachman, D., Folstein, M., Katzman, R., Price, D. and Stadlan, E. M. 1984. Clinical diagnosis of Alzheimer's disease: Report of the NINCDS-ADRDA Work Group under the auspices of Department of Health and Human Services Task Force on Alzheimer's Disease. *Neurology,* 34**,** 939-44.

Mckhann, G. M., Knopman, D. S., Chertkow, H., Hyman, B. T., Jack, C. R., Kawas, C. H., et al. 2011. The diagnosis of dementia due to Alzheimer's disease: Recommendations from the National Institute on Aging-Alzheimer's Association workgroups on diagnostic guidelines for Alzheimer's disease. *Alzheimers Dement,* 7**,** 263-9.

Mcmahon, H. T. and Boucrot, E. 2011. Molecular mechanism and physiological functions of clathrin-mediated endocytosis. *Nat Rev Mol Cell Biol,* 12**,** 517-33.

Mcmillan, P., Korvatska, E., Poorkaj, P., Evstafjeva, Z., Robinson, L., Greenup, L., et al.

2008. Tau isoform regulation is region- and cell-specific in mouse brain. *J Comp Neurol,* 511**,** 788-803.

Meinecke, M., Boucrot, E., Camdere, G., Hon, W. C., Mittal, R. and Mcmahon, H. T. 2013. Cooperative recruitment of Dynamin and BAR domain-containing proteins leads to GTP-dependent membrane scission. *J. Biol. Chem,* 288**,** 6651-61.

Meister, M., Zuk, A. and Tikkanen, R. 2014. Role of dynamin and clathrin in the cellular trafficking of flotillins. *FEBS J*, 281, 2956-76.

Mellman, I. and Nelson, W. J. 2008. Coordinated protein sorting, targeting and distribution in polarized cells. *Nat Rev Mol Cell Biol*, 9, 833-45.

Miller, J. D., Ganat, Y. M., Kishinevsky, S., Bowman, R. L., Liu, B., Tu, E. Y., et al. 2013. Human iPSC-based Modeling of Late-Onset Disease via Progerin-induced Aging. *Cell Stem Cell,* 13**,** 691-705.

Miyagawa, T., Ebinuma, I., Morohashi, Y., Hori, Y., Young Chang, M., Hattori, H., et al. 2016. BIN1 regulates BACE1 intracellular trafficking and amyloid-beta production. *Hum Mol Genet,* 25**,** 2948-58.

Mizuguchi, H., Hashioka, Y., Utoguchi, N., Kubo, K., Nakagawa, S. and Mayumi, T. 1994. A comparison of drug transport through cultured monolayers of bovine brain capillary and bovine aortic endothelial cells. *Biol Pharm Bull*, 17, 1385-90.

Montagne, A., Barnes, S. R., Sweeney, M. D., Halliday, M. R., Sagare, A. P., Zhao, Z., et al. 2015. Blood-Brain Barrier Breakdown in the Aging Human Hippocampus. *Neuron,* 85**,** 296-302.

Moody, P. R., Sayers, E. J., Magnusson, J. P., Alexander, C., Borri, P., Watson, P., et al. 2015. Receptor Crosslinking: A General Method to Trigger Internalization and Lysosomal Targeting of Therapeutic Receptor:Ligand Complexes. *Mol Ther,* 23**,** 1888-98.

Moore, G. K., Speckmann, W., Herzug, R.P. 2007. The Use of siRNA to Validate Immunofluorescence Studies. *In:* Tatlor, D. L., Haskins, J. R., Giuliano, K. (ed.) *High Content Screening: A Powerful Approach to Systems Cell Biology and Drug Discovery*. Totowa, NJ: Humana Press, Inc.

Motley, A., Bright, N. A., Seaman, M. N. and Robinson, M. S. 2003. Clathrin-mediated endocytosis in AP-2–depleted cells. *J Cell Biol*, 162, 909-18.

Mougeolle, A., Poussard, S., Decossas, M., Lamaze, C., Lambert, O. and Dargelos, E. 2015. Oxidative stress induces caveolin 1 degradation and impairs caveolae functions in skeletal muscle cells. *PLoS One,* 10**,** e0122654.

Mousavi, S. A., Malerod, L., Berg, T. and Kjeken, R. 2004. Clathrin-dependent endocytosis. *Biochem J,* 377**,** 1-16.

Mukherjee, S., Zha, X., Tabas, I. and Maxfield, F. R. 1998. Cholesterol distribution in living cells: fluorescence imaging using dehydroergosterol as a fluorescent cholesterol analog. *Biophys J*, 75, 1915-25.

Muller, A. J., Baker, J. F., Duhadaway, J. B., Ge, K., Farmer, G., Donover, P. S., et al. 2003. Targeted Disruption of the Murine Bin1/Amphiphysin II Gene Does Not Disable Endocytosis but Results in Embryonic Cardiomyopathy with Aberrant Myofibril Formation. *Mol Cell Biol,* 23**,** 4295-306.

Muller, A. J., Duhadaway, J. B., Donover, P. S., Sutanto-Ward, E. and Prendergast, G. C. 2005. Inhibition of indoleamine 2,3-dioxygenase, an immunoregulatory target of the cancer suppression gene Bin1, potentiates cancer chemotherapy. *Nat Med,* 11**,** 312-9.

Muller, T., Meyer, H. E., Egensperger, R. and Marcus, K. 2008. The amyloid precursor protein intracellular domain (AICD) as modulator of gene expression, apoptosis, and cytoskeletal dynamics-relevance for Alzheimer's disease. *Prog Neurobiol,* 85**,** 393-406.

Muller, F.-J., Schuldt, B. M., Williams, R., Mason, D., Altun, G., Papapetrou, E. P., et al. 2011. A bioinformatic assay for pluripotency in human cells. *Nat Meth,* 8**,** 315-17.

Murata, M., Peranen, J., Schreiner, R., Wieland, F., Kurzchalia, T. V. and Simons, K. 1995. VIP21/caveolin is a cholesterol-binding protein. *Proc Natl Acad Sci USA*, 92, 10339-43.

Naj, A. C., Jun, G., Beecham, G. W., Wang, L.-S., Vardarajan, B. N., Buros, J., et al. 2011. Common variants at MS4A4/MS4A6E, CD2AP, CD33 and EPHA1 are associated with late-onset Alzheimer's disease. *Nature Genet,* 43**,** 436-41.

Nakajo, A., Yoshimura, S. I., Togawa, H., Kunii, M., Iwano, T., Izumi, A., et al. 2016. EHBP1L1 coordinates Rab8 and Bin1 to regulate apical-directed transport in polarized epithelial cells. *J Cell Biol,* 212**,** 297-306.

Nasreddine, Z. S., Phillips, N. A., Bedirian, V., Charbonneau, S., Whitehead, V., Collin, I., et al. 2005. The Montreal Cognitive Assessment, MoCA: a brief screening tool for mild cognitive impairment. *J Am Geriatr Soc,* 53**,** 695-9.

Nelson, P. T., Alafuzoff, I., Bigio, E. H., Bouras, C., Braak, H., Cairns, N. J., et al. 2012. Correlation of Alzheimer Disease Neuropathologic Changes With Cognitive Status: A Review of the Literature. *J Neuropathol Exp Neurol,* 71**,** 362-81.

Nemes, C., Varga, E., Tancos, Z., Bock, I., Francz, B., Kobolak, J., et al. 2016. Establishment of PSEN1 mutant induced pluripotent stem cell (iPSC) line from an Alzheimer's disease (AD) female patient. *Stem Cell Res,* 17**,** 69-71.

Neu, U., Woellner, K., Gauglitz, G. and Stehle, T. 2008. Structural basis of GM1 ganglioside recognition by simian virus 40. *Proc Natl Acad Sci USA*, 105, 5219-24.

Nichols, B. J., Kenworthy, A. K., Polishchuk, R. S., Lodge, R., Roberts, T. H., Hirschberg, K., et al. 2001. Rapid Cycling of Lipid Raft Markers between the Cell Surface and Golgi Complex. *J Cell Biol*, 153, 529-42.

Niessen, C. M. 2007. Tight junctions/adherens junctions: basic structure and function. *J Invest Dermatol,* 127**,** 2525-32.

Nikolaev, A., Mclaughlin, T., O'leary, D. and Tessier-Lavigne, M. 2009. N-APP binds DR6 to cause axon pruning and neuron death via distinct caspases. *Nature,* 457**,** 981-9.

Nixon, R. A., Wegiel, J., Kumar, A., Yu, W. H., Peterhoff, C., Cataldo, A., et al. 2005. Extensive involvement of autophagy in Alzheimer disease: an immuno-electron microscopy study. *J Neuropathol Exp Neurol*, 64, 113-22.

Noble, L. J., Kalinyak, J. E., Pitts, L. H. and Hall, J. J. 1994. Fluid-phase endocytosis of horseradish peroxidase by cerebral endothelial cells in primary culture: characterization and kinetic analysis. *J Neurosci Res*, 38, 654-63.

O'rahilly, R. and Muller, F. 1994. Neurulation in the normal human embryo. *Ciba Found Symp,* 181**,** 70-89.

Ochalek, A., Nemes, C., Varga, E., Tancos, Z., Kobolak, J. and Dinnyes, A. 2016. Establishment of induced pluripotent stem cell (iPSC) line from a 57-year old patient with sporadic Alzheimer's disease. *Stem Cell Res,* 17**,** 72-4.

Oddo, S., Caccamo, A., Shepherd, J. D., Murphy, M. P., Golde, T. E., Kayed, R., et al. 2003. Triple-transgenic model of Alzheimer's disease with plaques and tangles: intracellular Abeta and synaptic dysfunction. *Neuron,* 39**,** 409-21.

Oh, P., Mcintosh, D. P. and Schnitzer, J. E. 1998. Dynamin at the neck of caveolae mediates their budding to form transport vesicles by GTP-driven fission from the plasma membrane of endothelium. *J Cell Biol,* 141**,** 101-14.

Ohtsuki, S., Sato, S., Yamaguchi, H., Kamoi, M., Asashima, T. and Terasaki, T. 2007. Exogenous expression of claudin-5 induces barrier properties in cultured rat brain capillary endothelial cells. *J Cell Physiol,* 210**,** 81-6.

Okita, K., Ichisaka, T. and Yamanaka, S. 2007. Generation of germline-competent induced pluripotent stem cells. *Nature,* 448**,** 313-7.

Olabarria, M., Noristani, H. N., Verkhratsky, A. and Rodriguez, J. J. 2010. Concomitant astroglial atrophy and astrogliosis in a triple transgenic animal model of Alzheimer's disease. *Glia,* 58**,** 831-8.

Olson, M. I. and Shaw, C. M. 1969. Presenile dementia and Alzheimer's disease in mongolism. *Brain,* 92**,** 147-56.

Olusanya, O., Andrews, P. D., Swedlow, J. R. and Smythe, E. 2001. Phosphorylation of threonine 156 of the mu2 subunit of the AP2 complex is essential for endocytosis in vitro and in vivo. *Curr Biol*, 11, 896-900.

Orlandi, P. A. and Fishman, P. H. 1998. Filipin-dependent inhibition of cholera toxin: evidence for toxin internalization and activation through caveolae-like domains. *J Cell Biol,* 141, 905-15.

Owen, D. J., Wigge, P., Vallis, Y., Moore, J. D., Evans, P. R. and Mcmahon, H. T. 1998. Crystal structure of the amphiphysin-2 SH3 domain and its role in the prevention of dynamin ring formation. *EMBO J,* 17**,** 5273-85.

Owen, D. J., Vallis, Y., Noble, M. E., Hunter, J. B., Dafforn, T. R., Evans, P. R., et al. 1999. A structural explanation for the binding of multiple ligands by the alpha-adaptin appendage domain. *Cell,* 97**,** 805-15.

Owen, D., Vallis, Y., Pearse, B., Mcmahon, H. and Evans, P. 2000. The structure and function of the β2-adaptin appendage domain. *EMBO J,* 19**,** 4216-27.

Owen, D. J., Collins, B. M. and Evans, P. R. 2004. Adaptors for clathrin coats: structure and function. *Annu Rev Cell Dev Biol,* 20**,** 153-91.

Oyama, F., Sawamura, N., Kobayashi, K., Morishima-Kawashima, M., Kuramochi, T., Ito, M., et al. 1998. Mutant presenilin 2 transgenic mouse: effect on an age-dependent increase of amyloid beta-protein 42 in the brain. *J Neurochem,* 71**,** 313-22.

Pahlman, S., Ruusala, A. I., Abrahamsson, L., Mattsson, M. E. and Esscher, T. 1984. Retinoic acid-induced differentiation of cultured human neuroblastoma cells: a comparison with phorbolester-induced differentiation. *Cell Differ,* 14**,** 135-44.

Palade, G. E. and Bruns, R. R. 1968. Structural modulations of plasmalemmal vesicles. J *Cell Biol*, 37, 633-49.

Pant, S., Sharma, M., Patel, K., Caplan, S., Carr, C. M. and Grant, B. D. 2009. AMPH-1/Amphiphysin/Bin1 functions with RME-1/Ehd1 in endocytic recycling. *Nat Cell Biol*, 11, 1399-410.

Paquet, D., Kwart, D., Chen, A., Sproul, A., Jacob, S., Teo, S., et al. 2016. Efficient introduction of specific homozygous and heterozygous mutations using CRISPR/Cas9. *Nature,* 533**,** 125-9.

Parikh, I., Fardo, D. W. and Estus, S. 2014. Genetics of PICALM Expression and Alzheimer's Disease. *PLoS One*, 9, e91242.

Park, H. R., Cockrell, L. M., Du, Y., Kasinski, A., Havel, J., Zhao, J., Reyes-Turcu, F., Wilkinson, K. D., Fu, H. 2008. Protein-Protein Interactions. In: WALKER, J. M., RAPLEY, R. (ed.) *Molecular Biomethods Handbook*. 2nd ed. Totowa, USA: Humana Press.

Parker, S., Walker, D. S., Ly, S. and Baylis, H. A. 2009. Caveolin-2 Is Required for Apical Lipid Trafficking and Suppresses Basolateral Recycling Defects in the Intestine of Caenorhabditis elegans. *Mol Biol Cell,* 20**,** 1763-71.

Parton, R. G., Way, M., Zorzi, N. and Stang, E. 1997. Caveolin-3 Associates with Developing T-tubules during Muscle Differentiation. *J Cell Biol*, 136, 137-54.

Parton, R. G. and Collins, B. M. 2016. Unraveling the architecture of caveolae. *Proc Natl Acad Sci USA*, 113, 14170-2.

Parvathy, S., Hussain, I., Karran, E. H., Turner, A. J. and Hooper, N. M. 1999. Cleavage of Alzheimer's amyloid precursor protein by alpha-secretase occurs at the surface of neuronal cells. *Biochemistry,* 38**,** 9728-34.

Pavlides, S., Gutierrez-Pajares, J. L., Iturrieta, J., Lisanti, M. P. and Frank, P. G. 2014. Endothelial caveolin-1 plays a major role in the development of atherosclerosis. *Cell Tissue Res*, 356, 147-57.

Pelkmans, L., Kartenbeck, J. and Helenius, A. 2001. Caveolar endocytosis of simian virus 40 reveals a new two-step vesicular-transport pathway to the ER. *Nat Cell Biol*, 3, 473-83.

Perusini, G. 1909. Über klinisch und histologisch eigenartige psychische Erkrankungen des späteren Lebensalters. *In:* NISSL, F. & ALZHEIMER, A. (eds.) *Histologische und Histopathologische Arbeiten.* Jena: Verlag G Fischer.

Peter, B. J., Kent, H. M., Mills, I. G., Vallis, Y., Butler, P. J., Evans, P. R., et al. 2004. BAR domains as sensors of membrane curvature: the amphiphysin BAR structure. *Science,* 303**,** 495-9.

Petersen, R. C., Aisen, P., Boeve, B. F., Geda, Y. E., Ivnik, R. J., Knopman, D. S., et al. 2013. Mild cognitive impairment due to Alzheimer disease in the community. *Ann Neurol,* 74**,** 199-208.

Picas, L., Viaud, J., Schauer, K., Vanni, S., Hnia, K., Fraisier, V., et al. 2014. BIN1/M-Amphiphysin2 induces clustering of phosphoinositides to recruit its downstream partner dynamin. *Nat Commun*, 5, 5647.

Pineda-Lucena, A., Ho, C. S., Mao, D. Y., Sheng, Y., Laister, R. C., Muhandiram, R., et al. 2005. A structure-based model of the c-Myc/Bin1 protein interaction shows alternative splicing of Bin1 and c-Myc phosphorylation are key binding determinants. *J Mol Biol,* 351**,** 182-94.

Pitas, R. E., Boyles, J. K., Lee, S. H., Foss, D. and Mahley, R. W. 1987. Astrocytes synthesize apolipoprotein E and metabolize apolipoprotein E-containing lipoproteins. *Biochim Biophys Acta,* 917**,** 148-61.

Platt, F. M., Boland, B. and Van Der Spoel, A. C. 2012. Lysosomal storage disorders: The cellular impact of lysosomal dysfunction. *J Cell Biol*, 199, 723-34.

Polo, J. M., Liu, S., Figueroa, M. E., Kulalert, W., Eminli, S., Tan, K. Y., et al. 2010. Cell type of origin influences the molecular and functional properties of mouse induced pluripotent stem cells. *Nat Biotechnol,* 28**,** 848-55.

Pooler, A. M., Phillips, E. C., Lau, D. H. W., Noble, W. and Hanger, D. P. 2013. Physiological release of endogenous tau is stimulated by neuronal activity. *EMBO Rep,* 14**,** 389-94.

Poteryaev, D., Datta, S., Ackema, K., Zerial, M. and Spang, A. 2010. Identification of the switch in early-to-late endosome transition. *Cell,* 141**,** 497-508.

Preston, J. E., Joan Abbott, N. and Begley, D. J. 2014. Transcytosis of macromolecules at the blood-brain barrier. *Adv Pharmacol.* 2014, 71, 147-63.

Prince, M., Knapp, M., Guerchet, M., Mccrone, P., Prina, M., Comas-Herrera, A., Wittenberg, R., Adelaja, B., Hu, B., King, D., Rehill, A., Salimkumar, D. 2014. *Dementia UK Second edition - Overview,* London, Alzheimer's Society 2014.

Prince, M., Wimo, A., Guerchet, M., Ali, G., Wu, Y., Prina, M. 2015. *World Alzheimer Report 2015, The Global Impact of Dementia: An analysis of prevalence, incidence, cost and trends World Alzheimer Report 2015, The Global Impact of Dementia: An analysis of prevalence, incidence, cost and trends,* London, Alzheimer's Disease International.

Prindull, G., Prindull, B. and Meulen, N. 1978. Haematopoietic stem cells (CFUc) in human cord blood. *Acta Paediatr Scand,* 67**,** 413-6.

Prokic, I., Cowling, B. S. and Laporte, J. 2014. Amphiphysin 2 (BIN1) in physiology and diseases. *J Mol Med (Berl),* 92**,** 453-63.

Raiborg, C., Bache, K. G., Gillooly, D. J., Madshus, I. H., Stang, E. and Stenmark, H. 2002. Hrs sorts ubiquitinated proteins into clathrin-coated microdomains of early endosomes. *Nat Cell Biol*, 4, 394-8.

Raj, T., Shulman, J., Keenan, B., Chibnik, L., Evans, D., Bennett, D., et al. 2012. Alzheimer Disease Susceptibility Loci: Evidence for a Protein Network under Natural Selection. *Am J Hum Genet,* 90**,** 720-6.

Ramjaun, A. R., Micheva, K. D., Bouchelet, I. and Mcpherson, P. S. 1997. Identification and characterization of a nerve terminal-enriched amphiphysin isoform. *J Biol Chem,* 272**,** 16700-6.

Ramjaun, A. R. and Mcpherson, P. S. 1998. Multiple amphiphysin II splice variants display differential clathrin binding: identification of two distinct clathrin-binding sites. *J Neurochem,* 70**,** 2369-76.

Ramjaun, A. R., Philie, J., De Heuvel, E. and Mcpherson, P. S. 1999. The N terminus of amphiphysin II mediates dimerization and plasma membrane targeting. *J Biol Chem,* 274**,** 19785-91.

Rapoport, M., Dawson, H. N., Binder, L. I., Vitek, M. P. and Ferreira, A. 2002. Tau is essential to beta -amyloid-induced neurotoxicity. *Proc Natl Acad Sci USA,* 99**,** 6364-9.

Raub, T. J. and Audus, K. L. 1990. Adsorptive endocytosis and membrane recycling by cultured primary bovine brain microvessel endothelial cell monolayers. *J Cell Sci*, 97, 127-38.

Razani, B. and Lisanti, M. P. 2001. Caveolins and caveolae: molecular and functional relationships. *Exp Cell Res*, 271, 36-44.

Razani, B., Engelman, J. A., Wang, X. B., Schubert, W., Zhang, X. L., Marks, C. B., et al. 2001. Caveolin-1 null mice are viable but show evidence of hyperproliferative and vascular abnormalities. *J Biol Chem*, 276, 38121-38.

Razani, B., Wang, X. B., Engelman, J. A., Battista, M., Lagaud, G., Zhang, X. L., et al. 2002. Caveolin-2-Deficient Mice Show Evidence of Severe Pulmonary Dysfunction without Disruption of Caveolae. *Mol Cell Biol*, 22, 2329-44.

Reese, T. S. and Karnovsky, M. J. 1967. Fine structural localization of a blood-brain barrier to exogenous peroxidase. *J Cell Biol*, 34, 207-17.

Refolo, L. M., Malester, B., Lafrancois, J., Bryant-Thomas, T., Wang, R., Tint, G. S., et al. 2000. Hypercholesterolemia accelerates the Alzheimer's amyloid pathology in a transgenic mouse model. *Neurobiol Dis*, 7, 321-31.

Reiman, E. M., Chen, K., Liu, X., Bandy, D., Yu, M., Lee, W., et al. 2009. Fibrillar amyloid-beta burden in cognitively normal people at 3 levels of genetic risk for Alzheimer's disease. *Proc Natl Acad Sci U S A,* 106**,** 6820-5.

Ren, G., Vajjhala, P., Lee, J. S., Winsor, B. and Munn, A. L. 2006. The BAR domain proteins: molding membranes in fission, fusion, and phagy. *Microbiol Mol Biol Rev,* 70**,** 37-120.

Rentz, D. M., Locascio, J. J., Becker, J. A., Moran, E. K., Eng, E., Buckner, R. L., et al. 2010. Cognition, reserve, and amyloid deposition in normal aging. *Ann Neurol,* 67**,** 353-64.

Reubinoff, B. E., Pera, M. F., Fong, C.-Y., Trounson, A. and Bongso, A. 2000. Embryonic stem cell lines from human blastocysts: somatic differentiationin vitro. *Nature Biotechnology,* 18**,** 399-404.

Riddell, D. R., Christie, G., Hussain, I. and Dingwall, C. 2001. Compartmentalization of beta-secretase (Asp2) into low-buoyant density, noncaveolar lipid rafts. *Curr Biol*, 11, 1288-93.

Ridge, P. G., Mukherjee, S., Crane, P. K. and Kauwe, J. S. 2013. Alzheimer's disease: analyzing the missing heritability. *PLoS One,* 8**,** e79771.

Robert, J., Button, E. B., Stukas, S., Boyce, G. K., Gibbs, E., Cowan, C. M., et al. 2017. High-density lipoproteins suppress Aβ-induced PBMC adhesion to human endothelial cells in bioengineered vessels and in monoculture. *Molecular Neurodegener,* 12**,** 60.

Roberts, R. L., Fine, R. E. and Sandra, A. 1993. Receptor-mediated endocytosis of transferrin at the blood-brain barrier. *J Cell Sci,* 104**,** 521-532.

Rohan De Silva, H. A., Jen, A., Wickenden, C., Jen, L. S., Wilkinson, S. L. and Patel, A. J. 1997. Cell-specific expression of beta-amyloid precursor protein isoform mRNAs and proteins in neurons and astrocytes. *Brain Res Mol Brain Res,* 47**,** 147-56.

Rosen, W. G., Mohs, R. C. and Davis, K. L. 1984. A new rating scale for Alzheimer's disease. *Am J Psychiatry,* 141**,** 1356-64.

Rothberg, K. G., Heuser, J. E., Donzell, W. C., Ying, Y. S., Glenney, J. R. and Anderson, R. G. 1992. Caveolin, a protein component of caveolae membrane coats. *Cell*, 68, 673-82.

Rovelet-Lecrux, A., Hannequin, D., Raux, G., Meur, N. L., Laquerrière, A., Vital, A., et al. 2005. APP locus duplication causes autosomal dominant early-onset Alzheimer disease with cerebral amyloid angiopathy. *Nature Genet,* 38**,** 24-26.

Ruiz, A., Dols-Icardo, O., Bullido, M. J., Pastor, P., Rodriguez-Rodriguez, E., De Munain, A. L., et al. 2014. Assessing the role of the TREM2 p.R47H variant as a risk factor for Alzheimer's disease and frontotemporal dementia. *Neurobiol Aging,* 35**,** 4.

Sabuncu, M. R., Desikan, R. S., Sepulcre, J., Yeo, B. T., Liu, H., Schmansky, N. J., et al. 2011. The dynamics of cortical and hippocampal atrophy in Alzheimer disease. *Arch Neurol,* 68**,** 1040-8.

Sachse, M., Urbe, S., Oorschot, V., Strous, G. J. and Klumperman, J. 2002. Bilayered clathrin coats on endosomal vacuoles are involved in protein sorting toward lysosomes. *Mol Biol Cell*, 13, 1313-28.

Sakamuro, D., Elliott, K. J., Wechsler-Reya, R. and Prendergast, G. C. 1996. BIN1 is a novel MYC-interacting protein with features of a tumour suppressor. *Nat Genet,* 14**,** 69-77.

Sannerud, R., Esselens, C., Ejsmont, P., Mattera, R., Rochin, L., Tharkeshwar, A. K., et al. 2016. Restricted Location of PSEN2/gamma-Secretase Determines Substrate Specificity and Generates an Intracellular Abeta Pool. *Cell,* 166**,** 193-208.

Sasaguri, H., Nilsson, P., Hashimoto, S., Nagata, K., Saito, T., De Strooper, B., et al. 2017. APP mouse models for Alzheimer's disease preclinical studies. *EMBO J*, 36, 2473-87.

Saunders, A. M., Strittmatter, W. J., Schmechel, D., George-Hyslop, P. H., Pericak-Vance, M. A., Joo, S. H., et al. 1993. Association of apolipoprotein E allele epsilon 4 with late-onset familial and sporadic Alzheimer's disease. *Neurology,* 43**,** 1467-72.

Saura, C. A., Choi, S. Y., Beglopoulos, V., Malkani, S., Zhang, D., Shankaranarayana Rao, B. S., et al. 2004. Loss of presenilin function causes impairments of memory and synaptic plasticity followed by age-dependent neurodegeneration. *Neuron,* 42**,** 23-36.

Scheiffele, P., Verkade, P., Fra, A., Virta, H., Simons, K. and Ikonen, E. 1998. Caveolin-1 and -2 in the Exocytic Pathway of MDCK Cells. *J Cell Biol,* 140**,** 795-806.

Scherer, P. E., Okamoto, T., Chun, M., Nishimoto, I., Lodish, H. F. and Lisanti, M. P. 1996. Identification, sequence, and expression of caveolin-2 defines a caveolin gene family. *Proc Natl Acad Sci USA*, 93, 131-5.

Scheuner, D., Eckman, C., Jensen, M., Song, X., Citron, M., Suzuki, N., et al. 1996. Secreted amyloid beta-protein similar to that in the senile plaques of Alzheimer's disease is increased in vivo by the presenilin 1 and 2 and APP mutations linked to familial Alzheimer's disease. *Nat Med,* 2**,** 864-70.

Schlachetzki, F. and Pardridge, W. M. 2003. P-glycoprotein and caveolin-1alpha in endothelium and astrocytes of primate brain. *Neuroreport*, 14, 2041-6.

Schlegel, A. and Lisanti, M. P. 2000. A molecular dissection of caveolin-1 membrane attachment and oligomerization. Two separate regions of the caveolin-1 C-terminal domain mediate membrane binding and oligomer/oligomer interactions in vivo. *J Biol Chem*, 275, 21605-17.

Schlossman, D. M., Schmid, S. L., Braell, W. A. and Rothman, J. E. 1984. An enzyme that removes clathrin coats: purification of an uncoating ATPase. *J Cell Biol,* 99**,** 723-33.

Schmechel, D. E., Saunders, A. M., Strittmatter, W. J., Crain, B. J., Hulette, C. M., Joo, S. H., et al. 1993. Increased amyloid beta-peptide deposition in cerebral cortex as a consequence of apolipoprotein E genotype in late-onset Alzheimer disease. *Proc Natl Acad Sci U S A,* 90**,** 9649-53.

Schneider, A., Rajendran, L., Honsho, M., Gralle, M., Donnert, G., Wouters, F., et al. 2008. Flotillin-dependent clustering of the amyloid precursor protein regulates its endocytosis and amyloidogenic processing in neurons. *J Neurosci*, 28, 2874-82.

Schnitzer, J. E., Oh, P., Pinney, E. and Allard, J. 1994. Filipin-sensitive caveolae-mediated transport in endothelium: reduced transcytosis, scavenger endocytosis, and capillary permeability of select macromolecules. *J Cell Biol*, 127, 1217-32.

Schöler, H. R., Hatzopoulos, A. K., Balling, R., Suzuki, N. and Gruss, P. 1989. A family of octamer-specific proteins present during mouse embryogenesis: evidence for germline-specific expression of an Oct factor. *EMBO J,* 8**,** 2543-50.

Schonheit, B., Zarski, R. and Ohm, T. G. 2004. Spatial and temporal relationships between plaques and tangles in Alzheimer-pathology. *Neurobiol Aging,* 25**,** 697-711.

Schopperle, W. M. and Dewolf, W. C. 2007. The TRA-1-60 and TRA-1-81 human pluripotent stem cell markers are expressed on podocalyxin in embryonal carcinoma. *Stem Cells,* 25**,** 723-30.

Schubert, W., Frank, P. G., Razani, B., Park, D. S., Chow, C. W. and Lisanti, M. P. 2001. Caveolae-deficient endothelial cells show defects in the uptake and transport of albumin in vivo. *J Biol Chem*, 276, 48619-22.

Schuff, N., Woerner, N., Boreta, L., Kornfield, T., Shaw, L. M., Trojanowski, J. Q., et al. 2009. MRI of hippocampal volume loss in early Alzheimer's disease in relation to ApoE genotype and biomarkers. *Brain,* 132**,** 1067-77.

Seki, T., Yuasa, S., Oda, M., Egashira, T., Yae, K., Kusumoto, D., et al. 2010. Generation of induced pluripotent stem cells from human terminally differentiated circulating T cells. *Cell Stem Cell,* 7**,** 11-4.

Selkoe, D. J. 1991. The molecular pathology of Alzheimer's disease. *Neuron,* 6**,** 487-98.

Selkoe, D. J. 1994. Cell biology of the amyloid beta-protein precursor and the mechanism of Alzheimer's disease. *Annu Rev Cell Biol*, 10, 373-403.

Selkoe, D. J. and Hardy, J. 2016. The amyloid hypothesis of Alzheimer's disease at 25 years. *EMBO Mol Med,* 8**,** 595-608.

Sengupta, U., Portelius, E., Hansson, O., Farmer, K., Castillo-Carranza, D., Woltjer, R., et al. 2017. Tau oligomers in cerebrospinal fluid in Alzheimer's disease. *Ann Clin Transl Neurol,* 4**,** 226-35.

Serrano-Pozo, A., Frosch, M. P., Masliah, E. and Hyman, B. T. 2011. Neuropathological Alterations in Alzheimer Disease. *Cold Spring Harb Perspect Med,* 1.

Seshadri, S., Fitzpatrick, A. L., Ikram, M., Destefano, A., Gudnason, V., Boada, M., et al. 2010. Genome-wide Analysis of Genetic Loci Associated with Alzheimer's Disease. *JAMA,* 303**,** 1832-1840.

Seubert, P., Vigo-Pelfrey, C., Esch, F., Lee, M., Dovey, H., Davis, D., et al. 1992. Isolation and quantification of soluble Alzheimer's beta-peptide from biological fluids. *Nature,* 359**,** 325-7.

Sharma, D. K., Choudhury, A., Singh, R. D., Wheatley, C. L., Marks, D. L. and Pagano, R. E. 2003. Glycosphingolipids internalized via caveolar-related endocytosis rapidly merge with the clathrin pathway in early endosomes and form microdomains for recycling. *J Biol Chem*, 278, 7564-72.

Sherrington, R., Froelich, S., Sorbi, S., Campion, D., Chi, H., Rogaeva, E. A., et al. 1996. Alzheimer's disease associated with mutations in presenilin 2 is rare and variably penetrant. *Hum Mol Genet,* 5**,** 985-8.

Shi, Y., Kirwan, P. and Livesey, F. J. 2012a. Directed differentiation of human pluripotent stem cells to cerebral cortex neurons and neural networks. *Nat. Protocols,* 7**,** 1836-1846.

Shi, Y., Kirwan, P., Smith, J., Maclean, G., Orkin, S. H. and Livesey, F. J. 2012b. A Human Stem Cell Model of Early Alzheimer's Disease Pathology in Down Syndrome. *Science Translational Medicine,* 4, 124-9.

Shi, Y., Kirwan, P., Smith, J., Robinson, H. P. C. and Livesey, F. J. 2012c. Human cerebral cortex development from pluripotent stem cells to functional excitatory synapses. *Nature Neuroscience,* 15**,** 477-486.

Shibata, M., Yamada, S., Kumar, S. R., Calero, M., Bading, J., Frangione, B., et al. 2000. Clearance of Alzheimer's amyloid-β1-40 peptide from brain by LDL receptor–related protein-1 at the blood-brain barrier. *J Clin Invest, 106, 1489-9.*

Shih, W., Gallusser, A. and Kirchhausen, T. 1995. A clathrin-binding site in the hinge of the beta 2 chain of mammalian AP-2 complexes. *J Biol Chem,* 270**,** 31083-90.

Shivas, J. M., Morrison, H. A., Bilder, D. and Skop, A. R. 2010. Polarity and endocytosis: reciprocal regulation. *Trends Cell Biol,* 20**,** 445-52.

Shpetner, H. S., Herskovits, J. S. and Vallee, R. B. 1996. A binding site for SH3 domains targets dynamin to coated pits. *J Biol Chem,* 271**,** 13-6.

Shupliakov, O., Low, P., Grabs, D., Gad, H., Chen, H., David, C., et al. 1997. Synaptic vesicle endocytosis impaired by disruption of dynamin-SH3 domain interactions. *Science,* 276**,** 259-63.

Silva, J., Nichols, J., Theunissen, T. W., Guo, G., Van Oosten, A. L., Barrandon, O., et al. 2009. Nanog Is the Gateway to the Pluripotent Ground State. *Cell,* 138**,** 722-37.

Simons, K. and Sampaio, J. L. 2011. Membrane organization and lipid rafts. Cold Spring *Harb Perspect Biol*, 3, a004697.

Simons, M., Keller, P., De Strooper, B., Beyreuther, K., Dotti, C. G. and Simons, K. 1998. Cholesterol depletion inhibits the generation of beta-amyloid in hippocampal neurons. *Proc Natl Acad Sci USA*, 95, 6460-4.

Simpson, I. A., Chundu, K. R., Davies-Hill, T., Honer, W. G. and Davies, P. 1994. Decreased concentrations of GLUT1 and GLUT3 glucose transporters in the brains of patients with Alzheimer's disease. *Ann Neurol,* 35**,** 546-51.

Sims, R., Van Der Lee, S. J., Naj, A. C., Bellenguez, C., Badarinarayan, N., Jakobsdottir, J., et al. 2017. Rare coding variants in PLCG2, ABI3, and TREM2 implicate microglial-mediated innate immunity in Alzheimer's disease. *Nat Genet*, 49, 1373-84.

Singh, P. P., Singh, M. and Mastana, S. S. 2006. APOE distribution in world populations with new data from India and the UK. *Ann Hum Biol,* 33**,** 279-308.

Singh, R. D., Puri, V., Valiyaveettil, J. T., Marks, D. L., Bittman, R. and Pagano, R. E. 2003. Selective Caveolin-1–dependent Endocytosis of Glycosphingolipids. *Mol Biol Cell*, 14, 3254-65.

Sinha, S., Anderson, J. P., Barbour, R., Basi, G. S., Caccavello, R., Davis, D., et al. 1999. Purification and cloning of amyloid precursor protein beta-secretase from human brain. *Nature,* 402**,** 537-40.

Sivadon, P., Bauer, F., Aigle, M. and Crouzet, M. 1995. Actin cytoskeleton and budding pattern are altered in the yeast rvs161 mutant: the Rvs161 protein shares common domains with the brain protein amphiphysin. *Mol Gen Genet,* 246**,** 485-95.

Slepnev, V. I., Ochoa, G. C., Butler, M. H., Grabs, D. and De Camilli, P. 1998. Role of phosphorylation in regulation of the assembly of endocytic coat complexes. *Science*, 281, 821-4.

Smith, M. W. and Gumbleton, M. 2006. Endocytosis at the blood-brain barrier: from basic understanding to drug delivery strategies. *J Drug Target,* 14**,** 191-214.

Sowa, G., Pypaert, M., Fulton, D. and Sessa, W. C. 2003. The phosphorylation of caveolin-2 on serines 23 and 36 modulates caveolin-1-dependent caveolae formation. *Proc Natl Acad Sci USA,* 100**,** 6511-6.

Sowa, G. 2011. Novel Insights into the Role of Caveolin-2 in Cell- and Tissue-Specific Signaling and Function. *Biochem Res Int*, 809259.

Spires, T. L., Orne, J. D., Santacruz, K., Pitstick, R., Carlson, G. A., Ashe, K. H., et al. 2006. Region-specific dissociation of neuronal loss and neurofibrillary pathology in a mouse model of tauopathy. *Am J Pathol,* 168**,** 1598-607.

Sproul, A. A., Jacob, S., Pre, D., Kim, S. H., Nestor, M. W., Navarro-Sobrino, M., et al. 2014. Characterization and molecular profiling of PSEN1 familial Alzheimer's disease iPSC-derived neural progenitors. *PLoS One,* 9**,** e84547.

Stowell, M. H., Marks, B., Wigge, P. and Mcmahon, H. T. 1999. Nucleotide-dependent conformational changes in dynamin: evidence for a mechanochemical molecular spring. *Nat Cell Biol,* 1**,** 27-32.

Stratman, A. N., Malotte, K. M., Mahan, R. D., Davis, M. J. and Davis, G. E. 2009. Pericyte recruitment during vasculogenic tube assembly stimulates endothelial basement membrane matrix formation. *Blood,* 114**,** 5091-101.

Szaruga, M., Veugelen, S., Benurwar, M., Lismont, S., Sepulveda-Falla, D., Lleo, A., et al. 2015. Qualitative changes in human gamma-secretase underlie familial Alzheimer's disease. *J Exp Med,* 212**,** 2003-13.

Takahashi, K. and Yamanaka, S. 2006. Induction of pluripotent stem cells from mouse embryonic and adult fibroblast cultures by defined factors. *Cell,* 126**,** 663-76.

Takahashi, K., Tanabe, K., Ohnuki, M., Narita, M., Ichsaka, T., Tomoda, K., Yamanaka, S. 2007. Induction of Pluripotent Stem Cells from Adult Human Fibroblasts by Defined Factors. *Cell,* 131**,** 861-872.

Tamai, I., Sai, Y., Kobayashi, H., Kamata, M., Wakamiya, T. and Tsuji, A. 1997. Structure-internalization relationship for adsorptive-mediated endocytosis of basic peptides at the blood-brain barrier. *J Pharmacol Exp Ther,* 280**,** 410-5.

Tamboli, I. Y., Hampel, H., Tien, N. T., Tolksdorf, K., Breiden, B., Mathews, P. M., et al. 2011. Sphingolipid storage affects autophagic metabolism of the amyloid precursor protein and promotes Abeta generation. *J Neurosci*, 31, 1837-49.

Tan, M. S., Yu, J. T. and Tan, L. 2013. Bridging integrator 1 (BIN1): form, function, and Alzheimer's disease. *Trends in Molecular Medicine,* 19**,** 594-603.

Tancos, Z., Varga, E., Kovacs, E., Dinnyes, A. and Kobolak, J. 2016. Establishment of induced pluripotent stem cell (iPSC) line from a 75-year old patient with late onset Alzheimer's disease (LOAD). *Stem Cell Res,* 17**,** 81-83.

Tanzi, R. E. 2012. The Genetics of Alzheimer Disease. *Cold Spring Harb Perspect Med,* 2.

Tao-Cheng, J., Nagy, Z. and Brightman, M. 1987. Tight junctions of brain endothelium in vitro are enhanced by astroglia. *J Neurosci,* 7**,** 3293-3299.

Te Vruchte, D., Lloyd-Evans, E., Veldman, R. J., Neville, D. C., Dwek, R. A., Platt, F. M., et al. 2004. Accumulation of glycosphingolipids in Niemann-Pick C disease disrupts endosomal transport. *J Biol Chem*, 279, 26167-75.

Ter Haar, E., Harrison, S. C. and Kirchhausen, T. 2000. Peptide-in-groove interactions link target proteins to the beta-propeller of clathrin. *Proc Natl Acad Sci USA,* 97**,** 1096-100.

Thinakaran, G., Borchelt, D. R., Lee, M. K., Slunt, H. H., Spitzer, L., Kim, G., et al. 1996. Endoproteolysis of presenilin 1 and accumulation of processed derivatives in vivo. *Neuron,* 17**,** 181-90.

Thomas, R. S., Lelos, M. J., Good, M. A. and Kidd, E. J. 2011. Clathrin-mediated endocytic proteins are upregulated in the cortex of the Tg2576 mouse model of Alzheimer's disease-like amyloid pathology. *Biochem Biophys Res Commun,* 415**,** 656-61.

Thomas, R. S., Henson, A., Gerrish, A., Jones, L., Williams, J. and Kidd, E. J. 2016. Decreasing the expression of PICALM reduces endocytosis and the activity of β-secretase: implications for Alzheimer's disease. *BMC Neurosci, 17*.

Thomas, S., Mercado, J. M., Duhadaway, J., Diguilio, K., Mullin, J. M. and Prendergast, G. C. 2016. Novel Colitis Immunotherapy Targets Bin1 and Improves Colon Cell Barrier Function. *Dig Dis Sci,* 61**,** 423-32.

Thompson, A., Nessler, R., Wisco, D., Anderson, E., Winckler, B. and Sheff, D. 2007. Recycling Endosomes of Polarized Epithelial Cells Actively Sort Apical and Basolateral Cargos into Separate Subdomains. *Mol Biol Cell*, 18, 2687-97.

Thomson, J. a. T., Itskovitz-Eldor, J., Shapiro, S. S., Waknitz, M. A., Swiergiel, J. J., Marshall, V. S., et al. 1998. Embryonic Stem Cell Lines Derived from Human Blastocysts. *Science,* 282**,** 1145-1147.

Torgersen, M. L., Skretting, G., Van Deurs, B. and Sandvig, K. 2001. Internalization of cholera toxin by different endocytic mechanisms. *J Cell Sci*, 114, 3737-47.

Tousseyn, T., Thathiah, A., Jorissen, E., Raemaekers, T., Konietzko, U., Reiss, K., et al. 2009. ADAM10, the rate-limiting protease of regulated intramembrane proteolysis of Notch and other proteins, is processed by ADAMS-9, ADAMS-15, and the gamma-secretase. *J Biol Chem,* 284**,** 11738-47.

Tremblay, R. G., Sikorska, M., Sandhu, J. K., Lanthier, P., Ribecco-Lutkiewicz, M. and Bani-Yaghoub, M. 2010. Differentiation of mouse Neuro 2A cells into dopamine neurons. *J Neurosci Methods,* 186**,** 60-7.

Trokovic, R., Weltner, J., Nishimura, K., Ohtaka, M., Nakanishi, M., Salomaa, V., et al. 2014. Advanced Feeder-Free Generation of Induced Pluripotent Stem Cells Directly From Blood Cells. *Stem Cells Transl Med,* 3**,** 1402-9.

Tsutsui, K., Maeda, Y., Seki, S. and Tokunaga, A. 1997. cDNA cloning of a novel amphiphysin isoform and tissue-specific expression of its multiple splice variants. *Biochem Biophys Res Commun,* 236**,** 178-83.

Ubelmann, F., Burrinha, T., Salavessa, L., Gomes, R., Ferreira, C., Moreno, N., et al. 2017. Bin1 and CD2AP polarise the endocytic generation of beta-amyloid. *EMBO Rep,* 18**,** 102-22.

Uchida, Y., Ohtsuki, S., Katsukura, Y., Ikeda, C., Suzuki, T., Kamiie, J., et al. 2011. Quantitative targeted absolute proteomics of human blood-brain barrier transporters and receptors. *J Neurochem,* 117**,** 333-45.

Ungewickell, E., Ungewickell, H., Holstein, S. E., Lindner, R., Prasad, K., Barouch, W., et al. 1995. Role of auxilin in uncoating clathrin-coated vesicles. *Nature,* 378**,** 632-5.

Urich, E., Lazic, S. E., Molnos, J., Wells, I. and Freskgard, P. O. 2012. Transcriptional Profiling of Human Brain Endothelial Cells Reveals Key Properties Crucial for Predictive In Vitro Blood-Brain Barrier Models. *Plos One,* 7**,** 16.

Valencia-Sanchez, M. A., Liu, J., Hannon, G. J. and Parker, R. 2006. Control of translation and mRNA degradation by miRNAs and siRNAs. *Genes Dev,* 20**,** 515-24.

Van Assema, D. M., Lubberink, M., Bauer, M., Van Der Flier, W. M., Schuit, R. C., Windhorst, A. D., et al. 2012. Blood-brain barrier P-glycoprotein function in Alzheimer's disease. *Brain,* 135**,** 181-9.

Van Der Meer, A. D., Poot, A. A., Feijen, J. and Vermes, I. 2010. Analyzing shear stress-induced alignment of actin filaments in endothelial cells with a microfluidic assay. *Biomicrofluidics,* 4**,** 11103.

Vance, J. E. 2012. Dysregulation of cholesterol balance in the brain: contribution to neurodegenerative diseases. *Dis Model Mech*, 5, 746-55.

Vassar, R., Bennett, B. D., Babu-Khan, S., Kahn, S., Mendiaz, E. A., Denis, P., et al. 1999. Beta-secretase cleavage of Alzheimer's amyloid precursor protein by the transmembrane aspartic protease BACE. *Science,* 286**,** 735-41.

Vazin, T., Ball, K. A., Lu, H., Park, H., Ataeijannati, Y., Head-Gordon, T., et al. 2014. Efficient derivation of cortical glutamatergic neurons from human pluripotent stem cells: A model system to study neurotoxicity in Alzheimer's disease. *Neurobiol Dis,* 62**,** 62-72.

Vera, E., Bosco, N. and Studer, L. 2016. Generating Late-Onset Human ipsc-Based Disease Models By Inducing Neuronal Age-Related Phenotypes Through Telomerase Manipulation. *Cell Rep,* 17**,** 1184-92.

Vercauteren, D., Vandenbroucke, R. E., Jones, A. T., Rejman, J., Demeester, J., De Smedt, S. C., et al. 2010. The Use of Inhibitors to Study Endocytic Pathways of Gene Carriers: Optimization and Pitfalls. *Mol Ther,* 18**,** 561-9.

Von Rotz, R. C., Kohli, B. M., Bosset, J., Meier, M., Suzuki, T., Nitsch, R. M., et al. 2004. The APP intracellular domain forms nuclear multiprotein complexes and regulates the transcription of its own precursor. *J Cell Sci,* 117**,** 4435-48.

Wahrle, S., Das, P., Nyborg, A. C., Mclendon, C., Shoji, M., Kawarabayashi, T., et al. 2002. Cholesterol-dependent gamma-secretase activity in buoyant cholesterol-rich membrane microdomains. *Neurobiol Dis*, 9, 11-23.

Wang, H. W., Pasternak, J. F., Kuo, H., Ristic, H., Lambert, M. P., Chromy, B., et al. 2002. Soluble oligomers of beta amyloid (1-42) inhibit long-term potentiation but not long-term depression in rat dentate gyrus. *Brain Res,* 924**,** 133-40.

Wang, Y., Wang, N., Cai, B., Wang, G., Li, J. and Piao, X. 2015. In vitro model of the blood-brain barrier established by co-culture of primary cerebral microvascular endothelial and astrocyte cells. *Neural Regen Res,* 10**,** 2011-7.

Ward, R. V., Jennings, K. H., Jepras, R., Neville, W., Owen, D. E., Hawkins, J., et al. 2000. Fractionation and characterization of oligomeric, protofibrillar and fibrillar forms of beta-amyloid peptide. *Biochem J,* 348**,** 137-44.

Warnock, D. E., Hinshaw, J. E. and Schmid, S. L. 1996. Dynamin self-assembly stimulates its GTPase activity. *J Biol Chem,* 271**,** 22310-4.

Wechsler-Reya, R., Sakamuro, D., Zhang, J., Duhadaway, J. and Prendergast, G. C. 1997.

Structural analysis of the human BIN1 gene. Evidence for tissue-specific transcriptional regulation and alternate RNA splicing. *J Biol Chem,* 272**,** 31453-8.

Weingarten, M. D., Lockwood, A. H., Hwo, S. Y. and Kirschner, M. W. 1975. A protein factor essential for microtubule assembly. *Proc Natl Acad Sci USA,* 72**,** 1858-62.

Weisgraber, K. H., Rall, S. C., Jr. and Mahley, R. W. 1981. Human E apoprotein heterogeneity. Cysteine-arginine interchanges in the amino acid sequence of the apo-E isoforms. *J Biol Chem,* 256**,** 9077-83.

Weksler, B. B., Subileau, E. A., Perriere, N., Charneau, P., Holloway, K., Leveque, M., et al. 2005. Blood-brain barrier-specific properties of a human adult brain endothelial cell line. *FASEB J,* 19**,** 1872-4.

Weksler, B. B., Romero, I. A. and Couraud, P. O. 2013. The hCMEC/D3 cell line as a model of the human blood brain barrier. *Fluids Barriers CNS,* 10**,** 16.

Wertkin, A. M., Turner, R. S., Pleasure, S. J., Golde, T. E., Younkin, S. G., Trojanowski, J. Q., et al. 1993. Human neurons derived from a teratocarcinoma cell line express solely the 695-amino acid amyloid precursor protein and produce intracellular beta-amyloid or A4 peptides. *Proc Natl Acad Sci USA,* 90**,** 9513-7.

West, M. J., Kawas, C. H., Martin, L. J. and Troncoso, J. C. 2000. The CA1 region of the human hippocampus is a hot spot in Alzheimer's disease. *Ann NY Acad Sci,* 908**,** 255-9.

Wigge, P., Kohler, K., Vallis, Y., Doyle, C. A., Owen, D., Hunt, S. P., et al. 1997a. Amphiphysin heterodimers: Potential role in clathrin-mediated endocytosis. *Mol Biol Cell,* 8**,** 2003-2015.

Wigge, P., Vallis, Y. and Mcmahon, H. T. 1997b. Inhibition of receptor-mediated endocytosis by the amphiphysin SH3 domain. *Curr Biol,* 7**,** 554-60.

Wigge, P. and Mcmahon, H. T. 1998. The amphiphysin family of proteins and their role in endocytosis at the synapse. *Trends Neurosci,* 21**,** 339-344.

Wilson, P. G. and Stice, S. S. 2006. Development and differentiation of neural rosettes derived from human embryonic stem cells. *Stem Cell Rev,* 2**,** 67-77.

Wingo, T. S., Lah, J. J., Levey, A. I. and Cutler, D. J. 2012. Autosomal Recessive Causes Likely in Early-Onset Alzheimer Disease. *Arch Neurol,* 69**,** 59-64.

Winkler, E. A., Nishida, Y., Sagare, A. P., Rege, S. V., Bell, R. D., Perlmutter, D., et al. 2015. GLUT1 reductions exacerbate Alzheimer's disease vasculoneuronal dysfunction and degeneration. *Nat Neurosci,* 18**,** 521-30.

Wisniewski, T., Castano, E. M., Golabek, A., Vogel, T. and Frangione, B. 1994. Acceleration of Alzheimer's fibril formation by apolipoprotein E in vitro. *Am J Pathol,* 145**,** 1030-5.

Wolburg, H., Wolburg-Buchholz, K., Kraus, J., Rascher-Eggstein, G., Liebner, S., Hamm, S., et al. 2003. Localization of claudin-3 in tight junctions of the blood-brain barrier is selectively lost during experimental autoimmune encephalomyelitis and human glioblastoma multiforme. *Acta Neuropathol,* 105**,** 586-92.

Wolfe, M. S., De Los Angeles, J., Miller, D. D., Xia, W. and Selkoe, D. J. 1999. Are presenilins intramembrane-cleaving proteases? Implications for the molecular mechanism of Alzheimer's disease. *Biochemistry,* 38**,** 11223-30.

Wolff, A., Antfolk, M., Brodin, B. and Tenje, M. 2015. In Vitro Blood-Brain Barrier Models-An Overview of Established Models and New Microfluidic Approaches. *J Pharm Sci,* 104**,** 2727-46.

Wu, L. J., Leenders, A. G., Cooperman, S., Meyron-Holtz, E., Smith, S., Land, W., et al. 2004. Expression of the iron transporter ferroportin in synaptic vesicles and the blood-brain barrier. *Brain Res*, 1001, 108-17.

Xia, D., Watanabe, H., Wu, B., Lee, S. H., Li, Y., Tsvetkov, E., et al. 2015. Presenilin-1 knockin mice reveal loss-of-function mechanism for familial Alzheimer's disease. *Neuron,* 85**,** 967-81.

Xiao, Q., Gil, S.-C., Yan, P., Wang, Y., Han, S., Gonzales, E., et al. 2012. Role of Phosphatidylinositol Clathrin Assembly Lymphoid-Myeloid Leukemia (PICALM) in Intracellular Amyloid Precursor Protein (APP) Processing and Amyloid Plaque Pathogenesis. *J Biol Chem,* 287**,** 21279-21289.

Xu, R. H., Sampsell-Barron, T. L., Gu, F., Root, S., Peck, R. M., Pan, G., et al. 2008. NANOG is a direct target of TGFbeta/activin-mediated SMAD signaling in human ESCs. *Cell Stem Cell,* 3**,** 196-206.

Yagi, T., Ito, D., Okada, Y., Akamatsu, W., Nihei, Y., Yoshizaki, T., et al. 2011. Modeling familial Alzheimer's disease with induced pluripotent stem cells. *Hum Mol Gen,* 20**,** 4530-4539.

Yagishita, S., Morishima-Kawashima, M., Tanimura, Y., Ishiura, S. and Ihara, Y. 2006. DAPT-induced intracellular accumulations of longer amyloid beta-proteins: further implications for the mechanism of intramembrane cleavage by gamma-secretase. *Biochemistry,* 45**,** 3952-60.

Yamada, M., Tsukagoshi, H., Otomo, E. and Hayakawa, M. 1987. Cerebral amyloid angiopathy in the aged. *J Neurol,* 234**,** 371-6.

Yamada, M. 2002. Risk factors for cerebral amyloid angiopathy in the elderly. *Ann N Y Acad Sci,* 977**,** 37-44.

Yamada, M. 2015. Cerebral Amyloid Angiopathy: Emerging Concepts. *J Stroke,* 17**,** 17-30.

Yamamizu, K., Iwasaki, M., Takakubo, H., Sakamoto, T., Ikuno, T., Miyoshi, M., et al. 2017. In Vitro Modeling of Blood-Brain Barrier with Human iPSC-Derived Endothelial Cells, Pericytes, Neurons, and Astrocytes via Notch Signaling. *Stem Cell Rep,* 8**,** 634-47.

Yamamoto, N., Fukata, Y., Fukata, M. and Yanagisawa, K. 2007. GM1-ganglioside-induced Abeta assembly on synaptic membranes of cultured neurons. *Biochim Biophys Acta*, 1768, 1128-37.

Yamazaki, T., Chang, T. Y., Haass, C. and Ihara, Y. 2001. Accumulation and aggregation of amyloid beta-protein in late endosomes of Niemann-pick type C cells. *J Biol Chem*, 276, 4454-60.

Yan, S. D., Chen, X., Fu, J., Chen, M., Zhu, H., Roher, A., et al. 1996. RAGE and amyloid-beta peptide neurotoxicity in Alzheimer's disease. *Nature,* 382**,** 685-91.

Young, S. P., Bomford, A. and Williams, R. 1984. The effect of the iron saturation of transferrin on its binding and uptake by rabbit reticulocytes. *Biochem J*, 219, 505-10.

Young, M. J., Lee, R. K., Jhaveri, S. and Wurtman, R. J. 1999. Intracellular and cell-surface distribution of amyloid precursor protein in cortical astrocytes. *Brain Res Bull,* 50**,** 27-32.

Young, A. 2007. Structural insights into the clathrin coat. *Semin Cell Dev Biol,* 18**,** 448-58.

Yu, Y. J., Zhang, Y., Kenrick, M., Hoyte, K., Luk, W., Lu, Y., et al. 2011. Boosting brain uptake of a therapeutic antibody by reducing its affinity for a transcytosis target. *Sci Transl Med*, 3, 84ra44.

Yuan, S. H., Martin, J., Elia, J., Flippin, J., Paramban, R. I., Hefferan, M. P., et al. 2011. Cell-Surface Marker Signatures for the Isolation of Neural Stem Cells, Glia and Neurons Derived from Human Pluripotent Stem Cells. *Plos One,* 6**,** 16.

Zelhof, A. C., Bao, H., Hardy, R. W., Razzaq, A., Zhang, B. and Doe, C. Q. 2001. Drosophila Amphiphysin is implicated in protein localization and membrane morphogenesis but not in synaptic vesicle endocytosis. *Development,* 128**,** 5005-15.

Zhang, D. D., Cheng, L. J., Badner, J. A., Chen, C., Chen, Q., Luo, W., et al. 2010. Genetic Control of Individual Differences in Gene-Specific Methylation in Human Brain. *Am J Hum Gen,* 86**,** 411-419.

Zhang, Y., Chen, K., Sloan, S. A., Bennett, M. L., Scholze, A. R., O'keeffe, S., et al. 2014. An RNA-Sequencing Transcriptome and Splicing Database of Glia, Neurons, and Vascular Cells of the Cerebral Cortex. *J Neurosci*, 34, 11929-47.

Zhang, S., Lv, Z., Liu, L., Li, Q., Gong, W., Sha, H., et al. 2017. Characterization of human induced pluripotent stem cell (iPSC) line from a 72year old male patient with later onset Alzheimer's disease. *Stem Cell Res,* 19**,** 34-36.

Zhao, Z., Sagare, A. P., Ma, Q., Halliday, M. R., Kong, P., Kisler, K., et al. 2015. Central role for PICALM in amyloid-beta blood-brain barrier transcytosis and clearance. *Nat Neurosci,* 18**,** 978-87.

Zhong, Y., Hennig, B. and Toborek, M. 2010. Intact lipid rafts regulate HIV-1 Tat protein-induced activation of the Rho signaling and upregulation of P-glycoprotein in brain endothelial cells. *J Cereb Blood Flow Metab*, 30, 522-33.

Zhou, L., Brouwers, N., Benilova, I., Vandersteen, A., Mercken, M., Van Laere, K., et al. 2011. Amyloid precursor protein mutation E682K at the alternative β-secretase cleavage β'-site increases Aβ generation†. *EMBO Mol Med,* 3**,** 291-302.

Zhu, X. C., Tan, L., Wang, H. F., Jiang, T., Cao, L., Wang, C., et al. 2015. Rate of early onset Alzheimer's disease: a systematic review and meta-analysis. *Ann Transl Med,* 3.

Zipser, B. D., Johanson, C. E., Gonzalez, L., Berzin, T. M., Tavares, R., Hulette, C. M., et al. 2007. Microvascular injury and blood-brain barrier leakage in Alzheimer's disease. *Neurobiol Aging,* 28**,** 977-86.

Zlokovic, B. V. 2005. Neurovascular mechanisms of Alzheimer's neurodegeneration. *Trends Neurosci,* 28**,** 202-8.

Zlokovic, B. V., Deane, R., Sagare, A. P., Bell, R. D. and Winkler, E. A. 2010. Low-density lipoprotein receptor-related protein-1 : a serial clearance homeostatic mechanism controlling Alzheimer's amyloid β-peptide elimination from the brain. *J Neurochem,* 115**,** 1077-89.

Appendix I

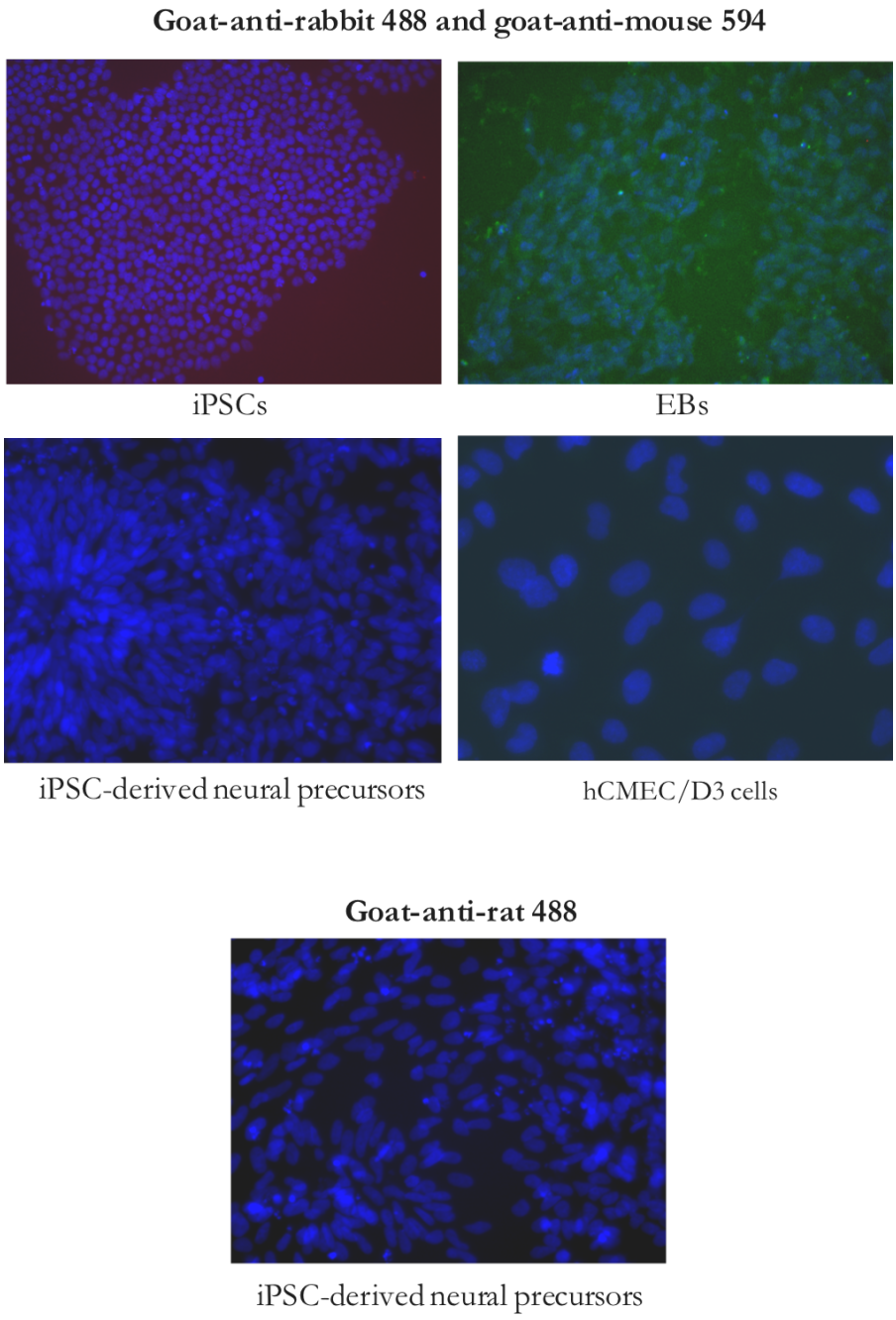

Figure A1: Omission of primary antibodies for immunocytochemistry negative controls

Representative images showing the application of goat-anti-rabbit 488 with goat-anti-mouse 594 without primary antibody and goat-anti-rat 488 without primary antibody to demonstrate the minimal level of background staining in immunocytochemistry experiments.

Appendix II

The PICALM antibody used in Chapter 5 was developed by a collaboration with Millipore and was validated by Thomas et al. (2016) using siRNA targeting PICALM (Figure A2).

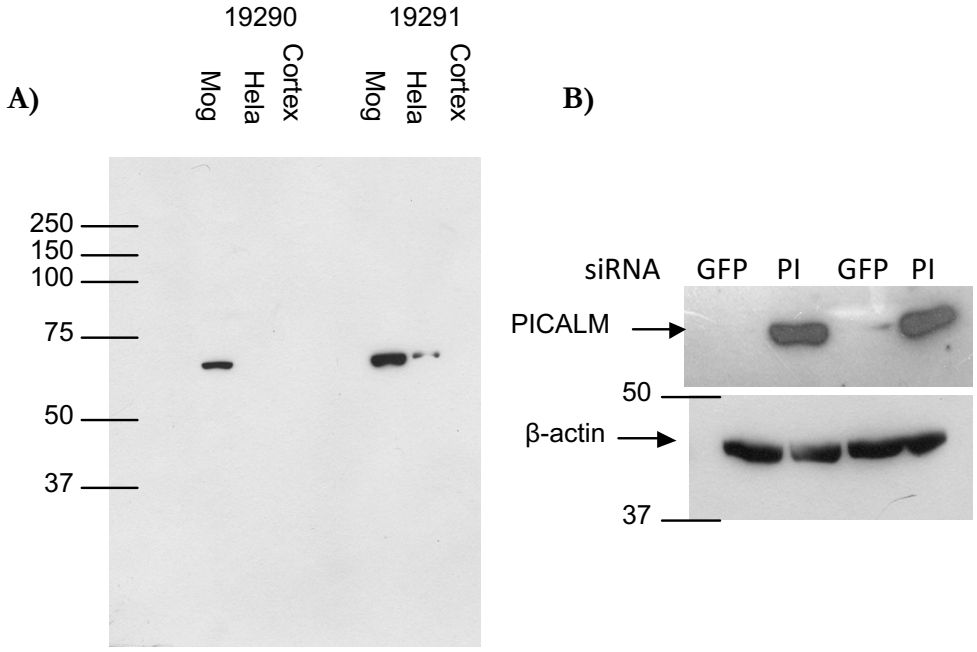

Figure A2: Validity report for PICALM 19291 antibody showing specificity and depletion with PICALM siRNA

A) Western blot showing PICALM bands using Millipore corporation antibody 19291 in Mog cells, HeLa cells and Mouse cortex. Mog = MOG G UVW Human brain astrocytoma Established from an anaplastic astrocytoma of normal adult brain

B) Western blot showing PICALM bands using the Millipore corporation 19291 antibody after GFP siRNA and PICALM siRNA (PI) treatment.